Enantioenriched Helicenes and Helicenoids Containing Main-Group Elements (B, Si, N, P)

Kais Dhbaibi, Ludovic Favereau, Jeanne Crassous

Enantioenriched helicenes and helicenoids containing main-group elements (B,Si,N,P)

Kais Dhbaibi,[†,#] Ludovic Favereau,[†] Jeanne Crassous[*,†]

[†] Univ Rennes, CNRS, ISCR (Institut des Sciences Chimiques de Rennes) - UMR6226, F-35000 Rennes, France; [#] University of Gabés, Faculty of Science of Gabès, Zrig, 6072 Gabès, Tunisia.

Email: jeanne.crassous@univ-rennes1.fr

ABSTRACT: In this review, we discuss the rich chemistry of helicenes and helicenoids containing main-group elements. Enantioenriched helicenic derivatives containing main-group elements B, Si, N and P, either incorporated within the helical backbone or grafted to it, will be thoroughly presented. We will describe their synthesis, resolution, and asymmetric synthesis, their structural features, electronic and chiroptical properties, emission, together with other photochemical properties and applications.

OUTLINE

4.1. N-incorporating helicenes

4.1.1. Azahelicenes with fused pyridine cycles (pyridohelicenes)

4.1.1.1. Synthesis, chiroptical and physicochemical properties

4.1.1.1.1. Oxidative photocyclization

4.1.1.1.2. Coupling reactions

4.1.1.1.3. [2+2+2] Alkyne cyclotrimerization

4.1.1.1.4. Alkyne-arene cycloisomerization

4.1.1.1.5. Other cyclization processes

4.1.1.1.6. Substitution of pyridohelicenes

4.1.1.2. Application in optoelectronics

4.1.1.2.1. Conductance

4.1.1.2.2. Optoelectronic devices

4.1.1.3. Coordination chemistry of pyridohelicenes

4.1.1.4. Applications in asymmetric organocatalysis

4.1.2. Azahelicenes with fused carbazole cycles (pyrrolohelicenes)

4.1.2.1. Carbazoles from oxidative photocyclization

4.1.2.2. Carbazoles from palladium-catalyzed cyclodehydrogenation

4.1.2.3. Intramolecular N-arylation

4.1.2.4. Double Bucherer-carbazole-synthesis

4.1.2.5. Enantioselective Fischer indolization

4.1.2.6. Oxidative fusion of pyrroles

4.1.2.7. Diels-Alder reactions

4.1.3. Pyrazine-containing helicenes

4.1.4. Helicene-dimide systems

4.1.5. Helicene-imidazole derivatives

4.1.5.1. Fused helicene-imidazole derivatives

4.1.5.2. Imidazole-substituted helicenes

4.1.6. Azahelicenes with N-bridging fused rings

4.1.6.1. Helicenic bridged triarylamines

4.1.6.1.1. Carboxy-bridged triarylamine heterohelicenes

4.1.6.1.2. Oxygen-bridged triarylamine heterohelicenes

4.1.6.1.3. Thia-bridged triarylamine heterohelicenes

4.1.6.2. Polyaza[7]helicenes

4.1.7. Cationic helicenes

1. Introduction and scope

1.1. General structural and stereochemical aspects

Chirality is ubiquitous in life and Nature has chosen the homochiral helical topology for its biological systems at work, namely the right-handed α-helix in proteins and the right-handed double helix in DNA.[1] In the chemist's artificial synthetic world, remarkable progress has been accomplished in the construction of helical systems, not only because they can mimic biological functions, but also because they enable to examine and develop chirality-related new phenomena, properties and functionalities.[2,3,4] [*n*]Helicenes are formed of *ortho*-fused aromatic rings; the steric repulsive interaction between the terminal aromatic rings, makes them chiral helical molecules, even though they are devoid of any stereogenic center.[5,6,7,8,9] The chemistry of heterohelicenes can be traced back to 1903 when the first two azahelicenes, namely 7*H*-dibenzo[*c*,*g*]carbazole **1** and benzo[*f*]naphtho[2,1-*c*]cinnoline **2** (Figure 1), were prepared by Meisenheimer and Witte.[10] Helicenes chemistry experienced a boom since the seminal work of Newman and Lednicer, who performed the first synthesis of enantioenriched carbo[6]helicene (**3**).[11] The first preparation of enantioenriched heterohelicene was accomplished by Wynberg in 1968, when hexa- and heptathiahelicenes were prepared by oxidative photocyclization reaction.[12] Since then, there has been a growing interest in the chemistry and applications of helicenes containing main-group elements, concomitantly to the development of polycyclic aromatic hydrocarbons (PAHs).[13] Heterohelicenes can indeed be regarded as heterographenes with a helical topology.[14] In this context, flexible as well as convenient methods for their syntheses are highly desirable for structural modification. For this purpose, the introduction of main-group elements can endow the basic carbohelicenic backbone with particular structural features and properties that will be used for targeted applications. Indeed, organic semiconductors based on heteroatomic π-conjugated molecules have attracted great attention in the past few decades due to their interesting optical and electronic properties, and their wide applications in organic light-emitting diodes (OLEDs), organic field-effect transistors (OFETs), and organic photovoltaics (OPVs), spintronics.

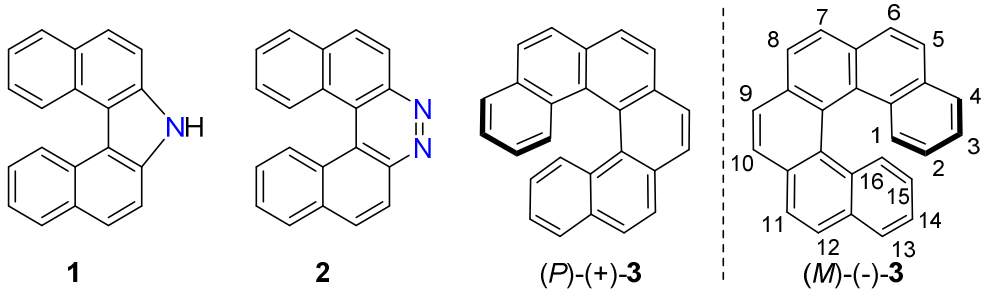

1 **2** (*P*)-(+)-**3** (*M*)-(-)-**3**

Figure 1. Structures of first aza[5]helicenes prepared in 1903[10] and of carbo[6]helicene enantiomers.[11] Official IUPAC numbering for hexahelicenes.

When symmetrically substituted, helicenes possess C_2 symmetry axis that is perpendicular to the axis of helicity (Figure 2a) but in most cases, they are C_1-symmetric chiral molecules. Their configurational stability depends on the number of fused aromatic rings and substituents and they typically start to display

high racemization barriers (>27 kcal mol^{-1}) when n ≥ 5 (or for n=4 with particularly highly-crowded systems). The highly delocalized large π-electron system of fully aromatic helicenes along with their inherent chirality predetermines their unique optical and electronic properties,[6] as well as their use in many fields of research including supramolecular chemistry and molecular recognition, biology,[6] materials science,[7,8,9] and asymmetric organo- or transition metal catalysis.[15,16,17] Note that systems formed of non fully aromatic *ortho*-fused rings are called helicenoid or helicene-like molecules and will be also considered here whenever they are obtained in enantioenriched forms. Binaphthyl systems may indeed give rise to helicene-like structures upon different types of ring closures; some of them will be discussed in this review.

According to IUPAC nomenclature, the term carbo[n]helicene is used to denote a helical molecule formed of n *ortho*-fused benzene rings. The prefix penta-, hexa-, hepta-, and so on, can also be used to specify the number of fused benzenes (for example hexahelicene). As far as a heteoratom is incorporated into the helical backbone, the general term hetero[n]helicene is used, where 'hetero' refers to 'aza', 'bora', 'oxa', 'phospha', 'thia'. When possible, the position of the heteroatom is given by using IUPAC numbering. It must be pointed out that the same generic term can correspond to very different helical structures. For example, an aza[6]helicene or hexaazahelicene may refer indifferently to a pyrido[6]helicene or to a pyrrolo[6]helicene. Similarly, thiahelicene is used as a generic name for all classes of helicenes incorporating a sulfur atom in the helical scaffold. As a consequence, this general nomenclature may be confusing. It is therefore recommended to specify the type of heteroaromatic ring included in the helical backbone (such as for instance pyrrolo[6]helicene rather than aza[6]helicene) and/or to use the full IUPAC chemical name.

As the number of fused rings increases, the helicene spirals up along the helical axis to form a cylindrical structure with a constant pitch (in both the inner and the outer helices, see Figure 2a). Carbohelicenes composed of six-membered aromatic rings can cover a complete 360° rotation of a screw, overlapping the terminal rings. The term helicity is generally used to define the dihedral angle between the two terminal rings. On the basis of the helicity rule proposed, a left-handed helix is designated “minus” and denoted as (*M*) whereas a right-handed one is designated “plus” and denoted as (*P*) (Figure 2b).[18] The replacement of one or more carbons by a heteroatom in a helicenic structure, above all, modifies the geometric parameters of the helix (Table 1) and therefore its propensity to racemize more or less rapidly. DFT calculations performed on pentahelicenic structures, incorporating a central CH_2 element or a heteroatom, showed that the type of heteroatom significantly affects the torsion angles where for example a silicon or a phosphorus atom induces a larger overlap of the two terminal benzene rings, which increases the resistance to racemization,[19] while a nitrogen or an oxygen atom reduces the overlap and therefore the inversion barrier.[20]

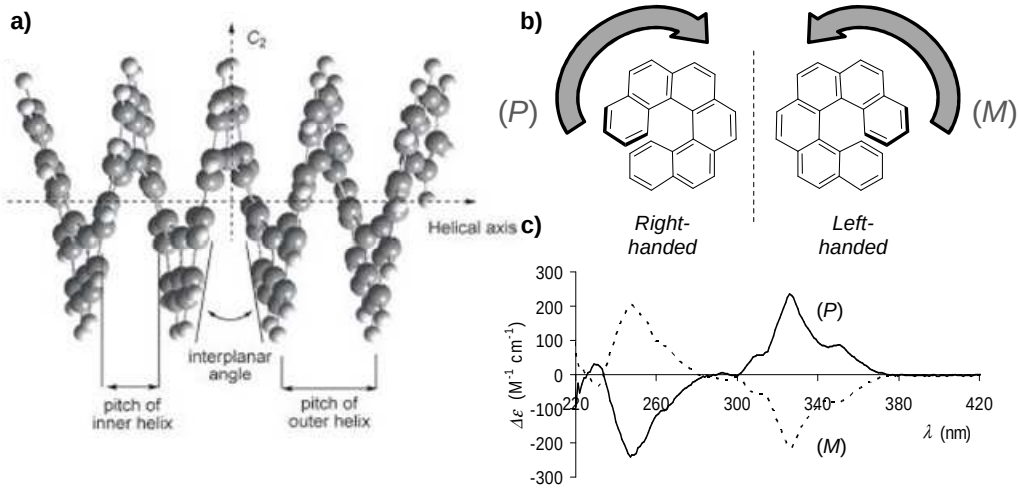

Figure 2. a) Helicenes helical structure, b) (*M*) and (*P*) chirality in helicenes, c) ECD spectra of (*P*) (plain lines) and (*M*)-carbo[6]helicene (dotted lines). Adapted from ref. [5]. Copyright 2012, American Chemical Society.

Table 1. Optimized Torsion Angles (θ) for [6]helicene derivatives.[a] Reproduced from ref. [20]. Copyright 2016, American Chemical Society.

Z	CH_2	NH	O	SiH_2	P(=O)H
∠*C*–*Z*–*C* / degree	102.6	109.4	105.9	91.9	91.4
θ / degree	21.5	18.7	17.0	32.3	29.1

[a]Estimated for the structure optimized by DFT at the B3LYP/6-31G(d) level of theory.

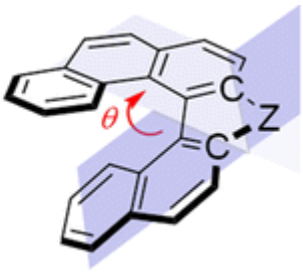

1.2. Photophysical and chiroptical properties, absolute configuration

The presence of a heteroatom in the fused polycyclic systems considerably alters the electronic structure and enables to fine-tune various optoelectrical properties. (Hetero)helicenes can be considered as chiral organic semi-conductors. Although not as efficiently as in planar PAHs, the π-electrons are delocalized *via* the helical structure which generally absorbs from the near-UV to the visible and in some cases to the near-IR domain. While the HOMO-LUMO gap (E_{gap}) is quite high in carbohelicenes, it can be significantly modified by the introduction of heteroatoms. For instance, the band gaps of carbo[n]helicenes, thia[n]helicenes with alternating benzene and thiophene rings, and carbon-sulfur [n]helicenes were estimated by density functional theory (DFT) studies in the gas phase: due to ineffective conjugation, carbon-sulfur helicenes have the largest energy gap(4.1 eV), while the thiahelicenes show smaller gap (2.5 eV) than that of carbohelicenes (2.9 eV).[21]

Regarding emission properties, it will be seen that most of organic B, Si, P, N-containing helicenes display blue fluorescence due to the electron-withdrawing effect of the heteroatoms, but this emission can be significantly tuned by taking advantage of the presence of vacant orbital (B) or lone pair (P, N) through reactivity with a variety of reagents (proton, halide, metallic ion, lanthanide, etc) thus giving the opportunity to achieve stimuli responsiveness and chiroptical switching.[22] Importantly, endowing the

helical backbone with strong charge transfer significantly modifies the absorption and emission properties. The helical nature of the π-conjugated system has also a direct impact on the emission properties since it promotes singlet to triplet intersystem crossing, thanks to the large spin-orbit coupling in helical molecules.[23] Therefore at low temperature, fluorescence is often accompanied by phosphorescence emission. Finally, helicenes can self-assemble in the solid state thus giving rise to solid state optical properties different from the liquid state.

Due to their helical shape and extended π-electronic conjugation, helicenes are archetypes in chirality. They display particularly intense electronic circular dichroism (ECD) spectra thanks to the strong π–π* transitions within a helical scaffold associated resulting from strong dipolar magnetic transition moments coupled with dipolar electric transition moments. As a direct consequence, the absolute configuration (relating the handedness and the sign of a chiroptical property, typically the specific rotation at the sodium line,[24] or the sign of ECD band at a defined wavelength)[25] can very often be deduced from the experimental ECD spectrum. This feature is very convenient to directly know which enantiomer is obtained after a stereoselective method. There is also a general relationship between the absolute configuration and the optical rotation at the sodium D line: (*P*) helicenes are dextrorotatory, while (*M*) helicenes are levorotatory (exceptions will be clearly stated in the text). Note that the units for specific and molar rotations will not be given in the text are specified on note #. The optical rotatory dispersion (ORD), *i.e.* dependence of optical rotation as a function of the wavelength, was also often used in the early stages of helicenes chemistry to characterize the chirality of helicenes. Vibrational circular dichroism (VCD) and Raman optical activity (ROA) are also valuable chiroptical techniques acting in the infrared region. In this regards helicenes display typical vibrational chiroptical activity, with for instance nice signature in VCD spectroscopy for the coupled C=C stretching modes along the helical axis.[26] Being emissive and chiral, helicenes containing main-group element often display circularly polarized luminescence (CPL)[27] and this aspect is a growing interest in materials science.[28] As will be illustrated, the presence of heteroatoms can significantly change the shape of the molecule and its π-system thus changing strongly the chiroptical response.

1.3. Scope

In this review, *enantioenriched* helicenes containing main-group elements B, Si, N and P,[29] either incorporated within the helical backbone or grafted to it (Figure 3), will be thoroughly presented. As a result, the classical carbo[n]helicenes, their radical anions and related graphene-type scaffolds will not be discussed here. Thus the hexahelicene radical anions generated from elements of the main groups I and II (Li, Na, K salts) will not be discussed.[30,31] Similarly, helicenic structures including Li^+, Na^+ or K^+ cation through cation-π interactions yielding a closed helical structure have been considered theoretically and observed experimentally by mass spectrometry with the Li element[32] but have not yet been obtained in enantioenriched forms. In addition, we only consider substituted systems where the heteroatom is either directly linked or close to the helical backbone; we thus discard systems linked to carbohelicenes through carbon π-systems such as alkynyl or ethynyl bridges but discuss helicenes substituted with small hetero-functions (alkoxy, amino, cyano, phosphine, etc) and heteroaromatics (pyridine, pyrrole, phosphole, etc).

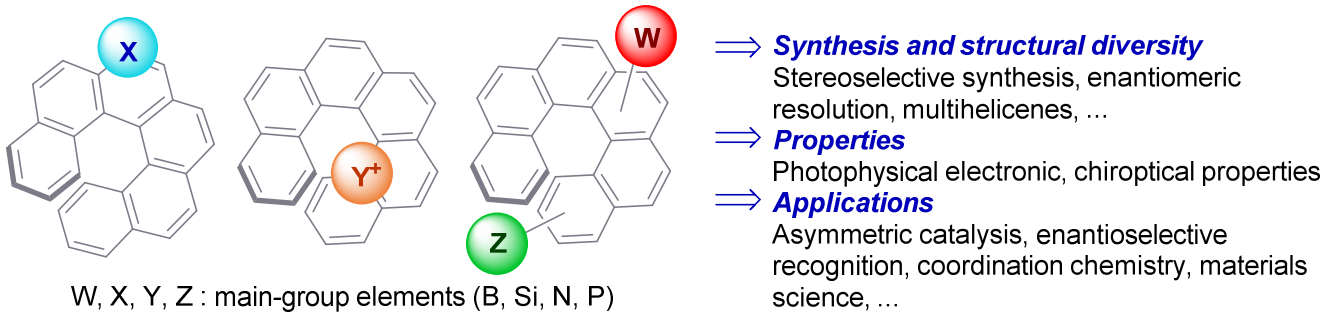

Figure 3. Helicenic structures either incorporating or substituted with main-group elements.

Since many reviews and a monography dealing with the general aspects of carbohelicenes and heterohelicenes are already existing, in this review, we will deal with the helicenic structures that have properties originating from their chirality, *i.e.* helicenes that are configurationally stable and that have been obtained in enantioenriched forms, and for which their chirality has been emphasized either from the synthetic point of view or for their chirality-related properties. From the synthetic point of view, stereoselective synthetic methods and other preparation methods of enantioenriched molecules will be presented. The universally utilized chromatographic enantiomeric resolution methods will be given for each compound. An important aspect is the configurational stability of the helical derivatives, which can depend on the chemical structure and may be influenced by the presence of heteroelement, will be discussed in this review. Furthermore, particular attention will be paid on the chiroptical properties, especially the optical rotations (OR) and the electronic circular dichroism (ECD) spectra and how they vary as a function of the topological structure considered (geometrical parameters) and of special features such as charge transfer, π-conjugation, self-assembly, etc. The non-polarized and polarized photophysical properties, namely emission and CPL will be also detailed. Finally, the other physico-chemical properties related to and influenced by the chirality of helicenes, such as their heterochiral/homochiral supramolecular assembly (in 2 and 3 dimensions), their chiral recognition abilities, their charge transport in relation with their enantiopurity, and the tuning of their chirality/chiroptical activity, will be detailed. Enantioenriched heteroatomic multihelicenic systems will also be described. Note that helicenes including oxygen and sulfur atoms are not treated in the present review and will be published elsewhere. For related reviews see: [33,34,35,36,37,38,39].

2. Helicenes Substituted with boron

2.1. Helicenes incorporating boron atoms: borahelicenes

Incorporating boron atoms into helical PAHs is an efficient strategy to create novel chiral materials with tailored properties, providing heterohelicenes for high-performance organic chiral molecular materials. For instance, thanks to the electron-accepting and Lewis acidic character of boron, introducing one or several B atoms into carbohelicenes generally results in strongly blue emitting fluorophores due to the higher energy of the LUMO levels. The efficient conjugation between the vacant p orbital of boron and adjacent π-electron cloud for compounds with a three-coordinate boron atom or the π-σ / π-σ* type interactions for compounds incorporating four-coordinate B atoms are also important features influencing

the absorption and emission. Furthermore, B atoms usually affect the intramolecular and intermolecular charge transfers by creating permanent dipole moments that have a great impact on the ionic mobilities in the solid state.[40] However, due to the intrinsic reactivity of tricoordinated organoboranes to oxygen and moisture, the synthesis of "B-doped" helical PAHs is rather difficult. To overcome this issue, N or O atoms are often concomitantly introduced as B-N or B-O units. Indeed, the interaction between the lone pair of electrons on the N/O atoms and the empty p orbital of the B atom enhances the stability. Thus, the class of helicenes incorporating boron atoms most generally includes N or O atoms and are therefore named azaborahelicenes and oxaborahelicenes. Thanks to the three or four-coordinate nature of the boron atom, monohelicenic or multihelicenic structures can be built-up.

2.1.1. Borahelicenes from intramolecular electrophilic arene borylation

In 2012, Hatakeyama and coworkers reported an azaboradibenzo[6]helicene (**6**, Scheme 1) as a new type of semi-conducting material displaying helical chirality.[41] This compound was synthesized in its racemic form by a tandem bora-Friedel-Crafts type reaction on intermediate **5** and was subsequently resolved through chiral HPLC on a Daicel Chiralpak IA-3 column (eluent: *n*-hexane/CH_2Cl_2). An inversion barrier of 42 kcal/mol was obtained by theoretical calculations showing great configurational stability. Mirror-imaged ECD spectra were measured for the pure enantiomers, with a negative-positive signature at 268-287 nm and a positive-negative one between 329-380 nm ((*P*)-isomer, see Figure 4d). Note that this ECD signature is not the typical one of helicenes, and was assigned by other authors in 2013 as mainly resulting from exciton-coupling of the *ortho*-fused aromatic rings.[42] Similarly, the specific rotation values are small compared to fully carbon hexahelicene (333 *vs.* +3300 in CH_2Cl_2, Table 2).[24]

Using a similar synthetic procedure, the same group prepared in 2015 oxabora[6]helicene **9** from 1,3-bis(naphthalen-2-yloxy)benzene **8** (see Scheme 1).[43] Compound **9** displayed a helical topology which was ascertained by X-ray crystallography (Figure 4c). Subsequent enantiomeric resolution of **9** was conducted by chiral HPLC over a Daicel Chiralpak IA-3 (eluent: toluene); however, its activation energy for racemization appeared low ($\Delta H^{\neq}$ = 26.6 kcal mol^{-1}) *i.e.* between those of [6]helicene and [5]helicene.[44] Calculations and X-ray crystallography enabled to assign the (*P*)-(+) absolute configuration for azaborahelicene **6** and for enantiopure dibromo derivative **10** (with Br in *para* position of the N atoms) which was also prepared from enantiopure **6**. X-ray structure crystallography and calculated Nuclear Independent Spin Chemical Shifts (NICS) (Figures 4a and 4c) revealed low aromaticity of the central BNC4 rings of **6**.[41] As a consequence, azabora[6]helicene **6** (and in a similar way in **9**[43]) revealed fully extended π-conjugation, which was further evidenced in the calculated HOMO and LUMO (Figure 4b).

Azabora[6]helicene **6** displayed appealing charge transport properties. Indeed, carrier inversion was observed between the racemate, acting as a p-type semi-conductor, with higher hole mobility μ_h than electron mobility μ_e (measured by time of flight (TOF) technique on a thin amorphous films obtained by vacuum-deposition between Al electrodes) and the pure enantiomer acting as a n-type semi-conductor, with higher μ_e than μ_h. This effect was explained by their different packing in the solid state between racemate and pure enantiomers. Indeed, the heterochiral and homochiral supramolecular assembly, found in the packing of *rac*-**6** and (*P*)-**6**, respectively, impose different arrangements of the dipole moments and therefore different holes or electrons transport in films.[41]

Scheme 1. Synthesis of azaboradibenzo[6]helicene **6**[41] and oxabora[6]helicene **9**[43]. Structure of dibrominated helicene (*P*)-**10**.[41]

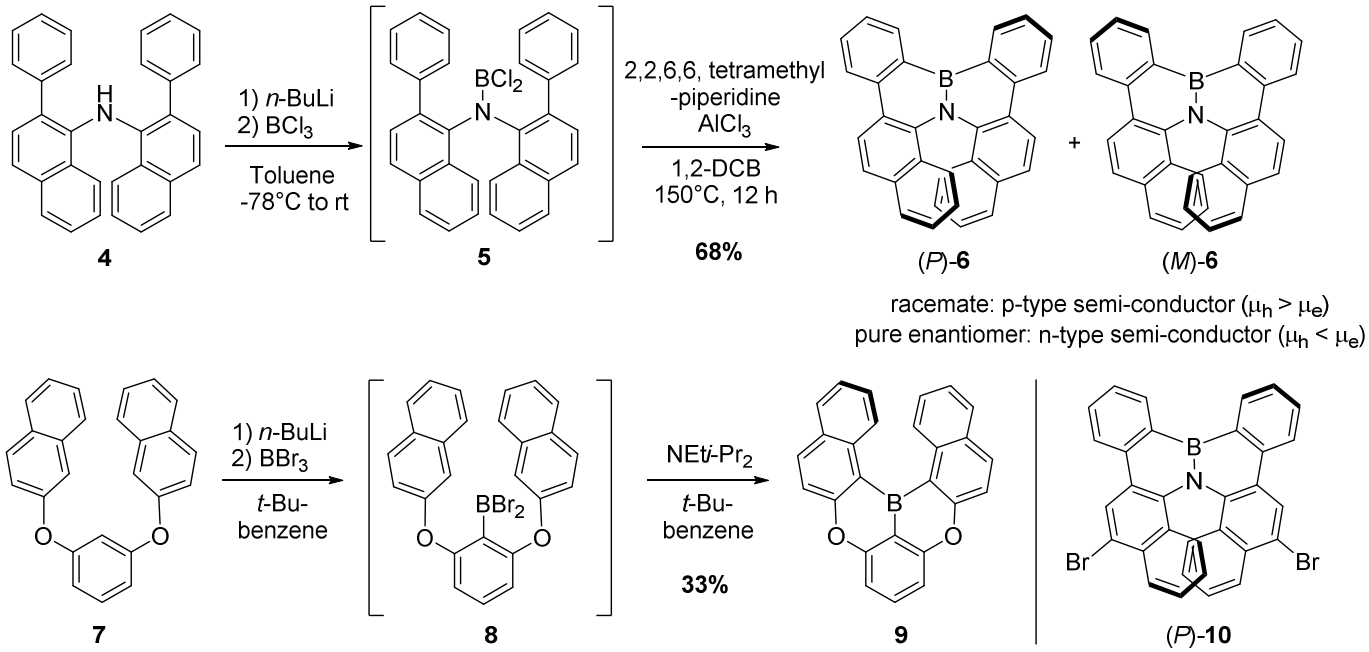

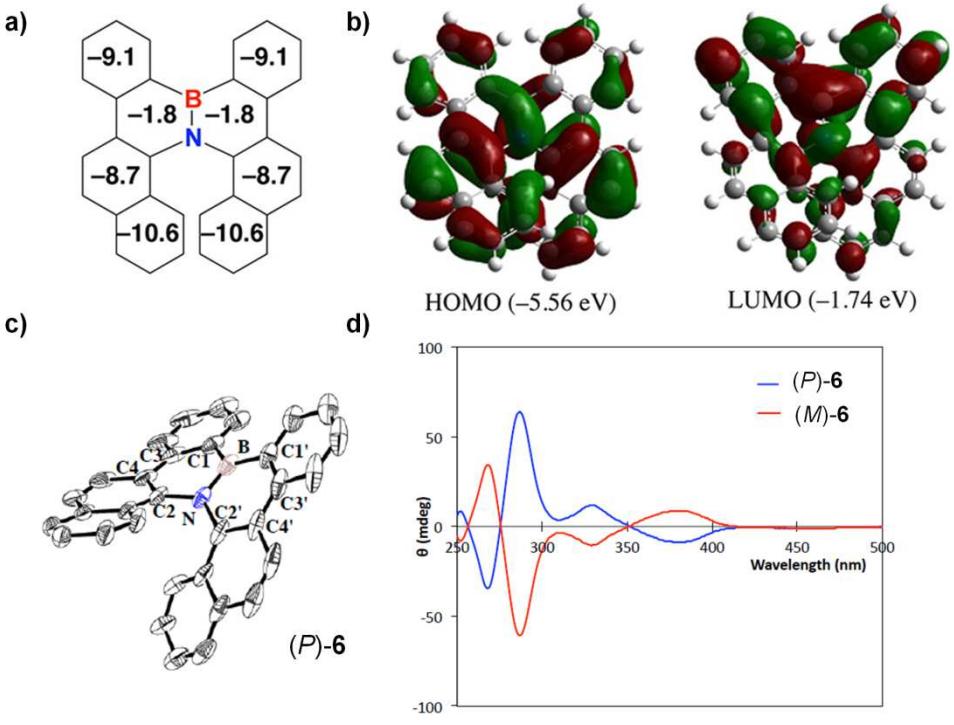

Figure 4. a) Calculated Nuclear Independent Spin Chemical Shifts (NICS(1)) of azaboradibenzo[6]helicene **6**; b) Kohn-Shan HOMO and LUMO, c) X-ray (ORTEP drawing) of

enantiopure (*P*)-**6** showing the helical structure, d) ECD spectra (ellipticity) of (*P*) and (*M*)-**6** enantiomers. Adapted from ref.[41]. Copyright 2012, American Chemical Society.

2.1.2. Borahelicenes from *ortho*-cycloborylation

In 2017, Autschbach, Crassous, *et al.* synthesized enantiopure hexa-, octa- and deca-azaborahelicenes **12a-d** and studied the influence of the helicene's size and the number of four-coordinate boron atoms on the chiroptical properties (both in absorption and emission).[45] These azaborahelicenes were prepared using a two-step process *i.e.* a cycloborylation reaction of 2-phenylpyridine type precursor using BBr_3 in the presence of $N^iPr(Et)_2$ affording a *B,B*-dibromo-azaborole system, which was then reacted with $AlMe_3$ (Scheme 2). The method takes advantage of the nitrogen atom which directs the electrophilic aromatic borylation to the *ortho*-position. Then the pure enantiomers were obtained using HPLC separation over chiral stationary phases (see Table 2). Azaborahelicenes **12a-d** display strong absorption between 250-450 nm (see Figure 5) and blue fluorescence (λ_{em} ~ 420-450 nm) with rather strong quantum yields (0.21-0.49) for azaborahexahelicenes **12a**,**c** and more modest ones (~ 7%) for the octa- and decahelicenes **12b**,**d**. Indeed, the introduction of one additional boron atom on **12c** strongly increases the emission efficiency compared to **12a**, but at the same time strongly decreases the configuration stability (an enantiomerization barrier $\Delta G^{\neq}$ of 27.5 kcal mol^{-1} at 78 °C, in ethanol was experimentally estimated for **12c** by racemization kinetic studies) due to the presence of two azaborapentacycles that give a more open and more easily racemizing structure. The HOMO and LUMO of **12a-d** show extended π-conjugation over the helical frame, while other MOs show conjugation between the B-CH_3 σ-bonds and the π-system of the aromatic scaffold.[45] In the UV-vis spectra depicted in Figure 5, one can see that the longer are the helicene, the stronger the absorption coefficients and the more red-shifted the absorption wavelengths. Similarly, the ECD spectra were more red-shifted and more intense for azaboraoctahelicene **12b** and azaboradecahelicene **12d** as compared to azaborahexahelicenes **12a**,**c**. This is also reflected in the specific rotations that show values around $+1000^{\#}$ for the (*P*)-[6]helicenes and $+3000^{\#}$ for the (*P*)-[8] or (*P*)-[10]helicenes. Note that, except for **12c**, the overall ECD signature appeared typical of helicene derivatives and that the (*P*)-enantiomers display positive optical rotation values. On the contrary, the CPL responses of these azaborahelicenes do not follow a general trend, with negative g_{lum} values found for (*P*)-**12a-c** and a positive one for (*P*)-**12d** (see Table 2). It was indeed noticed[46,26] that the sign of CPL greatly varies with the substituents grafted onto the helicenic core and generally follows the sign of the lower energy ECD-active band. However, the absolute values of g_{lum} (between 7×10^{-4} and 10^{-3}) for **12a-d** are typical of enantiopure organic helicenes.[27]

Recently a very similar strategy was used to prepare enantiopure azabora[5]helicenes **13-15** (Scheme 2b).[47] Overall, the ECD spectra and optical rotation values of **13-15** appeared very different from azaborahelicenes **12a-d**, with for instance negative specific rotations for all (*P*) enantiomers (see Table 2). Enantiopure azabora[5]helicenes **13-15** displayed different charge transfer characters and fluorescence quantum yields ranging from 0.13 and 0.30 in toluene, governed by the electron-donor substitution (*p*-MeO-phenyl, *p*-Me_2N-phenyl) on the helicene.[47] The dimethylamino-substituted derivative emitted at the most red-shifted wavelength and showed the highest Stokes shift in toluene. These helicenes also show CPL activity with dissymmetry factors (g_{lum}) up to 3.5×10^{-3} . It was shown that the sign of the ECD

band corresponding to the first transition and the CPL spectrum depend on the electron-donor substitution (Figures 6a,b).

Scheme 2. a) Synthetic routes to azabora[*n*]helicenes **12a-d**. *i*) BBr_3, $N^iPr(Et)_2$, CH_2Cl_2, 25 °C, 24 hrs; *ii*) $AlMe_3$, CH_2Cl_2, 30 min.[45] b) Chemical structure of azabora[*5*]helicenes **13-15**.[47]

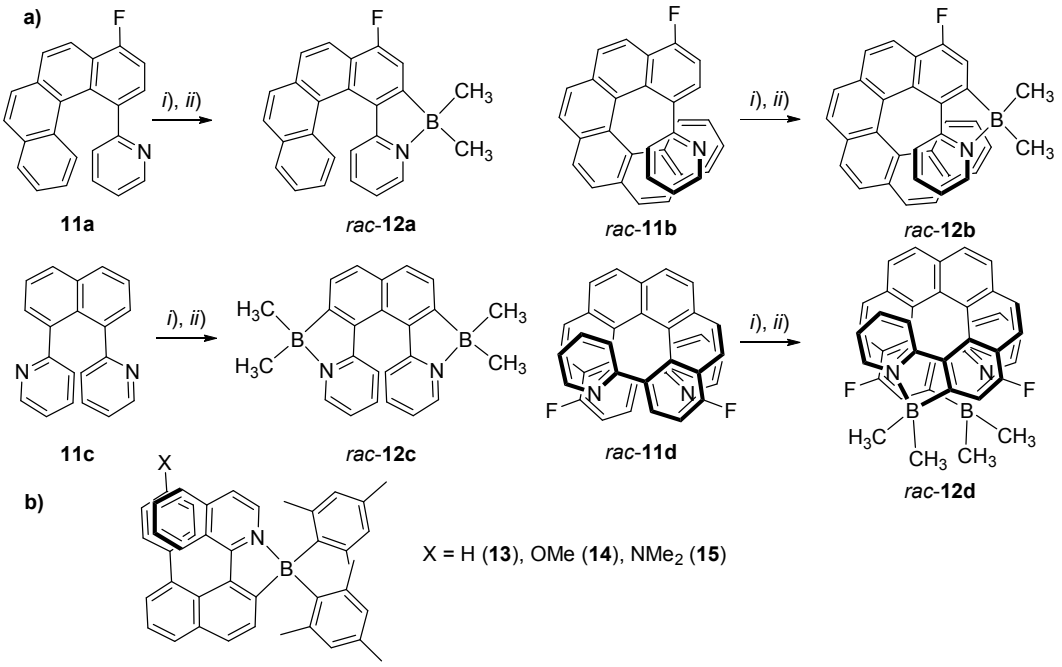

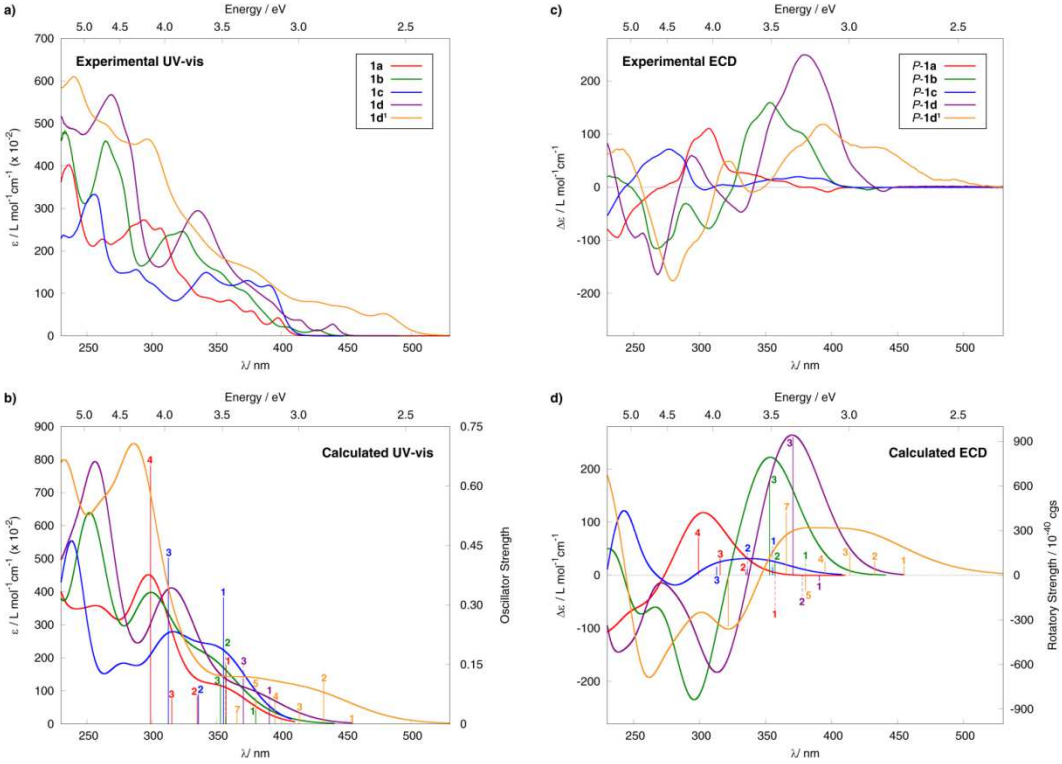

Figure 5. Experimental UV-vis (a) and ECD (c) spectra of azaborahelicenes (*P*)-**12a-d** and of bis-platina[10]helicene complex ((*P*)-**334h** see section 4.2.3.) in CH_2Cl_2, and their corresponding simulated

spectra (panels b and d, respectively) using TD-DFT LC-PBE0* calculations with continuum solvent model for dichloromethane at BP-D3 optimized geometries. No spectral shift has been applied. Calculated excitation energies and rotatory strengths are indicated as 'stick' spectra. Reproduced from ref. [45]. Copyright 2017, Wiley.

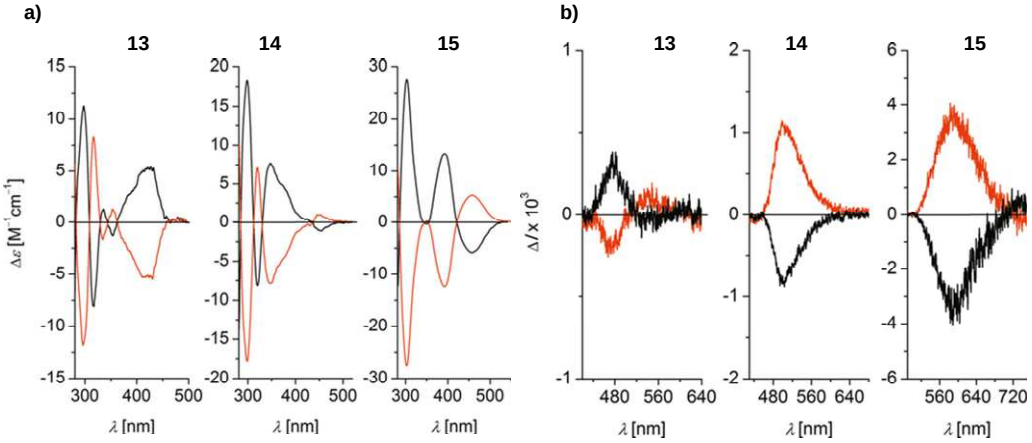

Figure 6. a) ECD spectra and b) CPL spectra of **13-15** in aerated toluene solution of (*P*)-isomers (red) and (*M*)-isomers (black). The corresponding fluorescence spectra have been normalized so that the ΔI value at the emission maximum reflects directly the $|g_{lum}|$ value. Reproduced with permission from ref. [47]. Copyright 2018, Wiley.

2.1.3. Multihelicenic structures

Multihelicenic structures can give access to multiple conformations, increased non planarity, and three dimensional inter/intramolecular interactions.[48,49,50] In this regards, several groups have devoted intensive efforts to the synthesis of double heterohelicenes[48,49] consisting of structures with two heterohelicenes fused together. Almost simultaneously in 2016, the groups of Hatakeyama[51] and Müllen[52] reported the preparation of fused double [5] and [7]heterohelicene containing OBO units (**19a**,**b** and **c** depicted in Scheme 3a) from hexabromobenzene *via* a Hart reaction followed by a tandem demethylation-borylation (Scheme 3b). X-ray structures (Scheme 3a for **19a** and **19c**) demonstrated a significantly twisted structure with the terminal aromatic rings overlapping at both ends, giving in the case of **19a**, an example of a double helicenes with intramolecular π-layers. Indeed, DFT calculations of the isomerization process yielded isomerization barrier ($\Delta G^{\neq}$) of 23.0 kcal mol^{-1} (at 298 K) from the chiral (*P*,*P*)-**19a** isomer to *meso* (*P*,*M*)-**19a** which is comparable to that of [5]helicene.[53] The isomerization barrier was substantially increased (31.8 kcal mol^{-1}) by introducing *tert*-butyl groups in **19c**, which enabled to separate (*P*,*P*)- and (*M*,*M*)-**19b** by chiral HPLC on a Daicel Chiralpak IE-3 column (eluent: toluene). By using one of the pure enantiomers, the isomerization barrier was experimentally determined as 29.0 kcal mol^{-1}, and agreed well with the calculated ones. Double [5]helicenes **19a** and **b** show two sets of strong absorption bands around 310 nm and 410 nm, with the longer ones corresponding to HOMO-LUMO transitions. The ECD spectra of (*P*)- and (*M*)-**19b** in CH_2Cl_2 displayed mirror-image relationship, with typical negative-positive Cotton effects around 270 and 330 nm, respectively, with an additional broad negative ECD-band around 430 nm corresponding to HOMO-LUMO transition displaying strong rotational strength in this case (Scheme 3d).

The absorption spectrum of **19c** recorded in CH_2Cl_2 solutions exhibited a maximum at 376 nm which is significantly red shifted compared with that of double [5]helicene **19a** (310 nm) due to the more extended π-conjugation in **19c**. According to TD-DFT calculations, the low-energy absorption band from 400 to 500 nm is assignable to the HOMO→LUMO transition corresponding to a π–π* transition of the fully conjugated bis-helical system. DFT calculations revealed a very high theoretical isomerization barrier of 45.1 kcal/mol for the (*P*,*P*)/(*M*,*M*)-**19c** stereoisomer, *i.e.* 4.4 kcal/mol higher than the (*P*,*M*) stereoisomer (not observed experimentally). The high configurational stability of **19c** enabled to obtain the pure (*P*,*P*)- and (*M*,*M*)-**19c** by chiral HPLC (Daicel Chiralcel IE column; EtOAc/MeOH = 9:1 as eluent) and to study their chiroptical properties. The ECD spectrum of (*P*,*P*)-**19c** in CH_2Cl_2 displayed two strong positive bands at 275 and 320 nm, a strong negative one at 375 nm and a broad and less intense one between 425-475 nm.[52] Note that the isomerization barrier of the OBO-fused double [7]helicene is much higher than for oxabora[6]helicene **9** (*vide supra*) and higher than carbo[7]helicene (42.0 kcal/ mol), indicating the advantage of double helicenes over monohelicenes in terms of conformational stability. Indeed no racemization was observed upon heating enantiomer (*P*,*P*) and (*M*,*M*)-**19c** for 24 h up to 200 °C.[52] Note that in 2017 a longer double OBO-helicene analogue was deposited on a Au(111) under UHV conditions and its surface-assisted cyclodehydrogenation into a planar OBO-perihexacene was observed by STM.[54]

Similarly to **6** and **9**, the strong bond alternation found in the BOC4 rings of **19a**[51] may account for the small NICS value of 1.3 while the surrounding C6 rings, including the distorted central benzene ring, show large negative NICS values (Scheme 3c). For comparison, in the all-carbon analogue tetrabenzo-[*a*,*f*,*j*,*o*]perylene shown in Scheme 3c, the central C6 ring shows a positive NICS value, indicating substantial antiaromatic character. Notably, molecular orbital calculations of **19a** indicate that the HOMO and LUMO are spread over the C6 rings rather than on the boron and oxygen atoms, accounting for the substantial stability of **19a** (Scheme 3c).

Borahelicenes are efficient blue fluorophores. Indeed, azabora[6]helicene **6** displays blue fluorescence at 447 nm (Table 2), while smaller achiral [4]helicenic systems were successfully used as host materials in phosphorescent OLEDs with efficiencies better than the classical 4,4'-bis(9-carbazolyl)-1,1'-biphenyl (**CBP**) host.[43] The emission properties of oxabora[6]helicenes **19a** and **b** were also studied (see Table 2 for **19b**); **19b** revealed deep and almost pure blue fluorescence with Commission Internationale de l′Eclairage coordinates of (0.15, 0.08). Its enantiomers showed circularly polarized luminescence activity with g_{lum} of 1.7×10^{-3} at ~ 435 nm. Notably, the absolute fluorescence quantum yields of **19a** and **b** are 0.68 and 0.65 at 430 and 436 nm, respectively, which correspond to very high values for double helicenes. Achiral structures similar to **19a** and **b** have indeed proven efficient as B-containing PAH dopants in organic OLEDs and in field-effect transistors.[55] Compound **19c** has a green yellow fluorescence with the emission maximum at 487 nm and a quantum yield of 0.26, *i.e.* less efficient and more red-shifted compared to **19a**,**b**. Note that such BN and BO aromatic compounds also display increasing interest in the domain of thermally activated delayed fluorescence (TADF).[56]

Carrier-transport properties were also examined by TOF measurements on a stable amorphous film of double [5]helicene **19a**. It showed balanced ambipolar conductivity ($\mu_h = 5.7 \times 10^{-3}$ cm^2 V^{-1} s^{-1}, $\mu_e = 7.9 \times 10^{-3}$ cm^2 V^{-1} s^{-1}) superior to those of representative amorphous ambipolar materials, thus revealing high potential for materials science applications. These examples highlight the direct impact that enantiopurity can have on a chiral material incorporated into an optoelectronic device.[28]

Scheme 3. a) Chemical structures of oxaborahelicenes **19a-c** and X-ray structure of **19a** (heterochiral assembly) and of **19c**; b) synthetic scheme for the preparation of **19a-c**; c) NICS, HOMO and LUMO of **19a** compared to its all-carbon analogue; d) ECD (solid lines) and CPL (dashed lines) spectra of (*P*)-**19b** (red) and (*M*)-**19b** (blue). Adapted refs [51] and [52]. Copyright 2016, American Chemical Society.

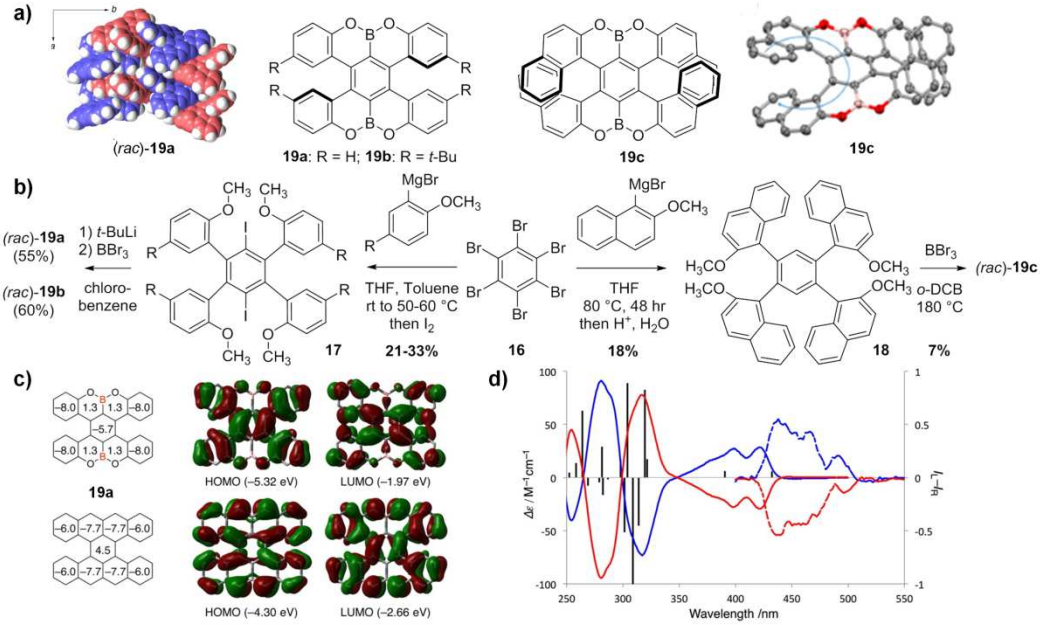

Overall, the use of CH borylation to create boron-rich helicenic structures appears efficient to access novel helicenic derivatives with efficient emission properties such as deep blue fluorescence and good electron, holes or ambiphilic mobilities, which can combine with the typical strong ECD spectra and CPL activity of organic helicenes. Other potential applications of 3 and 4-coordinate boron-PAH's are photoresponsive materials, sensors and imaging materials.[57,58,59]

2.2. Helicenes grafted with a boron atom

Another obvious feature of boron derivatives is their use as key intermediates in the preparation of novel derivatives, by taking advantage of the reactivity of boronic acids and boronate esters in a diversity of reactions (diverse couplings among which Suzuki or Chan-Lam). In this regard, we recently prepared 2-carbo[6]helicene-boronate esters (*P*)- and (*M*)-**21a** and **21b**[1,2] by classical oxidative photocyclization process and used them as intermediates for the preparation of enantioenriched amino-helicene derivatives.[60] Indeed, carbo[6]helicene-2-boronic pinacol and pinanediol esters were obtained by a classical photocyclization reaction of stilbenic precursors decorated with the boronic ester functions (Scheme 4a). Although the pinanediol derivatives exist as (*P*,1'*S*,2'*S*,4'*S*)-**21b**[1] and (*M*,1'*S*,2'*S*,4'*S*)-**21b**[2] diastereomers (more conveniently written as (*P*)- and (*M*)), no diastereoselectivity was observed during the cyclization. Compounds **21a** and **21b**[1,2] were therefore prepared in enantiopure forms by using chiral HPLC separation methods (see Table 2). Their ECD spectra displayed the same shape as those hexahelicene enantiomers and their molar rotations, which take into account the molecular weight, appeared of very similar magnitude as for **3** (~12000). A racemization Gibbs energy $\Delta G^{\neq}$ of 36.7 kcal mol^{-1} at 182 °C in 1,2-dichlorobenzene was evaluated experimentally for **21a**.[60] Note that enantiopure

boronate esters may be directly prepared from enantiopure 2-bromo-carbo[6]helicene.[61] Boronic acid **21c** was obtained from **21a** using sodium periodate in the presence of ammonium acetate (Scheme 4b).

Scheme 4. Preparation of enantiopure carbo[6]helicene-2-boronic pinacol esters **21a,b**[1,2] (a) and of boronic acid **21c** (b).[60]

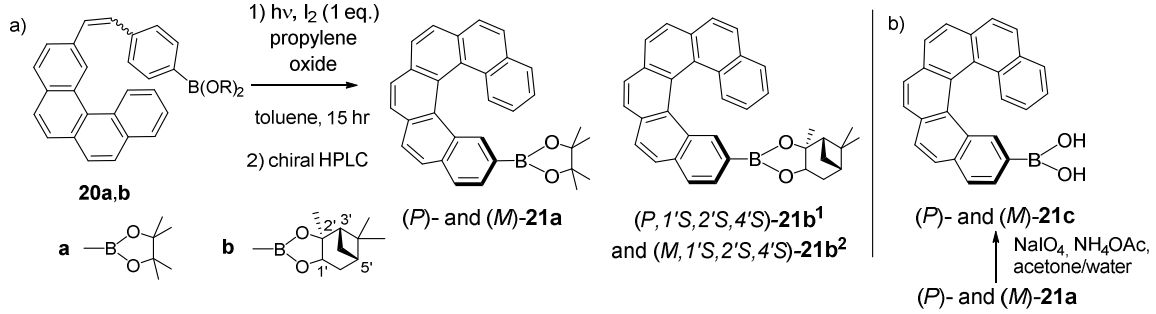

Table 2. Specific rotation values and photophysical data of enantioenriched borahelicenes.

Compound	Method of obtention	$[\alpha]_D$[a]	Enantio-purity	Conditions[b] (solvent/Conc.[c])	λ_{Abs} (nm)	λ_{Em} (nm)	Φ (% / solvent)	g_{lum}	Ref
(*P*)-**6**	Chiral HPLC[e]	+300	N.d.	CH_2Cl_2/0.1	310,373	447	-	-	41
(*P*)-**12a**	Chiral HPLC[f]	+1390	>96% *ee*[g]	$CH_2Cl_2/10^{-3}$ M	See Fig. 5	404, 425, 450sh	21/CH_2Cl_2	-9×10^{-4}	45
(*P*)-**12b**	Chiral HPLC[h]	+3010	>99% *ee*[h]	$CH_2Cl_2/10^{-3}$ M	See Fig. 5	435, 458	6.9/CH_2Cl_2	-7×10^{-4}	45
(*P*)-**12c**	Chiral HPLC[i]	+1440	>96% *ee*[i]	$CH_2Cl_2/10^{-3}$ M	See Fig. 5	427	49/CH_2Cl_2	-2.3×10^{-3}	45
(*P*)-**12d**	Chiral HPLC[j]	+5320	>97% *ee*[k]	$CH_2Cl_2/10^{-3}$ M	See Fig. 5	443, 471, 502, 541	7.4/CH_2Cl_2	$+1 \times 10^{-3}$	45
(*P*)-**13**	Chiral HPLC[l]	-106.4	>98% *ee*[l]	$CHCl_3$/0.1	414[d]	480	29/toluene	-2.5×10^{-4}	47
(*P*)-**14**	Chiral HPLC[l]	-96.8	>98% *ee*[l]	$CHCl_3$/0.05	420[d]	502	30/toluene	$+9.5 \times 10^{-4}$	47
(*P*)-**15**	Chiral HPLC[l]	-72.7	>98% *ee*[l]	$CHCl_3$/0.1	433[d]	586	13/toluene	$+3.5 \times 10^{-3}$	47
(*P*,*P*)-**19b**	Chiral HPLC[m]	+940.2	>99% *ee*[m]	$CHCl_3$/4.96	315,411	436,460	65/CH_2Cl_2 26/solid	-1.7×10^{-3}	51
(*P*)-**21a**	Chiral HPLC[n]	+2600	>98% *ee*[n]	$CH_2Cl_2/2 \times 10^{-4}$ M	353[d]	-			60
(*P*)-**21b**	Chiral HPLC[o]	+2370	>99.5 % *ee*[o]	$CH_2Cl_2/2 \times 10^{-4}$ M	355[d]	-			60
(*M*)-**21b**	Chiral HPLC[o]	-2640	>99.5 % *ee*[o]	$CH_2Cl_2/1 \times 10^{-4}$ M	355[d]	-			60

[a] In $deg \cdot mL \cdot g^{-1} \cdot dm^{-1}$. [b] Temperature between 20-25 °C. [c] In g/100 mL otherwise precised. [d] Longer-wavelength absorption band. [e] Chiralpak IA-3, *n*-hexane/CH_2Cl_2. [f] Chiralcel OD-H, *n*-hexane/EtOH. [g] Chiralcel OD-3, *n*-heptane/EtOH. [h] Lux-Cellulose-2, *n*-heptane/EtOH. [i] (*S*,*S*)-Ulmo, *n*-hexane/*i*-PrOH. [j] (*S*,*S*)-Ulmo, *n*-heptane/*i*-PrOH/$CHCl_3$. [k] Chiralpak IF, *n*-hexane/*i*-PrOH/ $CHCl_3$. [l] Chiralpak IA, *n*-hexane/isopropanol. [m] Chiralpak IE, toluene. [n] (*S*,*S*)-Whelk-O1, *n*-hexane/*i*-PrOH/ CH_2Cl_2. 90:5:5. [o] Chiralpak IB, *n*-hexane/*i*-PrOH.

3. Helicenes substituted with silicon

The most straightforward way to introduce silicon atoms into helicenic backbones is to fuse biphenyl rings with siloles in *ortho* positions, resulting in (di)benzosiloles (or silafluorenes). Siloles are silacyclopentadienes in which the σ* orbital of two exocyclic σ-bonds of the silicon atom and the π* orbital of the 1,3-butadiene moiety interact to provide a σ*–π* conjugated system.[62] The resulting low LUMO level gives rise to various characteristic photophysical features such as strong luminescence. Moreover, the high electron transport ability of siloles has been used as a key component in organic light-emitting diodes (OLEDs).[63] Incorporating silole into helicenic frameworks thus leads to chiral helical π-conjugated molecules with fluorescence emission and potential charge-carrier transport ability.

3.1. Helicenes incorporating a silicon atom: silahelicenes

3.1.1. Enantioselective [2+2+2] cycloaddition

In 2012, Shibata and coworkers described for the first time the synthesis of enantioenriched sila[7]helicenes **25a-d** incorporating silole units, by performing consecutive stereoselective and stereospecific inter- and intramolecular [2+2+2] cycloadditions (Scheme 5).[64] Indeed, these silahelicenes containing two dibenzosiloles in a helically chiral structure were synthesized by 1) an enantioselective Ir-catalyzed intermolecular [2+2+2] cycloaddition of a tetrayne (**22a-c)** with a diyne (**23**) yielding enantioenriched axially chiral system **24a-d** with up to 94% *ee's* when using the $[IrCl(cod)]_2$/(*S*,*S*)-EtFerroTANE catalytic system (see list of catalysts), followed by 2) a stereospecific Ni-mediated intramolecular [2+2+2] cycloaddition yielding (*M*)-**25a-d** with 90-99% *ee's* when using the $[Ni(cod)_2]$/2PPh_3 system. These sila[7]helicenes **25a-d** displayed blue fluorescence and high specific rotations (see Table 3). Note however that the absolute configurations are not consistent with the classical one; indeed while the (*M*) stereochemistry was obtained for **25a** by X-ray crystallography and specified as (*M*) in the synthetic scheme, the specific rotations were found to be positive. Furthermore, sila[7]helicenes **25a-d** display blue fluorescence (quantum yields of 0.029-0.084, see Table 3).

Scheme 5. Consecutive asymmetric inter- and intramolecular [2+2+2] cycloadditions yielding enantioenriched (*M*)-**25a-d**.[64]

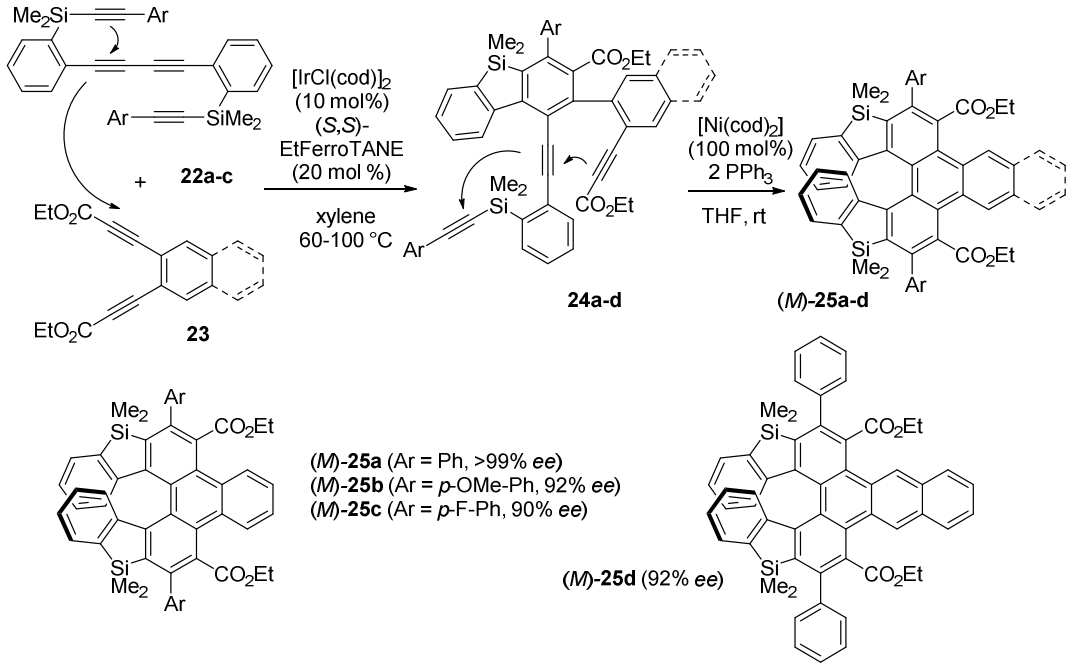

In 2015, Tanaka applied enantioselective double [2+2+2] cycloaddition (Scheme 6, *vide infra* for phospha- and oxahelicenes) to prepare enantioenriched 1,1'-bis-triphenylene-based sila[7]helicenes (*P*)-**28** with 91% *ee* (analyzed using Chiralpak AD-H, *n*-hexane/*i*-PrOH) when using the $[Rh(cod)_2]BF_4$/(*S*)-Segphos catalytic system (see list of catalysts).[65,66] Compared to sila[7]helicene **32** (*vide infra*), **28** displayed red-shifted absorption and fluorescence responses explained by the presence of fused 1,1'-bistriphenylenes resulting in more extended π-conjugation. Probably for the same reason, enantiopure **28** show high g_{lum} values, *i.e.* 1.6×10^{-2}, which is uncommonly high for an organic helicene. These values appear larger than that for the 3,3-biphenanthrene-based sila[7]helicene **32** (g_{lum} = -0.0035 at 470 nm, Table 3) but smaller than that for the 1,1-bitriphenylene based carbo[7]helicene (g_{lum} = -0.030 at 428 nm).[67] On the contrary, the optical rotation magnitude is of lower intensity compared to **32**.

Scheme 6. Enantioselective synthesis of 1,1'-bistriphenylene-based sila[7]helicenes (*P*)-**28** by Rh^I-catalyzed [2+2+2] cycloadditions.[65]

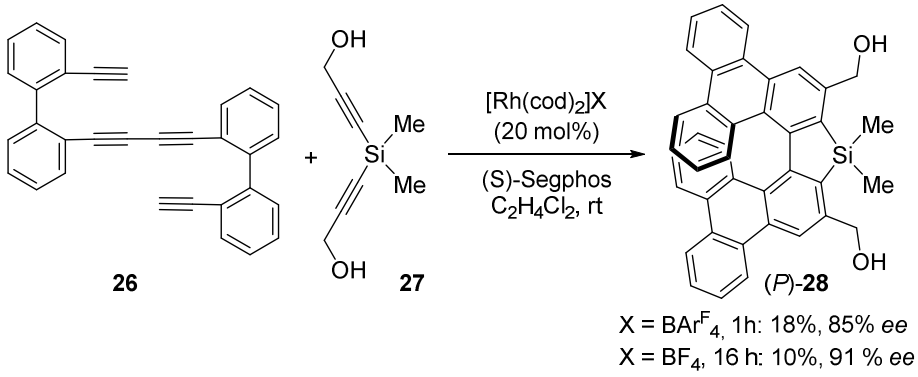

3.1.2. Alkyne-arene cycloisomerization

In 2013, Nozaki and coworkers reported a facile synthetic route to sila[7]helicene **32**, with a silole as the central cycle.[68] Bis-brominated dibenzosilole **30** was readily obtained from 2,2',6,6'-tetrabromobiphenyl **29** (Scheme 7). Introduction of two ethynylphenyl units through a Negishi coupling/deprotection sequence yielded 1,9-bis-(2-ethynylphenyl)dibenzosilole **31**, which was finally cyclized into racemic **32** using [$PtCl_2$]. Enantiopure (*P*)- and (*M*)-**32** were then obtained by HPLC separation over a chiral stationary phase (see Table 3) and the absolute stereochemistry was ascertained by X-ray crystallography of the (*P*) enantiomer. Thermal racemization was studied experimentally and no racemization was found at 220 °C in *o*-dichlorobenzene.

Scheme 7. Synthetic scheme of racemic sila[7]helicene (*rac*)-**32**.[68]

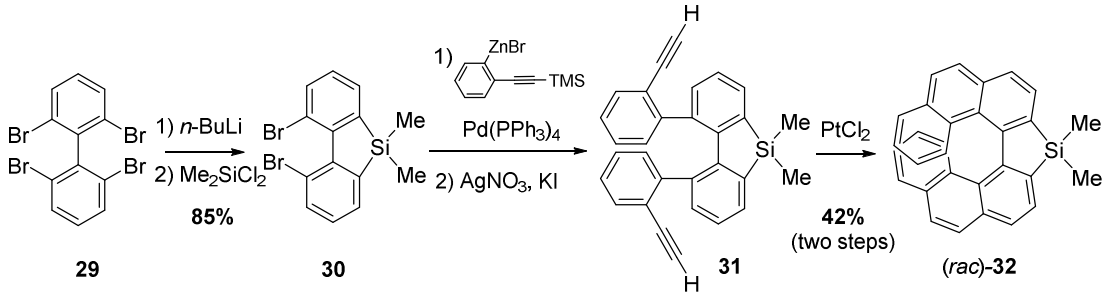

The UV-vis absorption spectrum of (*rac*)-**32** is depicted in Figure 7 and shows longest absorption at 412 nm, that is much longer than pristine phenanthrene (293 nm) and dibenzosilole (286 nm), due to extended delocalization of the π-electrons over the molecule, as further evidenced in the HOMO and the LUMO (see Figure 7). The absorption edge of (*rac*)-**32** at 431 nm is similar to that of λ^5-phospha[7]helicene (432 nm, *vide infra*) and red-shifted compared to the related aza- and oxa-[7]helicenes (425 nm for aza[7]helicene and 409 nm for oxa[7]helicene, *vide infra*). Upon excitation at 320 nm, compound (*rac*)-**32** exhibits a strong blue fluorescence with λ_{max} at 450 nm and good quantum yields in solution and in the solid state (see Table 3). Electrochemical properties were also studied by differential pulse voltammetry which displayed two oxidation waves at 1.15 and 1.34 V (*vs.* Fc/Fc^+), attributed to the oxidation of the two phenanthrene parts. Enantiopure sila[7]helicene (*P*)-**32** displayed specific rotation of +2980 (Table 3), which is larger than the related oxa- and aza[7]helicenes, but smaller than λ^5-phospha[7]helicenes (*vide infra*). this is in agreement with the general trend giving higher helicity for Si,P containing helicenes, compared to N,O ones (see Table 1). The ECD spectrum of (*P*)-**32** exhibits typical ECD for organic helicenes, *i.e.* mainly a large negative around 250 nm and a large positive one at 340 nm and resembles the one of λ^5-phospha[7]helicenes (*vide infra*). According to TD-DFT calculations results (M06/6-31G(d) level of theory), the intense signal around 340 nm can be assigned to a mixed π-π* transition.

Figure 7 shows the mirror-image CPL spectra of enantiopure sila[7]helicene (*P*)- and (*M*)-**32**, with positive and negative sign, respectively; dissymmetry factors of 3.5×10^{-3} at 470 nm were measured, *i.e.* of similar magnitude as λ^5-phospha[7]helicene, oxa[7]helicene, and aza[7]helicene.[69,70] The authors

conclude that the g_{lum} derives mainly from the helical biphenanthryl moiety while the heterole moiety plays essential roles in the luminescent properties.

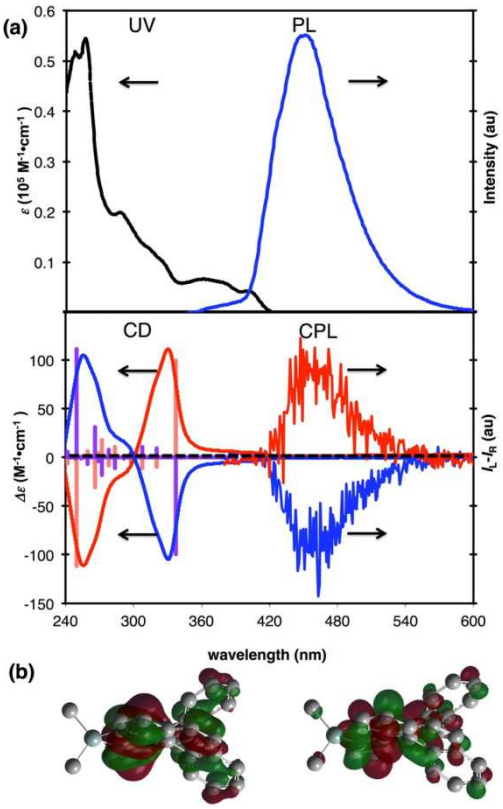

Figure 7. (a) UV-vis/fluorescence spectra and ECD/CPL spectra of sila[7]helicene **32** in CH_2Cl_2. Blue lines in ECD and CPL spectra: (*M*)-isomer. Red lines: (*P*)-isomer. The blue and red bars show the calculated CD spectra. (b) HOMO (left) and LUMO (right) orbitals of (*P*)-**32**. Reproduced from ref. [68]. Copyright 2013, American Chemical Society.

3.1.3. Dehydrogenative silylation

In 2016, Murai, Takai, *et al.*[20] reported the synthesis of enantioenriched sila[6]helicene (*M*)-**34** *via* a Rh^I-catalyzed dehydrogenative silylation of a C-H bond, a convenient way for incorporating silicon atoms into π-conjugated backbones (Scheme 8). They first prepared **34** in its racemic form starting from (*rac*)-**33** and found $[RhCl(cod)]_2$/(*R*)-(*S*)-BPPFA in 1,4-dioxane as the best catalytic system. They could then achieve a partial axial to helical transfer of chirality when starting from enantiopure (*R*)-**33** (separated by HPLC over a Daicel CHIRALPAK IB column, hexane as the eluent) yielding (*M*)-**34** with up to 78% *ee*. The chiroptical properties of (*M*)-**34** were measured on an enantiopure sample obtained by chiral HPLC separation (similar conditions as for **33**) and a $[\alpha]_D^{25}$ of -1625 in $CHCl_3$ was obtained, along with an experimental racemization barrier of 28.8 kcal mol^{-1} which is 7 kcal mol^{-1} lower than for carbo[6]helicene (36 kcal mol^{-1})[71] but high enough for configurational stability. As former silahelicenes, **34** displayed a blue fluorescence (at 420 nm upon excitation at 290 nm) with moderate quantum yield (0.16 in CH_2Cl_2) and some conjugation between σ and π bonds was also found in the calculated LUMO.

Scheme 8. Stereospecific synthesis of sila[6]helicene (*M*)-**34** from biaryl (*R*)-**33**.[20]

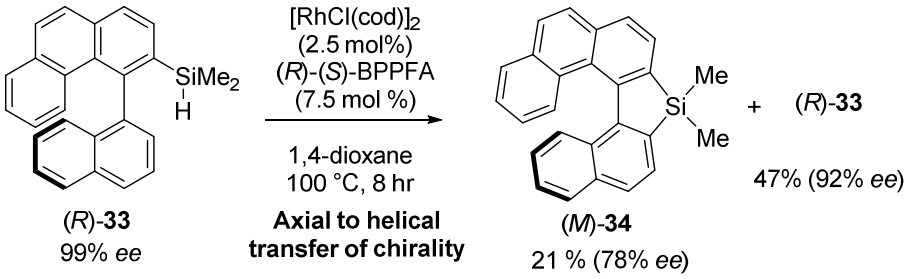

Table 3. Specific rotation values and photophysical data of enantioenriched silahelicenes.

Compound	Method of obtention	$[\alpha]_D$ [a]	Enantiopurity	Conditions[b] (solvent/Conc.[c])	λ_{Abs} [d] (nm)	λ_{Em} (nm)	Φ (%/solvent)	g_{lum}	Ref
25a[e]	Enantioselective catalysis	1063	>99% *ee*[f]	$CHCl_3$/0.45	296	464	3		64
25b[e]	Enantioselective catalysis	709	92% *ee*[g]	$CHCl_3$/0.705	293	466	3.3		64
25c[e]	Enantioselective catalysis	1063	90% *ee*[h]	$CHCl_3$/1.025	295	465	2.9		64
25d[e]	Enantioselective catalysis	561	92% *ee*[f]	$CHCl_3$/0.77	320	457	8.4		64
(*P*)-**28**	Enantioselective catalysis	+1254	91% *ee*[i]	$CHCl_3$/0.088	390	482	15/$CHCl_3$	$+1.6 \times 10^{-2}$	65
(*P*)-**32**	Chiral HPLC	+2980	>99% *ee*[j]	$CHCl_3$/0.1	See Fig. 7	450	23/CH_2Cl_2 26/solid	-3.5×10^{-3}	68
(*M*)-**34**	Axial to helical chirality transfer		78% *ee*[k]		362	420	16/CH_2Cl_2		20
	Chiral HPLC	-1625	>99% *ee*[k]	$CHCl_3$/0.09					

[a] In $deg \cdot mL \cdot g^{-1} \cdot dm^{-1}$. [b] Temperature between 20-25 °C. [c] In g/100 mL otherwise precised. [d] Longer-wavelength absorption band. [e] Some inconstancy was found between the sign of the specific rotation and the stereochemitry reported in ref [64]. [f] Chiralpak IA, *n*-hexane/CH_2Cl_2. [g] Chiralpak IA (double), *n*-hexane/*i*-PrOH. [h] Chiralpak IA (double), *n*-hexane/CH_2Cl_2. [i] Chiralpak AD-H, *n*-hexane/*i*-PrOH. [j] Chiralpak IF, *n*-hexane/CH_2Cl_2. [k] CHIRALPAK IB, hexane.

3.2. Helicenes grafted with silicon

In helicenes chemistry, silylated substituents mainly serve as protecting groups in thiahelicenes, either during multistep synthesis or in order to protect redox active site from oxidation and subsequent polymerization side reactions.[72] In addition, silane- and siloxane-substituted thiahelicenes have been shown to display more intense and bathochromically shifted ECD spectra as compared to non-substituted ones, together with high specific rotations.[73] Another interest in using silylated substituents is to modify the solid state properties by changing the packing.[74] Chiral menthyl-siloxane groups have been used by Rajca and coworkers to separate thiahelicenes through silica gel column chromatography of diastereomers.[73] Finally, silicon atom may serve as a tetrahedral bridge to covalently assemble several helicenes within multihelicenic systems yielding spiro compounds.[75] For a review on Rajca's thiahelicenes see: [38].

4. Helicenes substituted with nitrogen

Nitrogen-containing helicenes correspond to the widest class of enantioenriched helicenic structures. There are many ways of introducing nitrogen atoms into helicenic structures. Indeed, diverse heterocycles (pyridyl, pyrrole, pyrazine, imidazole, thiadiazole) or triarylamines can be incorporated within a helical scaffold. Otherwise, the N atom can be part of a classical organic substituent (CN, NH_2, etc…) or a N-heteroaromatic acting as a grafted functionality onto the helical scaffold. Through both methods, monohelicenic or multihelicenic scaffolds can be obtained. Regarding properties, the nitrogen and its lone pair strongly modify the characteristics of an aromatic ring. The N-electronegativity changes the inherent properties of the whole ring such as its electron-richness or electron-poorness, its redox potentials, its aromaticity, its reactivity towards electrophiles and nucleophiles. The N-lone pair in pyridyl units is not involved in the π-conjugation and is therefore available for reactivity with other systems (basicity, oxidation, coordination, …), while for example in pyrroles the N-lone pair is engaged in ring aromaticity. As will be illustrated below, all these different features directly affect the photophysical and chiroptical properties of the helicene, together with other properties of azahelicenes (such as conduction, complexation, or catalysis).

4.1. N-incorporating helicenes

The first helical N-heteroaromatics to be known were prepared in 1903 when Meisenheimer and Witte prepared pentahelicenic molecules **1** and **2** corresponding respectively to 7*H*-dibenzo[*c*,*g*]carbazole and benzo[*f*]naphtho[2,1-*c*]cinnoline.[10] These derivatives contain five *ortho*-fused aromatic rings; however, to our knowledge their enantioenriched forms have not been prepared. In the next paragraphs, we describe the main synthetic strategies to prepare aza[n]helicenes, especially those which have led to enantioenriched derivatives.[76,77]

4.1.1. Azahelicenes with fused pyridine cycles (pyridohelicenes)

Pyridohelicenes having N-atom placed at different positions of the helicene backbone have been synthesized using different synthetic strategies. We depict below the different synthetic pathways which have led to enantioenriched systems, and describe their resulting properties.

4.1.1.1. Synthesis, chiroptical and physicochemical properties

4.1.1.1.1. Oxidative photocyclization

The oxidative photocyclization is among the most common methods to prepare aza[n]helicenes. Aza[5]helicenes are good models for illustrating the many parameters that influence the synthesis in terms of choice of precursors, regioselectivity, yields, side reactions, and configurational stability. In 2005, Caronna *et al.* used the classical oxidative photocyclization of stilbene derivative using a visible light, to obtain aza or diaza[5]helicenes.[78] First, a photochemical process proceeds with a *trans* to *cis* isomerization process followed by a conrotatory electrocyclization to generate a primary dihydroaromatic product with *trans* configuration. Then oxidative conditions yielded fully aromatized system thanks to

open air (see Scheme 9a).[79,80] A diversity of stilbenic systems were prepared using a Wittig reaction between the corresponding aldehydes and phosphonium salts. After photocyclization, aza[5]helicenes (Scheme 9b) or diaza[5]helicenes (Scheme 9c) where nitrogens are placed at positions 4,5,6 and 4-6/9-11, respectively, were prepared with high yields and high regioselectivities. The photocyclizations were performed in EtOAc and with lamps irradiating in the visible range during 24-36 hours. Some monoaza[5]helicenes could not be obtained using this method. Indeed, the photochemical cyclization leading to 7-aza[5]helicene **35a**^{7} was unsuccessful (Scheme 9e), whereas the attempt to obtain 2-aza[5]helicene **35a**^{2} gave the 7-azabenzo[*ghi*]perylene **37** as the only product (Scheme 9d). In a following article, the series was completed and better yields were obtained using improved synthetic pathways.[81] For example, regioselective issues were solved by starting from other types of stilbenic derivatives, as depicted in Scheme 10. The whole family of bis-aza[5]helicenes was completed but only in their racemic forms.[82]

Aza[5]helicenes are good models for studying the racemization process of pentahelicenic structures. In 2005, Abbate and coworkers studied the X-ray structures and the chiroptical properties of monoaza[5]helicenes **35a**^{4}, **35a**^{5}, and **35a**^{6} (Scheme 9).[83] Their X-ray structures display the typical helical topology but with an open geometry enabling facile racemization. 5-Aza[5]helicene **35a**^{5} crystallized as a conglomerate of enantiomorphic crystals in the non-centrosymmetric space group *P*21*nb*. 4-Aza[5]helicene **35a**^{4} was found to be isomorphic with the parent [5]-helicene of *C*2/*c*, with some additional orientational disorder[84] while 6-aza[5]helicene **35a**^{6} crystallized in the *P*21/*n* space group. Helicities (dihedral angles between the terminal rings) of 51.13, 45.70 and 45.15° were found for these three azapentahelicenic models. Enantiomeric separations were achieved by preparative HPLC separation using columns packed with a Chiralcel OD-type stationary phase. Under conditions using *n*-heptane/ethanol (90:10) as eluent and at 22 °C, some racemization was observed during the separation and enantioenriched samples with resulting *ee*'s smaller than 87%. Kinetics of racemization was performed on each isomer by following their ECD spectra with time (see the example of **35a**^{5} in Figure 8). The evolution was typical of a first-order process and half-life times $t_{1/2}$ of 47 min for **35a**^{4}, 12 min for **35a**^{5}, and 35 min for **35a**^{6} were obtained at 23 °C or room temperature. Therefore, the compounds had to be stored at -20 °C. The half-life times were completed in 2007 for the all series of aza[5]helicenes.[85]

Scheme 9. Synthesis of mono- and bis-aza-[5]helicenes investigated by oxidative photocyclization, except **35b**^{2} which was prepared by an acid cyclization process.[78,86,87]

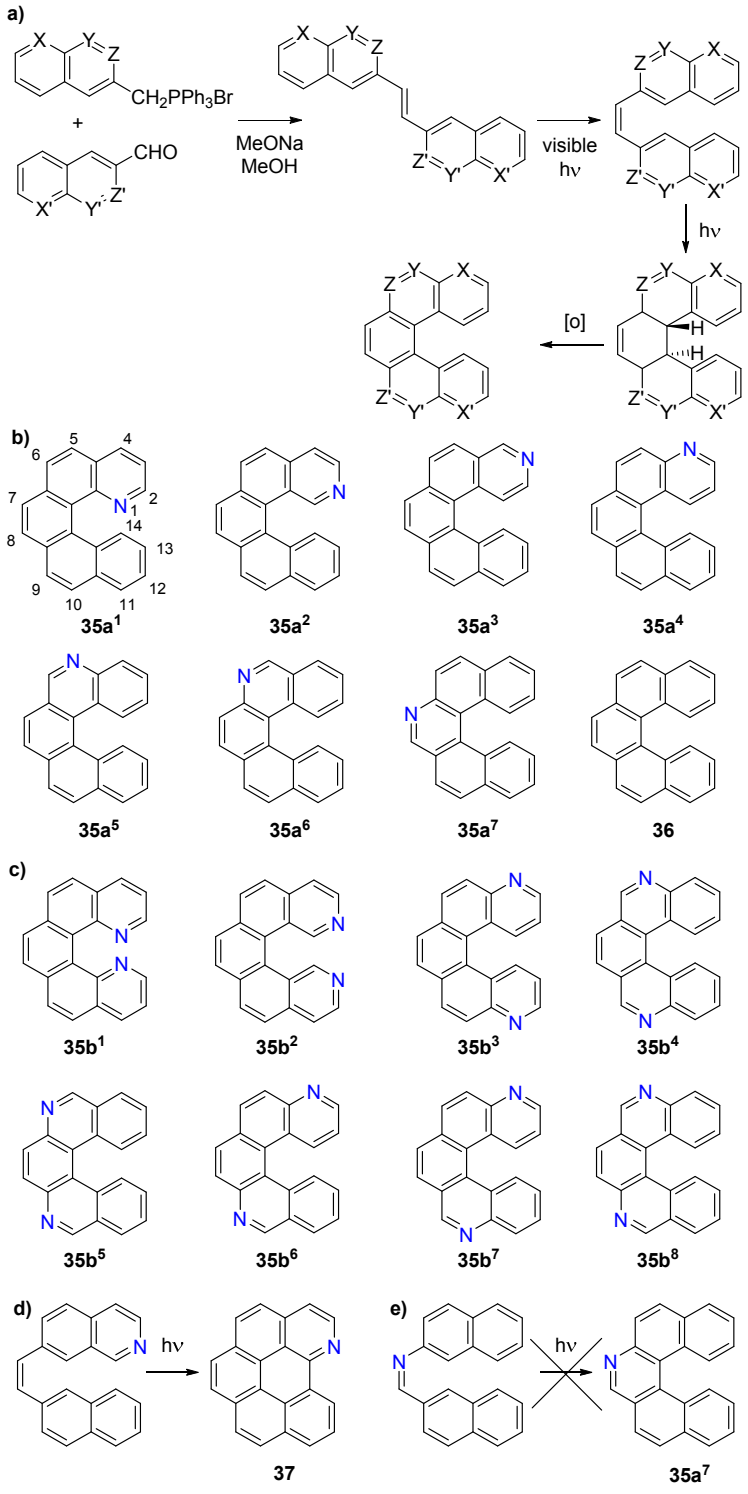

Scheme 10. Regioselective issues of photocyclization reactions leading to **35a^1** and/or **35a^3**.[81]

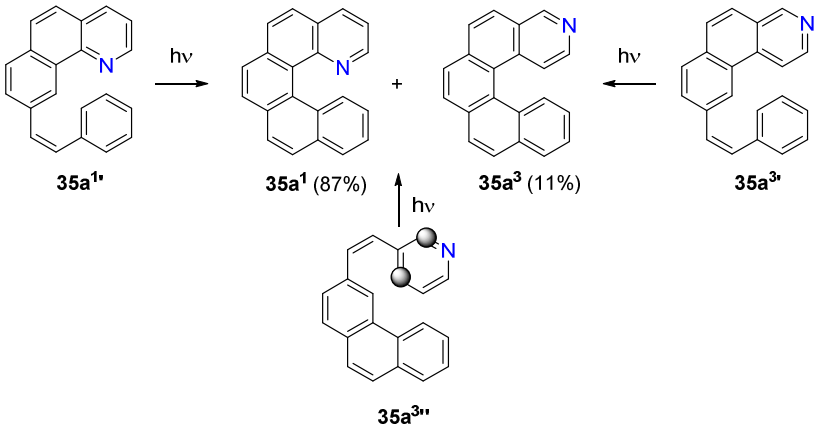

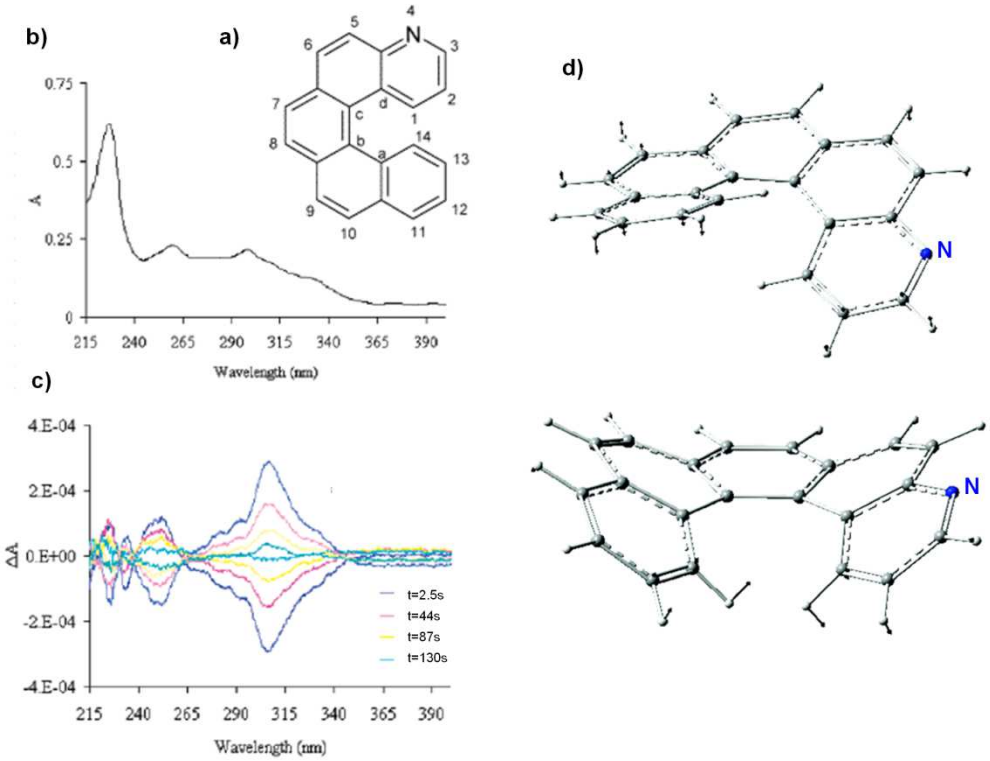

Figure 8. a) Numbering, b) UV-vis spectrum of 4-aza[5]helicene **35a^4** (methanol) and c) its racemization process observed by ECD spectroscopy, recorded every 2.5 min, with the first taken just after dissolving the solid sample at -4 °C in methanol; d) calculated stable conformation and transition state. Adapted from ref. [83]. Copyright 2004, American Chemical Society.

Thanks to their rapid racemization, the enantiomerization barriers[88] of **35a$^{1\text{-}7}$** and **36** (Scheme 9) could also be studied by enantioselective dynamic HPLC (DHPLC) in normal phase mode using *n*-hexane/2-propanol as the eluent and a diversity of coated and immobilized derivatized polysaccharide stationary phases at temperatures below 10 °C. Enantiomerization barriers $\Delta G^{\neq}$ were determined using the unified equation of dynamic chromatography[89] and an Eyring-plot analysis was performed to obtain activation

parameters $\Delta H^{\neq}$ and $\Delta S^{\neq}$ from the temperature-dependent kinetic measurements.[90] DFT calculations at the B3LYP/6-311G(d,p) level of theory performed in the gas phase were also performed and are reported in Table 4, they show reasonable agreement with the experimental ones except for **35a^1** which shows 7 kcal mol^{-1} underestimation. The authors interpret this discrepancy as the strong influence of the eluent, especially the propanol which establishes a N…HO hydrogen bond with the 1-N atom (see below the strong basicity of such compounds). Note also that the half-life times measured by Caronna *et al.* nicely follow the tendency of $\Delta G^{\neq}$ measured by (DHPLC). Overall, the measurements confirm the lower activation barriers of aza[5]helicenes as compared to carbo[5]helicene, with the lowest barrier obtained for **35a^1**. This has been also observed by Stary and Stara in 2014.[91]

Table 4. Activation parameters of the enantiomerization of aza[5]helicenes **35a$^{1\text{-}7}$**, carbo[5]helicene **36**, and carbo[6]helicene **3** obtained by DHPLC[90] together with calculated enantiomerization barriers. Half-life times of racemization of **35a^1, 35a$^{3\text{-}6}$** obtained by ECD spectroscopy.[83,85] Racemization barriers of bis-aza[6]helicenes **41a^{1,2}** [92] and carbo[6]helicenes **3**.[71]

Compd.	Exp. $\Delta G^{\neq}_{298\,K}$ (kJ mol^{-1} / kcal mol^{-1})	$\Delta H^{\neq}$ [kJ·mol^{-1}]	$\Delta S^{\neq}_{298\,K}$ [J·(mol K)$^{-1}$]	$t_{1/2}$ (min)[b]	Theor. $\Delta G^{\neq}_{298\,K}$[a] (kJ mol^{-1})
35a^1	90.7 / 21.7	52.9±0.8	−127±5	49.5	60.2
35a^2	90.9 / 21.75	63.5±0.8	−92±3		94.0
35a^3	91.2 / 21.8	61.5±1.5	−100±5	44	95.2
35a^4	92.3 / 22	44.9±1.4	−159±23	47	94.7
35a^5	89.5 / 21.4	61.5±0.8	−94±3	12	91.2
35a^6	91.2 / 21.8	41.7±0.5	−166±10	35	94.2
35a^7	87.6 / 20.95	45.6±0.9	−141±8	6.6	88.5
36	96.3 / 23	60.8±0.6	−119±3		98.9
41a^1	134.7/ 32.25[c]				
41a^2	147.7 / 35.35[c]				
3	154.6 / 37[d]			187[d]	

[a] DFT calculations at the B3LYP/6-311G(d,p) level of theory.[90] [b] Half-life times obtained experimentally from ECD spectra evolution (see the case of **35a^4** on Figure 8) and taken from ref. [85] at rt or at 23 °C. [c] Racemization barriers measured at 140 °C in 1-decanol.[92] [d] Racemization barriers measured at 461 K in naphthalene.[71]

Dehaen *et al.* prepared racemic chloro-substituted diaza[5]helicene derivative **39** in 57% yield by oxidative photocyclization of stilbenic system **38** containing two 2-chloroquinoline units, in toluene for 10 hours using iodine as the oxidant, and then transformed **39** to (1:1) diastereomeric mixture **40a^{1,2}** in 72% yield by a Buchwald−Hartwig coupling with enantiopure (*S*)-α-methylbenzylamine (Scheme 11). While trying to separate the diastereomers (*P*,*S*,*S*)-**40a^1** and (*M*,*S*,*S*)-**40a^2** by column chromatography at 10 °C, they found that these compounds were not configurationally stable, with half-life times $t_{1/2}$ of 26 min at 25 °C ($\Delta G^{\#}$ = 22.4 kcal mol^{-1} for racemization) and 4.2 h at 10 °C.[93] These results confirm that helicenes incorporating 1 or 2 N atoms racemize more readily than the corresponding carbo[5]helicenes.

Scheme 11. Synthesis of diastereomeric aza[5]helicene derivatives[93] separated by column chromatography.

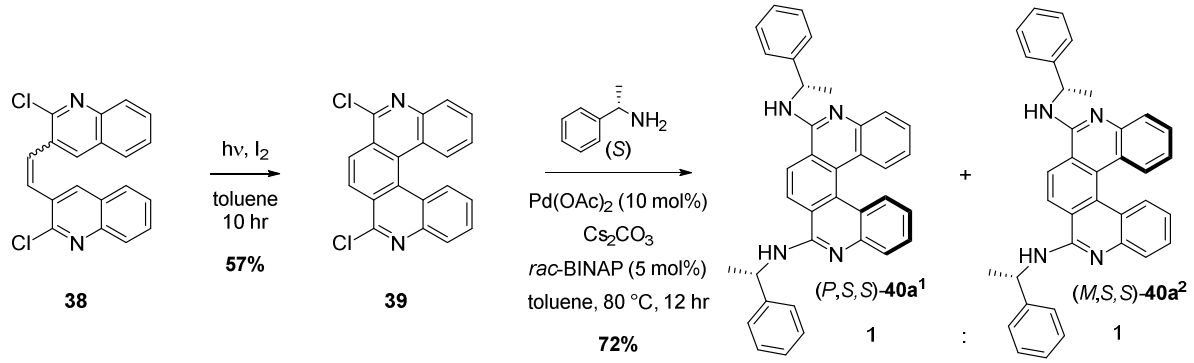

Monoaza[6]helicenes **41a**$^{1\text{-}5}$ and diaza[6]helicenes **41b**$^{1\text{-}5}$ depicted in Figure 9 were also prepared by the oxidative photocyclization method. Ben Hassine *et al*. expanded the original synthesis published by Caronna for the unsubstituted 3-aza[6]helicene **41a**^{3} [94] and for methoxy-substituted **41a**^{3,OMe} [95] as depicted on Scheme 12.[95] The synthesis first involved a Mizoroki-Heck coupling reaction between bromobenzophenanthrenes **42a,b** and 3-vinyl-pyridine **43** yielding *trans* olefin **44a,b**, then an oxidative photocyclization step of **44b** yielded **41a**^{3,OMe}. Note that the final photocyclization was not fully regioselective since 8% of 14-methoxy-1-aza[6]helicene **41a**^{1,OMe} isomer was also isolated by column chromatography. HPLC separation of **41a**^{3,OMe} over a Chiralcel OD stationary phase (eluent *n*-hexane/*i*-PrOH) afforded pure (*P*)-(+) and (*M*)-(-)-**41a**^{3,OMe} enantiomers which were characterized by ECD spectroscopy and specific rotations (Table 6). The ECD spectrum of the dextrorotatory enantiomer (*P*)-(+)- **41a**^{3,OMe} exhibited a positive maximum at 333 nm and a negative maximum at 253 nm showing no significant change as compared to unsubstituted hexahelicene.[96] Finally, a demethylation using classical conditions yielded (*P*)-(+) and (*M*)-(-)- **41a**^{3,OH} derivatives. The same strategy was also applied to olefin **44a** to prepare (*rac*)-**41a**^{3} (50% yield) accompanied with (*rac*)-**41a**^{1} (7%).[94] In 2013, Mori and Inoue reported the chiral HPLC separations of (*rac*)-**41a**^{1} and (*rac*)-**41a**^{2} and obtained pure enantiomers with >99 *ee*'s (see Table 6).[97] In addition, 4-aza[6]helicene **41a**^{4} [98,99] and 5-aza[6]helicenes **41a**^{5} [26,100] were also prepared in enantiopure forms by this method, that is by the photocyclization method followed by chiral HPLC resolution. Their chiroptical properties (optical rotation, ECD and VCD and CPL) were studied and they were used as ligands for coordination to platinum (see paragraph 4.1.1.3.).

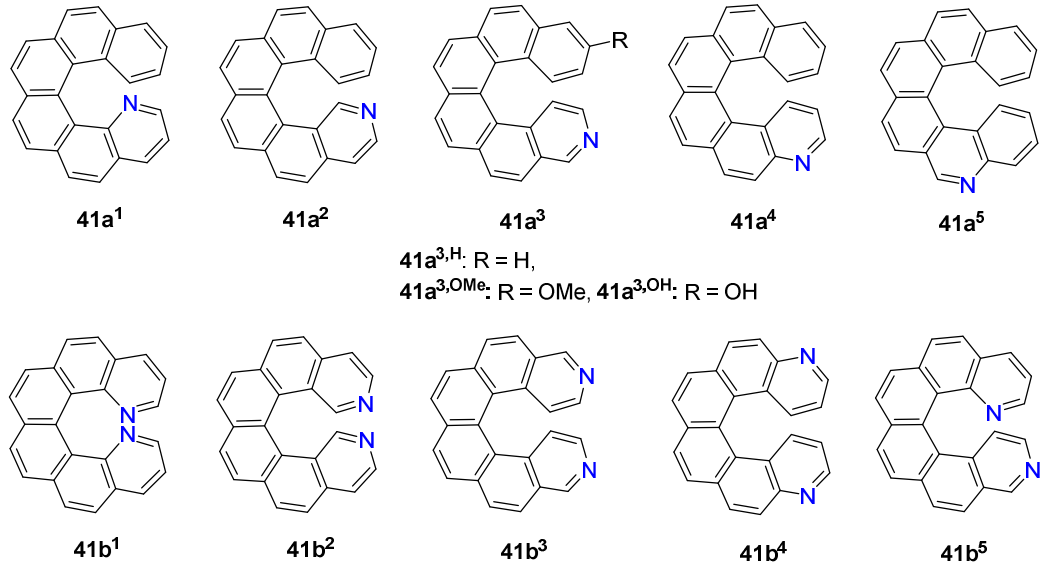

Figure 9. Mono- and bis-aza-[6]helicenes prepared by oxidative photocyclization.

Scheme 12. Synthesis of 3-aza[6]helicenes derived with H or OMe and OH groups.[95]

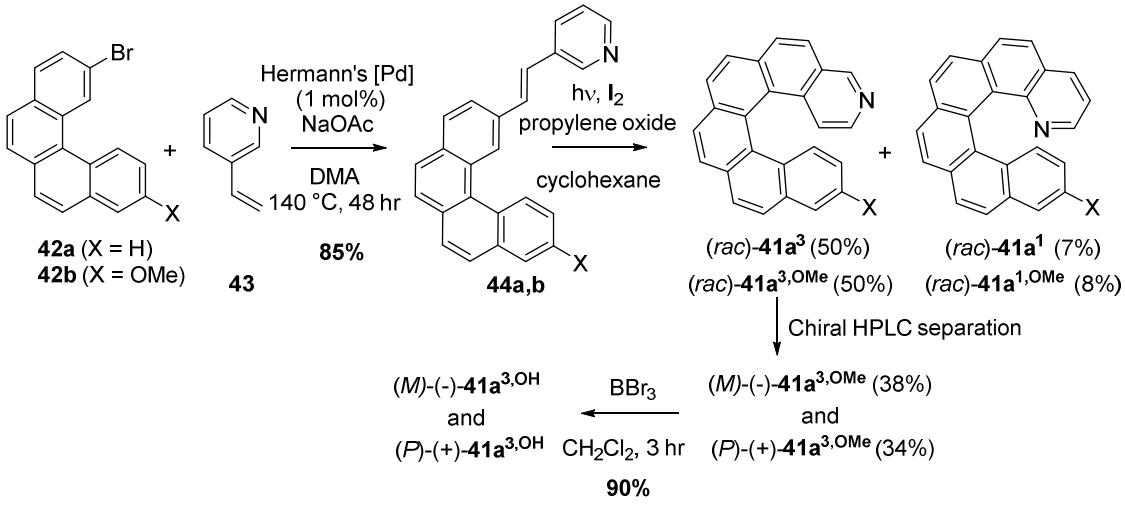

Racemization barriers of **41a**^{1,2} were also studied. Samples were heated at high temperature in 1-decanol and their racemization process was followed by HPLC over a Chiralcel OD-H column (see Table 6). In the case of carbo[6]helicene **3**, racemization process is characterized by a free energy barrier of 37 kcal mol^{-1} at 188 °C (461 K) in naphthalene.[71] These data show that 2-aza[6]helicene **41a**^{2} behaves similarly to parent [6]helicene **3**, while 1-aza[6]helicene **41a**^{1} behaves differently. The significantly lower energy barrier to racemization of **41a**^{1} reflects the smaller steric repulsion between the lone pair of electrons on N(1) and the H-C(16) proton in **41a**^{1} than that between the H-C(1) and H-C(16) protons in **41a**^{2}, which is expected to occur on formation of a C_s transition state.[44]

The proton affinities (PAs) of 1- and 2-aza[6]helicene **41a**^{1} and **41a**^{2} respectively, were determined using mass spectrometry and DFT calculations.[101] PAs around 1000 kJ mol^{-1} were found,[102,103,104,] showing that these azahelicenes are chiral superbases with affinities similar to 'proton sponge' 1,8-bis(dimethylamino)-naphthalene **35'** (Table 5). The combination of helical topology and high PAs are

good opportunities for enantioselective reactions of these helical nitrogen bases as evidenced by Takenaka's achievements (see paragraph 4.1.1.4.). In 1989, Staab and coworkers had already described **35b[1]** as a proton sponge similar to **35'** with an experimental pKA value of 10.3.[105] According to Staab, the high basicity of these proton sponges is ascribed to the destabilization of the free bases due to repulsive lone-pair interaction of two closely neighboring nitrogen atoms (despite the helical topology of the molecule) and to the release of this strain on monoprotonation leading to a strong N...H...N hydrogen bond.

Table 5. Physicochemical properties of azahelicene bases **41a[1]**, **41a[2]** and **35b[1]** taken from ref. [92].

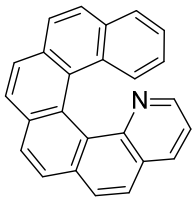

41a[1]

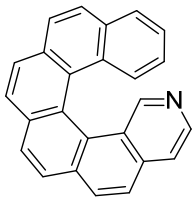

41a[2]

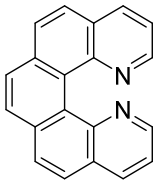

35b[1]

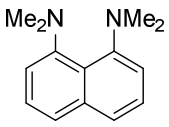

35'

Base B	pKa of BH^+ (exptl) [a]	PA of B (calcd) [kJ mol^{-1}] [b]	pKa of BH^+ (calcd) [c]
41a[1]	5.16	1012	4.9
41a[2]	5.77	992	6.2
35b[1]	8.75	1064	11.6

[a] Measured by capillary electrophoresis in methanol (25 mm ion strength of the background electrolyte used and 25 °C). [b] Gas-phase proton affinity (ΔG_{298K}) of B determined by DFT (PBE) calculations. [c] Related to the Gibbs energy of deprotonation (ΔG_{deprot}) of BH^+ in ethanol, as calculated by means of the COSMO method.

In 2013,[46,97] Mori, Inoue *et al.* scrutinously examined the ECD signature of a series of azahelicenes and their protonated systems and described the bands using the Platt classification.[106] They found that these ECD bands are dependent on geometric and electronic features of the considered helicene. For instance, carbo[6]helicene **3** exhibits strong bisignate Cotton effects signals in the ^1B_a and ^1B_b transition regions with molar ECD intensities ($\Delta\varepsilon$) of -267 $M^{-1}\cdot cm^{-1}$ at 246 nm and +259 $M^{-1}\cdot cm^{-1}$ at 324 nm together with a very weak $\Delta\varepsilon$ of -0.3 $M^{-1}\cdot cm^{-1}$ observed for the ^1L_b band at 410 nm.[107]

Mono and diaza-[6]helicenes and their protonated monoazonia-, and diazonia[6]helicenes appeared as an interesting series of neutral, monocationic, and dicationic helicenes for examining the electronic versus structural effects of protonation on the chiroptical properties of helicene. Indeed, the attractive cation-π interaction in monoazonia[6]helicenes and the repulsive cation–cation interactions in diazonia[6]helicenes were expected to cause the opposite structural changes in addition to the even stronger electronic effects. The authors conducted theoretical calculations and showed that the dispersion-corrected DFT method better described the geometry of the neutral and charged helicenes. Neutral aza[6]helicenes were very similar in structure to carbo[6]helicene **3**. In 1-aza- and 1,1′-diaza[6]helicenes (**41a[1]** and **41b[1]** respectively), the terminal ring(s) were slightly deformed, probably due to the smaller size of nitrogen, compared with the CH group. The overall change in the helical structure was very slight, compared with

[6]helicenes bearing substituents. Monocationic azonia[6]helicenes revealed essentially the same structures as the corresponding aza[6]helicenes. The cation-π interaction was not strong enough to alter the helical backbone geometry. In contrast, the structures of diazonia[6]helicenes deviated from those of the corresponding neutral helicenes, most probably due to the repulsive cation–cation interaction. Then the effect of protonation on the ECD spectra was studied (Figure 10A). The bisignate Cotton effects at the $^1B_a/^1B_b$ bands (bands B/D) of neutral aza[6]helicenes (**41a**[1]) appeared in the same wavelength region, but with reduced intensities, in monoazonia[6]helicenes (**41a1.**H^+). The lowest-energy ^1L_b band (band A) became more apparent and strongly red-shifted, while the intensity was enhanced significantly (1–2 orders of magnitude) with the *g* factor on the order of 10^{-3}. Regarding the diaza analogues such as **41b**[1], upon protonation, the changes in ECD pattern appeared insignificant, but the relative excitation energy and rotational strength were significantly changed. Indeed, the ^1B_b band of the positive signal was red-shifted and broadened and presumably overlapped with some additional transitions, while the signal intensity was significantly reduced. The Cotton effect at the ^1L_b band was sensitive to the electronic effect with a red-shifted wavelength but remained similar in strength (with the same sign) upon dual protonation. Due to the increased number of additional bands, the assignment of the ^1B_a band appeared difficult. These extensive ECD spectral changes caused by protonation are expected to occur upon association with other electrophiles such as Lewis acids and some metal cations and therefore can be used as a tool for evaluating the influence of association on the chiroptical properties. For example, similar behavior was indeed observed in protonation of (*M*) and (*P*)-**51** and enabled to perform acid/base triggered chiroptical switching (*vide infra*).[108]

Vibrational circular dichroism (VCD) spectra of 5-aza[6]helicene **41a**[5] were measured in $CDCl_3$ and compared to theoretically calculated spectra. Characteristic common VCD fingerprints were found: 1) Negative VCD feature at 1608 cm^{-1} for which calculations indicate that it is due to two vibrational features with the same sign (degenerate pair, see modes a and b); these are in-plane HCC bendings coupled to CC stretchings in the inner and in the outer periphery of the molecule. Particularly the b component is a normal mode that is delocalized over the entire structure. The normal modes in this region (modes c and d of Figure 10B) are also delocalized and show a helical-responsive feature (H character); using the nomenclature of modes typical of graphene, they correspond to the important Raman G feature.[13] 2) Negative VCD doublet at 1508 and 1499 cm^{-1}; this doublet was also assigned of H character; the modes underneath, modes e and f of Figure 10B, have still some resemblance to G modes and are mainly HCC bendings coupled to CC stretchings with a relative phase such that half of the molecule is moving opposite to the other. G modes are strictly correlated to D modes (radial CC stretchings, from the nomenclature used for polycyclic aromatics, like graphene), which are calculated here at 1370 cm^{-1} (mode g of Figure 10B) and are observed as the most intense peak of the Raman spectrum (see ref. [26]). In conclusion, all modes commented above involve the whole conjugated system and, irrespective of substituent and helix length, are helical sensitive, H. 3) Positive VCD feature at 930 cm^{-1}; this feature has quite large rotational strength and is in correspondence of a rather intense IR band. A substituent-responsive feature (S character) was assigned to this mode, corresponding to an out of plane CH bending mode close to the nitrogen is taking place.

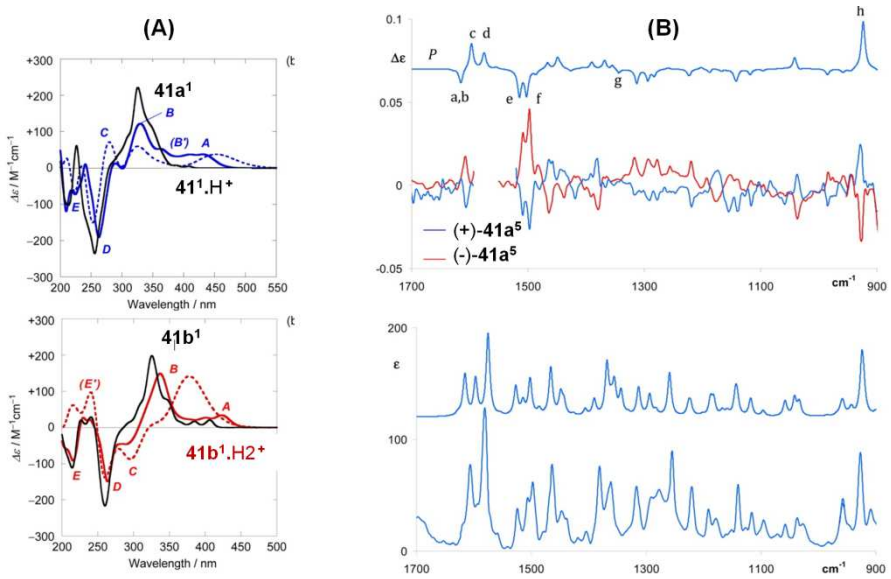

Figure 10. (A) Modification of ECD spectra of monoaza[6]helicene **41a**[1] and of bisaza[6]helicenes **41b**[1] upon protonation. Experimental ECD spectra of aza[6]helicenes (black line) and experimental (solid blue line) and theoretical (dotted blue line) ECD spectra of azonia[6]helicenes. Experimental CD spectra of diaza[6]helicenes (black line) and experimental (solid red line) and theoretical (dotted red line) CD spectra of diazonia[6]helicenes. Adapted from ref. [97]. Copyright 2013, American Chemical Society. (B) Comparison of the experimental spectra of both enantiomers of 5-aza-hexahelicene **41a**[5] with calculated VCD spectrum for the (*P*)-**41a**[5] (top two panels). Corresponding IR spectra (lower panels). Computed wavenumbers have been scaled. Reproduced from ref. [26]. Copyright 2014, American Chemical Society.

In 2007, Schmidt, Brédas and co-workers examined the intersystem crossing processes in nonplanar aromatic heterocyclic molecules and especially in aza[5]helicene and carbo[5]helicenes. Using optical spectroscopy (absorption and time-resolved luminescence measurements) and quantum chemistry studies, they demonstrated that the magnitude of spin-orbit coupling is directly correlated with the deviation from planarity.[23] They showed that the introduction of a nitrogen atom into the [5]helicene backbone results in large variations in the luminescence properties, which depends strongly on the nitrogen substitution site. Furthermore, they showed that both the intersystem crossing rates and the radiative phosphorescence decay rates are enhanced in aza[5]helicenes with respect to carbo[5]helicene. As was demonstrated with the help of monoaza[5]helicenes as model systems, introduction of a heteroatom into a nonplanar conjugated molecule can affect its Inter-System Crossing (ISC) behavior not only by introducing lower-lying n-π^* transitions (relevant for small molecules), but also by changing its deviation from planarity, an effect that is expected to dominate the former for larger compounds. For calculations of phosphorescence see recent review [109].

Abbate *et al.* reported the CPL activity of blue-fluorescent **41a**[5] enantiomers in relation to their ECD spectrum and they showed that the sign of the CPL signal was controlled by the sign of the lower energy ECD named S-type band in relation to Mori's nomenclature (Figure 11).[26,97] In 2016, Longhi and Santoro reported the vibronically resolved calculated UV-vis, ECD, emission, and CPL spectra of 5-aza[6]helicene **41a**[5]. A CPL dissymmetry factor g_{lum} of $+5.9 \times 10^{-3}$ for (*M*)-**41a**[5] was experimentally measured and used as a helically shaped chiral model to test the validity of advanced theoretical calculations of chiroptical techniques.[110] In 2018, Mori *et al.* try to see whether there was a correlation

between excitation and emission dissymmetry factors; they examined the experimental ratio g_{lum}/g_{abs} for a series of chiral organic emissive molecules among which helicenes. They found that this ratio significantly depended on the structure of the helicenic molecule and varied between 0.16 and 28.[27]

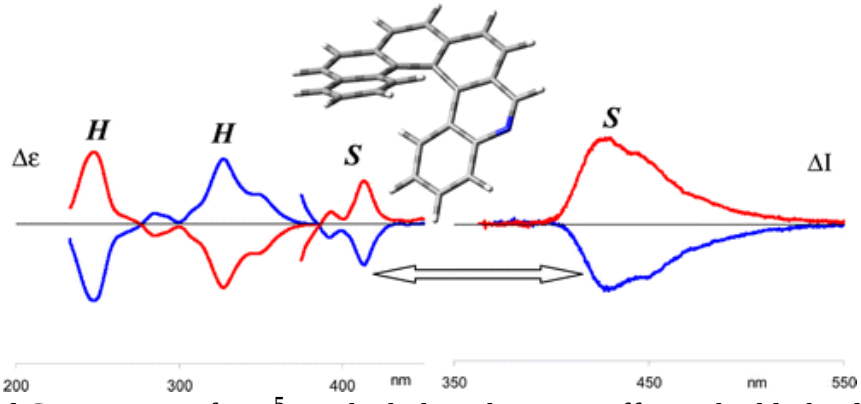

Figure 11. ECD and CPL spectra of **41a**[5] in which the substituent effect is highlighted. Reproduced from ref. [26]. Copyright 2014, American Chemical Society.

In 2016, Srebro-Hooper, Crassous, *et al.* has prepared bis-helicenic terpyridine ligand **48** (Scheme 13).[111] The synthesis of ligand **48** was accomplished by a Wittig reaction between terpyridine bis-aldehyde **45** and (benzo[c]phenanthren-3-ylmethyl)triphenyl-phosphonium bromide **46** giving **47** as a mixture of three isomers (*E,E* - major compound, *Z,Z*, and *E,Z*) followed by photo-irradiation (700 W Hg lamp) of **47** in a toluene/THF mixture at room temperature in the presence of catalytic iodine. The bis-helicene-terpyridine **48** was obtained as a statistical mixture of (*meso*)-**48** and racemic (*P,P*)- and (*M,M*)-**48**, which were separated by chiral HPLC separation (see Table 6). High specific and molar optical rotation values were obtained ((*P,P*)-**48**: $[\alpha]_D^{23}$= +2150, $[\phi]_D^{23}$= +15790 (±5%, CH_2Cl_2, 2.2 × 10^{-4} M) and found twice as high as for 4-aza[6]helicene (*P*)-**41a**[4] ($[\alpha]_D^{23}$= +2290,$[\phi]_D^{23}$= +7735 (±5%, CH_2Cl_2, *C* 1.7 g/100mL)[99] in agreement with the presence of two azahelicene moieties. Note that a similar strategy was applied by Srebro-Hooper, Crassous, *et al.* to the preparation of helicene-bipy **51** (Scheme 13 and Table 6).[108] Very few examples of helicenes bearing bi-pyridine units are known in literature (for racemic helicene-bipyridine-type ligands see ref. [112]). Katz *et al.* reported in 1999 the synthesis of enantioenriched [8]helicene derivatives fused with 4,7-diaza-1,10-phenanthroline acting as *N^N'* chelating ligand (*vide infra*, Scheme 30).[113]

Scheme 13. Synthesis of bis-helicenic terpyridine **1**. *i*) *n*-BuLi, THF, rt, 5 hr, 82-92%; *ii*) hν, cat. I_2, toluene/THF, rt, 7 hr, 45-90%.[111,108]

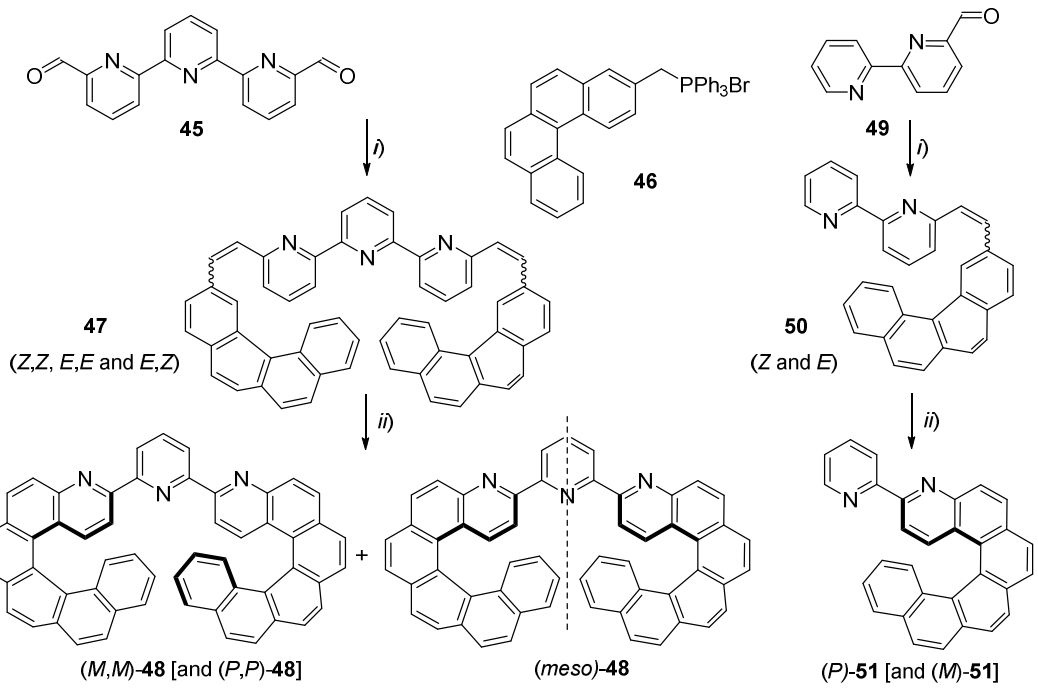

Table 6. Specific rotation values of enantioenriched aza[6]helicenes.

Compound	*Method of obtention*	$[\alpha]_D$[a]	Conditions[b] (solvent/Conc.[c])	Enantio/diastereo-purity	Ref.
(*M*)-**41a**^{3,OMe}	Chiral HPLC[d]	-1373	CH_2Cl_2/0.2	>99% *ee*[e]	95
(*M*)-**41a**^{3,OH}	From (*M*)-**N13**^{OMe}	-1559	MeOH /0.30	>99% *ee*[e]	95
(*M*)- **41a**^{1}	Chiral HPLC[e]	-3500 ± 100	ACN/0.0011	> 99% *ee*[e]	97
(*M*)-**41a**^{1}	Diastereomeric crystallization[f]	-3631	CH_2Cl_2/0.001	>99% *ee*[g]	92
(*M*)-**41a**^{2}	Chiral HPLC[g]	-3840	$CHCl_3$/0.001	> 99% *ee*[g]	92
(*M*)-**41a**^{3}	Chiral HPLC[e]	-3300 ± 100 (> 99% ee)	ACN/0.0011	> 99% *ee*[e]	97
(*M*)-**41a**^{4}	Chiral HPLC[h]	-2540 ± 5%	CH_2Cl_2/1.7	> 99% *ee*[i]	99
(*M*)-**41a**^{5}	Chiral HPLC[j]	-3241	$CHCl_3$/0.002	99% *ee*[j]	26
(*P*)-**41b**^{1}	Chiral HPLC[k]	+3600 ± 100	ACN/0.00381	> 99% *ee*[k]	46
(*P*)-**41b**^{3}	Chiral HPLC[k]	+2900 ± 100	ACN/0.00460	97% *ee*[k]	46
(*P*)-**41b**^{5}	Chiral HPLC[k]	+2600 ± 100	ACN/0.0093	97% *ee*[k]	97
(*P*,*P*)-**48**	Chiral HPLC[l]	+2150 ± 5%	CH_2Cl_2/2.2 × 10^{-4} M	>98% *ee*[l]	111
(*P*)-**51**	Chiral HPLC[m]	+2955 ± 5%	CH_2Cl_2, 6.5 × 10^{-5} M	>99% *ee*[m]	108

(*P*)-[**51**,2H$^+$][2BF$_4^-$]	From (*P*)-**51**	+1700 ± 5%	CH_2Cl_2/1.7 × 10^{-4} M	>99% *ee*	[108]
(*P*)-[**41a**^{1}.H$^+$]TFPB$^-$	From (*P*)-**41a**^{1}	+1778	$CHCl_3$/0.1		[114]
(*P*)-**70**	Chiral HPLC^n	+2666	$CHCl_3$/0.00012	> 99% *ee*^{h}	[115]
(*P*)-**71**	Chiral HPLC^n	+3595	$CHCl_3$/0.0002	> 99% *ee*^{h}	[115]
(*P*)-**72**	Chiral HPLC^n	+2255	$CHCl_3$/0.0006	> 99% *ee*^{h}	[115]
(*M*)-**105a**	From (*M*)-**71**	-2670	$CHCl_3$/0.1		[114]
(*P*)-**105b**	From (*P*)-**72**	+2274	$CHCl_3$/0.1		[114]
(*P*)-[**105b**.H$^+$]TFPB$^-$	From (*P*)-**105b**	+1803	$CHCl_3$/0.1		[114]
(*M*)-**105c**	From (*M*)-**72**	-2974	$CHCl_3$/0.1		[114]
(*M*)-[**105c**.H$^+$]TFPB$^-$	From (*M*)-**103c**	-1299	$CHCl_3$/0.1		[114]
(*P*)-**105d**	From (*P*)-**72**	+2140	$CHCl_3$/0.1		[114]
(*P*)-[**103d**.H$^+$]TFPB$^-$	From (*P*)-**103d**	+1509	$CHCl_3$/0.1		[114]
(*P*)-**105e**	From (*P*)-**72**	+1860	$CHCl_3$/0.1		[114]
(*P*)-[**105e**.H$^+$]TFPB$^-$	From (*P*)-**105e**	+1790	$CHCl_3$/0.1		[114]
(*M*)-**105f**	From (*M*)-**105a**	-4348	$CHCl_3$/0.1		[114]
(*M*)-[**105f**.H$^+$]TFPB$^-$	From (*M*)-**105f**	-1960	$CHCl_3$/0.1		[114]
(*P*)-**105g**	From (*P*)-**105b**	+3040	$CHCl_3$/0.1		[114]
(*P*)-[**105g**.H$^+$]TFPB$^-$	From (*P*)-**105g**	+1581	$CHCl_3$/0.1		[114]
(*P*)-**106**	From (*P*)-**72**	+2618	$CHCl_3$/0.1		[116]

[a] In deg·mL·g^{-1}·dm^{-1}. [b] Temperature between 20-25 °C. [c] In g/100 mL otherwise stated. [d] cellulose-tris(3,5-dimethylphenylcarbamate) column, *n*-heptane/*i*-PrOH. [e] Chiralcel OD, *n*-hexane/*i*-PrOH (95:5). [f] (+)-*O*,*O*'-dibenzoyl-d-tartaric acid. [g] Chiralcel OD-H, *n*-heptane/*i*-PrOH (3:1). [h] Chiralpak IA, CO_2/EtOH, 80:20. [i] Chiralpak IA, Hexane/*i*-PrOH/$CHCl_3$ (90:5:5). [j] Chiralpak-IA, *n*-hexane/*i*-PrOH. [k] Chiralpak IB, *n*-hexane/EtOH/CH_2Cl_2, *N*,*N*-diethylamine (90:8:2:0.1). [l] Chiralpak ID, *n*-hexane/EtOH + triethylamine 0.1% /dichloromethane (85:5:10). [m] Chiralpak IC, hexane/EtOH/$CHCl_3$ (90:5:5). [n] CHIRALCEL OD-H, 40% *i*-PrOH in hexanes. [o] Daicel Chiralpak OD-R, aqueous 0.1 M KPF_6/acetonitrile (50:50). TFPB$^-$ = B(Ar)$_4^-$, Ar =3,5-(CF$_3$)$_2$C$_6$H$_3$.

In 2000, Branda *et al.* reported the synthesis of [7]helicene-bis-pyridinones by using the classical oxidative photocyclization process.[117] For this purpose, a mixture of (*Z*,*Z*)-, (*Z*,*E*)- and (*E*,*E*)-**52** obtained by a Wittig reaction afforded, after irradiation in the presence of iodine as oxidizing agent and propylene oxide as HI scavenger, the desired [7]helicene **53a** but in only minor amounts (Scheme 14). Instead, the major product was the extended aromatic **54a**. Removal of the benzyl groups from **53a** with trifluoroacetic acid cleanly afforded pyridinone **56a** as a yellow solid. The incorporation of a bromine atom onto the central benzene ring of the [7]helicene enabled to prevent the formation of **54b** in favor of **53b** and to increase solubility. The self-assembly of these racemic [7]helicenes was characterized both in solution and in the solid state where only enantiomerically pure homochiral dimers such as (*P*,*P*)-**57c** were formed and held together by two pairs of cooperative hydrogen bonds. Related work was published by Tanaka in which intermolecular hydrogen bonding between the nitrogen atom of one helicene and the hydroxyl group of the adjacent one forms homochiral binary aggregates.[118]

Scheme 14. Synthesis of bis-aza[7]helicene-bis-pyridinone **56a-c** and dimerization by hydrogen bonding. X-ray structure of homochiral dimeric structure (*P*,*P*)-**57c** (from (*rac*)-**56c**). Adapted from ref. [117]. Copyright 2000, American Chemical Society.

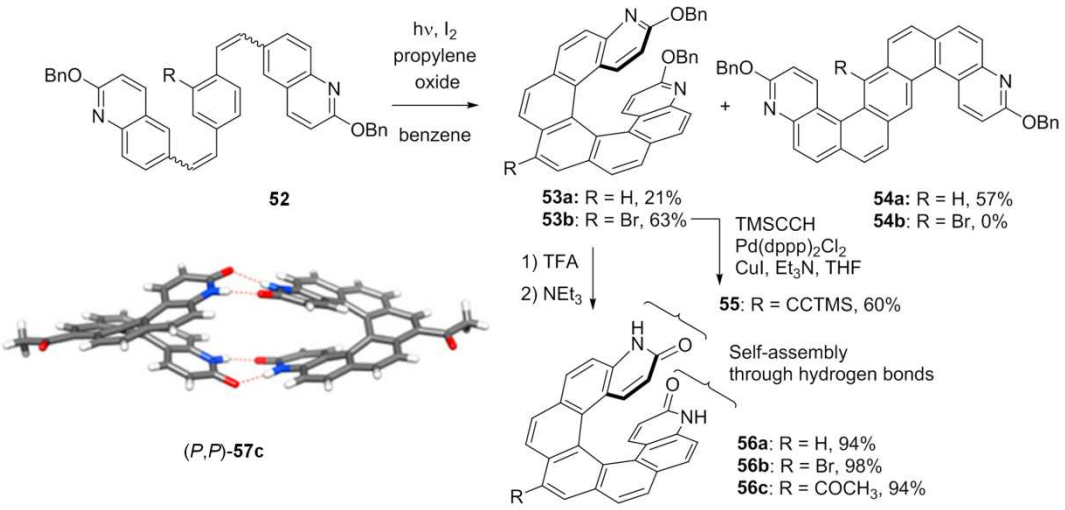

In 2013, Dehaen and co-workers reported the synthesis of enantioenriched diazadithia[7]helicenes (*P*)- and (*M*)-**58** and (*P*,*S*,S)- and (*M*,*S*,*S*)-**59**,[119] heterohelicenic molecules which combine both features of aza- and thiahelicenes molecules, by including two different main-group elements in their backbone (Figure 12). The thiophene ring at the extremity of the helical molecule offers a variety possible substitutions *via* the α-functionalization while the pyridine moiety can act as hydrogen acceptor or metal chelating group for chiral recognition applications. The synthetic strategy to access **59** involved Wittig reaction followed by oxidative photocyclization and then a Buchwald-Hartwig amination with L-(-)-α-methyl-benzylamine.[119] The 1:1 mixture of (*M*,*S*,*S*)/(*P*,*S*,*S*)-**59** diastereomers was finally separated by column chromatography. Analogue **58** revealed a racemization Gibbs energy $\Delta G^{\#}$ of 40.26 ±0.14 kcal mol^{-1} and a half-time of (6.5±0.7) h at 220 °C, which is similar to other known [7]helicenes. The ECD spectra of enantioenriched azathia[7]helicene **58** and diastereomers **59** were recorded in $CHCl_3$ (Figure 12). For **58**, the spectra showed mirror-image signal with opposite sign for (*P*) and (*M*) helicity; the ECD response was slightly red-shifted in comparison with other known [7]helicene that incorporates an alternation of benzene and thiophene rings.[120] The spectra for **59** diastereomers possess a strong similarity to **58** signal, the main difference is the absorption band around 300 nm which could be explained by the contribution of the additional stereogenic centers.

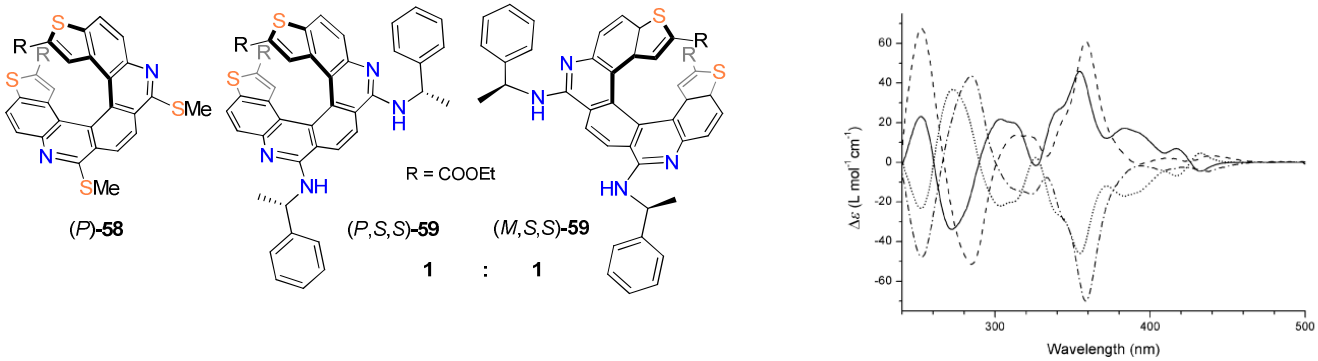

Figure 12. Chemical structures and ECD spectra of enantiomers (*P*)-(+)- (solid) and (*M*)-(-)-**58** (dotted) and (*P*,*S*,*S*)-(+)- (dashed) and (*M*,*S*,*S*)-(-)-**59** (dashed-dotted). Adapted from ref. [119]. Copyright 2013, Wiley.

4.1.1.1.2. Coupling reactions

Another synthetic strategy to obtain pyridohelicenes is the use of coupling reactions. The regioselective preparation of racemic 1,16- (**41b**[1]), 1,14- (**41b**[5]) and 3,14-diaza[6]helicenes (**41b**[3]) by photocyclization of bis-olefine **60** was studied by Staab *et al.* in 1994 and pure diazahelicenes were obtained in respective 1.7, 25 and 11% yields (Scheme 15). In order to increase the quantity of (*rac*)-**41b**[1] an alternative strategy was chosen, which consisted of an intramolecular Stille coupling of tetrabrominated bis-olefin **61**, which occurred with 52% yield.[121] These procedures were reproduced in 2013 by Mori, Inoue *et al.*[46] to obtain pure enantiomers of **41b**[1,3,5] after chiral HPLC separations (see Table 6).

Scheme 15. Oxidative photocyclization *vs.* Pd-coupling reaction for the synthesis of bis-aza[6]helicenes.[105]

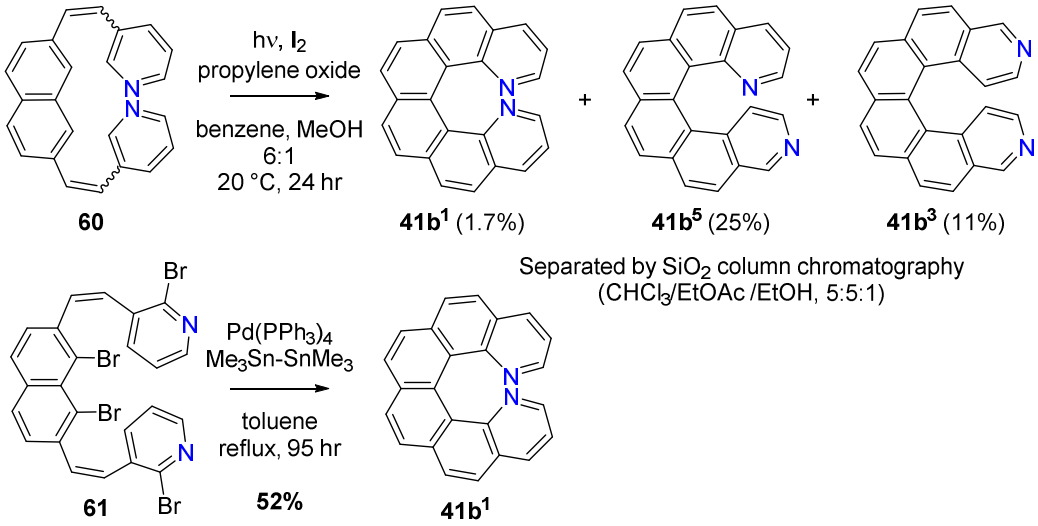

In 2008, Takenaka reported the synthesis of helically chiral pyridine N-oxides as a new family of asymmetric catalysts. They prepared **35a**[1], **41a**[1] and **69** by a *Z*-selective Wittig reaction between

phosphonium salts **62**, **63** and **64** respectively and aldehyde **65**, followed by a Stille-Kelly reaction of the dihalogenated olefins (Scheme 16).[115] Good yields and high quantities of racemic helicenes were obtained, which were subsequently transformed, upon reaction with *m*-CPBA in dichloromethane, to their corresponding helicenic N-oxides **70**-**72**, whose enantiomers were subsequently resolved by chiral HPLC methods (Table 6). Note that the racemization barrier of **70** was not reported but from its X-ray structure (Figure 13), one can see that the oxide induces steric hindrance and helical shape, hence sufficient configurational stability in the reaction conditions of asymmetric catalysis (see paragraph 4.1.1.4.).

Scheme 16. Synthesis of enantiopure aza[5] and [6]helicene oxides ((*P*) enantiomers shown) by a sequence of 1) Wittig reaction, 2) Stille-Kelly coupling, and 3) a final HPLC chiral resolution step.[115]

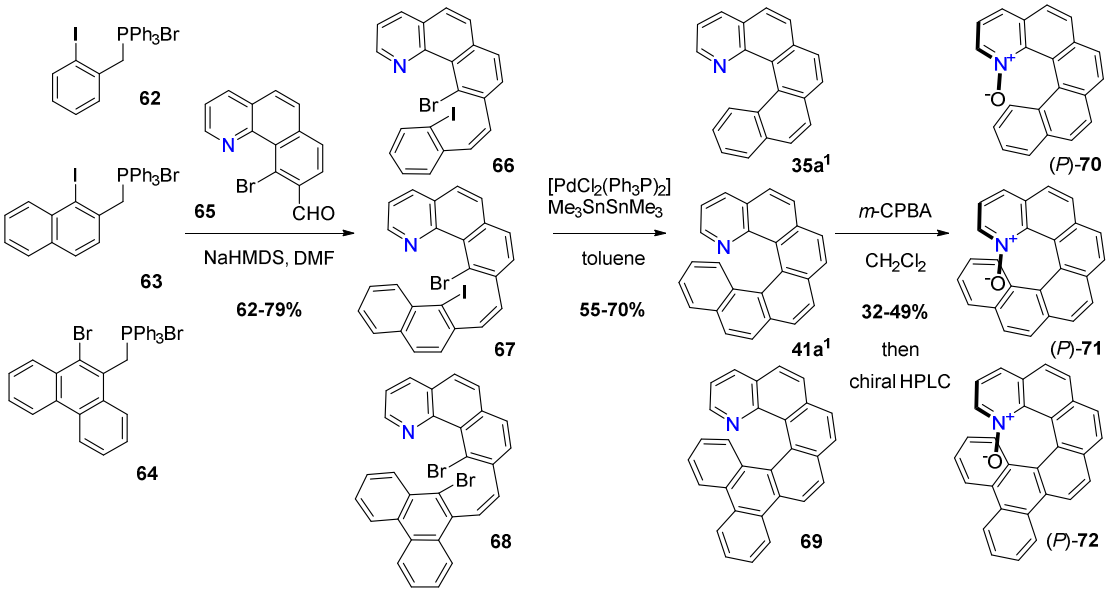

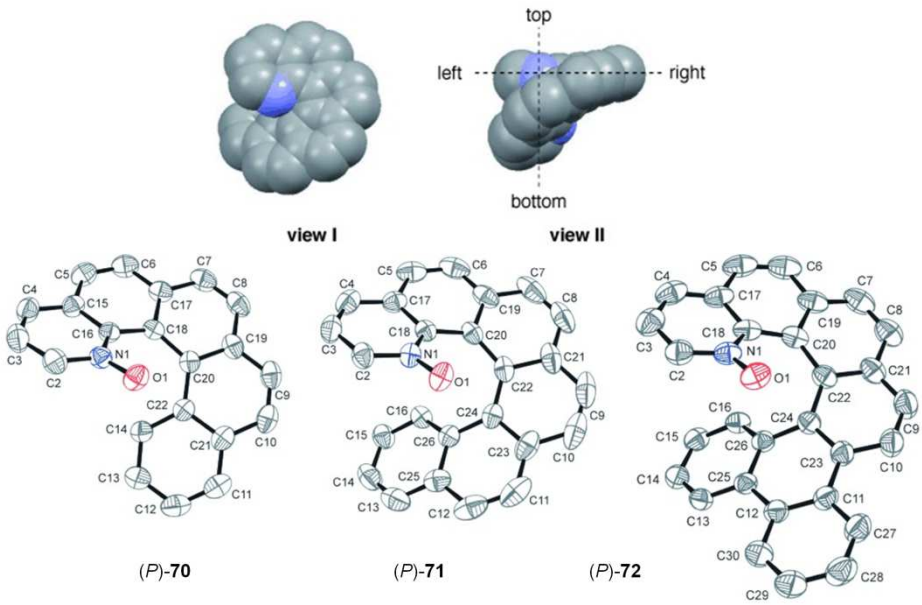

Figure 13. Schematic top-bottom and left-right view of 1-aza[6]helicene **41a**[1]. ORTEP of **70**-**72** ((*P*) enantiomers shown). Adapted from ref. [122]. Copyright 2009, Wiley.

4.1.1.1.3. [2+2+2] Alkyne cyclotrimerization

The use of [2+2+2] cyclotrimerization is a very efficient methodology to prepare many different helicenes incorporating N atoms. In 2008, Stary and Stara reported a convenient synthesis of 1,14-diaza[5]helicene (**35b**[1]), by using a cobalt-catalyzed [2+2+2] cyclotrimerization as the key-step, followed by aromatization with MnO_2 in combination with microwave irradiation (Scheme 17).[92] Similarly, racemic helical pyridazines (including **2**) were prepared by this method.[123]

Scheme 17. Synthesis of 1,14-diaza[5]helicene by [2+2+2] Alkyne cyclotrimerization.[92]

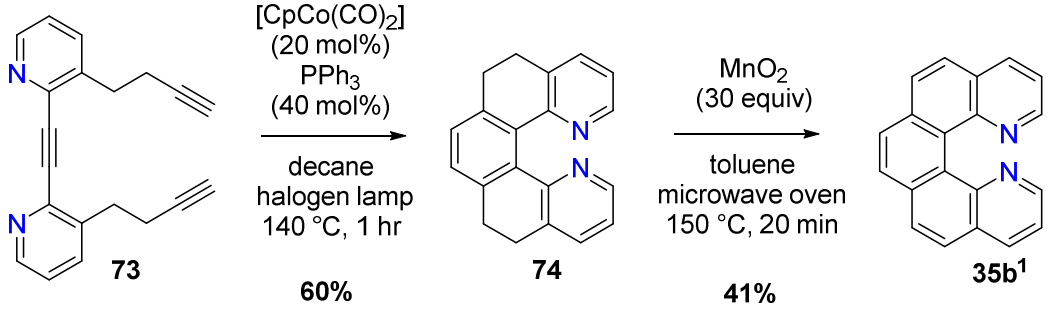

This method has also been used thoroughly to prepare several pyridohelicenes especially 1-aza[6]helicene (**41a**[1]), and 2-aza[6]helicene (**41a**[2], Scheme 18). The basicity of nitrogen in **41a**[1] and **41a**[2] was used to prepare a 2:1 complex with of (+)-*O*,*O*'-dibenzoyl-d-tartaric acid and to perform diastereomeric separation by preferential crystallization. After trituration of the yellow solid in diethyl ether at reflux, subsequent formation of the free base with sodium hydroxide, and its recrystallization led to optically pure 1-aza[6]helicene (+)-**41a**[1] with 99% *ee* as measured by chiral HPLC analysis on a Chiralcel OD-H column. The enantiomer (-)-**41a**[1] (>99% *ee*) was separated from the mother liquor by using (-)-*O*,*O*'-dibenzoyl-l-tartaric acid using the same procedure. As for 2-aza[6]helicene enantiomers, they were obtained with more than 99% *ee* by semi-preparative HPLC separation over a Chiralcel OD-H column. The absolute configurations of **41a**[1,2] were straightforwardly deduced from the ECD signatures and their racemization barriers were also measured experimentally (see Table 4). (**41a**[1]: $\Delta G^{\#}$ = 32.2 kcal mol^{-1}, $t_{1/2}$ = 71.9 min, at 423 K in 1-decanol; **41a**[2]: $\Delta G^{\#}$ = 35.4 kcal mol^{-1}, $t_{1/2}$ = 32.4 min, at 461 K in 1-decanol).

Scheme 18. Synthesis of (*rac*)-**41a**[1] and (*rac*)- **41a**[2] by [2+2+2] cycloisomerization.[92]

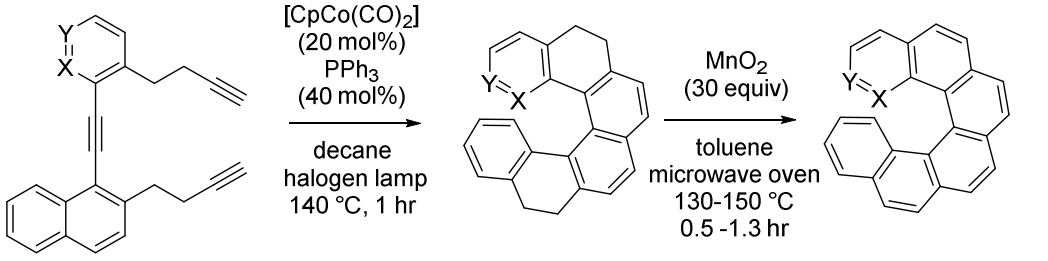

The exploration of this synthetic strategy was pursued by the group of Stary and Stara and several helicenic systems were prepared in their racemic forms such as 1,14-diaza[5]helicene[124] and dibenzo-aza[6]helicene.[125] Note that [2+2+2] cycloisomerization of either 3 alkynes (**77a^1**) or two alkynes and one nitrile (**77a^2**) can be performed and lead to different regioisomeric benzo-fused aza[6]helicenes, *i.e.* **78a^1** and **78a^2**, respectively (Scheme 19). Furthermore, while these N-containing [6]helicenes were obtained as racemic mixtures only,[126] the enantioselective synthesis of dibenzo-carbo[6]helicene (*P*)-**80** bearing two tolyl groups in positions 9 and 10 were reported when using $Ni(COD)_2$/(*R*)-QUINAP as the catalytic system.[125]

Scheme 19. Synthesis of (*rac*)-**78a^{1,2}** [126] and of (*P*)-**80**[125] by [2+2+2] cycloisomerization.

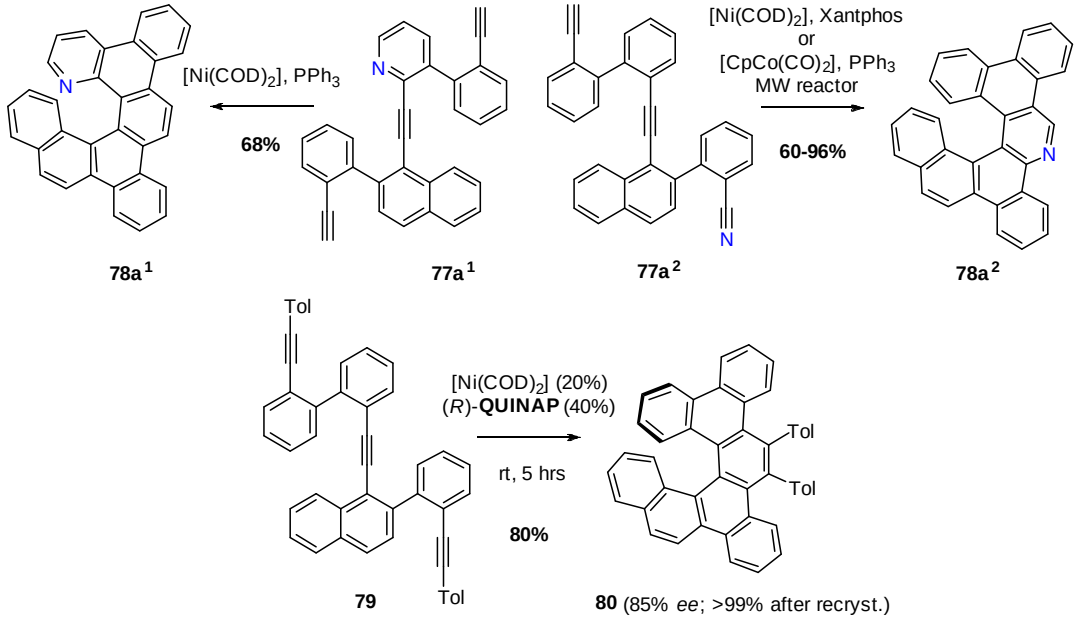

The same group was able to synthesize nonracemic pyrido[6]helicene-like compounds using a diastereoselective version of the [2+2+2] cyclization, and prepared centrally chiral cyanodiynes, *i.e.* (*R*)-(-)-**81** as a precursor of the pyrido[5]helicene-like molecule (*M*,*R*)-(-)-**85**, and (*R*)-(-)-**82**, as a precursor of the pyrido[6]helicenelike molecule (*M*,*R*)-(-)-**86** (Scheme 20).[126] This was achieved using a substoichiometric amount of $[CpCo(CO)_2]/PPh_3$ under microwave irradiation and only one diastereomer was seen by NMR spectroscopy. This chiral substrate-controlled diastereoselective cyclization stems from the fact that the pyridohelicene-like products are forced to adopt a helicity that prevents the disfavoured 1,3-allylic-type strain between the methyl substituent at the stereogenic center and adjacent tolyl group.[127] As the absolute configuration of the stereogenic center determines helicity, the (*M*) helicity was predicted when starting from (*R*)-cyanodiynes. The comparison of the ECD spectra (*M*,*R*)-(-)-**85** and (*M*,*R*)-(-)-**86** with carbonated analogues enabled to assign their absolute configuration. Similar asymmetric synthesis, corresponding to a tandem of [2+2+2] cycloisomerization of a centrally chiral triyne ((*R*)-(-)-**83** and **84**) followed by a thermodynamic equilibration of diastereomeric tetrahydrohelicene derivatives, being ultimately controlled by the 1,3-allylic-type strain, enabled to

prepare other enantioenriched aza[5] and aza[6]helicenic systems **88** and **90**. This nicely illustrates a point-to-helical chirality transfer utilizing a traceless chiral auxiliary.[128] Using similar strategies, the same group prepared pseudohelicenic 2,2′-bipyridines (**91-95**),[129] together with pseudohelicenic N-containing structures **96-98**,[130] in almost diastereomerially pure forms (Figure 14 and Table 7).

Scheme 20. Stereoselective synthesis of tolyl-substituted azahelicenes.[126,128]

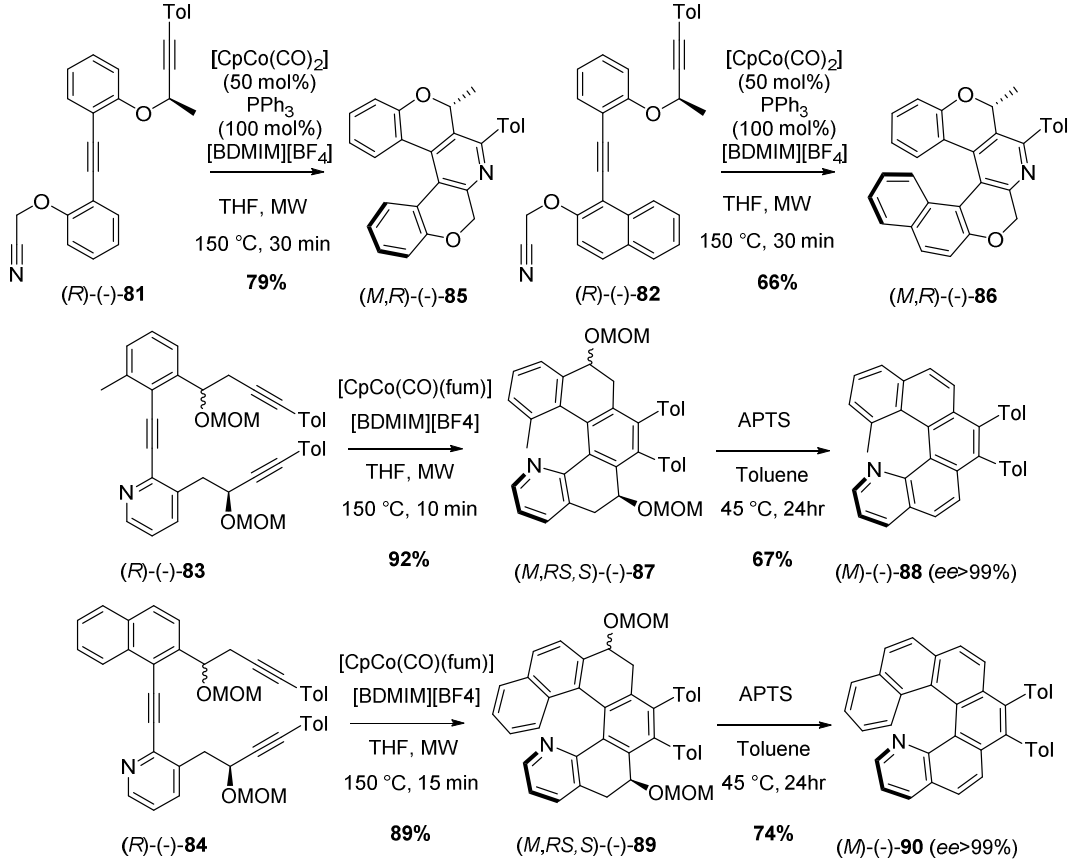

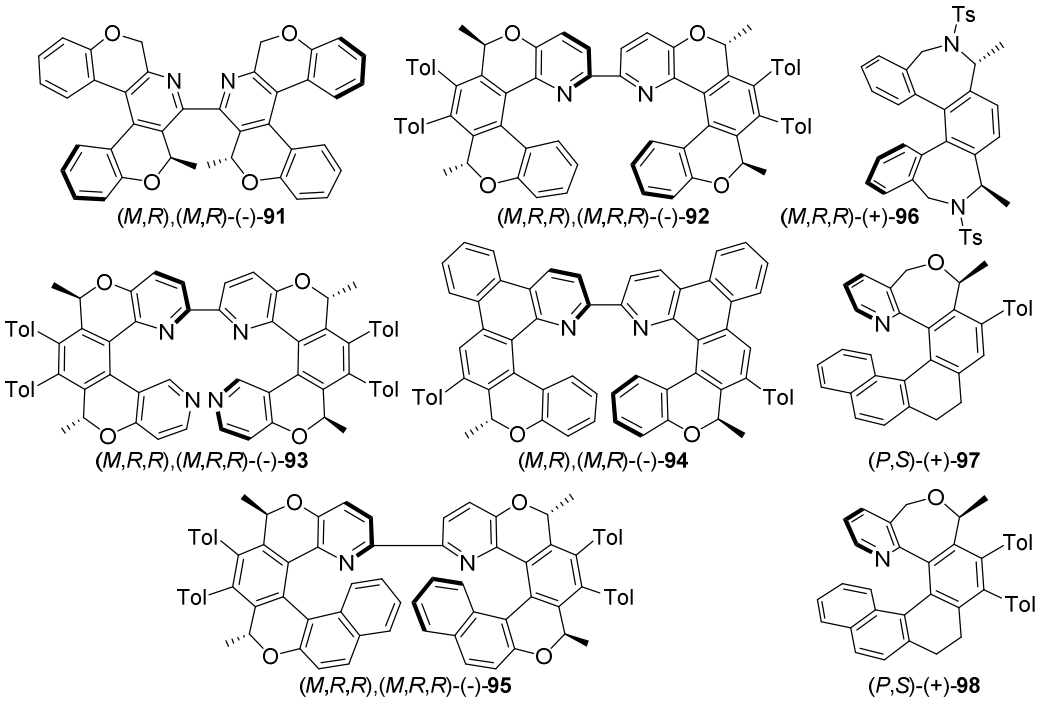

Figure 14. Enantioenriched bioxahelicene 2,2′-bipyridines (**91-95**) and pseudohelicenic N-containing structures **96-98**.[129]

Table 7. Specific rotation values of enantioenriched tolyl-substituted azahelicenes.

Compound	Method of obtention	$[\alpha]_D$[a]	Conditions[b] (solvent / Conc.[c])	Enantio/diastereo-Purity (determination method)	Ref.
(*M*,*R*)-**85**	Diastereoselective synthesis	-549	$CHCl_3$/0.2	>99% *de* [d,e]	[126]
(*M*,*R*)-**86**	Diastereoselective synthesis	-606	$CHCl_3$/0.267	>99% *de* [d,e]	[126]
(*M*,*RS*,*S*)-**87**	Diastereoselective synthesis	-183	$CHCl_3$/0.326		[128]
(*M*)-**88**	Diastereoselective synthesis	-458	$CHCl_3$/0.260	>99% *ee*[f]	[128]
(*M*,*RS*,*S*)-**89**	Diastereoselective synthesis	-334	$CHCl_3$/0.360		[128]
(*M*)-**90**	Diastereoselective synthesis	-1423	$CHCl_3$/0.253	>99% *ee*[f]	[128]
(*M*,*R*),(*M*,*R*)-**91**	Diastereoselective synthesis	-422	$CHCl_3$/0.327		[129]
(*M*,*R*,*R*),(*M*,*R*,*R*)-**92**	Diastereoselective synthesis	-765	$CHCl_3$/0.220		[129]
(*M*,*R*,*R*),(*M*,*R*,*R*)-**93**	Diastereoselective synthesis	-621	$CHCl_3$/0.208		[129]
(*M*,*R*),(*M*,*R*)-**94**	Diastereoselective synthesis	-1485	$CHCl_3$/0.138		[129]
(*M*,*R*,*R*),(*M*,*R*,*R*)-**95**	Diastereoselective synthesis	-1308	$CHCl_3$/0.199		[129]
(*M*,*R*,*R*)-**96**	Diastereoselective synthesis	+225	CH_2Cl_2/0.2	100:0 dr[d]	[130]

(*P*,*S*)-**97**	Diastereoselective synthesis	+237	CH_2Cl_2/0.37	92:8 dr[d]	[130]
(*P*,*S*)-**98**	Diastereoselective synthesis	+105	CH_2Cl_2/0.12	100:0 dr[d]	[130]

[a] In deg·mL·g^{-1}·dm^{-1}. [b] Temperature between 20-25 °C. [c] In g/100 mL otherwise stated. [d] NMR. [e] Chiralpak IA column, hexane/$CHCl_3$, 85:15. [f] Chiralpak IA column, heptane/$CHCl_3$, 70:30 (0.1% of diethylamine).

4.1.1.1.4. Alkyne-arene cycloisomerization

2-Aza-6,10-dimethyl[6]helicene was obtained by Storch *et al.* in its racemic form by an alkyne-arene cycloisomerization process using a combination of [$PtCl_4$] and $InCl_3$.[131] Using a similar cycloisomerization process with [$PtCl_4$] in dichloroethane, at high temperature, Fuchter *et al.* showed in 2013 that it was possible to transform stereospecifically axially chiral (R_a)-**99** (92% *ee)* to helical (*M*)-**41a^1** (90%) and (S_a)-**99** (94% *ee*) to helical (*P*)- **41a^1** (92% *ee*), as depicted in Scheme 21.[132] Note that the enantioenriched axially chiral precursors **99** were obtained by a chiral HPLC resolution step *i.e.* through separation on semi-preparative HPLC using the chiral OD-H column and hexane/isopropanol (95:5) as the eluent. Assignment of the absolute stereochemistry was made by comparison of the experimentally obtained electronic circular dichroism (ECD) spectra with theoretically predicted ones or by comparison with literature.[92] Finally, thermal racemization of **41a^1** was studied and less than 0.2% loss of *ee* was observed at 80 °C over 6 hours in 1-nonanol.

Scheme 21. Synthesis of 1-aza[6]helicene **41a^1** through a central to helical chiral relay.[132]

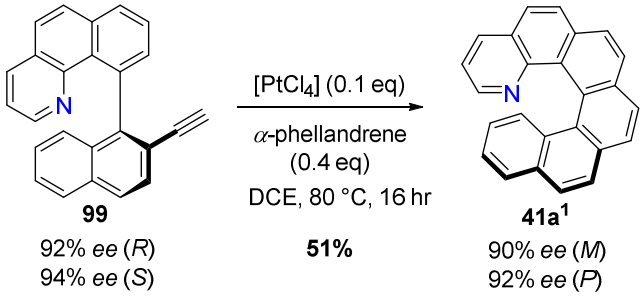

4.1.1.1.5. Other cyclization processes

Tanaka and coworkers reported in 2014 the transition-metal-catalyzed sequential intramolecular hydroarylation of alkynes (Scheme 22).[133,134] They performed the enantioselective synthesis of monoazahelicenes and S-shaped double azahelicenes *via* the Au-catalyzed sequential intramolecular hydroarylation of alkynes in the presence of AgOTf and using (*R*)-BINAP as the chiral ligand. The use of an excess AgOTf compared to Au(I) complex was necessary for this transformation. Using the same strategy, Tanaka *et al.* prepared S-shaped double azahelicene **100h** and **100i** as described in Scheme 22. The photophysical properties of azahelicenes (**100f** and **100g**) and S-shaped double azahelicenes (**100h** and **100i**) are summarized in Table 8. Double azahelicenes showed red shifts of absorption and emission maxima as compared with azahelicenes. They also showed higher quantum yields in $CHCl_3$ solution than for azahelicenes. The optical rotation values of double azahelicenes **100h** and **100i** were smaller than

those of single azahelicenes **100f** and **100g** which was tentatively explained by the presence of two pseudo-axially chiral methoxyphenyl groups. Interestingly, the CPL activity of the S-shaped double azahelicenes was significantly higher than that of the monoazahelicenes. Indeed, while CPL measurements showed that intensities for azahelicenes **100f** and **100g** were below their measurable limit (g_{lum}<0.001), double azahelicenes **100h** and **100i** exhibited strong CPL activities, with g_{lum} = 0.028 at 492 nm for (+)-**100h** and g_{lum} = −0.011 at 454 nm for (-)-**100i** in chloroform.[133] In 2016, Tanaka and coworkers applied similar strategy based on enantioselective transition-metal-catalyzed sequential intramolecular hydroarylation of alkynes on a substrate which, upon a double process, using (*R*)- and (*S*)-difluorophos respectively as the chiral ligand, afforded (-)- and (+)-aza[10]helicenes **100e'** . They found that **100e'** displayed $g_{abs} = 4.5 \times 10^{-3}$ at 303 nm which correspond to a smaller value than for *S*-shaped **100i** ($g_{abs} = 6.5 \times 10^{-3}$ at 331 nm). On the contrary, the optical rotation of **100e'** (3182) was significantly larger than for **100i** (1086).[134]

Scheme 22. Synthesis of enantioenriched aza[6]ahelicenes **100a-e,f** and bisaza[10]ahelicenes **100e'** by enantioselective Au-catalyzed intramolecular hydroarylation and transformation of **100f** to **100g**. Synthesis of S-shaped double helicene **100h** and **100i**.[133,134]

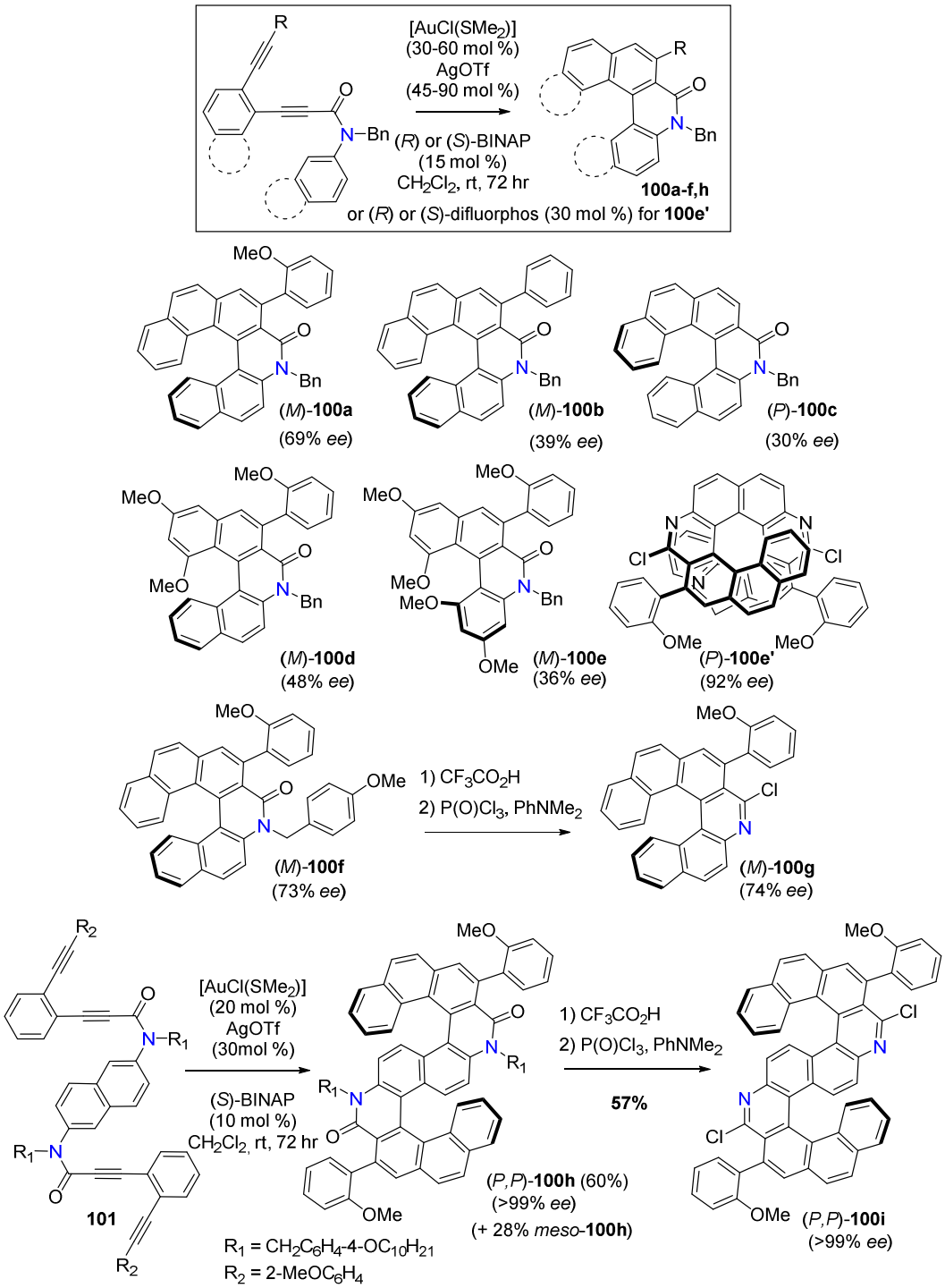

Table 8. Specific rotation values and photophysical data of enantioenriched azahelicenes **100a-i**.[133,134]

Compound	Method of obtention	$[\alpha]_{D\ exp}$[a]	*Enantio-purity*	$[\alpha]_{max}$[a]	Conditions[b] (solvent / Conc.[c])	λ_{Abs} (nm)	λ_{Em} (excitation) (nm)	Φ (%/solvent)	g_{lum}[d]
(*M*)-**100a**	Enantioselective intramolecular hydroarylation	-561.9	69%[e]		$CHCl_3$/2.52				
(*M*)-**100b**	Ibid.	-346.7	39%[e]		$CHCl_3$/1.355				
(*P*)-**100c**	Ibid.	+359.2	30%[e]		$CHCl_3$/1.645				
(*M*)-**100d**	Ibid.	-145.5	48%[e]		$CHCl_3$/1.640				
(*M*)-**100e**	Ibid.	-81.0	36%[e]		$CHCl_3$/2.380				
(*P*)-**100e'**	Ibid.	+2928	92%[f]		$CHCl_3$/0.635	261,442	477,509 (261)	1.4/$CHCl_3$	
(*M*)-**100f**	Ibid.	-989.0	73%[e]	-1355	$CHCl_3$/1.150	317,381	467 (317)	5.1/$CHCl_3$	<0.001
(*M*)- **100g**	From (*M*)-**100f**	-929.0	74%[g]	-1273	$CHCl_3$/1.645	325	467 (317)	2.1/$CHCl_3$	<0.001
(*P*,*P*)-**100h**	Enantioselective intramolecular hydroarylation	+373.1	>99%[h]	377	$CHCl_3$/0.543	284,448	471,492 (284)	19/$CHCl_3$	0.028±0.002
(*P*,*P*)- **100i**	From (*P*,*P*)-**100h**	1075.2	>99%	1075.2	$CHCl_3$/0.320	260, 329, 445	454,480 (329)	9.4/$CHCl_3$	0.011±0.002

[a] In $deg \cdot mL \cdot g^{-1} \cdot dm^{-1}$. [b] Measured at 25 °C. [c] In g/100 mL. [d] Excitation at 375 nm. [e] CHIRALPAK AD-H, hexane/2-PrOH = 80:20. [f] CHIRALPAK IA, hexane/IPA= 85:15. [g] CHIRALCEL OD-H, hexane/*i*-PrOH = 95:5. [h] CHIRALPAK AD-H, hexane/*i*-PrOH = 85:15.

To explain the enhancement of CPL in double azahelicenes, Mori *et al.* proposed in 2018 a protocol for rationally aligning multiple chiral units to boost the chiroptical responses.[135] They used hexahelicene as a prototype; they aligned two hexahelicenes in various orientations and examined by theoretical calculations which orientation resulted in the highest chiroptical performance from either X-shaped (**101**, Figure 15) or S-shaped (**102**) double hexahelicenes. Compound **101** and **102** exhibited more than a twofold increase in intensity of circular dichroism and circularly polarized luminescence. Indeed, **101** and **102**, constructed by merging two hexahelicenes **3** in D_2 and C_2 symmetry, showed absorption dissymmetry factors per benzene unit (g_{abs}/n) for the ^1B_b band that are larger by a factor of up to 1.5 than that of parent **3**. This enhancement was well rationalized by the electric (μ_e) and magnetic (μ_m) transition dipole moments and their relative angle (θ) evaluated theoretically. In the double helicenes, μ_e and μ_m were parallel-aligned (θ=0) to maximize the orientation factor (cos θ) up to 1, which was mere 0.24 (cos 76°) in **3**, while $|\mu_e|$ and $|\mu_m|$ were comparable or only slightly improved. Similarly, the luminescence dissymmetry factor per benzene unit (g_{lum}/n) was up to 1.7-fold larger for the double helicenes than for **3**, due to increase of $|\mu_e|$ and θ. The enhanced g_{abs}/n and g_{lum}/n values for double helicenes mean that merging two helicenes is 50-70% more efficient than simply assembling them, in favor of the molecular, rather than supramolecular strategy for constructing advanced chiroptical devices.

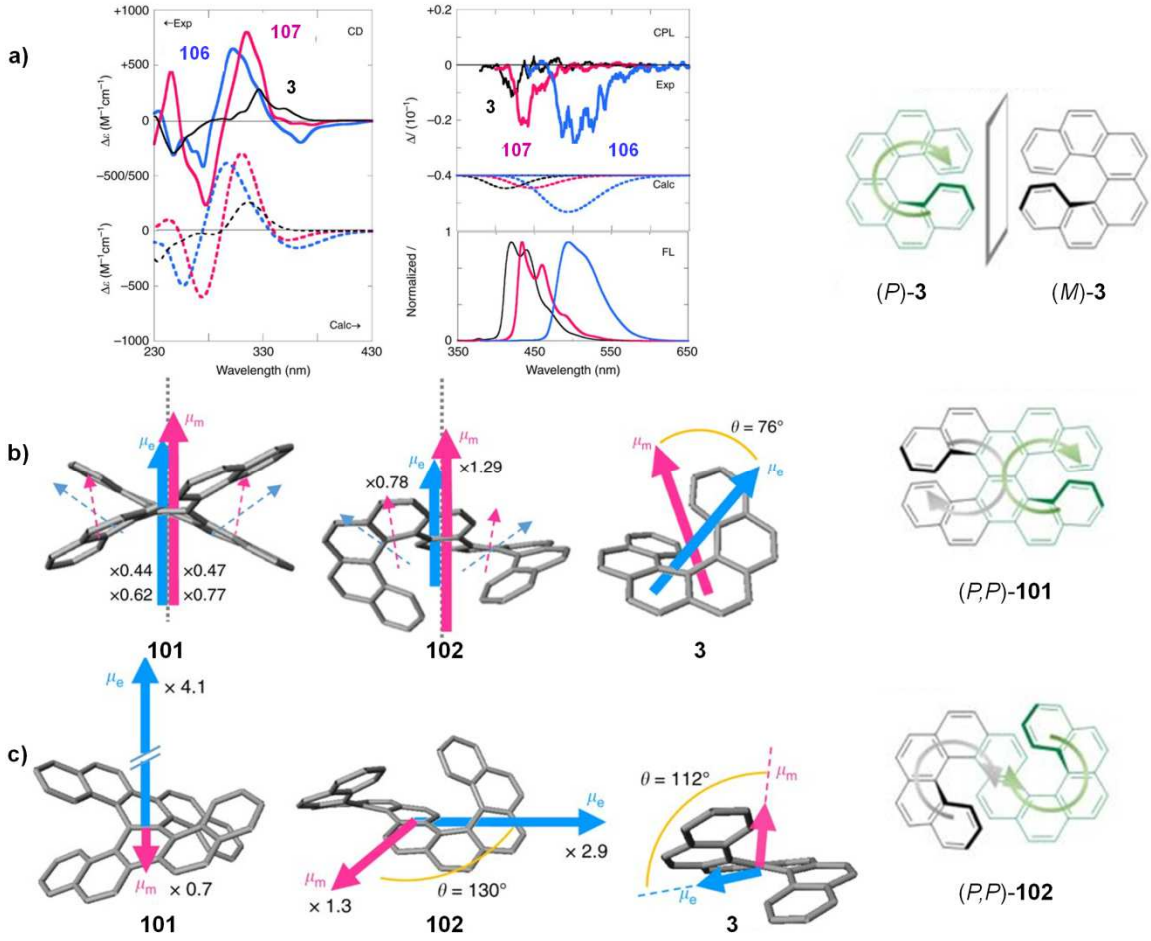

Figure 15. a) Experimental and calculated ECD and CPL responses of **3**, **101** and **102** ((*P*) enantiomers). b) Transition dipole moments in the ground state. Schematic representations of electric (μ_e, blue) and magnetic (μ_m, red) transition dipole moments of the ^1B_b band for X-shaped and S-shaped double hexahelicenes **101** and **102**, with the magnitudes relative to parent helicene **3**, calculated at the RI-CC2/def2-TZVPP level. Dashed arrows in double helicenes indicate the transition dipole moments of component helicene units. c) Transition dipole moments in the excited state. Schematic representations of the electric (μ_e, blue) and magnetic (μ_m, red) transition dipole moments of the ^1L_b band of **101** and **102** in the excited states, with the magnitudes relative to those for parent helicene **3**, calculated at the RI-CC2/def2-TZVPP level. Adapted from ref. [135]. Copyright 2018, Nature Publishers.

In 1976, Schuster showed that crude **103** dissolved in concentrated sulfuric acid gave almost quantitatively dibenzo-fused diaza[6]helicene **104** which precipitated in water (Scheme 23).[136] The enantiomeric resolution of **104** was carried out through an acid-base complex with the chiral resolving agent 2-(2,4,5,7-tetranitro-9 fluorenylideneaminooxy)-propionic acid (TAPA),[137] and later on through HPLC over a chiral stationary phase based on binaphthyl-2,2′-diyl-hydrogenphosphate ((*P*)-(+)-**BPA** linked through a 3-aminopropyl spacer to silica gel).[138] Its emission properties were also studied.[139]

Scheme 23. Synthesis of dibenzo-fused diaza[6]helicene **104**.[136,137]

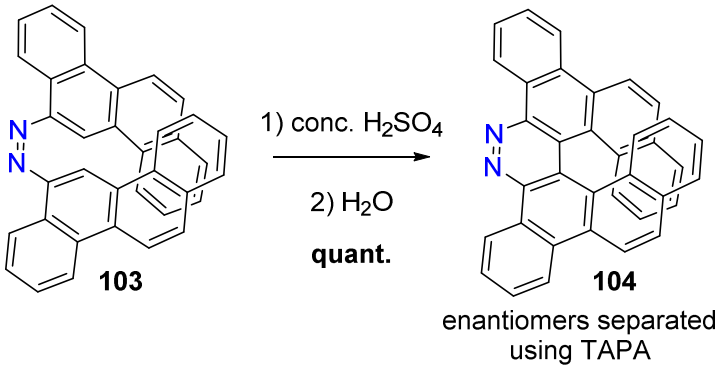

4.1.1.1.6. Substitution of pyridohelicenes

In 2010, the group of Takenaka prepared helical 2-aminopyridines (*P*) or (*M*)-**105a** to **105e** from enantiopure (*P*) or (*M*) helical pyridine-N-oxides **71** and **72** by reaction with an amine in the presence of tosyl anhydride (Scheme 24).[114] Then enantioenriched compounds **105a**,**b** were deprotected to **105f**,**g** using trifluoroacetic acid and the pyridinium salts were prepared using HCl. Enantioenriched pyridinium salts were also prepared from **105c-e** (see Table 6, Scheme 25). These compounds were efficiently used as hydrogen bond (H-bond) donors in organic catalysis (see paragraph 4.1.1.4. and Table 10). In 2011, the same group prepared helical 2,2'-bipyridine N-monoxide (*P*) and (*M*)-**106** from direct reaction of helical N-oxide (*P*) and (*M*)-**72** with 2-Li-pyridine followed by aromatization (Scheme 26).[116]

Scheme 24. Synthesis of pyridohelicenes **105a-e**, 2-substituted with amino groups.[114]

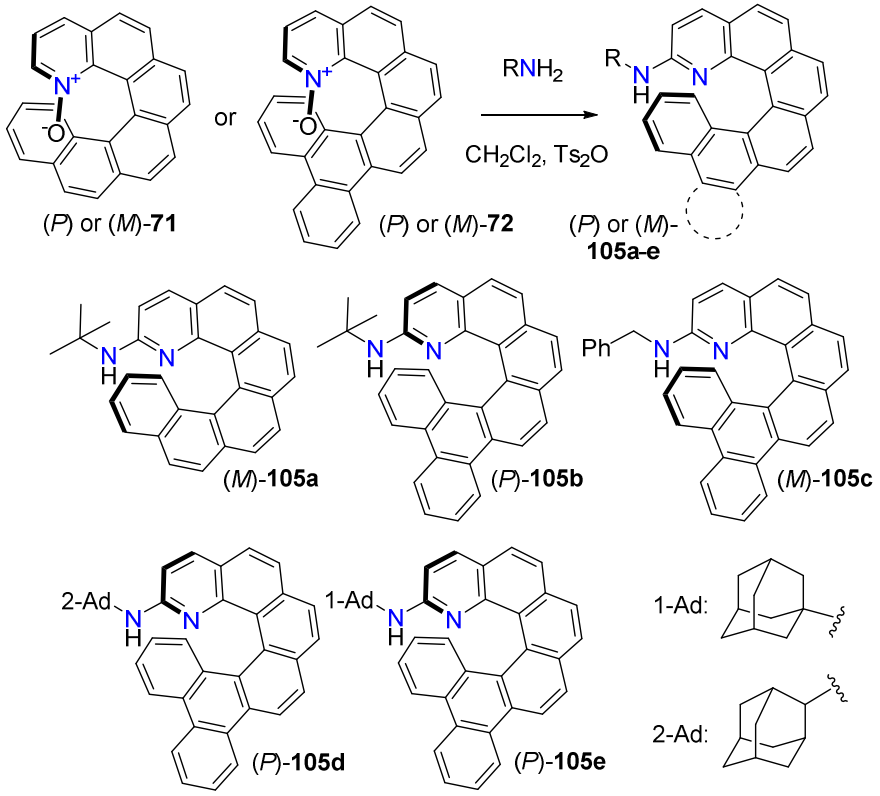

Scheme 25. Preparation of helical pyridinium salts from **105f**,**g**.[114]

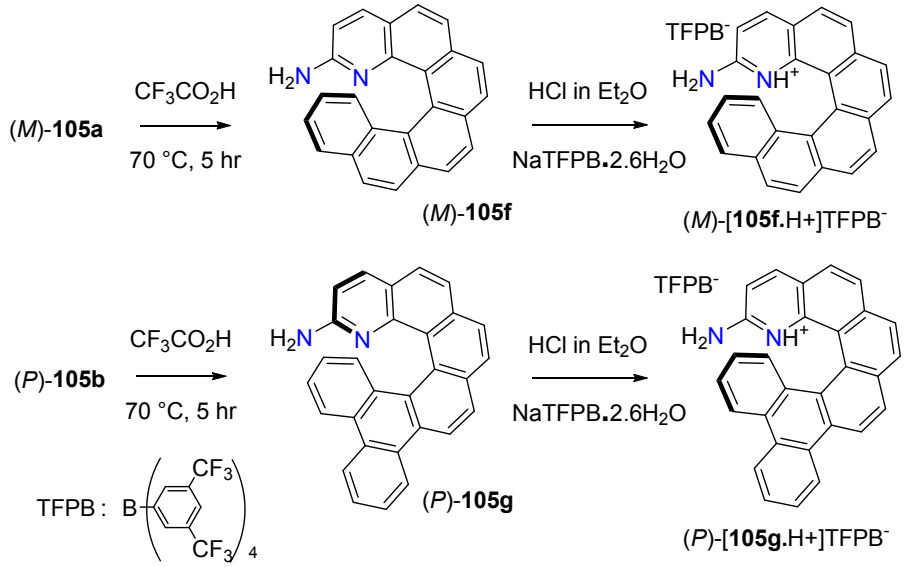

Scheme 26. Preparation of a helicenic bipyridine 1-N-oxide **106**.[116]

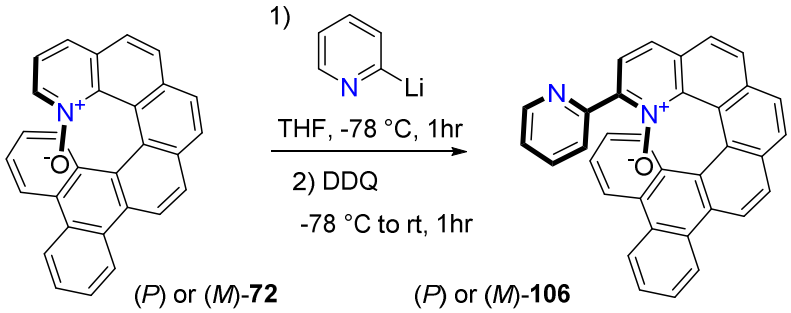

(*P*) or (*M*)-**72** (*P*) or (*M*)-**106**

4.1.1.2. Applications in optoeletronics

4.1.1.2.1. Conductance

As already mentioned, helicenes are helical graphene-like molecules with semi-conductive properties and as such they are interesting models to examine charge conduction at the molecular level. For this purpose, Vacek, Dubi, and co-workers used DFT and tight-binding calculations to study the mechanic tuning of conductance and thermopower in diaza[9]helicene (**107**) molecular junctions (MJs) (Figure 16A).[140] These MJs could be mechanically tuned from an insulating state (for example, Δr = 2 Å, 'OFF') to a metallic state (Δr = −2 Å, 'ON'). Furthermore, the thermoelectric figure of merit ZT could be tuned by helicene length and the distance between electrodes. Y. Xiao and coworkers studied the electronic transport of helicenes under stretching or compressing by first-principles calculations in a theoretical aza[12]helicene system, a helicene with 12 pyridine rings grafted to carbon electrodes (**107'**, see Figure 16B); this system is compared to another one, *i.e.* Au-[12]helicene-Au. They observed a U-shaped relationship between the pitch of the helicene (*d*) and the current (*I*) under a certain bias voltage.[141] Further analysis showed that it was the result of the nonmonotonic change of HOMO-LUMO gap with *d*. The change of overlap between orbitals induced by conformational deformation was found to be the underlying mechanism. This seems to correspond to an intrinsic characteristic of helicenes, which is independent of the electrode material or the heteroatoms in the skeletons used in the study.

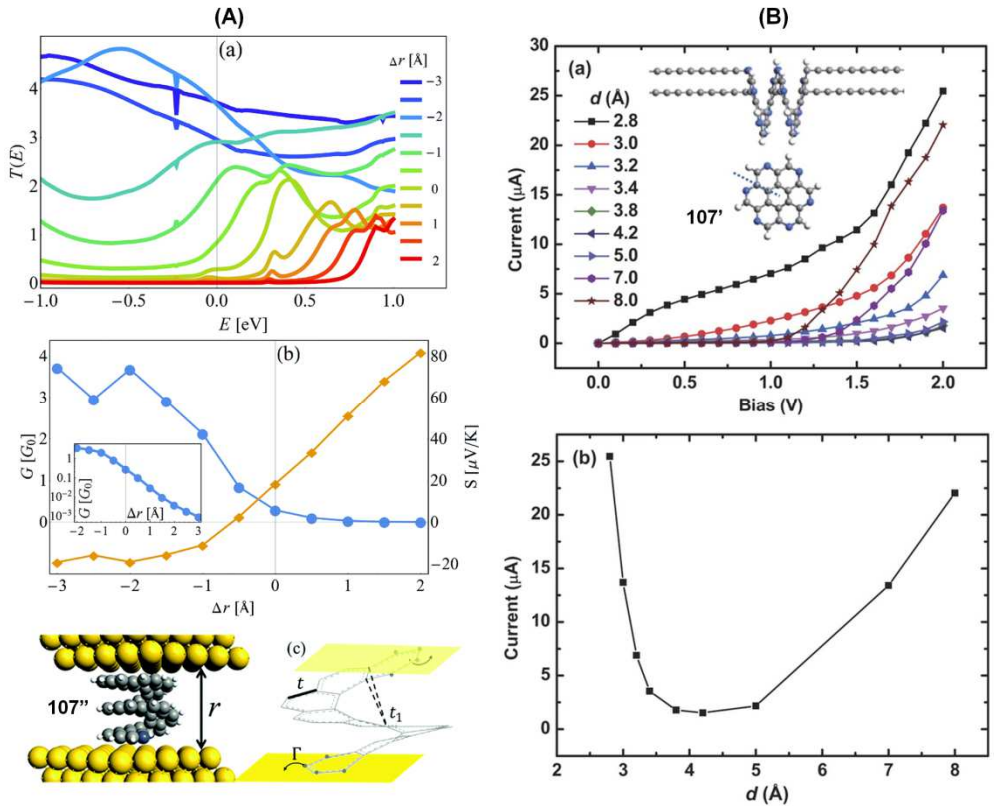

Figure 16. (A) Transmission and thermopower properties of a MJ formed by 2,21-diaza[9]helicene (**107**) and gold(1,1,1) electrodes: (a) transmission T(E) as a function of energy E for different inter-electrode distances incrementally changed about Δr = −3, 2.5, −2, …, 1, 2 Å (measured from the relaxed inter-electrode distance). (b) Conductance (blue circles) and thermopower (yellow diamonds) as a function of Δr. Inset: Conductance on a logarithmic scale, demonstrating the order of magnitude change in conductance with changing Δr. (c) Graphic representation of the tightbinding model of the 2,31-diaza[14]helicene (**107''**) based molecular junction. The tight binding parameters for nearest neighbor interaction (t), inter-stack coupling (t1) and molecule–electrode level broadening Γ are noted. Adapted from ref. [140]. Copyright 2015, Royal Society of Chemistry. (B) (a) $I-V$ curve under different pitch d. As shown in the inset, aza[12]helicene (**107'**) is composed of pyridines. (b) Current varies with d under the bias of 2.0 V. Adapted from ref. [141]. Copyright 2015, Nature Publishers.

4.1.1.2.2. Optoelectronic devices

In 2013, Fuchter, Campbell, *et al.* prepared an organic field-effect transistor (OFET) based on 1-aza[6]helicene **41a**[1] behaving as a hole-transporting material and giving layers of well-ordered crystallized domains upon annealation (Figure 17A). They explored the circularly polarized light responsivity of the enantiomerically pure transistors, and demonstrated a highly specific photoresponse, which was directly related to the handedness of the helicene. Indeed, the variation of illumination intensity at 365 nm with time of a right-handed and left-handed circularly polarized light was followed by the change in the drain current I_D of an annealed enantiopure 1-aza-[6]helicene OFET and the current appeared different for the two handednesses.[142] Later on, they showed that **41a**[1] can display up to an 80-

fold difference in hole mobility, together with differences in thin-film photophysics and morphology, solely depending on whether a single handedness or a 1:1 mixture of left- and right-handed molecules is employed under analogous fabrication conditions.[143] This is a result of the different bulk packing induced by chiral composition which has an impact on the charge transport. These results illustrate that chirality may be used as a key tuning parameter in future device applications.[144,145] The same authors reported the use of 1-aza[6]helicene **41a**[1] as a chiral dopant in light-emitting polymer, *i.e.* poly[9,9-dioctylfluorene-*co*-benzothiadiazole] (named **F8BT**, Figure 17B).[146] It was found that blends consisting of small amount (7%) of enantiopure 1-aza[6]helicene dopant gave a strong CP-PL response of the **F8BT** film. Increasing the 1-aza[6]helicene blending ratio resulted in improvements of the g_{PL} factor, up to a significantly high value of 0.5 for the 53% helicene blend (while the starting azahelicene displayed only modest g_{lum} ~10^{-4}-10^{-3}). To explain this behavior the authors suggest the formation of a chiroptical co-crystalline phase. The authors were then able to fabricate a single-layer polymer LED (PLED) device emitting circularly polarized light from the **F8BT** blends containing 7% of either the left-handed (-)-1-aza[6]helicene or the right-handed (+)-1-aza[6]helicene with a dissymmetry factor of electroluminescence (g_{EL}) factor as high as 0.2. The use of circularly polarized (CP) light is important in many technologies such as in highly efficient LCD backlights, for optical quantum information processing and communication, and in optical spintronics (see ref. [28] and references therein).

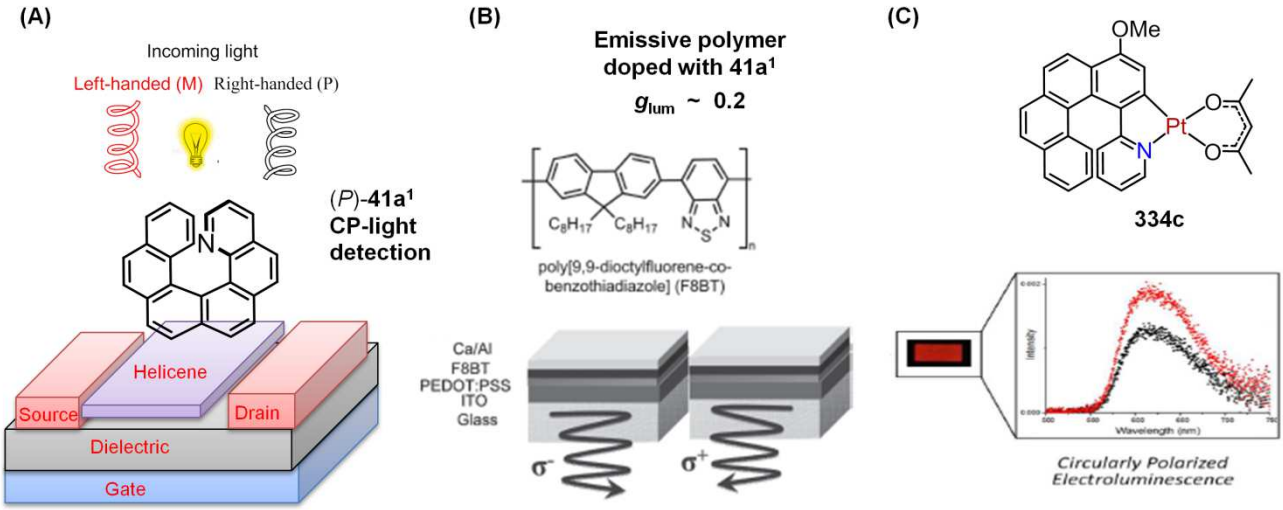

Figure 17. Three examples of devices using azahelicenes or platinahelicene derivatives in optoelectronic devices. (A) Chiral transistor based of enantiopure **41a**[1] capable of discriminating right-handed and left-handed CP-light.[146] (B) CP-PLED based on blends between enantiopure **41a**[1] and **F8BT**. Adapted from Ref. [142]. Copyright 2013, Wiley. (C) CP-PHOLED based on a pure enantiopure cycloplatinahelicene (see below **334c**). Adapted from ref. [147]. Copyright 2016, American Chemical Society.

4.1.1.3. Coordination chemistry of pyridohelicenes

Recent studies have demonstrated many potential applications of N-containing helicenes in coordination chemistry and in materials science. Indeed, their transition metal complexes may show interesting properties in harvesting (visible) light and re-emitting it at a wavelength that depends on the metallic ion used, thus allowing the development of light-emitting devices, chemosensors, photovoltaic dye-sensitized devices, etc. Furthermore, if the heteroaromatic ligand has more than one nitrogen atom in

its frame, large supramolecular complexes can be formed. Substituted N-containing helicenes are therefore useful in the development of asymmetric synthesis, receptors/sensors in molecular recognition, and components of supramolecular architecture.

In 2008, Stary *et al.* used racemic aza[6]helicenes **41a**^{1,2} (Figure 18) as N ligands for coordination, and 1:2 Ag^{I}-aza[6]helicene complexes such as **108** were prepared and characterized by X-ray crystallography. Complex **108** exhibited a T-shaped structure with two homochiral (*P*) or (*M*)-aza[6]helicene units coordinated and the silver atom embedded within the π-electron system. The coordination environment around the silver atom was best described as a trigonal bipyramid, in which each 1-aza[6]helicene actually binds as an η^3-*N,C,C* ligand, with the nitrogen atom and C=C bond occupying axial and equatorial positions, respectively.[92] The same group observed similar preferential formation of homochiral Ag^+ complexes in the gas phase.[148] Indeed, they prepared enantiopure deuterated 1-aza[6]helicene [7,8-D_2]-**41a**^{1} and probed the chiral discrimination in Ag^{I}-bound dimers of the type $[LAgL']^+$ (L,L' = **41a**^{1} or [7,8-D_2]-**41a**^{1}) by electrospray mass spectrometry. A pronounced preference for the formation of homochiral (*P,P*) and (*M,M*) dimers over the heterochiral (*M,P*) was observed. Competitive experiments with mixtures of 1- and 2-aza[6] helicene **41a**^{1,2} suggested a largely preferred coordination of 1-aza[6] helicene to the silver(I) cation, in agreement with stronger basicity (*vide supra*). The distinction between homochiral and heterochiral dimers of 1-aza[n]helicenes (n = 1,7) with alkaline cations (Li^+, Na^+, K^+) was studied by Alkorta *et al.* by DFT calculations and was found greater in the case of lithium with n = 6.[149] The racemization barriers of the 1:1 complexes were also examined and appeared larger in the complexes than in the non-coordinated ligands.

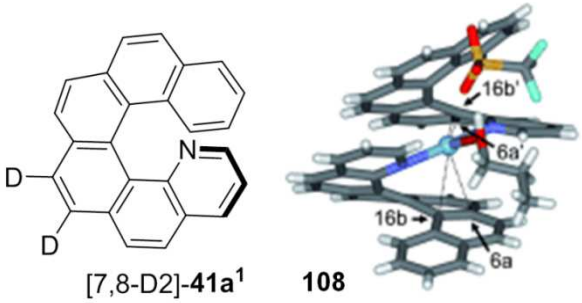

[7,8-D2]-**41a**^{1} **108**

Figure 18. Chemical structure of helicene [7,8-D_2]- **41a**^{1} and X-ray crystallographic structure of (*P,P*) Ag^{I}-bis-1-aza[6]helicene complex **108**. Adapted from ref. [92]. Copyright 2008, Wiley.

Later on in 2014, the coordination of 4-aza[6]helicene **41a**^{4} to square planar platinum(II) revealed a new aspect of reactivity in chiral transition metal complexes.[99] Indeed, our group has observed that *cis*-[$PtCl_2$(NCEt)PPh_3] (*cis*-**109**) reacted differently with either racemic or enantiopure 4-aza[6]helicene **41a**^{4} giving respectively *cis* (racemic, **110**) and *trans* (enantiopure, **110'**) [$PtCl_2$(**41a**^{4})PPh_3] complexes (Scheme 27). This unexpected reactivity is explained through a dynamic process (crystallization-induced diastereoselective transformation). Indeed, the racemic complex *cis*-**110** readily precipitated in refluxing toluene therefore displacing the *cis*-**109**/*trans*-**109'** equilibrium while the enantiopure series was soluble in refluxing toluene and yielded the more thermodynamically stable (*M*)- or (*P*)-*trans*-**110'**. Furthermore, X-ray crystallographic structure of racemic complex *cis*-**110** revealed the appearance of planar chirality around the square planar Pt center whose handedness was imposed by the helicene's one through efficient

chiral induction (Scheme 27). Note that a very similar phenomenon was also observed in the case of **41a**[5].[100] Pt complexes of aza[5]helicenes were also studied.[150,100]

Scheme 27. Different reactivity observed for racemic and enantiopure ligand **41a**[4], yielding respectively *cis*-**110** or *trans*-**110'** platinum complexes. X-ray crystallographic structure of *cis*-**110** (one enantiomer is shown) and dihedral angles used to define the (*M*) planar chirality around the Pt center.[99]

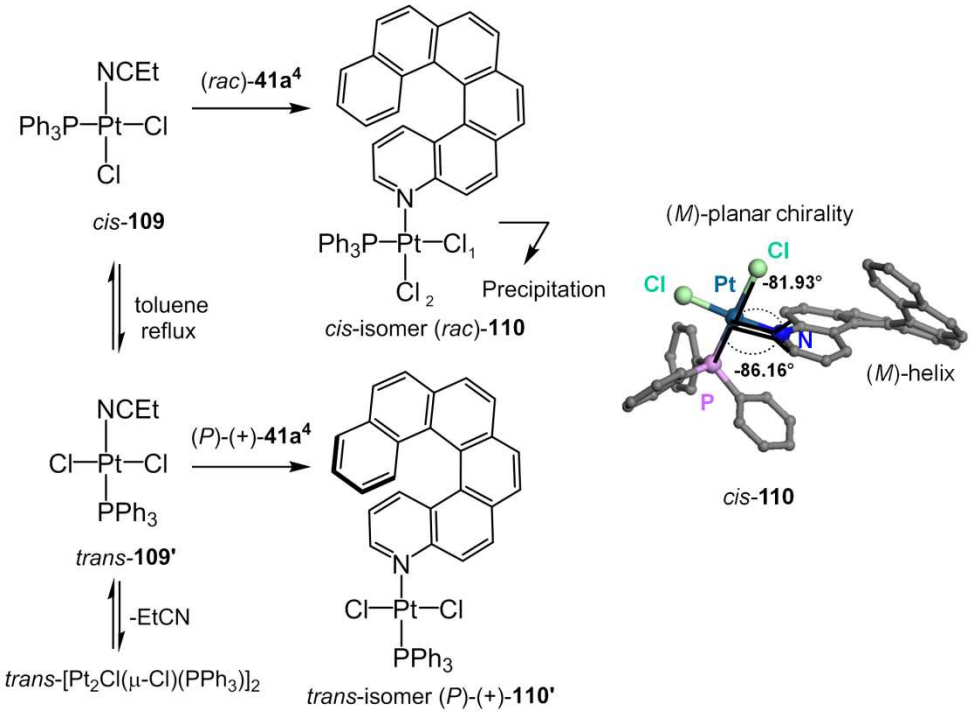

2,2'-Bipyridine ligands are classical N^N chelate ligands[151] but can also act as C^N ones toward different transition metal ions such as platinum.[152] In 2015, Autschbach, Crassous, *et al.* reported the preparation of enantiopure helical cycloplatinated complexes (*P*)- and (*M*)-**111** from a [6]helicene-bipyridine-type ligand, namely 3-(2-pyridyl)-4-aza[6]helicene ((*P*)- and (*M*)-**51** in Scheme 28). Due to the presence of an additional residual N atom in organometallic species (*P*)- and (*M*)-**111**, the acid-base triggering of UV-vis, ECD, phosphorescence and CPL was achieved, thus yielding the first acid-based CPL switch (see the increase of g_{lum} upon protonation in Scheme 28).[108] Furthermore, it was shown that organic helicene ligand (*P*)- and (*M*)-**51** was also an efficient chiroptical switch itself since, after double protonation, it displayed a strong bathochromic shift in emission wavelength while keeping strong CPL fluorescence signal ($g_{lum} = \pm 2 \times 10^{-3}$ in CH_2Cl_2). TD-DFT calculations showed that, upon protonation, the HOMO-to-LUMO transition changed from a π–π*-type to a charge transfer-type transition.

Scheme 28. Synthesis of cycloplatinated helicene (*M*)-**111** from (*M*)-**51** and reversible protonation and deprotonation process of organic and organometallic systems, observed by emission and CPL spectroscopies. *i*) $Pt(DMSO)_2(CH_3)_2$, acetone, 50 °C, 5 hrs, 90%.Variation of emission and CPL responses upon protonation.[108]

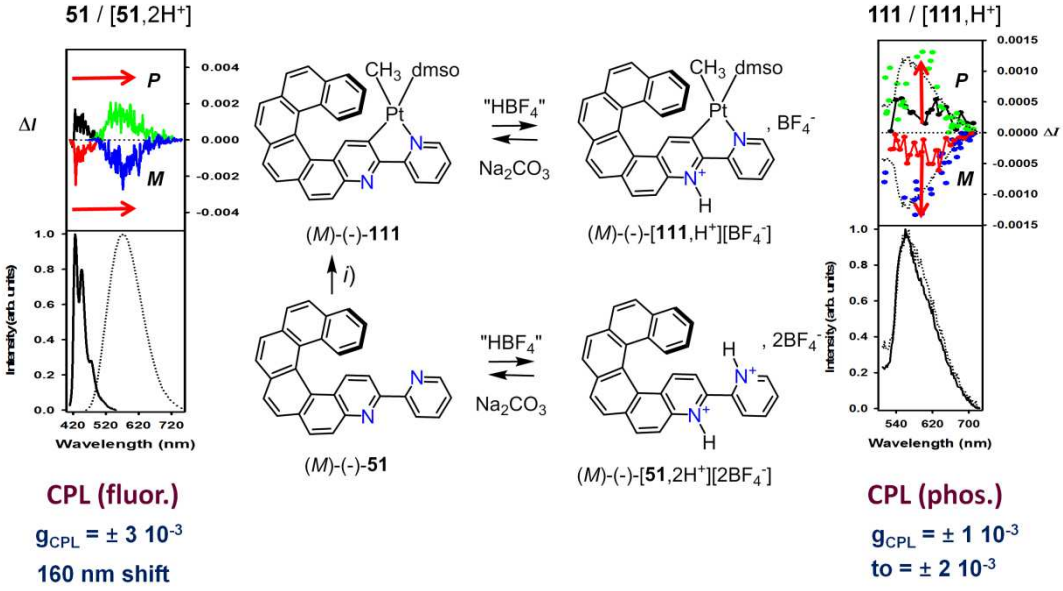

Rhenium(I)-chloro-tricarbonyl complexes bearing a bipy ligand are known to display efficient luminescence, usually a ^{3}CT emission from an excited state based on the bisimine ligand. [153] In this context, organic helicene-bipy ligand (*P*)- and (*M*)-**51** was used as N^N chelate to prepare enantio-enriched CPL-active helicene-bipyridine-rhenium complexes **112**, where carbon-metal bonds are established *via* the ancillary ligands (CO, isocyanide, see Scheme 29).[154] Starting from (*M*)-**51** ligand, two diastereomeric complexes, *i.e.* (*M*,A_{Re})-**112a^1** and (*P*,C_{Re})-**112a^2**, were formed, since the Re(I) atom is also a stereogenic center. These stereoisomers were separated by regular silica gel column chromatography and their chiroptical and emissive properties were studied. They revealed strong ECD spectra in CH_2Cl_2 (whose intensity depends on the rhenium stereochemistry, see Scheme 29), accompanied by substantial phosphorescence and CPL activity. Indeed (*M*,A_{Re})-**112a^1** and (*M*,C_{Re})-**112a^2** displayed phosphorescence emission (λ_{max}^{phos} = 673-680 nm, ϕ = 0.13-0.16%, τ = 27-33 ns) and good g_{lum} values ((*M*,C_{Re})-**114a^2**: g_{lum} ~ -3 × 10^{-3} around 670 nm). Upon reaction with AgOTf and 2,6-dimethylphenyl isocyanide in the presence of NH_4PF_6, (*M*,C_{Re}) and (*P*,A_{Re})-**112a^2** were transformed to cationic complexes (*P*)- and (*M*)-**113a^{1,2}**, respectively (see Scheme 29). The latter displayed stronger phosphorescence (λ_{max}^{phos} = 598 nm, ϕ = 6%, τ = 79 µs) and still good CPL activity (g_{lum} ~ ±1.5 × 10^{-3}). However, the stereochemical information at the Re(I) center was lost (epimerization to 50:50 mixture). Nevertheless, the ECD spectrum of (*P*)-**113a^{1,2}** displayed an additional positive ECD-active band around 450 nm as compared to (*P*,C_{Re})-**112a^1** and (*P*,A_{Re})-**112a^2**. According to TD-DFT calculations, this band does not involve the Re center but corresponds to the HOMO-to-LUMO transition with strong intraligand charge transfer from the π-helicene to the bipy moiety.[154] Autschbach, Crassous, *et al.* have thus shown that the incorporation of a rhenium atom within an extended helical π-conjugated bi-pyridine system can

impact the chiroptical and photophysical properties of the resulting neutral or cationic complexes, leading to the first rhenium-based circularly polarized phosphors.

Scheme 29. Synthesis of enantioenriched rhenium complexes (M,A_{Re})-**112a**^{1}, (M,C_{Re})-**112a**^{2}, and (M)-**113a**^{1,2} (mixture of two diastereomers). *i*) $Re(CO)_5Cl$, toluene, reflux; *ii*) AgOTf, EtOH/THF, then 2,6-dimethylphenyl isocyanide, THF, NH_4PF_6. X-ray crystallographic structure of **112a**^{2}. ECD spectra of (P,C_{Re})-**112a**^{1}, (P,A_{Re})-**112a**^{2} and (M)/(P)-**113a**^{1,2} isomers (CH_2Cl_2, C ~ 5×10^{-5} M).[154]

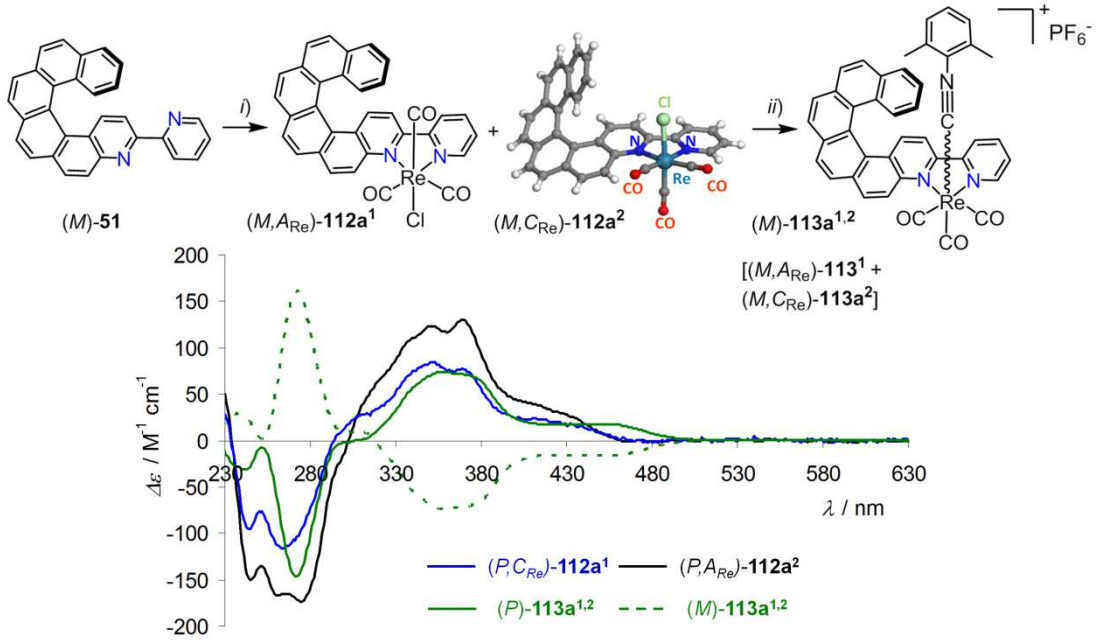

Note that in 1999, Katz and coworkers described the conversion of enantiopure helical quinone **114** into helical quinoxaline **117** (Scheme 30) in 48% yield using ethylenediamine.[113] Since **115** is an analogue of ligand 4,7-diaza-1,10-phenanthroline (pyrazino[2,3-f]quinoxaline), it was coordinated to metallic ions, especially it reacted with $Re(CO)_5Cl$ in toluene to give a complex **116**, which was isolated in 30% yield. Coordination with copper(I) was also examined but clear characterizations appeared difficult.

Scheme 30. Synthesis of bis-rhenium complex **116** from helicene-bis-quinoxaline derivative **115**.[113]

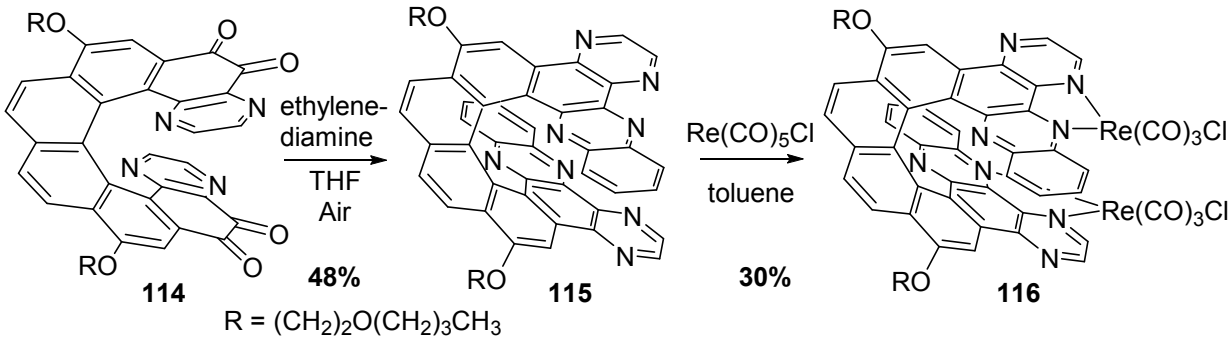

Taking advantage of differential assembly of racemate versus enantiopure species in the solid state enables to tune the physical properties of a material. In 2016, Pointillart, Crassous, Le Guennic, *et al.*

showed that the single molecule magnet (SMM) behavior of a chiral helicene-based dysprosium complex was different in its racemic and in its enantiopure forms.[155] For this purpose, racemic and enantiomerically pure [Dy(hfac)$_3$(**51**)] (**117a**, Figure 19) complexes were prepared and their structural and magnetic properties studied. It was shown that they behave as SMMs in their crystalline phase. Indeed, Dy(III) ion has a strong magnetic anisotropy and is an oblate ion placed within β-diketonate ligands and a bis-chelating nitrogenated ligand in a N_2O_6 coordination sphere, a geometry which often permits the detection of slow magnetic relaxation. Interestingly, the enantiopure SMM differs from the racemic one by two aspects. First, thanks to different dipolar interactions, the racemic complex showed antiferromagnetic behavior while the pure enantiomers were ferromagnetic (Figure 19b). Second, the presence of a hysteresis loop was found in the racemic system. These differences were explained by the different crystal packing between racemic complex (heterochiral dimeric assembly) and enantiopure one (homochiral columnar assembly) as described on Figure 19d) and 19e). Ab initio calculations on isolated complexes followed by determination of intermolecular dipolar couplings allowed the rationalization of the different low-temperature magnetic behaviors. Similar complexes, namely [Dy(**51**)(tta)$_3$] (**118**) (tta = 2-thienyltrifluoroaacetonate),[156] and [Ln$_2$(hfac)$_6$(**119**)]·nC_6H_{14} (Ln = Dy (**120a**) n = 0, Yb (**120b**) n = 1) with the **119** being 3,14-di-(2-pyridyl)-4,13-diaza[6]helicene racemic ligand (hfac = 1,1,1,5,5,5-hexafluoroacetylacetonate)[157] were synthesized in their racemic forms and structurally and magnetically characterized. All these complexes behaved as field-induced single molecule magnets in the crystalline phase. Their magnetic properties were rationalized by ab initio calculations.

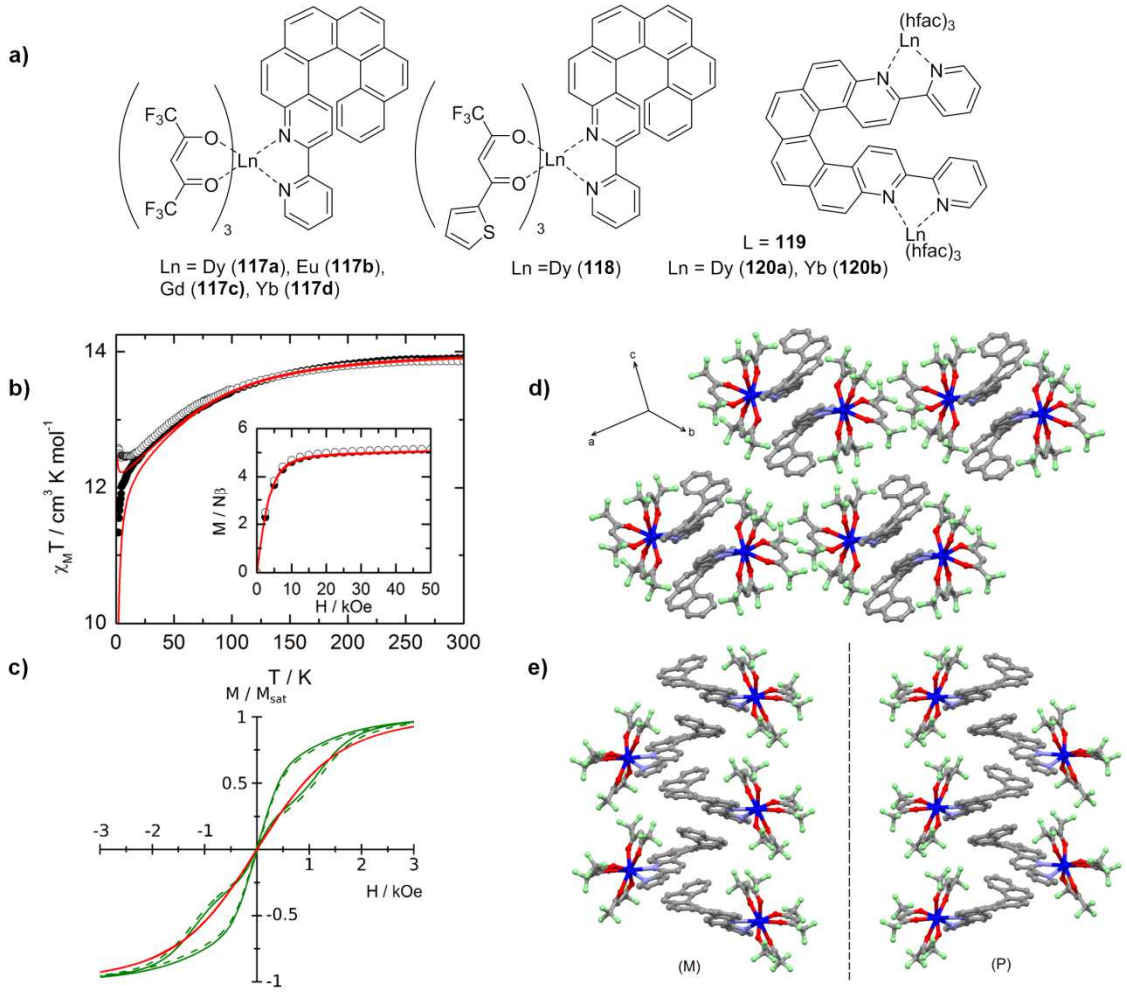

Figure 19. a) Chemical structures of Ln(III) complexes with helicene-bipy and helicene-bis(bipy) ligands **51** and **119**. b) Temperatures dependences of $\chi_M T$ for compounds (*rac*)-**117a**·0.5C_6H_{14} (black circles) and **(+)-117a** (white circles). In inset, the field variations of the magnetization at 2 K. Full red lines correspond to the simulated curves from *ab-initio* calculations. c) Magnetic hysteresis loops recorded at 500 mK and measured at a sweep rate of 16 Oe s^{-1} for (+)-**117a** (full green line), (-)-**117a** (dashed green line) and (*rac*)-**119a** ·0.5C_6H_{14} (red line). d) and e) Crystal packings of (*rac*)-**117a**, (*M*)-(-)-**117a** (left) and (*M*)-(+)-**117a** (right) highlighting the (*M*) and (*P*) helicoidal arrangements. The dashed line represents the mirror between both enantiomers. Adapted from ref. [155]. Copyright 2016, Royal Society of Chemistry.

The luminescence properties and singlet oxygen photosensitization were studied within the series of racemic [Ln(hfac)$_3$(**51**)] with Ln = Eu (**117b**), Gd (**117c**), Yb (**117d**) and were compared to those of the ligand **51**.[158] These studies indicated that non-emissive lanthanide act as heavy atoms strongly enhancing the singlet oxygen generation. It was also shown that sensitization of the f-f luminescence is in competition with singlet oxygen generation. Indeed, although the helicenic ligand used in this study is in itself a potent singlet oxygen sensitizer, which can be explained by the occurrence of aromatic backbone distortion that provides enhanced SOC, the coordination of lanthanide cations enables to tune the kinetics of intersystem crossing and therefore the balance between emission and singlet oxygen generation. The

outcome of this modulation greatly differs depending on the nature of the lanthanide cation. Gadolinium (**117c**), which presents f-f transitions much higher in energy than the lowest singlet excited state of the ligand, influences its photophysics solely by a "heavy-atom" effect, which results in an efficient singlet oxygen photosensitization. Conversely, in the ytterbium complex **117d**, the large difference in energy between the T_1 excited state and the lanthanide accepting level (*ca* 5000 cm^{-1}) results in a high-energy transfer which translates into a significant lowering in the singlet oxygen generation quantum yield and by the appearance of a characteristic ytterbium emission near 1000 nm. In between those two extremes, europium complex **117b** exhibits a more intricate behavior, with an interplay between competitive energy transfer and back transfer kinetics, resulting in a global increase in the kinetics of nonradiative events. Consequently, a rather ineffective sensitization of both lanthanide luminescence and singlet oxygen generation was observed for this complex.

The helical Terpyridine (Terpy) ligand **48** acted as a chiroptical switch upon reversible coordination-decoordination to zinc(II). The strong conformational changes induced lead to a multi-responsive chiroptical switch (Figure 20). The interconversion between the ligand and zinc-complexed states was analyzed *via* first-principles calculations, which highlighted the change from π–π* transitions in the organic ligand to charge transfer transitions in the Zn complex.[111]

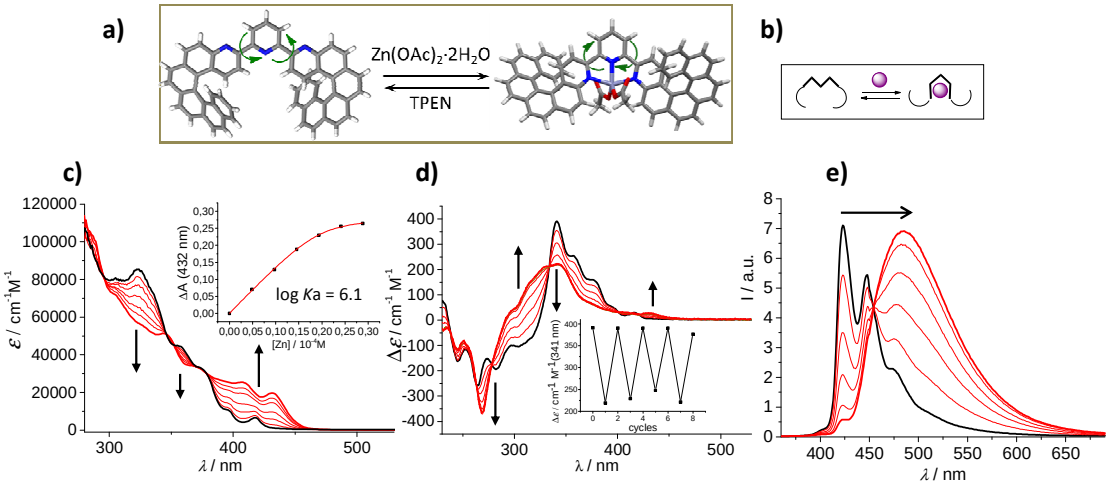

Figure 20. a) Reversible Zn(II) complexation-decomplexation process of (*P*,*P*)-**48** using $Zn(OAc)_2$ and TPEN as the chemical stimuli. b) Schematic modification of the geometry. c) Evolution of the UV-vis spectrum of (*P**,*P**)-**48** (3×10^{-5} M, CH_2Cl_2, rt) upon addition of $Zn(OAc)_2 \cdot 2H_2O$ aliquots (0.2 equiv. until saturation at 1.0-1.2 equiv.). Inset: Absorption at 432 nm and fitting with a 1:1 binding model. d) Evolution of the ECD spectrum of (*P*,*P*)-**48**. Inset: Reversible ECD_{341nm} switching process. e) Evolution of the fluorescence of (*P*,*P*)-**48** (λ_{ex} = 350 nm, 2.2×10^{-5} M, CH_2Cl_2, rt). Adapted from ref. [111]. Copyright 2016, Royal Society of Chemistry.

4.1.1.4. Applications in asymmetric organocatalysis

According to Takenaka and coworkers, the helically shaped 1-aza[6]helicene **41a**[1] having its nitrogen atom in the inner groove of the helix appeared an interesting "chiraphore" (For a discussion of terms

"catalaphore" and "chiraphore", see:[159]) because the pyridine ring is correctly desymmetrized in terms of "top-from-bottom" and "left-from-right" differentiations.[115] The helicene-N-oxides **70**, **71** and **72** were tested as catalysts in the desymmetrization of *meso* epoxides with chlorosilanes. Indeed, *c*is-stilbene epoxide reacted with $SiCl_4$ and gave the corresponding (*R*,*R*)-chlorohydrin with high *ee* values (Table 9, entry 1). The ring opening gave higher enantioselectivity for substrates bearing aromatic substituents rather than alkyl groups (Table 9, entries 1 and 2 versus 3 and 4). Catalyst **70** provided better *ee* values than **71** for acyclic epoxides (Table 1, entries 1-3), but the opposite was true for the cyclic epoxide (Table 1, entry 4). The scope of the reaction was additionally probed with catalyst **72** and the enantioselectivity was shown to be sensitive to electronic effects (Table 9, entries 5-7). Finally, the ring opening proceeded with a moderate *ee* value for an acyclic alkyl substituted epoxide (Table 9, entry 8), but with modest *ee*'s for a cyclic substrate (Table 9, entry 9).

Table 9. Desymmetrization of *meso* epoxides **121** by (*P*)-helical pyridine *N*-oxides (*P*)-**70**, (*P*)-**71** and (*P*)-**72** (see Scheme 16 and Figure 13).[115,122]

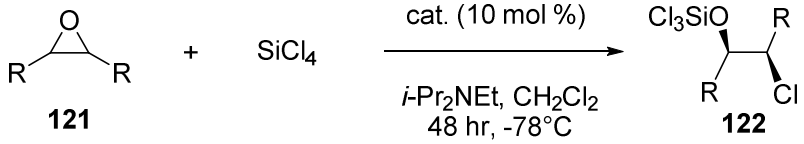

Entry	R	(*P*)-**70**	(*P*)-**71**	(*P*)-**72**
1	Ph	77 %, 93 % *ee*	80 %, 92 % *ee*	77 %, 94 % *ee*
2	2-Naphthyl	79 %, 81 % *ee*	77 %, 73 % *ee*	76 %, 92 % *ee*
3	$BnOCH_2$	71 %, 49 % *ee*	68 %, 42 % *ee*	72 %, 65 % *ee*
4	cyclooctene	70 %, 0 % *ee*	68 %, 22 % *ee*	74 %, 33 % *ee*
5	4-ClC_6H_4			84 %, 94 % *ee*
6	4-$CF_3C_6H_4$			83 %, 92 % *ee*
7	4-$CH_3C_6H_4$			83 %, 87 % *ee*
8	$CH_2O(CH_2)_3Ph$			63 %, 72 % *ee*
9	-CH_2OCH_2-			64 %, 33 % *ee*

The helical chiral 2-aminopyridinium ions (*P*)-[**105b-g**.H^+]$TFPB^-$ and (*P*)-[**41a**^{1}.H^+]$TFPB^-$ (Schemes 24 and 25) were presented in 2010 as a new class of hydrogen bond donor catalysts.[114] The approach of merging a 2-aminopyridinium core into the helical framework enabled to position an inherently chiral element at the H-bonding site and proved very successful. These helically chiral organic catalysts were tested on the addition of 4,7-dihydroindoles to nitroalkenes affording *β*-nitro-indol-2-yl products after subsequent oxidation (Table 10). An amount of 10 mol % of (*P*)-[**105f**.H^+]$TFPB^-$ efficiently promoted the reaction affording the product with moderate enantioselectivity (entry 1). Single H-bond donor (*P*)-[**41a**^{1}.H^+]$TFPB^-$ was found inefficient, indicating that the 2-amino group is required for asymmetric induction (entry 2). Benzo analogue (*P*)-[**105g**.H^+]$TFPB^-$ revealed more selective than (*P*)-

[**105f**.H$^+$]TFPB$^-$, even with 2 mol % catalyst loading (entries 3 and 4). Then, *N*-alkylated catalysts **105b-e** were evaluated (entries 5-8) and the enantioselectivity gradually improved as the alkyl substitution increased. The improved enantioselectivity was maintained when the catalyst loading was reduced to 0.5 mol % (entries 9).

Table 10. Evaluation of helical chiral 2-aminopyridinium catalysts (*P*)-[**105b-g**.H$^+$]TFPB$^-$ and (*P*)-[**41a**$^{\mathbf{1}}$.H$^+$]TFPB$^-$ in the asymmetric addition of 4,7-dihydroindole **123** to nitroalkene **124** yielding (*R*)-**125**.

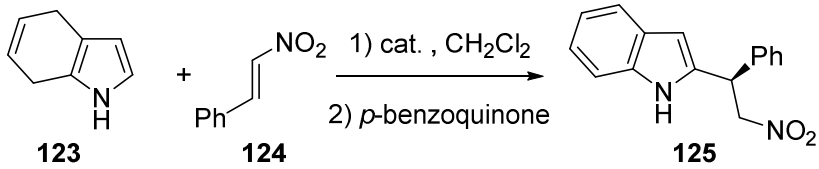

Entry	Catalyst	Mol %	Temp (°C)	Time (hr)	Yield (%)	*er*
1	(*P*)-[**105f**.H$^+$]TFPB$^-$	10	-40	20	80	64:36
2	(*P*)-[**41a**$^{\mathbf{1}}$.H$^+$]TFPB$^-$	10	-40	20	65	53:47
3	(*P*)-[**105g**.H$^+$]TFPB$^-$	10	-40	20	85	69:31
4	(*P*)-[**105g**.H$^+$]TFPB$^-$	2	-40	20	85	69:31
5	(*P*)-[**105c**.H$^+$]TFPB$^-$	2	-40	20	72	69:31
6	(*P*)-[**105d**.H$^+$]TFPB$^-$	2	-40	20	73	83:17
7	(*P*)-[**105b**.H$^+$]TFPB$^-$	2	-40	20	79	92:8
8	(*P*)-[**105e**.H$^+$]TFPB$^-$	2	-40	20	88	93:7
9	(*P*)-[**105e**.H$^+$]TFPB$^-$	0.5	-40	48	80	92:8

In 2011, Takenaka *et al.* used helical chiral 2,2'-bipyridine *N*-monoxides **106** (Scheme 26) in the enantioselective catalytic propargylation of aldehydes **126a**,**b** with allenyltrichlorosilane **127** to yield **128a**,**b** (Scheme 31).[116] The authors first examined the reactivity of allenyltrichlorosilane in Lewis base-catalyzed addition to benzaldehyde using as catalysts pyridyl-N-oxides (*P*)-**70**, (*P*)-**71** and (*P*)-**72** and chiral 2,2'-bipyridine N-monoxides (*P*)-**106** and found that **106** was the best catalyst. Then they applied the optimized conditions to a range of substitued benzaldehydes; for instance, the 2-substituted benzaldehydes gave the best yield and *ee*'s (see **128b** in Scheme 31). The authors proposed a mechanism involving coordination of the helical-bipy-N-oxide to allenyltrichlorosilane and accounting for the stereochemistry of the process.

Scheme 31. Enantioselective catalytic propargylation of aldehydes **126a**,**b** with allenyltrichlorosilane **127** to **128a**,**b** using chiral 2,2'-bipyridine *N*-monoxides **106**. Proposed model for explaining the preferred approach of catalyst (*P*)-**106**. Reproduced from ref. [116]. Copyright 2011, American Chemical Society.

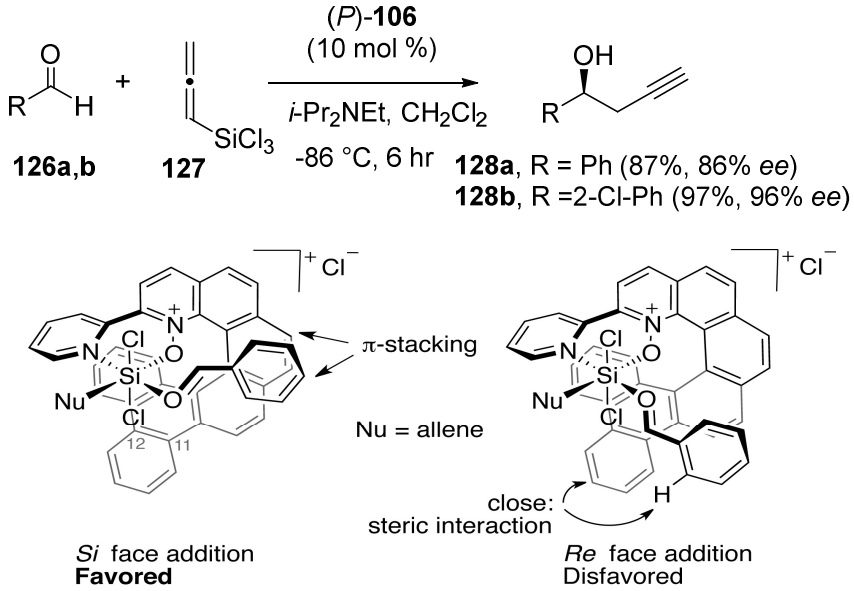

In 2009, Stara and Stary reported the successful utilization of a helicene-based organocatalyst in acylative kinetic resolution of racemic secondary alcohol (Scheme 32).[160] Employing racemic 1-phenylethanol (*rac*)-**129**, optically pure 2-aza[6]helicene (*M*)-**41a**^{2} (5-20 mol %), isobutyric anhydride and *N*-ethyldiisopropylamine in chloroform at 22–40 °C, an asymmetric acyl transfer reaction took place. Moderate reactivity, as well as selectivity factor (s = 9, 10) were observed. An effective control of the enantiodiscriminating step in acylative kinetic resolution by the helically chiral organocatalyst was proven for the first time.

Scheme 32. Kinetic resolution of secondary alcohol (*rac*)-**129** catalyzed by aza[6]helicene (*M*)-**41a**^{2}. Conditions: (*i*-PrCO)$_2$O (1.0 equiv.), (*M*)-**41a**^{2} (5 mole %), *N*-ethyldiisopropylamine (0.75 equiv.), chloroform, rt, 110 h, **129**:**129'** = 47:53 (GC).[160]

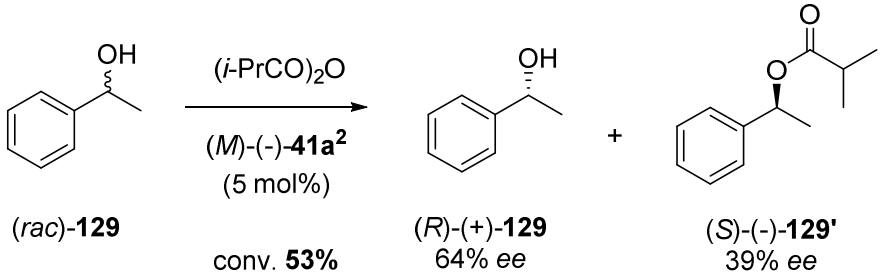

In 2017, Soai reported the reversal of the sense of enantioselectivity between 1- and 2-aza[6]helicenes, i.e. (*P*)-**41a**^{1} and (*P*)-**41a**^{2}, used as chiral inducers of asymmetric autocatalysis during the addition of diisopropyl-zinc to pyrimidine aldehyde **130** yielding secondary alcohols, either (*R*)- or (*S*)-**131** (Scheme 33).[161]

Scheme 33. Asymmetric autocatalytic Soai's reaction using (*P*)-**41a**^{1} and (*P*)-**41a**^{2}, with reversal of the sense of enantioinduction. Adapted from ref. [161]. Copyright 2017, Royal Society of Chemistry.

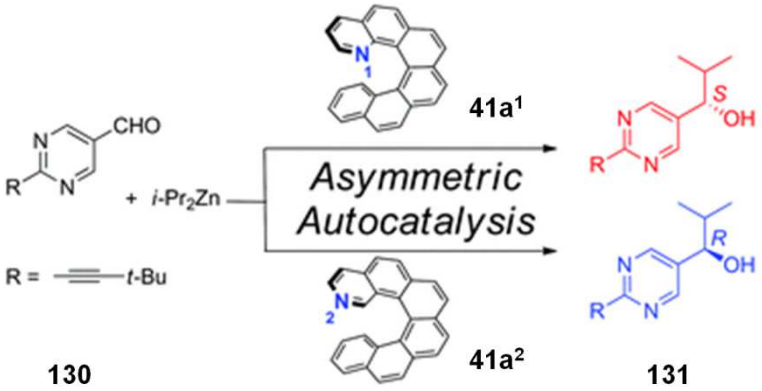

4.1.2. Azahelicenes with fused carbazole cycles (pyrrolohelicenes)

Pyrrole-incorporating PAHs have been shown to possess remarkable physical properties such as effective hole-transporting ability and bright emission. Heteroles such as furan, pyrrole, and thiophene are typical electron-rich heteroarenes. They have been used to constitute extended π-conjugated systems with a characteristic low oxidation potential.[162,163,164, 165,166] However, introduction of pyrroles in the helical backbone gives more open structures that are more prone to racemization. For this reason, few examples of enantioenriched carbazoles have been described in the literature. There are presented below.

4.1.2.1. Carbazoles from oxidative photocyclization

In 2015, precursor **132** bearing a chloro-quinoline and a carbazole unit was subjected to classical oxidative photocyclization (Scheme 34) to give a racemic [6]helicenic structure (*rac*)-**133** incorporating a pyridine and a pyrrole ring.[167] The chloro group was then substituted with (*S*)-(-)-α-methyl-benzylamine substituent by a Buchwald-Hartwig coupling to give **134a**,**b** (1:1 mixture of diastereomers). The diastereomers were readily separated *via* standard chromatography and characterized by ECD spectroscopy. These diastereomers were configurationally very stable at room temperature and no racemization was observed after heating the diastereomers at 150 °C for 12 hours. Other enantioenriched derivatives bearing bromo (**135**) and carboxaldehyde (**136**) substituents were also prepared by post-functionalization of **134a**,**b**.

Scheme 34. a) Synthesis of bis-aza[6]helicene diastereomers **134a**,**b**. Structure of their derivatives **135**,1**36** b) UV-vis spectra of compounds **133** (black), **134b** (red), **135** (green), and **136** (blue) in $CHCl_3$. (c) ECD spectra of diastereomers (*P*,*S*)-**134b** (black), (*M*,*S*)-**134a** (red), (*P*,*S*)-**135** (green), and (*P*,*S*)-**136** (blue) in $CHCl_3$. Adapted from ref. [167]. Copyright 2015, American Chemical Society.

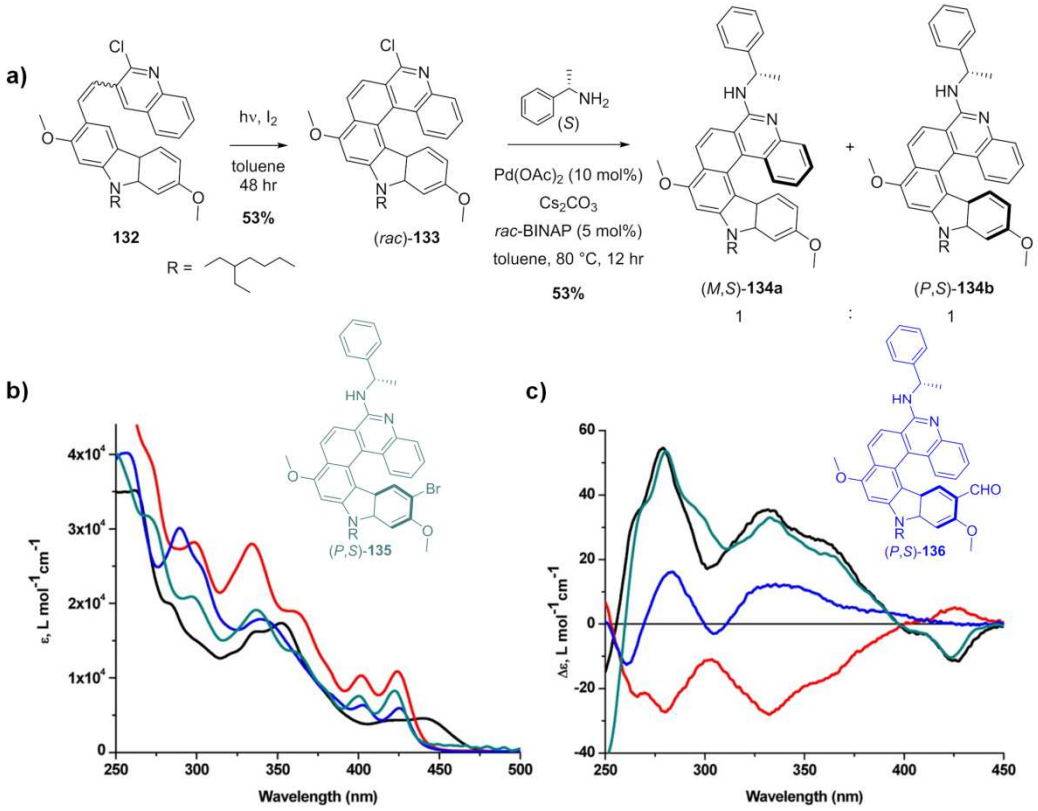

Bedekar *et al.* reported the synthesis of aza[7]helicene in 2014,[168] and aza[9]helicene in 2016,[169] bearing a central *N*-butyl-carbazole unit (Scheme 35). Upon classical oxidative photocyclization process, the "angular-angular" compound **139a** was obtained together with other isomeric structures named "angular-linear" **139b**, 'linear-linear" **139c** and "linear-fused-angular" **139d**. The authors found that the proportion of **139a** was increased in more diluted conditions. Nonahelicene **139a** was obtained in enantiopure forms by HPLC separations over a Chiralcel OD-H; IPA (10% in *n*-hexane). However their chiroptical properties were not reported, neither its configurational stability. From the X-ray structures (see Scheme 35) angle between two terminal rings, *i.e.* helicity for compound **139a** is 7.92° which means that they are almost parallel, while bis-fluorinated pyrrolo[7]helicene (**140d**) shows a helicity of 35.84.[168] The photophysical properties of **139a-d** and **140d** were studied (Table 11). They display blue-green emission with moderate quantum yields between 0.07-0.21 in solution.

Scheme 35. Synthesis of aza[7]-(**140d**)[168] and aza[9]helicenes (**139a**)[169] with a central *N*-butyl-carbazole units. Regioselectivity of the photocyclization to **139a**.

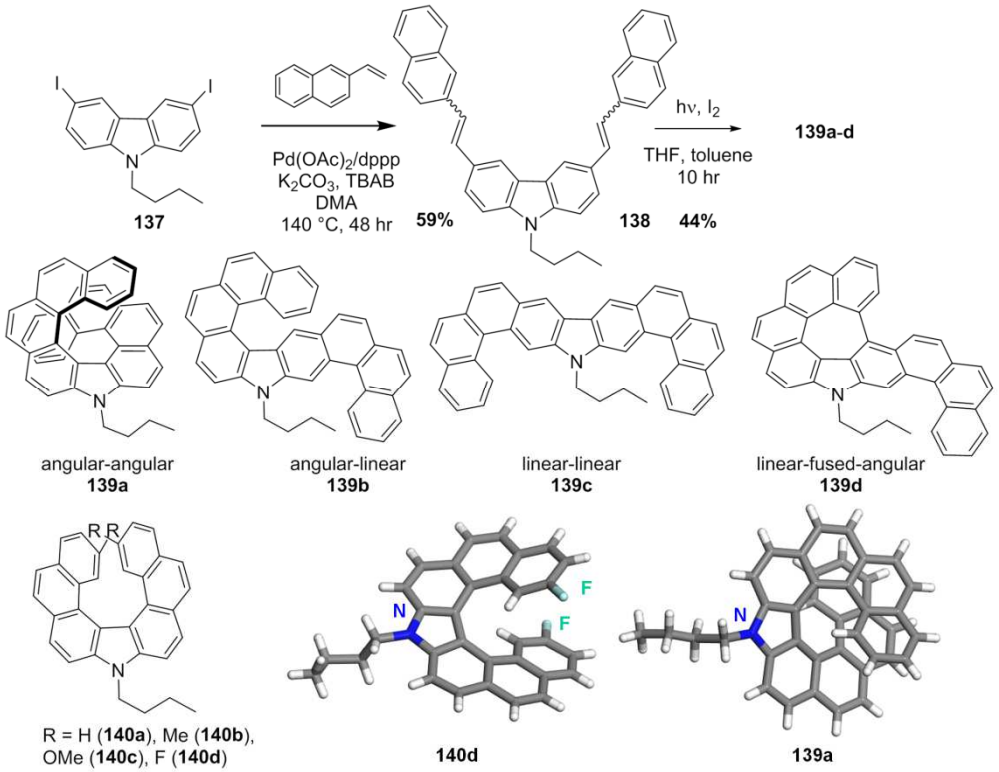

Table 11. Photophysical properties of **139a-d**.[169]

Compound	λ_{Abs} (nm)	λ_{Em} (nm)	Φ (CH_2Cl_2) (%)
139a	289	451	20
139b	348	465, 488	19
139c	299	477, 508	21
139d	338	529, 578	7

4.1.2.2. Carbazoles from palladium-catalyzed cyclodehydrogenation

A new hetero[7]helicene **142** (Scheme 36) incorporating a diazabenzo ring core[165] was successfully synthesized by Ryo Irie *et al.* by a catalytic domino cyclodehydrogenation using $Pd(OAc)_2$ and O_2 as the key step[170] (see also [171]). Significantly, **142** was stereochemically stable at room temperature and could be enantiomerically resolved by chiral HPLC using Chiralcel IC (eluent: hexane/THF = 9/1). Furthermore, a Gibbs energy of racemization $\Delta G^{\#}_{298K}$ = 31.7 kcal/mol was obtained experimentally. Its specific rotation was measured (Table 12) but the absolute configuration was not assigned. DFT calculations on *OO* (**143a**), *NO* (**143b**), and *NN* (**143c**) analogues ($\Delta G^{\#}_{298K}$ = 22.5, 24.8, and 26.5 kcal mol^{-1}, respectively) revealed that the stereochemical stability of the benzodiheterole-based helicenes was highly dependent

not only on the heteroaromatic ring component but also on the N-substituent of the pyrrole ring unit. Note that these compounds all contain a benzodiheterole core.

Scheme 36. Synthesis of heptahelicenic indolopyrrole **142** and structure of N,O analogues (**143a-c**).[170]

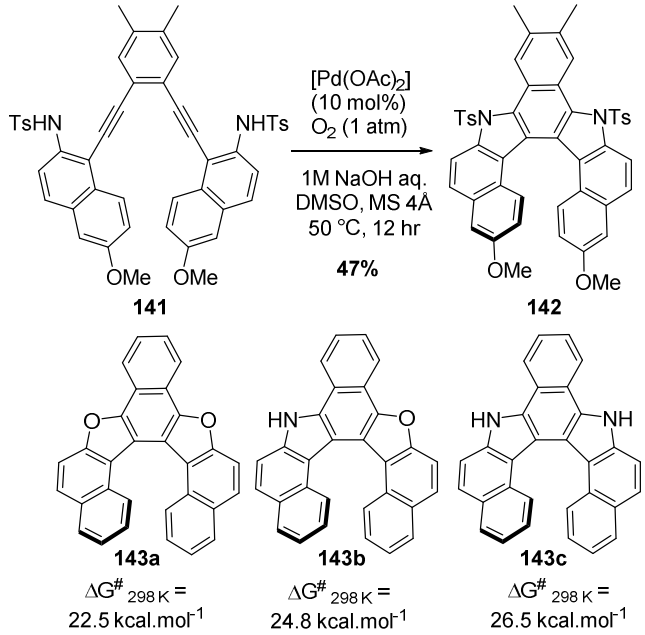

4.1.2.3. Intramolecular N-arylation

Dibenzofurans can be prepared through the intramolecular *O*-arylation of 2'-hydroxybiphenyl-2-yl halides while the related double *N*-arylation of primary amines with 2,2'-dihalobiphenyls or biphenylylene-2,2'-disulfonate can give access to carbazole derivatives. In 2005,[69] Nozaki's group applied this strategy to prepare racemic and enantioenriched aza[7]helicene (*P*)-**149** and oxa[7]helicene (*P*)-**147**, *i.e.* structural analogues of carbo[7]helicene where the central phenyl ring has been replaced by either a pyrrole or a furan cycle (Scheme 37). To do this, they first performed the enantiomeric resolution of 4,4'-biphenanthrene-3,3'-diol **144** through the column chromatography separation of its diastereomeric camphorsulfonyl esters (S_a,*S*,*S*)-**145a** and (R_a,*S*,*S*)-**145b** followed by their hydrolysis to (S_a)-**144** and (R_a)-**144**, respectively. Then, through the Pd-catalyzed double *N*-arylation of the bis-nonaflate (nonafluorobutanesulfonate) (S_a)-**148** in the presence of Xantphos under the conditions described in Scheme 37, (*P*)-**149** was obtained with 94% yield and 99% *ee*, while the Pd-catalyzed intramolecular double *O*-arylation of hydroxy-biphenanthryl-nonaflate (*S*)-**146** in the presence of a biphenyl phosphine ligand gave (*P*)-**147** with 49 % yield and 94% *ee*. The absolute configurations of **147** and **149** were obtained by measuring the specific optical rotations ((*P*)-**149**: $[\alpha]_D^{22}$ = +2310 ($CHCl_3$, *C* 0.1); ((*P*)-**147**: $[\alpha]_D^{22}$ = +1430 ($CHCl_3$, *C* 0.1)). Note that the oxa[7]helicene **147** was not configurationally stable at 100 °C (42% *ee* measured after heating at 100 °C in toluene for 88 hours), which forced the authors to perform the reaction during 13 hours only instead of 123 hours for the preparation of **149**. Note also that structural diversification can be achieved upon bromination of racemic aza[7]helicene at positions 5 and 7 followed by ester synthesis.

Scheme 37. Synthesis of enantioenriched aza[7]helicene (*P*)-**149** and oxa[7]helicene (*P*)-**147** from enantiopure (S_a)-**146/148**. Enantiomeric resolution of bisphenanthrol (*rac*)-**144**.[69]

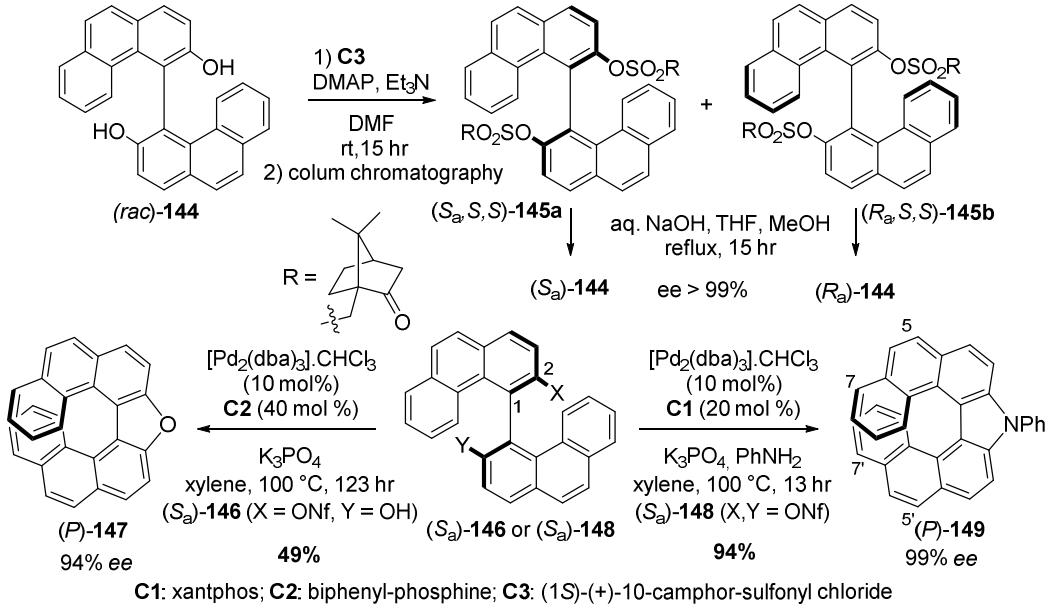

4.1.2.4. Double Bucherer-carbazole-synthesis

The first di-pyrrolo[6]helicene to be prepared was compound **152a** prepared in 1927 in racemic form by Fuchs and Niszel *via* a nonphotochemical approach (Scheme 38)[173] Following the same preparative pathway, Pischel *et al.* reported in 1996 the synthesis of the corresponding tetramethyl derivative **152b**[174] in less than 1% yield and succeeded in separating its enantiomers using chiral HPLC (Cellulose-tris (3,5-dimethylphenylcarbamate) (CDMPC), n-hexane/isopropanol, 9:1 as eluent).

Scheme 38. Synthesis of di-pyrrolo[6]helicene **152a** and **152b**.[173,174]

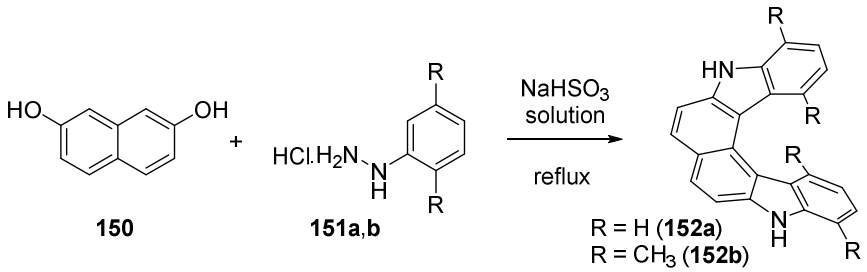

4.1.2.5. Enantioselective Fischer indolization

In 2014, List and coworkers reported the first asymmetric organocatalytic synthesis of helicenes, using a SPINOL-derived phosphoric acid bearing extended π-substituents as the chiral Brönsted acid asymmetric catalyst.[175] Upon condensation of a phenylhydrazine with an appropriate polyaromatic ketone, enantiopure Brönsted acid **157** might promoted asymmetric [3,3] sigmatropic rearrangement and furnished enantioenriched pseudo-helical (tetrahydro-helicene) **155a** and its corresponding azahelicenes

156a after oxidation. The approach appeared modular and a variety of azahelicenes (**155a-e**) could be obtained with good to excellent yields and enantioselectivities (see Scheme 39 and Table 12). ECD spectra enabled to recognize that the typical double Fischer indolization followed by oxidation led to diazahelicene (*P*)-**156f** with 88% *ee*, bearing one benzyl group, and then to (*P*)-**156g** after benzylation. The authors put forward the concept of asymmetric catalysis at the nanoscale and propose a catalytic intermediate (Figure 20) to account for the high enantioselectivities. Extended π-substituents in the 3,3'-position were needed for π–π stacking interaction with the polyaromatic system present in the formed enehydrazine, holding the intermediate in a chiral nanometer-sized pocket, and the catalyst could induce the screw sense of the helicene.[175]

Scheme 39. Asymmetric organocatalytic synthesis of helical tetrahydrohelicenes **155a-e, 156a** and helicenes **156f**,**g**

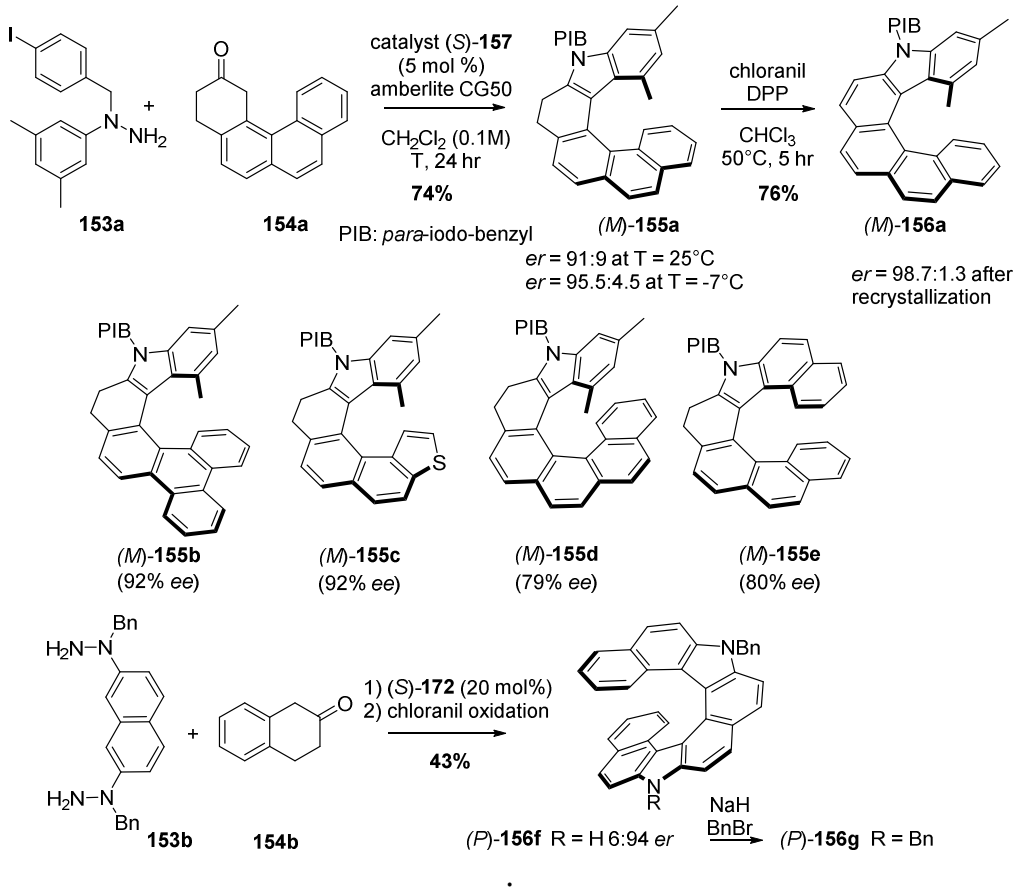

.

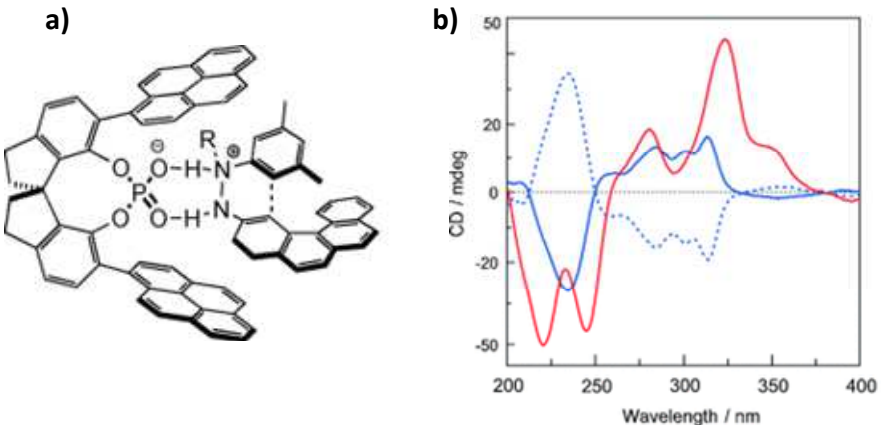

Figure 20. a) Catalytic intermediate model for (*S*)-**157**-enehydrazine intermediate. b) ECD spectra of (*P*)-**155a** (blue line), (*P*)-**156a** (red line), and (*M*)-**155a** (blue dashed line) in methanol. Adapted from ref. [175]. Copyright 2014, Wiley.

4.1.2.6. Oxidative fusion of pyrroles

In 2017, Osuka group reported the oxidative fusion reactions of ortho-phenylene bridged cyclic hexapyrroles and hexathiophenes yielding closed helicenic structures which were characterized by X-Ray diffraction analysis as a closed pentaaza[9]helicene (**159**), together with a double-helical structure of hexathia-[9]/[5]helicene (**161**), whose formation was assumed to result from multiple oxidative fusion along with a 1,2-aryl shift (Scheme 40).[176] The pentaaza[9]helicene exhibited well-defined emission with high fluorescence quantum yield (Φ_F = 0.31) among the known [9]helicenes. The racemic mixtures of **159** and **161** were enantiomerically resolved by HPLC using Chiralpak-IE as the chiral stationary phase and either *n*-hexane/THF (1:1) or *n*-hexane/$CHCl_3$ (3:1) as the eluents. ECD spectra of the enantiomers were recorded and showed mirror-imaged spectra (see Scheme 40c). The absolute configuration of each enantiomer was determined by comparison of experimental with the calculated ECD spectra at the B3LYP/6–311G(d,p) level of theory thus indicating that the first eluted samples corresponded to the (*P*)-**159** and (*P*,*P*)-**161**.[176]

Scheme 40. Synthesis and characterization of a pentaaza[9]helicene (**159**) and of a double-helical structure of hexathia-[9]/[5]helicene (**161**). (a)-(d) Photophysical properties (absorption and emission) together with ECD spectra. Adapted from ref. [176]. Copyright 2017, Wiley.

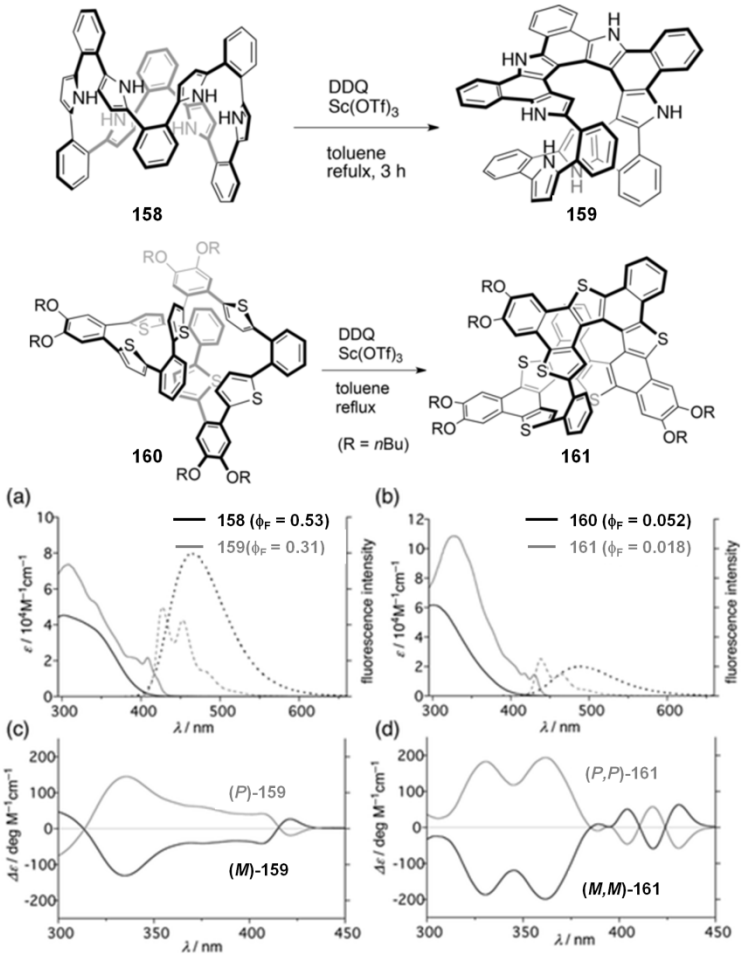

Using a similar procedure, Tanaka, Osuka *et al.* prepared in 2018 **163a-c** in their racemic forms (together with cyclic derivatives **164a**,**c**, Scheme 41); their enantiomers were obtained by chiral HPLC using a SUMICHIRAL OA3100 stationary phase (*n*-hexane/THF 60/40 as eluent).[177] The second-eluted sample was found to be the (*P*)-helicene through the ECD measurement and calculations. The racemization activation free energy was estimated by Eyring equation to be low ($\Delta G^{\#}_{298K}$ = 23.8 kcal mol^{-1} for **163b**).

Scheme 41. Synthesis of trisaza[7]helicenes **163a-c** from **164a-c**.[177]

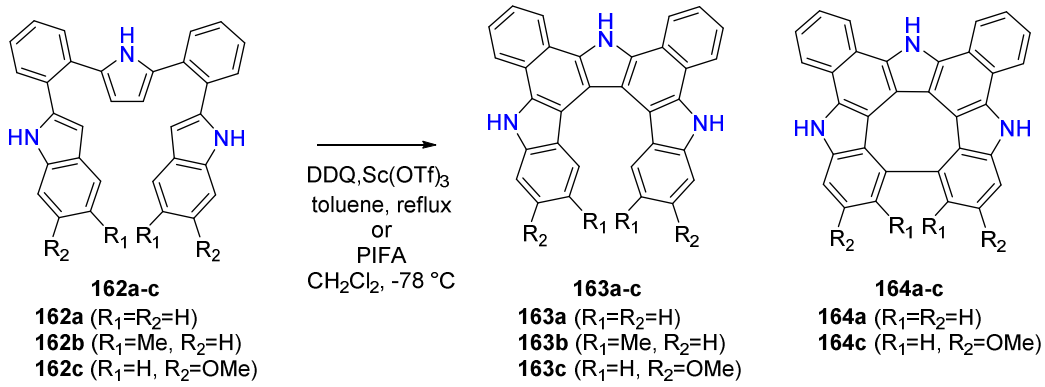

162a-c
162a (R_1=R_2=H)
162b (R_1=Me, R_2=H)
162c (R_1=H, R_2=OMe)

163a-c
163a (R_1=R_2=H)
163b (R_1=Me, R_2=H)
163c (R_1=H, R_2=OMe)

164a-c
164a (R_1=R_2=H)
164c (R_1=H, R_2=OMe)

In 2012, Hiroto, Shinokubo, *et al.* reported the selective oxidative fusion of 2 aminoanthracenes mediated by DDQ to provide pyrazine-fused bisanthracenes together with pyrrole-fused dimer **167a**,**b** obtained as by-products and displaying an aza[5]helicenic structure with a stable helical conformation thanks to the presence of bulky ethynylsilylated groups (Scheme 42).[178] ECD and CPL activity were indeed measured for enantiopure compounds prepared by chiral HPLC resolution over a CHIRALPAK-IA column using ethyl acetate/hexane (1:10) as the eluent.

In 2015, a double N-hetero[5]helicenes composed of two nitrogen-substituted heteropentacenes were synthesized by tandem oxidative C-N couplings reaction.[179] These double N-hetero[5]helicenes displayed larger helicities than typical [5]helicenes. Furthermore, their optical/electrochemical measurements revealed a significant increase in the electronic communication between the two heteropentacene moieties of the double helicenes compared with their cruciform dimers. The optical resolution of one of the double helicenes was successfully carried out, and their stability towards racemization was found significantly higher than those of typical [5]helicenes. Compounds **166a** and **167a** showed fluorescence with strong quantum yields in solution (Φ_F = 0.45 for **166a** and Φ_F = 0.36 for **167a**). The Stokes shift of **167a** (2220 cm^{-1}) was larger than that of **166a** (473 cm^{-1}), which reflected the distorted conformation of **167a**. Several carbazole-based azahelicenes have been reported but mostly in the [5]helicene series, *i.e.* displaying no configurational stability and few of higher helicenes have been reported yet. CPL anisotropy factor g_{lum} was measured to be 3×10^{-3} for both enantiomers of **167a**, which is comparable to the values observed for other helicenes.

Scheme 42. (A) Preparation of a configurationally stable azapentahelicenes **167a,b**. (B) X-ray structure of **167a** (hydrogen atoms, and silyl groups have been omitted for clarity). (C) Photophysical properties. a) UV/Vis absorption and b) emission spectra of **166a** (blue), **167a** (red), and **168** (black) in CH_2Cl_2 with excitation at 400 nm. c) ECD and CPL spectra of (*P*)-**167a** (black) and (*M*)-**167a** (red) in CH_2Cl_2. The blue lines show the ECD spectrum for (*P*)-**167a** calculated by TD-DFT at the B3LYP/6-31G(d) level. Adapted from ref. [178]. Copyright 2012, Wiley.

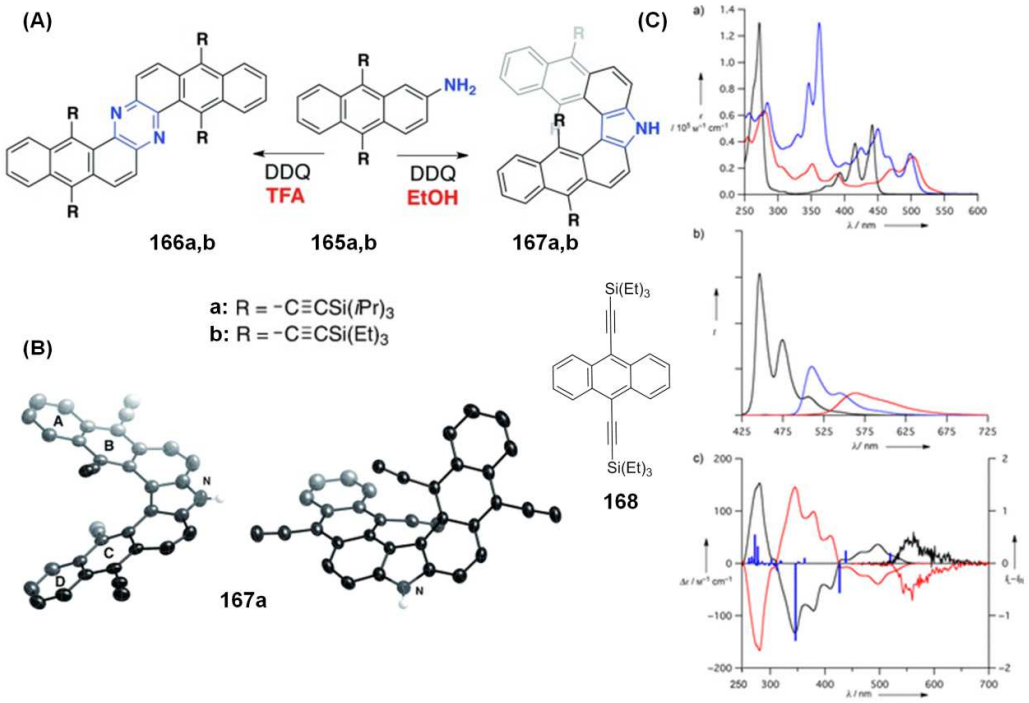

4.1.2.7. Diels-Alder reactions

In 1999, Katz and coworkers reported the preparation of heterocyclic helicenes **172a-d** (Scheme 43) that were easily prepared in gram quantities by a double Diels-Alder reaction between bis-dienes **184a-d** and *p*-benzoquinone to give **170a-d** (together with isomers that were easily separated either by crystallization or by column chromatography).[180] Then after deprotection of OTIPS groups followed by *O*-alkylation, heterohelicene-bis-quinones **171a-d** were resolved into their enantiomers. Reduction by zinc and esterification with (*S*)-(-)-camphanoyl chloride gave camphanate esters **172a-d** which were separated into almost pure diastereomers (>97% *ed*) by silica gel chromatography. The absolute configurations were deduced from the ECD spectra. The camphanate could then be removed by the action of MeLi or BuLi, and oxidation with chloranil to yield back **171a-d**. When solutions of **171a-c** in DMF were heated at 78 °C for 24 h, the ECD responses of **171b** and **c** decreased by 5-13%, and that of **171a** decreased by 45%. Moreover, the specific rotations of the (*P*)-(+)- and (*M*)-(-)-**171b** respectively, from the (+)- and (-)-diastereomers of **172b** are identical except for their signs: +1350 and -1300 (*c* 0.030, CH_2Cl_2). Note that specific rotations of **172a**,**c**, and **d** at the D wavelength could not be measured because the compounds absorb too strongly at 589 nm.

Scheme 43. Synthesis of heterocyclic helicenes **171a-d**/**172a-d**: *i*) CsF, *n*-BuI, DMF, 60 °C (86-99% yields); *ii*) (*S*)-(-)-camphanoyl chloride **C4**, Zn, $(Me_2NCH_2)_2$, PhMe, reflux (75-92% yields); *iii*) MeLi or BuLi, then chloranil.(63-88% yields).[180]

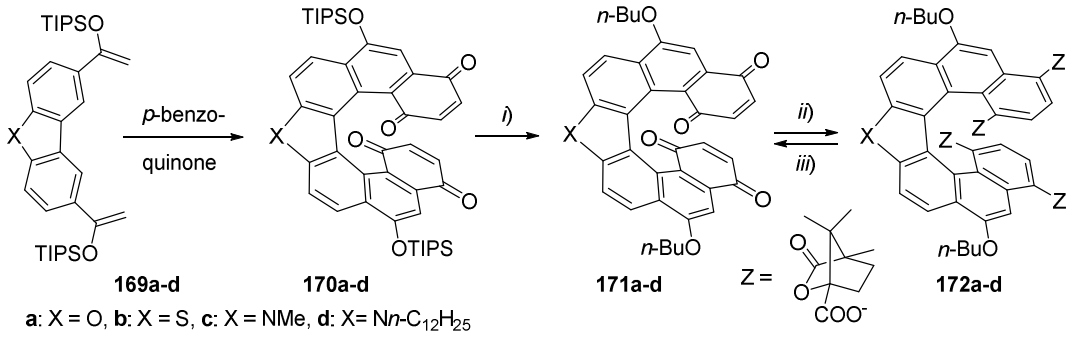

Table 12. Specific rotation values of enantioenriched helical carbazoles.

Compound	Method of obtention	$[\alpha]_{D\ exp}$ [a]	Conditions[b] (solvent/Conc.[c])	Enantio/diastereo-purity	Ref.
(+)-**142**	Chiral HPLC[d]	+98.5	$CHCl_3$/1.03	>99 % *ee*[d]	170
(*P*)-**147**	From (S_a)-**144**	+1430	$CHCl_3$/0.1	94% *ee*	69
(*P*)-**149**	From (S_a)-**144**	+2310	$CHCl_3$/0.1	>99% *ee*	69
(P)-**152b**	Chiral HPLC[e]	+588	$CHCl_3$/0.02		174
(*M*)-**155a**	Enantioselective Bronsted acid catalysis	-454.2	CH_2Cl_2/0.38	91% *ee*[f]	175
(*P*)-**156a**	From (*P*)-**170a** then recryst.	+1162	CH_2Cl_2/0.16	97.4% *ee*[g]	175
(*M*)-**155b**	Enantioselective Bronsted acid catalysis	-574.4	CH_2Cl_2/0.50	92% *ee*[f]	175
(*M*)-**155c**	Ibid.	-528.5	CH_2Cl_2/0.41	92% *ee*[g]	175
(*M*)-**155e**	Ibid.	-536.7	CH_2Cl_2/0.36	79% *ee*[f]	175
(*P*)-**156f**	Ibid.	+535.2	CH_2Cl_2/0.15	88% *ee*[g]	175
(*P*)-**156g**	From (*P*)-**156f**	+382.6	CH_2Cl_2/1.0	n.d.	175
(*M*)-**172c**	Separation of covalent diastereomers	-280	CH_2Cl_2/1.0	>97% *de*	180
(*P*)-**172c**	Ibid.	+220	CH_2Cl_2/0.045	>97% *de*	180

[a] In $deg \cdot mL \cdot g^{-1} \cdot dm^{-1}$. [b] Measured at 25 °C. [c] In g/100 mL. [d] Chiralcel IC, eluent: hexane/THF = 9/1. [e] (Cellulose-tris (3,5-dimethylphenylcarbamate) (CDMPC), *n*-hexane/isopropanol, 9:1, as eluent). [f] Chiralcel OD-RH, eluent: MeCN/H_2O mixture. [g] Chiralpak OD-3R, eluent: MeCN/H_2O mixture.

Note that VROA spectra of four representative helicenes, hexahelicene, tetrathia-[7]-helicene and its pyrrole and furan analogs, were simulated by Liegeois and Champagne and interpreted using computational and visualization tools in order to detect signatures of their helicity combined with π-electron conjugation.[181] Helicenes show intense VROA peaks attributed to their π-conjugated structure and associated with collective vibrational modes. In hexahelicene, the dominant VROA features are due to vibrational modes involving motions of the carbon skeleton and H-wagging but the intensity finds its source almost exclusively in the former. In the case of the three heterohelicenes, the previous statement is also verified where some fingerprints could therefore be associated with the helicity of the system. In particular, most of the VROA bands are positive for left-handed helicenes, and it was found that the major

role of the heteroatom is restricted to modifying the geometry and the normal modes. It would have been interesting to compare with VROA experiments but this is mostly prevented by the strong emission properties of these compounds at the measurement wavelength. Furthermore, a racemic radical cation and neutral radical with good persistence were generated from a pyrrolo-thia[7]helicene by Rajca *et al.* who showed by DFT calculations and by electrochemistry that the SOMO and HOMO energy levels were reversed in this case.[182]

4.1.3. Pyrazine-containing helicenes

Recently, oligoacenes containing pyrazine units have attracted much attention as promising compounds for electron-transporting materials because of their resistance to oxidation relative to the parent oligoacenes. A series of fluorescent "push-pull" tetrathia[9]helicenes **175a-d** based on quinoxaline (acceptor) fused with tetrathia[9]helicene (donor) derivatives was synthesized for control of the excited-state dynamics and circularly polarized luminescence (CPL) properties.[183] Introduction of a quinoxaline onto the tetrathia[9]helicene skeleton induced the "push–pull" character, which was enhanced by further introduction of an electron-releasing Me_2N group or an electron-withdrawing CN group onto the quinoxaline unit (**175c** and **175d**, respectively, Figure 21). Significant enhancements in the fluorescence quantum yields (Φ_F) were achieved. In particular, the maximum quantum yield of **175c** was 0.43 in benzene (Φ_F = 0.30 for **175d**), which is much larger than that of a pristine tetrathia[9]helicene (**TTH**; Φ_F = 0.02). These enhancements were also explained by the kinetics of the excited-state dynamics such as fluorescence and intersystem crossing (ISC) pathways. Such significant enhancements of the Φ_F values thus gave good CPL properties, with anisotropy factor g_{lum} estimated to be 3.0×10^{-3} for **175d**.

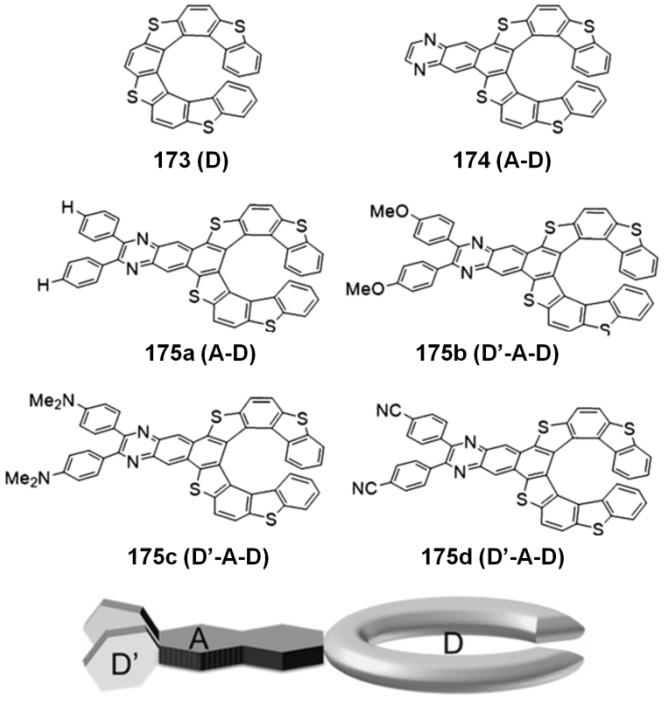

Figure 21. Push-pull systems **175a-d** with improved fluorescence and CPL emission. Adapted from ref. [183]. Copyright 2016, Wiley.

In 1999, phthalocyanines such as **176** (Figure 22) fused to four nonracemic [7]helicene units and bearing long chains have been prepared and studied by Katz, Persoons and collaborators. These molecules have shown to aggregate in appropriate EtOH-$CHCl_3$ solvent mixtures.[184] Chiral Langmuir-Blodgett films were also prepared and displayed very strong second-order NLO activity. In 1996, soluble helical conjugated ladder polymers with an average molecular weight of 7000 g/mol were also prepared by Katz *et al.*, by reaction of 1,2-phenylenediamine with enantiopure [6]helicene derivative in the presence of a metallic ion, through the well-known salophen coordination chemistry.[185,186]

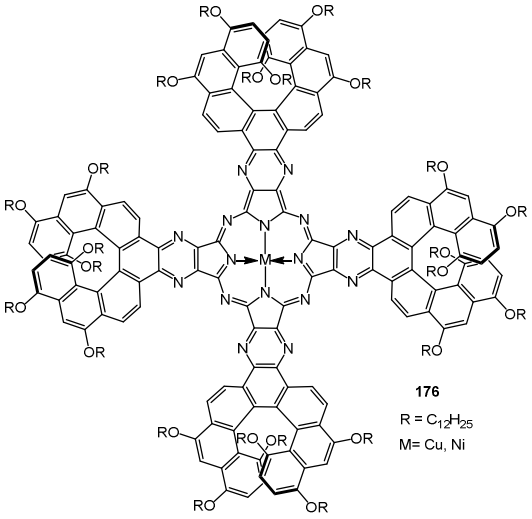

Figure 22. Phthalocyanine **176** capped with [7]helicene and displaying strong NLO activity.[184]

4.1.4. Helicene-dimide systems

In 2015, Dehaen et *al*. described a detailed study about the diastereoselective synthesis of thia[*n*]helicenes bearing a central maleimide cycle, using different types of chiral auxiliary motifs which were positioned at different places in the helicene scaffold, in order to enhance the selectivity and then the enantiomeric separation.[187] The strategy of placing the chiral unit at the maleimide moiety was not effective and the oxidative photocyclization generated non separable diastereomers (*P*,*S*) and (*M*,*S*)-**179** (Scheme 44). On the contrary, substitution of the helicene core at the most sterically hindered position yielded amplified chiral induction. Indeed, a chiral amine α-methyl-benzylamine moieties were attached at the two inner extremities of the olefin precursors **180** and the oxidative photocyclization to **181a,b** was carried out in a varieties of solvents in order to study the effect of the solvent in the diastereomeric ratios (Table 13). In toluene, after 1h, the diastereomeric ratio was 64:36 as determined *via* ^{1}H NMR spectra (entry 1). The use of polar solvents such as or 1-butyl-3-methyl-imidazolium chloride [bmim][Cl] (entry 2) gave inverted ratio 31:69 at around 55-60 °C. The effect of temperature was studied in DMF; a ratio of 38:62 at 55-60 °C (entry 3) led to an increased diastereoselectivity to 30:70 at temperature around 20-22 °C (entry 4). The authors suggest that the intramolecular hydrogen-bonding interactions play an important role in the diastereomeric ratio. In Table 14 is depicted the effect of different conditions on the cyclization of thiahelicenic derivative **182** substituted with chiral oxazolines to **183a**,**b**. Besides the solvent influence (entry 1 vs. entry 2), it was shown that the presence of $(CF_3SO_3Cu)_2.C_6H_5CH_3$ in toluene during the

photocyclization significantly improved the stereoselectivity as compared to similar conditions without any Cu(I) source, suggesting that the coordination to copper enabled to preorganize the system in a fixed geometry.

Scheme 44. Synthesis of thiahelicenes bearing a central imide ring.[187]

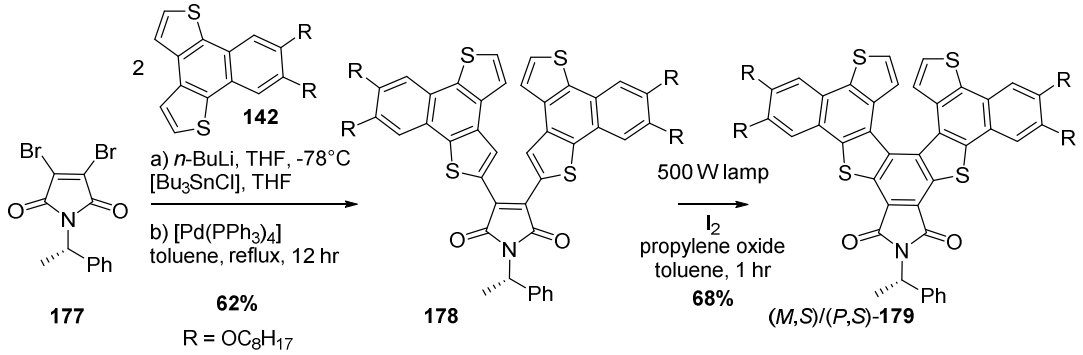

Table 13. Effect of the solvent and temperature on the diastereoselectivity of oxidative photocyclization of **180** to **181a**,**b**. [187]

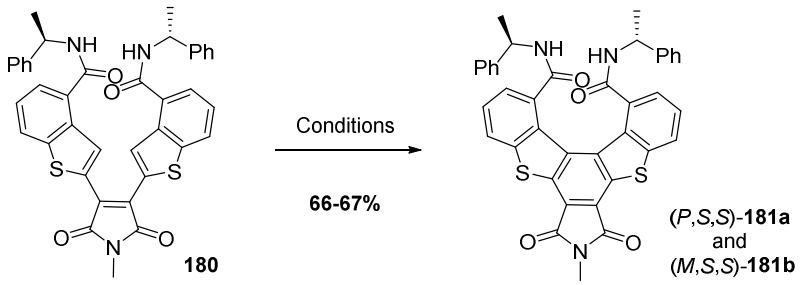

Entry	Conditions	*dr* (*P*,*S*,*S*):(*M*,*S*,*S*)
1	500W lamp, I_2, toluene, 1hr	64:36
2	500W lamp, I_2, or [bmim]Cl, 1hr, 55-60 °C	31:69
3	500W lamp, I_2, DMF, 1hr, 55-60 °C	38:62
4	500W lamp, I_2, DMF, 1hr, cooling, 20-22 °C	30:70

Table 14. Effect of the solvent and presence of copper (I) ion on the diastereoselectivity of oxidative photocyclization of **182** to **183a**,**b**.[187]

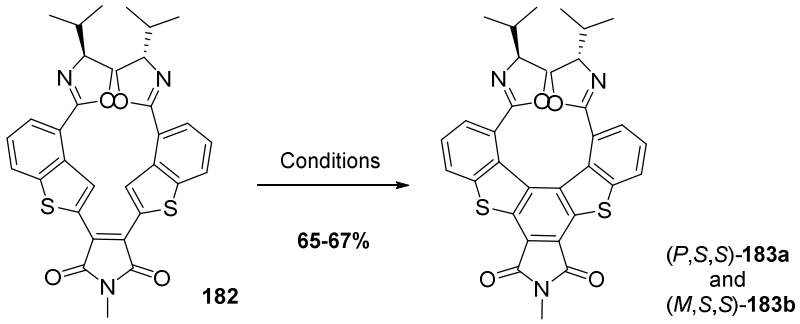

Entry	Conditions	*dr* (*P*,*S*,*S*):(*M*,*S*,*S*)
1	500W lamp, I_2, toluene, 2hr	66:34
2	500W lamp, I_2, DMF, 2hr	70:30
3	500W lamp, I_2, $(CF_3SO_3Cu)_2 \cdot C_6H_5CH_3$, toluene, 2hr	100:0

In 2016, Chuan-Feng Chen and coworkers reported the preparation of helical aromatic imide based enantiomers with full-color circularly polarized luminescence.[188] For this purpose they performed a Diels-Alder reaction of diene **184** with maleic anhydride to yields the helical anhydride **185** which was then oxidized to **186** (Scheme 45). Reaction with *n*-propylamine gave racemic imide (*rac*)-**187** which was then enantiomerically resolved by SFC chiral resolution (see conditions in Table 15). Each (*P*)-(-) and (*M*)-(+) enantiomer of **187** was then post-functionalized to (*P*)-(-)- and (*M*)-(+)-**188a-e.** A racemization Gibbs free energy $\Delta G^{\#}$ of 32.8 kcal mol^{-1} at 150 °C was found for **187**, which demonstrated that these helical imides are highly configurationally stable. Each pair of enantiomers displayed rather low opposite optical rotation values and mirror-image ECD spectra. The absolute configurations (Table 15) were found opposite to those of classical heterohelicenes. Aromatic imides are known to display bright emission properties. Indeed, each pair of enantiomers (*P*)-(-)- and (*M*)-(+)-**188a-e** exhibited full colour fluorescence emission (from 445 to 617 nm) and mirror-image CPL signals in THF (Scheme 45). The g_{abs} values of the enantiomers fell in the range of $\pm 1.5 \times 10^{-3}$ to $\pm 3.5 \times 10^{-4}$ and the g_{lum} values between $\pm 0.2 \times 10^{-3}$ and $\pm 1.5 \times 10^{-3}$ (Table 15).

Scheme 45. a) Synthesis of (*P*)-(-)- and (*M*)-(+)-**188a-e**: (i) maleic anhydride (5.0 equiv.), xylene, reflux, 3 h, 89%; (ii) Br_2 (2.0 equiv.), CH_2Cl_2, rt, 3 h, 56%; (iii) *n*-propylamine (5.0 equiv.), DMF, 70 °C, 24 h, 82%; (iv) SFC chiral resolution;(v) arylboronic acid (3.0 equiv.), $[Pd(PPh_3)_4]$ (5 mol%), K_2CO_3 (10.0 eq., equiv.), toluene/EtOH/H_2O (2:2:1), 75 °C, 12 h, 84-99%. b) Emission colours panel of **188a-e**. c) ECD spectra in THF of pure enantiomers. d) CPL spectra in THF of pure enantiomers. Adapted from ref. [188]. Copyright 2016, Royal Society of Chemistry.

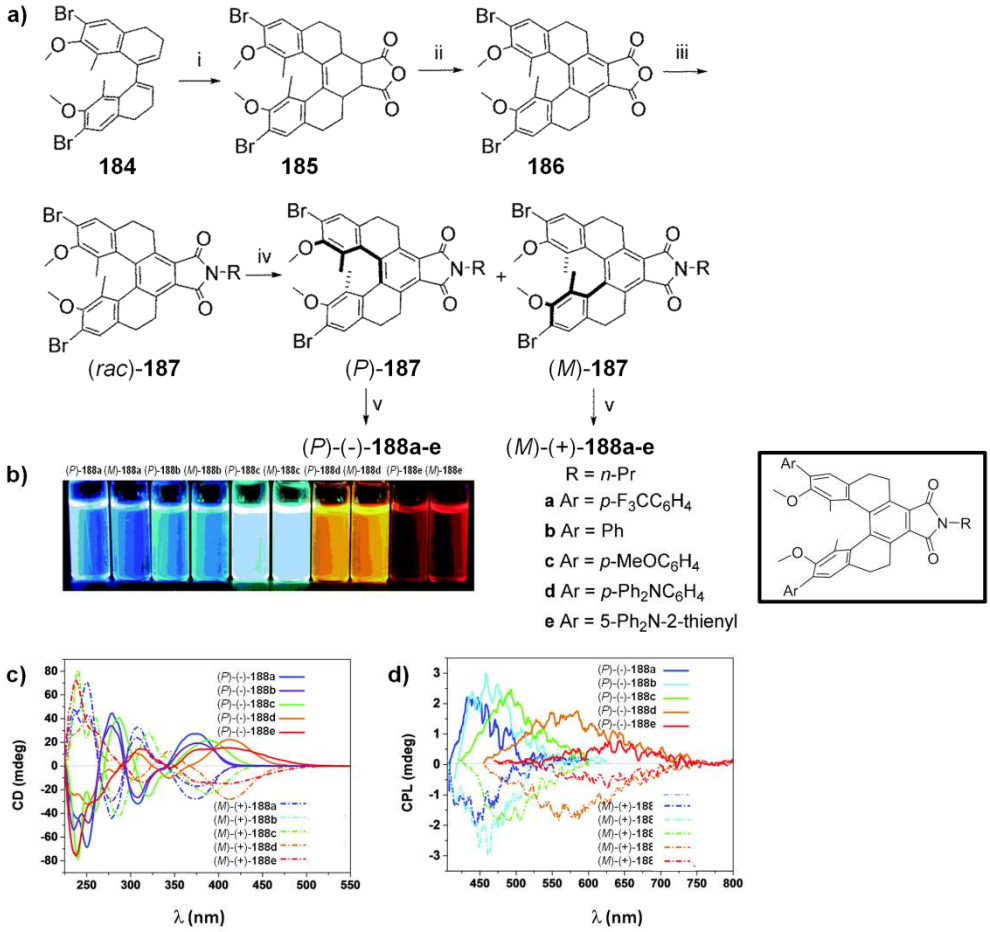

Table 15. Specific rotation values and photophysical data of helical imides **188a-e**.

Compound	Method of obtention	$[\alpha]_D$[a]	Conditions[b] (solvent/Conc.[c])	Enantio-purity	λ_{Abs} (nm)	λ_{Em} (nm)	Φ (% / THF)	g_{lum}	Ref
(*P*)-**188a**	From (*P*)-**187**	-32	N.d.	98.5%[d]	291, 366	445	12.8	-1.2×10^{-3}	188
(*P*)-**188b**	*Ibid.*	-40	N.d.	98.6%[d]	288, 366	457	19.2	-1.5×10^{-3}	188
(*P*)-**188c**	*Ibid.*	-234	N.d.	98.4%[d]	290, 371	482	64.8	-0.8×10^{-3}	188
(*P*)-**188d**	*Ibid.*	-221	N.d.	99%[d]	308, 387	556	40.3	-0.8×10^{-3}	188
(*P*)-**188e**	*Ibid.*	-213	N.d.	98.7%[d]	304, 415	617	7.4	0.2×10^{-3}	188

[a] In $deg \cdot mL \cdot g^{-1} \cdot dm^{-1}$. [b] Temperature between 20-25 °C. [c] In g/100 mL otherwise precised. [d] Chiralpak IC, CO_2/MeOH/CH_2Cl_2=40/30/30.

In 2013, Sasaki *et al.* reported chiral 1,14-dimethyl[5]helicene ligand **188f** containing a central maleimide cycle *N*-linked to a spermine moiety. This compound could enantioselectively bind with B- and Z-DNA, with (*P*)-**188f** displaying a preference for right-handed B-DNA and (*M*)-**188f** for left-handed Z-DNA (Figure 23).[189] The chiral recognition process was investigated by measuring the thermal denaturing temperature (T_m) and binding affinity (K_a) through isothermal titration calorimetry together with surface plasmon resonance experiments. according to the authors, the cationic spermine portion produces electrostatic interactions along the phosphate backbone of the minor groove, and the helicene part forms complexes in an end-stacking mode. **188f** was prepared according to a similar strategy as **188a-e** and enantiomerically resolved by HPLC over a DAICEL OJ-RH column (ACN as the eluent).[189] The same authors found that [5]helicene **188g** containing methoxy groups could bind to B-DNA in its racemic form, with induction of (*P*)-chirality accompanied with a B-to-Z helicity change of the duplex DNA, $[(dC\text{-}dG)_3]_2$. The (*P*)-chirality of the bound **188g**, in turn, transitioned to the (*M*)-chirality within the Z helicity of the DNA. These results illustrate the chirality synchronization between the DNA and the ligand.[190]

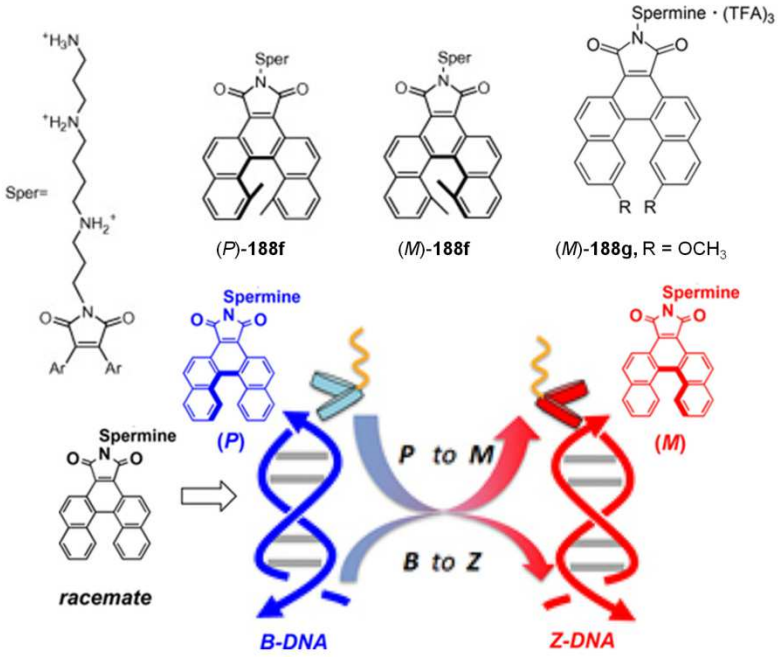

Figure 23. Chiral recognition of pentahelicenes **188f,g** to Z/B-DNA.Adapted from ref. [189]. Copyright 2013, Elsevier Ltd. Reproduced from ref. [190]. Copyright 2017, Wiley.

In 2016, Steigerwald, Nuckolls and coworkers reported the synthesis of a π-extended helical molecule made from the fusion of a perylene-3,4,9,10-tetracarboxylic-diimides (PDI) and helicene units. They first prepared naphthyl-linked PDI-dimer helicene (**190**) which consists of two PDIs incorporated within a [6]helicenic backbone (Figure 24).[191] The enantiomers were resolved by chiral HPLC over CHIRALPAK-IA-3 stationary phase; they were not racemized when heated at 250 °C in diphenyl ether for one hour, and they display intense ECD spectra with pronounced Cotton effects (Figure 24c). More recently, the same group showed that the fusion of two naphthalene subunits with three PDI monomers results in a naphthyl-linked PDI-trimer helix (**189**) displaying a shape-persistent nanoribbon architecture.[192] A racemic mixture of (*M*) and (*P*) helices was obtained after iterative cross-couplings and

oxidative visible-light cyclizations. X-ray diffraction study revealed extensive intramolecular overlap of the π-surface, which locks the nanoribbon into a helical superstructure. The crystal structure also showed formation of supramolecular columns of **189** in the solid state consisting of alternating (*M*) and (*P*)-**189** (Figure 24b). This structure combines the inherent properties of PDI (multi-electron acceptor) and those of helicenes (strong absorption, emission and helical chirality) which are strongly amplified in the superstructure, as evidenced in the very strong ECD response of **189** in comparison to its smaller homologue **190**. Interestingly, the *meso* form was not observed, probably due to the extensive π-to-π overlap between the PDI subunits which preclude inversion of the helicene units. The considerable ECD of **189** distinguishes this new π-helix from **190**, as well as from helicenes in general, with Δε values up to 820 M^{-1} cm^{-1} at 407 nm. Similarly, the g_{abs} values were very much increased since **189** displayed $|\Delta\varepsilon|/\varepsilon$ of 7.9×10^{-3} at 377 nm and 8.9×10^{-3} at 407 nm, a 7.2-fold and 5.9-fold increase over those transitions of **190** at 355 and 401 nm. The two helical structures display similar emission properties, *i.e.* fluorescence around 400 nm in THF. The electrochemical behavior was studied and showed that the system can accept four electrons. Therefore these compounds may be good n-type semiconductors in organic field effect transistors and organic photovoltaics (OPVs). It was for example shown by the same group that racemic similar helical nanoribbons may find application as ultra-narrow band photodetectors.[193] Recently, longer [7]helicenic systems similar to **190** were also prepared in enantiopure forms according to the same strategy.[194]

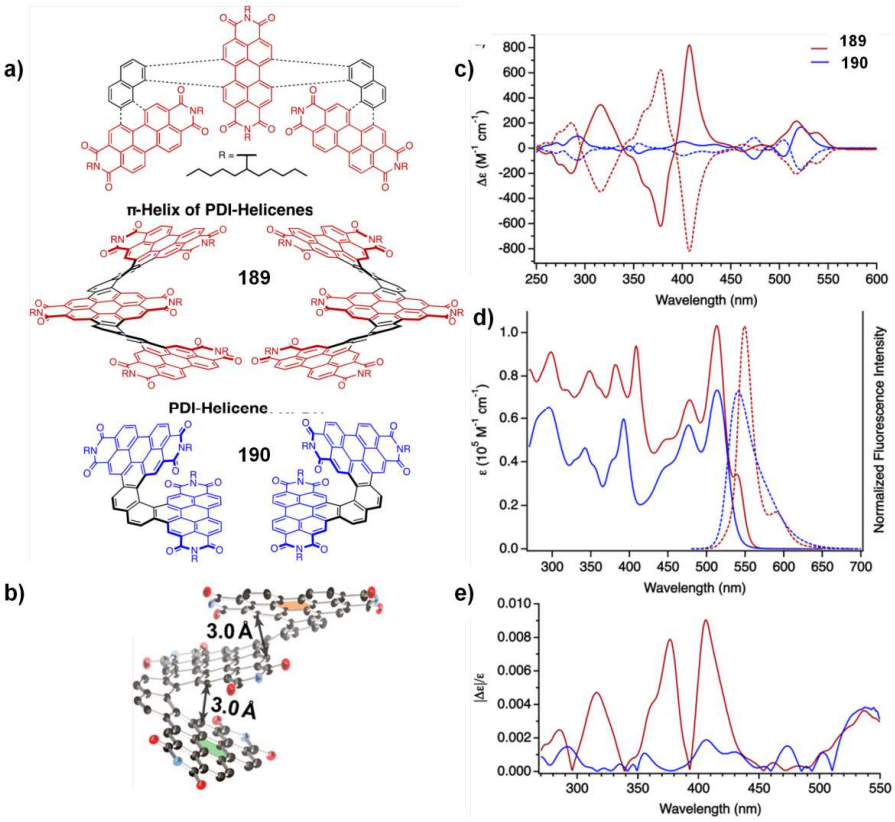

Figure 24. a) Structures of helicene-perylene-diimides **189** and **190**; b) solid state assembly of **189**; c) ECD, d) UV-vis and emission and e) g_{abs} of **189** and **190** enantiomers. Adapted from ref. [191]. Copyright 2016, Wiley. Adapted from ref. [192]. Copyright 2018, American Chemical Society.

4.1.5. Helicene-imidazole derivatives

Helicene-imidazole derivatives are a new series of nitrogen-containing helicenic derivatives that has appeared since 2016.[195,196,197,198] Up to now, only a few examples of imidazolium salts are known in the literature. They include one family of helicene-fused imidazole derivatives, and three families of helicenes grafted with imidazolium groups.

4.1.5.1. Fused helicene-imidazole derivatives

In 2017, our group has described the synthesis of the first helicene fused with an imidazole ring.[195,196,197] To do so, a carbo[4]helicene-1,2-diamine **192** was prepared by reduction of [5]helicene-thiadiazole **191**[199] and was then cyclized to imidazole **193** which exists as a mixture of two tautomeric forms **a** and **b**, as it was observed by NMR (Scheme 46). [5]Helicene-imidazole **193** was then substituted with a tolyl group at N3 position through a Chan-Lam coupling to give helical imidazole **194** and then by a methyl through a N-alkylation reaction to yield racemic [5]helicene-imidazolium (*rac*)-**195**. Note that this imidazolium salt could not be enantiomerically resolved using classical chiral HPLC methods because of its ionic character. It was thus transformed to a neutral Ir(I) complex for further stereochemical studies.[195]

Scheme 46. Preparation of [5]helicene-imidazolium salt (*rac*)-**195**. *i*) $LiAlH_4$, THF, Ar, rt, 5 hr; *ii*) $HC(OEt)_3$, cat. I_2, ACN, rt, 2 hr, 52% (two steps); *iii*) *p*-tolyl-boronic acid, anhydrous $Cu(OAc)_2$, pyridine, CH_2Cl_2, air, molecular sieves, rt, 24 hr, 69%; *iv*) CH_3I, ACN, reflux, 18 hr, 91%. X-ray structures of **193** in one of its tautomeric forms and of (*rac*)-**195** ((*P*) enantiomers are shown).[195]

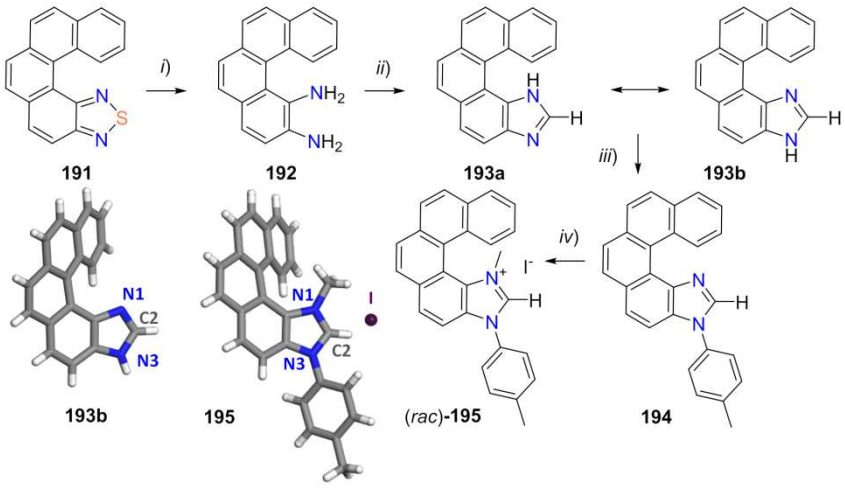

In the last two decades, octahedral cyclometalated iridium(III) complexes have attracted attention due to their appealing properties as phosphors in high-efficiency organic light-emitting devices (OLEDs)[200] and for their attractive biological activity as intracellular luminescence probes, anticancer or antibacterial agents.[201] In 2017, the first fused π-helical NHC system was prepared and examined through its diastereomerically pure cyclometalated complexes *mer*-(*P*,Λ_{Ir})-**196a**$^{\mathbf{1}}$ and *mer*-(*P*,Δ_{Ir})-**196a**$^{\mathbf{2}}$ (Scheme 47).[195] These chiral organometallic species display light-green phosphorescence with *i*) circular

polarization that depends on both the helical-NHC (*P*)/(*M*) stereochemistry and the iridium (*Δ*)/(*Λ*) one and *ii*) unusually long lifetimes (up to 250 μs as compared to 530 ns for model *mer*-**197**). The unprecedented features of **196a**^{1,2} can be attributed to extended π-conjugation within helical carbenic ligand. Note also that the two diastereomers **196a**^{1,2} display very different specific and molar rotations (Table 16).

Scheme 47. Preparation of cycloiridiated complexes **196a**^{1,2}. Structures and CPL spectra of iridium(III) complexes (*P*,*Λ*$_{Ir}$)-**196a**^{1}/(*M*,*Δ*$_{Ir}$)-**196a**^{1}, (*P*,*Δ*$_{Ir}$)-**196a**^{2}/(*M*,*Λ*$_{Ir}$)-**196a**^{2}, and (*Δ*$_{Ir}$)-**197**/(*Λ*$_{Ir}$)-**197**.[195]

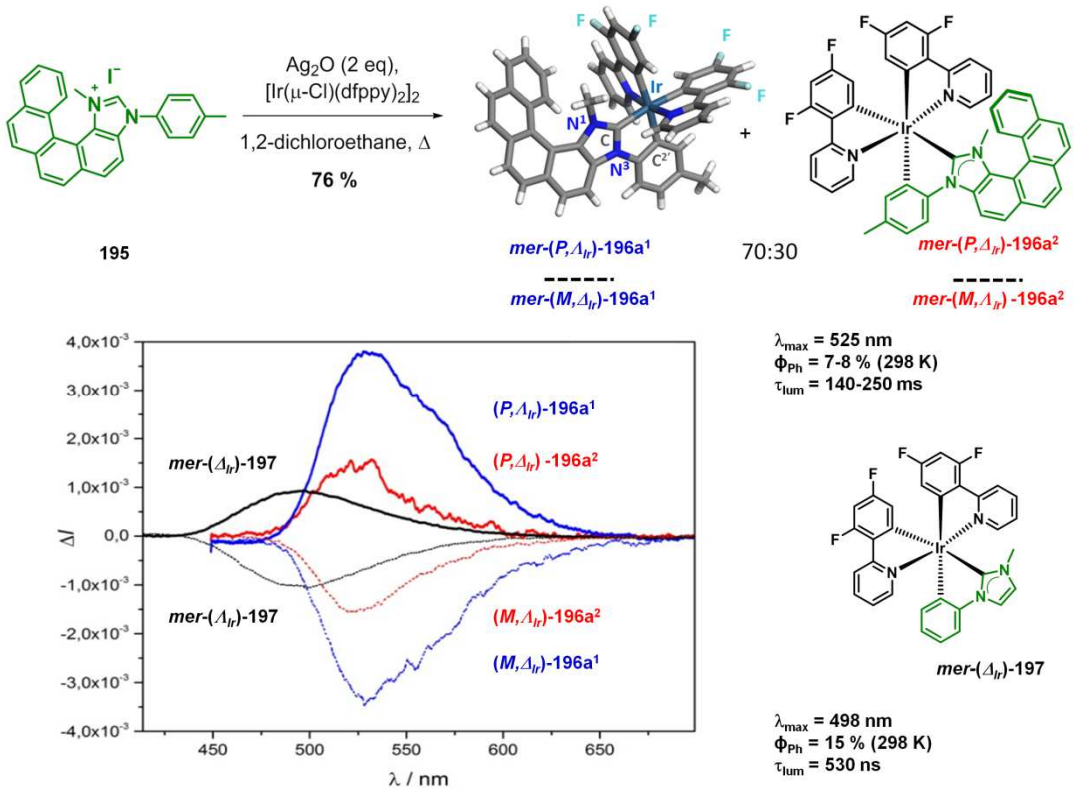

Table 16. Experimental specific and molar rotations for the Ir-carbene complexes **196a**^{1}, **196a**^{2}, and **197**.

	(*P*,*Λ*$_{Ir}$)-**196a**^{1}		(*P*,*Δ*$_{Ir}$)-**196a**^{2}		(*Λ*$_{Ir}$)-**197**	
	$[\alpha]^{23}$	$[\phi]^{23}$	$[\alpha]^{23}$	$[\phi]^{23}$	$[\alpha]^{23}$	$[\phi]^{23}$
589.3 nm						
Expt.	+920[a]	+8680	-	-	+610[a]	+4450
436 nm						
Expt.	+157[a]	+16520	-230	-2170		-

[a] Measured within an ± 5 % error. Conditions: CH_2Cl_2 / 3-4 × 10^{-5} M

4.1.5.2. Imidazole-substituted helicenes

In 2016, our group prepared the configurationally stable [6]helicene substituted with imidazolium according to a procedure known in the literature.[202] It was simply obtained by substitution of bromide by a methyl-imidazole to yield imidazolium salts 1-methyl-3-(2-methyl[4,6]helicenyl)-imidazolium **199a**,**b**.[198] These compounds were then deprotonated *in situ* to NHC ligand and cycloiridiated to complexes **200a**,**b** (Scheme 48). The neutral complexes were separated by HPLC over chiral stationary phases Chiralpak IC, heptane/EtOH/$CHCl_3$ (60/20/20) and Chiralpak IE, heptane/EtOH/CH_2Cl_2 (50/30/20) and their chiroptical properties were studied (see Figure 25). Due to their ionic character, charged derivatives such as helical imidazolium salts are difficult to resolve by classical HPLC techniques. In 2016, Vacek et al. tackled this problem and investigated the preparation of enantiopure samples of a *t*-Bu substituted (imidazolium **199c**) by different chromatographic methods *i.e.* classical HPLC, chiral supercritical fluid chromatography (SFC) methods and chiral electrophoresis.[203]

Scheme 48. Synthesis of chiral helicene-NHC cycloiridiated complexes **200a**,**b**. *i*) 1-Methylimidazole, acetone, reflux, overnight, 66-71%; *ii*) $[Cp^*IrCl_2]_2$, NaOAc, I, 80 °C, 15 hrs, 35-57%.[198]

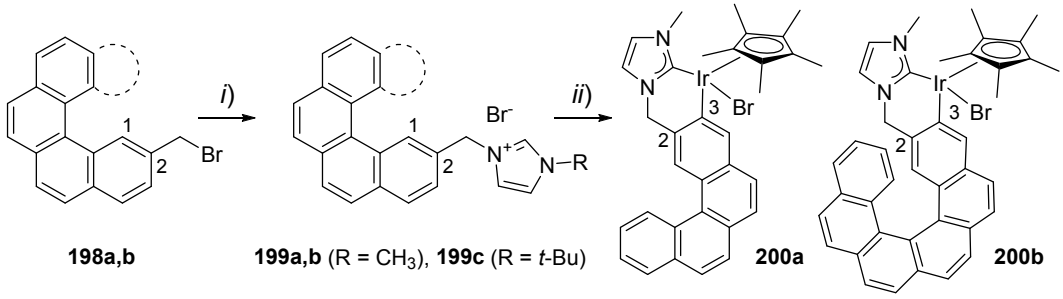

The electronic, chiroptical properties related to their stereochemical features of **200a**,**b** were experimentally and theoretically analyzed. Complex **200b** features two stereogenic elements, *i.e.* the [6]helicene unit and the tetrahedral Ir^{III}, but the (M,R_{Ir})- and (P,S_{Ir})-**200b** enantiomeric pair was the only diastereomer found, showing that the helicene's configuration controls the iridium stereochemistry, as shown in the X-ray crystal structure (Figure 25). On the contrary, complex **200a** displayed only two (R_{Ir}) and (S_{Ir}) enantiomers since the [4]helicene ligand was not configurationally stable. Kinetic studies, based on the evolution of the ECD at 254 nm with time at 60 °C, estimated the racemization barrier of (-)-**200a** around 26.3 kcal/mol and a half-life time of ca. 2 hours at 62 °C in chloroform. The differences between complexes **200a** and **200b** were clearly seen in their ECD spectra which showed very different signatures and magnitudes; these differences were analyzed by TD-DFT calculations which highlighted the involvement of helicene-CH_2-NHC orbitals in the chiroptical responses and enabled to assign their absolute configurations.[198]

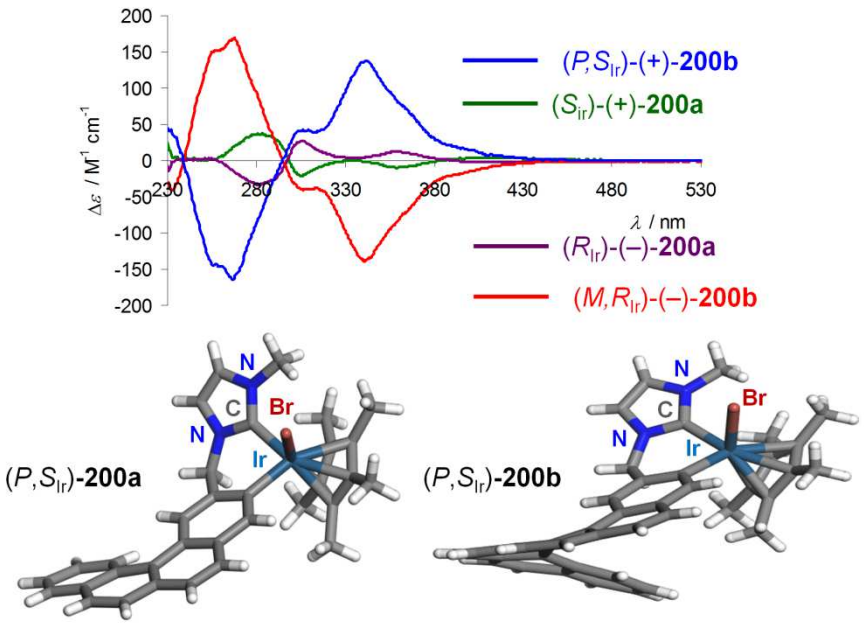

Figure 25. a) Electronic circular dichroism spectra of complexes (R_{Ir})- and (S_{Ir})-**200a** and (P,S_{Ir})- and (M,R_{Ir})-**200b** (CH_2Cl_2). b) X-ray structure of **200a** and **200b** (only one stereoisomer shown).[198]

Note that compounds **206-208** belong to the oxahelicene class (Figure 26). Contrary to fused helicene-imidazolium salts **195** and **200b**, all other helicenic imidazolium were obtained in enantioenriched forms (see their specific rotations in Table 17). In 2017, Stara and Stary developed a straightforward approach to access optically pure 2-aminooxa[5]helicenes (*M*,*R*,*R*)-(-)-**203a-g** and **205a-g** and 2-aminooxa[6]helicene (*M*,*R*,*R*)-(-)-**205h** employing the key [2+2+2] cycloisomerization of chiral functionalized triynes such as **202**.

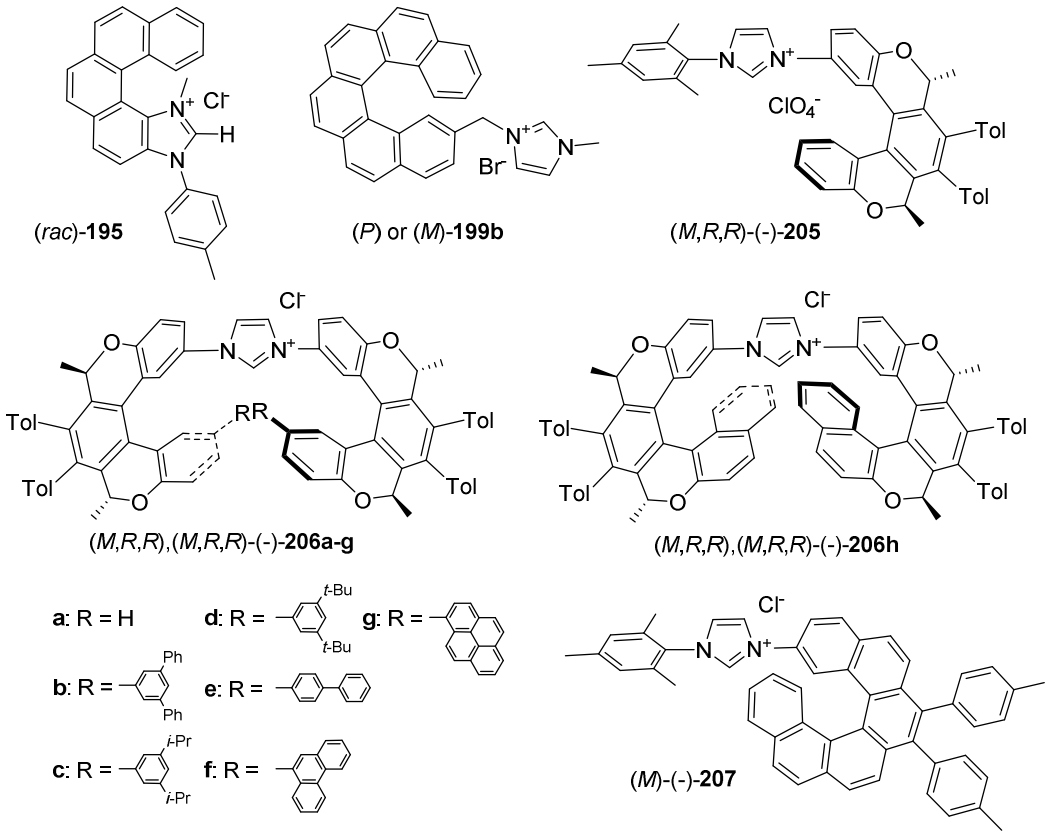

Figure 26. Helicenic imidazolium salts known up to now.[195,196,198]

Helicene-amine derivatives **202a,h** and chloro-substituted **203** were obtained by typical diastereoselective [2+2+2] cycloisomerization process; then **202a,h** were hydrolyzed to **2035a,h** while **203** was subjected to Suzuki couplings using a diversity of arylboronic acids or aryl-boronates yielding **202b-g** then **204b-g** after hydrolysis. All these steps occurred with very good yields (>63%, Scheme 49). Then the imidazolium salts **205** and **206a-h** were obtained by two different methods, depicted in Scheme 49, depending on the mono-helicenic or bis-helicenic structure obtained.

Scheme 49. Synthesis of helicene-amine derivatives **203** and **204a-h** and of imidazolium salts **205** and **206a-h** from **204a-h**.[196] See substituents on Figure 26.

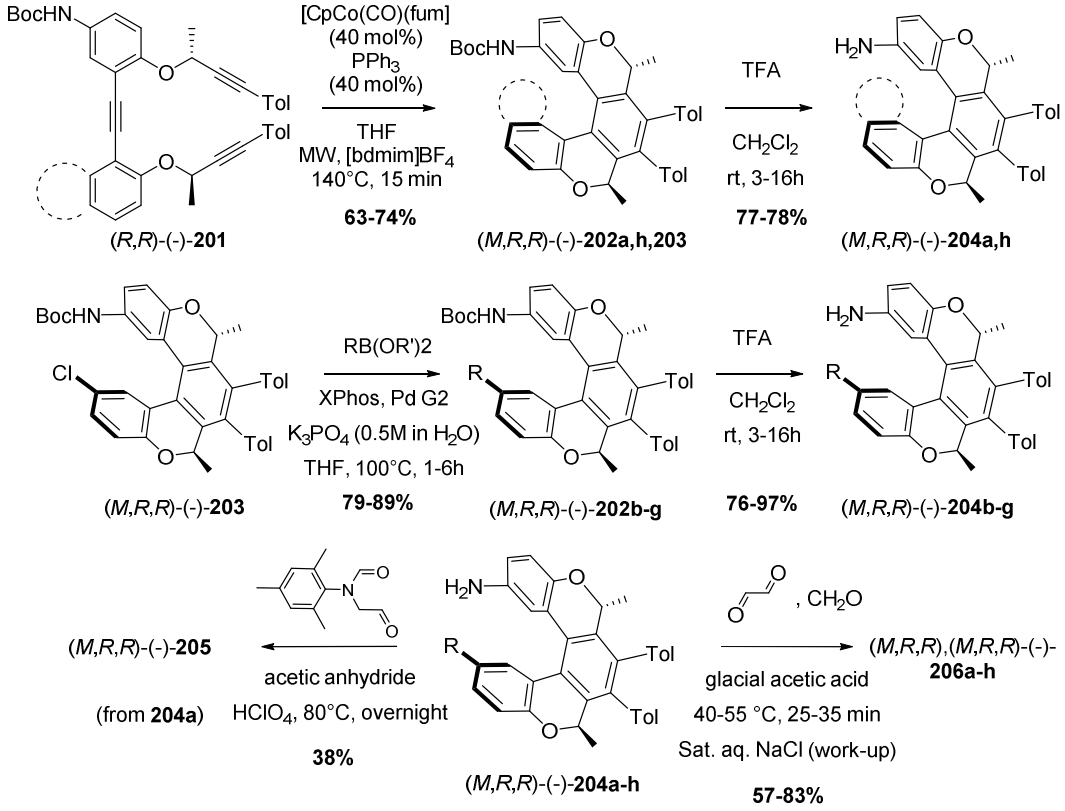

Table 17. Specific rotation values of enantioenriched helicenes-imidazole derivatives.[196]

Compound	Method of obtention	$[\alpha]_D$[a]	Conditions[b] (solvent / Conc.[c])	Ref.
(*M*,*R*,*R*)-**202a**	Diastereoselective catalytic [2+2+2] cycloisomerization	-546	$CHCl_3$/0.266	[196]
(*M*,*R*,*R*)-**202b**	*Ibid.*	-596	$CHCl_3$/0.311	[196]
(*M*,*R*,*R*)-**202c**	*Ibid.*	-657	$CHCl_3$/0.304	[196]
(*M*,*R*,*R*)-**202d**	*Ibid.*	-677	$CHCl_3$/0.359	[196]
(*M*,*R*,*R*)-**202e**	*Ibid.*	-674	$CHCl_3$/0.252	[196]
(*M*,*R*,*R*)-**202f**	*Ibid.*	-422	$CHCl_3$/0.303	[196]
(*M*,*R*,*R*)-**202g**	*Ibid.*	-481	$CHCl_3$/0.272	[196]
(*M*,*R*,*R*)-**202h**	*Ibid.*	-611	$CHCl_3$/0.340	[196]
(*M*,*R*,*R*)-**203**	*Ibid.*	-671	$CHCl_3$/0.250	[196]
(*M*,*R*,*R*)-**204a**	From (*M*,*R*,*R*)-**202a**	-629	$CHCl_3$/0.133	[196]
(*M*,*R*,*R*)-**204b**	From (*M*,*R*,*R*)-**202b**	-578	CH_2Cl_2/0.346	[196]
(*M*,*R*,*R*)-**204c**	From (*M*,*R*,*R*)-**202c**	-668	CH_2Cl_2/0.112	[196]
(*M*,*R*,*R*)-**204d**	From (*M*,*R*,*R*)-**202d**	-669	CH_2Cl_2/0.345	[196]
(*M*,*R*,*R*)-**204e**	From (*M*,*R*,*R*)-**202e**	-742	CH_2Cl_2/0.122	[196]
(*M*,*R*,*R*)-**204f**	From (*M*,*R*,*R*)-**202f**	-358	CH_2Cl_2/0.322	[196]
(*M*,*R*,*R*)-**204g**	From (*M*,*R*,*R*)-**202g**	-459	CH_2Cl_2/0.155	[196]
(*M*,*R*,*R*)-**204h**	From (*M*,*R*,*R*)-**202h**	-687	$CHCl_3$/0.191	[196]
(*M*,*R*,*R*)-**205**	From (*M*,*R*,*R*)-**204a**	-452	$CHCl_3$/0.215	[196]
(*M*,*R*,*R*),(*M*,*R*,*R*)-**206a**	From (*M*,*R*,*R*)-**204a**	-601	$CHCl_3$/0.091	[196]
(*M*,*R*,*R*),(*M*,*R*,*R*)-**206b**	From (*M*,*R*,*R*)-**204b**	-716	$CHCl_3$/0.313	[196]

(*M*,*R*,*R*),(*M*,*R*,*R*)-**207c**	From (*M*,*R*,*R*)-**204c**	-806	$CHCl_3$/0.275	[196]
(*M*,*R*,*R*),(*M*,*R*,*R*)-**206d**	From (*M*,*R*,*R*)-**204d**	-808	$CHCl_3$/0.258	[196]
(*M*,*R*,*R*),(*M*,*R*,*R*)-**206e**	From (*M*,*R*,*R*)-**204e**	-825	$CHCl_3$/0.273	[196]
(*M*,*R*,*R*),(*M*,*R*,*R*)-**206f**	From (*M*,*R*,*R*)-**204f**	-799	$CHCl_3$/0.301	[196]
(*M*,*R*,*R*),(*M*,*R*,*R*)-**206g**	From (*M*,*R*,*R*)-**204g**	-952	$CHCl_3$/0.353	[196]
(*M*,*R*,*R*),(*M*,*R*,*R*)-**206h**	From (*M*,*R*,*R*)-**205h**	-669	$CHCl_3$/0.247	[196]

Enantiopure helical NHC ligands generated from (*M*,*R*,*R*)-(-)-**205** and (*M*,*R*,*R*),(*M*,*R*,*R*)-(-)-**206a-g** were tested in the enantioselective Ni(0)-catalyzed [2+2+2] cycloisomerization of **213** to (*P*)-(+)-**214**. High yields and good *ee*'s were obtained for the mono-oxa[5]helicenic unsymmetrical imidazolium salt **205** (Table 18, entry 1) while symmetrical 1,3-bisoxahelicenyl imidazolium salts gave much better *ee*'s. The presence of bulky aryl group at the opposite terminus of the oxa[5]helicene backbone with respect to the position of the imidazolium unit led to an increase of the *ee* of (*P*)-(+)-**214**: from 41% *ee* (Table 18, entry 2) to 66% (Table 18, entry 6). The highest level of chirality transfer from a helical NHC ligand to a helical product was achieved in [2+2+2] cycloisomerization of the aromatic triyne **215** to dibenzo[7]helicene (*P*)-(+)-**216** (Table 19), with lower yield but with *ee*'s up to 86% when using NHC precursor **202c (**Table 19, Entry 3).

Table 18. Enantioselective [2+2+2] cycloisomerization of triyne **213** to dibenzo[6]helicene **214** in the presence of enantiopure NHC ligands generated from (*M*,*R*,*R*)-(-)-**205** and (*M*,*R*,*R*),(*M*,*R*,*R*)-(-)-**206a-h**.[196]

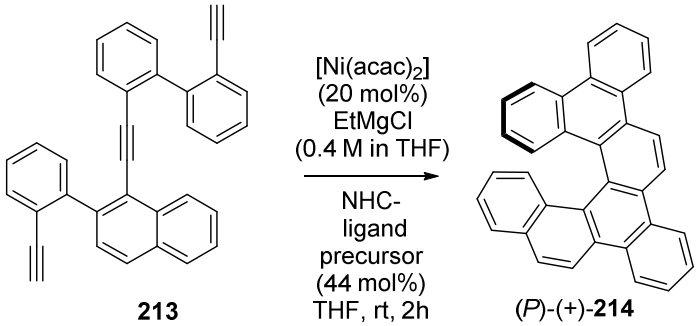

213 (*P*)-(+)-**214**

Entry	NHC precursor	Conv[a]	*ee*[b] (%) of **214**
1	(*M*,*R*,*R*)-(-)-**205**	>90	17 (+)
2	(*M*,*R*,*R*),(*M*,*R*,*R*)-(-)-**206a**	>90	41 (+)
3	(*M*,*R*,*R*),(*M*,*R*,*R*)-(-)-**206h**	>90	59 (+)
4	(*M*,*R*,*R*),(*M*,*R*,*R*)-(-)-**206b**	90	61 (+)
5	(*M*,*R*,*R*),(*M*,*R*,*R*)-(-)-**206c**	90	64 (+)
6	(*M*,*R*,*R*),(*M*,*R*,*R*)-(-)-**206d**	81	66 (+)
7	(*M*,*R*,*R*),(*M*,*R*,*R*)-(-)-**206e**	89	44 (+)
8	(*M*,*R*,*R*),(*M*,*R*,*R*)-(-)-**206f**	73	56 (+)
9	(*M*,*R*,*R*),(*M*,*R*,*R*)-(-)-**206g**	90	47 (+)

[a] Estimated by HPLC. [b] Determined by HPLC on a Chiralpak IA column.

Table 19. Enantioselective [2+2+2] cycloisomerization of triyne **215** to dibenzo[6]helicene **216** in the presence of enantiopure NHC ligands generated from (*M*,*R*,*R*),(*M*,*R*,*R*)-(-)-**206a**,**c**,**g**. [196]

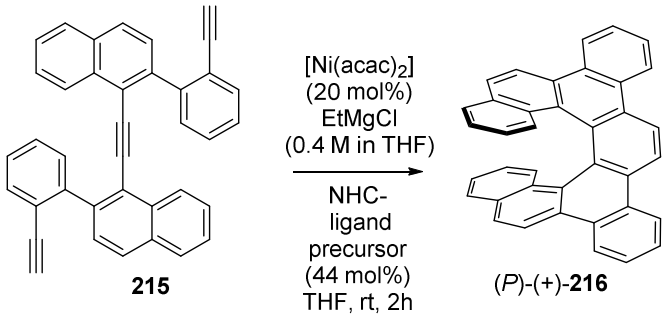

Entry	NHC precursor	Conv[a]	*ee*[b] (%) of **216**
1	(*M*,*R*,*R*),(*M*,*R*,*R*)-(-)-**206h**	76	74 (+)
2	(*M*,*R*,*R*),(*M*,*R*,*R*)-(-)-**206a**	64	72 (+)
3	(*M*,*R*,*R*),(*M*,*R*,*R*)-(-)-**206c**	86	86 (+)

[a] Estimated by HPLC. [b] Determined by HPLC on a Chiralpak IA column.

Using the same approach, an imidazolium salt bearing a pendant carbo[6] unit was also prepared (see Scheme 50), and its corresponding Ru-NHC complex **209** obtained from the first generation Hoveyda-Grubbs catalyst isolated and identified. This complex was then used for asymmetric catalysis (see Scheme 50).[197] Experimental UV-vis and ECD spectra of helical imidazolium salts were also studied. Indeed **209** was evaluated in asymmetric ring-closing metathesis (RCM) and ring-opening metathesis-cross metathesis (ROM/CM) reactions, which proceeded with good enantioselectivity (Scheme 51). Extensive NMR-spectroscopic investigations and a DFT geometry optimization were performed. These results led to a topographic steric map and calculation of percent-buried-volume values for each quadrant around the metal center, and enabled to have an insight into the approach of the substrate and the origin of enantioselectivity.[197]

Scheme 50. Synthesis of helical-NHC based Ru-complex (*M*)-**209**. Adapted from ref. [197]. Copyright 2018, Wiley.

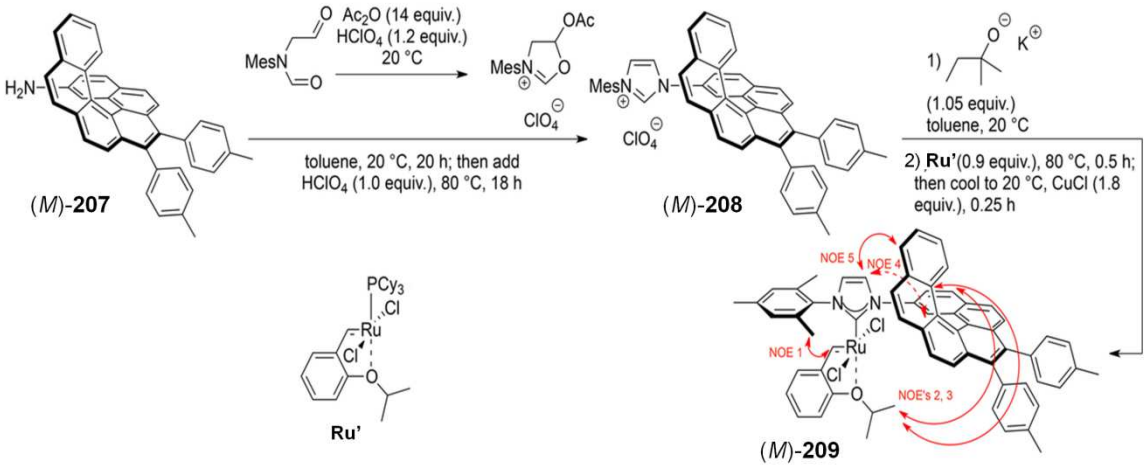

Scheme 51. a) Enantioselective RCM (a) and ROM-CM (b) catalyzed by (*M*)-**209**. b) Ball-and-stick-representation of DFT-geometry-optimized structure of (*M*)-**209**. c) Topographic steric map of (*M*)-**209**. View from the *z*-axis onto the *x*–*y*-plane. All scales are in Å. Adapted from ref. [197]. Copyright 2018, Wiley.

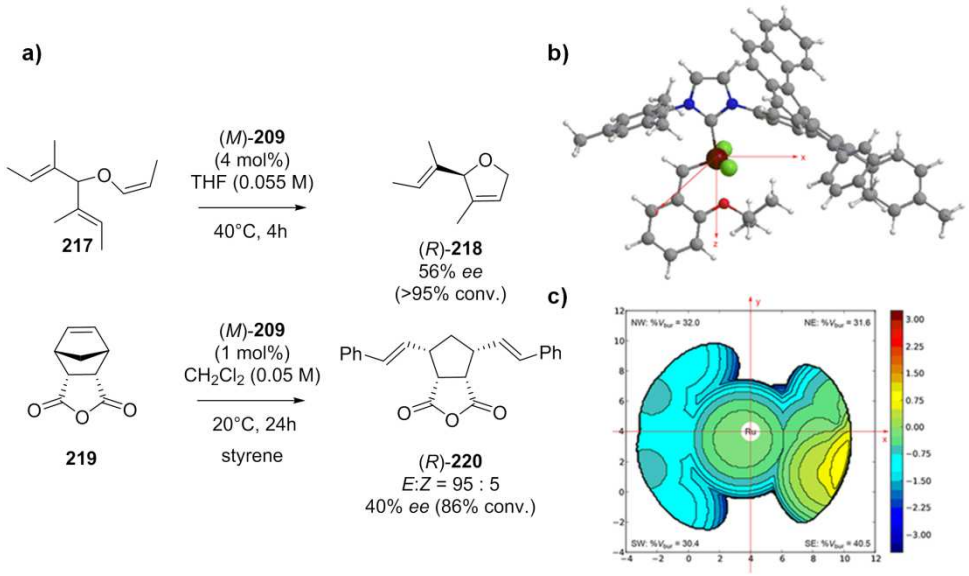

4.1.6. Azahelicenes with N-bridging fused rings

4.1.6.1. Helicenic bridged triarylamines

4.1.6.1.1. Carboxy-bridged triarylamine heterohelicenes

In 2003, Venkataraman *et al.* reported the first examples of CPL-active heterohelicenes, namely **226a**,**b** and **227a**,**b**, whose structure is based on triarylamine, a unit widely exploited in the OLED industry due to its electronic, photochemical, and physical properties.[204] They were synthesized as shown in Scheme 52. The coupling of **221** to diarylamine **222** was performed using the copper-catalyzed Ullmann conditions and gave **223** with 70% yield. After hydrolysis, the obtained bis-carboxylic acids were converted to acid chloride with thionyl chloride which underwent *in situ* cyclization with $SnCl_4$ to give (*rac*)-**224** with 80% yield. After deprotection of the methoxy group to (*rac*)-**225** and esterification using (1*S*)-camphanic acid, a 1:1 diastereomeric mixture of (*P*,*S*)-**226a** and (*M*,*S*)-**226b** was obtained which was then separated by column chromatography. Longer helical (*P*,*S*)- and (*M*,*S*)-**227a,b** were obtained in a similar way.

Scheme 52. Synthesis of the first helical triarylamines **226a**,**b** and chemical structure of longer helicene **227a**. *i*) CuI, K_2CO_3, *n*-Bu_2O, 150 °C, 96 hr, 70%; *ii*) NaOH, H_2O/EtOH (1:1), reflux, 24 hrs; *iii*) $SOCl_2$, CH_2Cl_2/DMF (cat.), reflux for 2 hr then $SnCl_4$, reflux, 18 hrs, 80%; iii) AcOH/HBr (2:1), reflux, 72 hr, 60%; (e) DMAP, (1*S*)-camphanic chloride, CH_2Cl_2, reflux, 12 hr, 85%.[204]

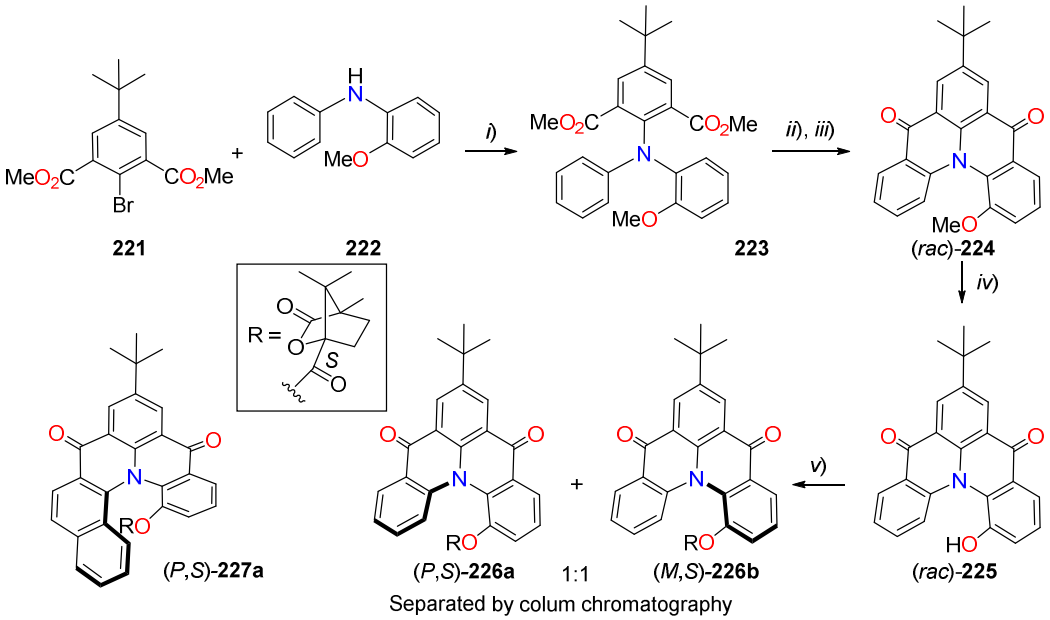

The two diastereomers of (*P*,*S*)-**226a** and (*M*,*S*)-**226b** displayed identical absorption spectra (Figure 27) in the UV-vis region with the absorption maxima occurring at 434 nm. ECD and CPL spectra of **226a,b** display mirror-image relationship showing that the (1*S*)-camphanate has no influence on the chiroptical properties and only serves to maintain the helicity and configurational stability of the molecule. The emission maximum occurs at 453 nm for helicene **226** and 478 nm for helicene **227**. The dissymmetry factors at the peak maxima for **226** and **227** were found to be ±0.001 and ±0.0008, respectively. In addition, for the same transition, g_{abs} and g_{lum} have essentially the same value for both helicenes showing no significant geometry change upon population of the emitting state. This is corroborated by the small Stokes shifts of the emission maxima. By comparing the results with those of Phillips *et al.*,[205] a 10-fold increase in the luminescence dissymmetry ratio is reported, *i.e.* $|g_{lum}| = 0.01$, for a system of aggregating helicenes. However, the increased ordering of these aggregates also results in a large degree of linear polarization ($P = 0.39$) which can greatly affect the CPL measurement.[206]
The homodimeric structure (*M*,*S*,*M*,*S*)-**229** was also prepared by Venkataraman by a Pd(0) Stille coupling of brominated bridged triarylamine (*M*,*S*)-**228** (Scheme 53). The properties of monomer and dimer were compared and the dimer was found more easily oxidizable than the monomer; this was explained by a more extended π-conjugation in the dimer.[207]

In 2006, Barnes and coworkers reported the fluorescence-detected circular dichroism (FDCD) from an individual molecule of (*P*,*S*)-**227a** or (*M*,*S*)-**227b** deposited on the surface of a polymer film (Zeonex).[208] Mirror-image dichroic responses averaged over ~500 molecules were obtained and the dissymmetry factors were found to be > 0.5, i.e. significantly larger than the ones observed in bulk solution, suggesting

a strong effect of orientation and of removing disorder present in condensed matter. A well-defined structure observed in the histograms was suggestive of specific molecular orientations at the polymer interface. However, these results have been reconsidered by the group of Cohen *et al.* Indeed these authors suggested that the broad distribution of *g*-values observed by Hassey *et al.* can be explained by *linear dichroism* in the randomly oriented helicene molecules, coupled with imperfect circular polarization of the illumination.[209,207] Consequently, one cannot conclude about the possibility of measuring FCDC from single molecules (see discussion between both groups in reference [210]). Note that bridged triarylamines were used as models for several calculations of ECD, VCD and CPL.[211,207,212,213,214]

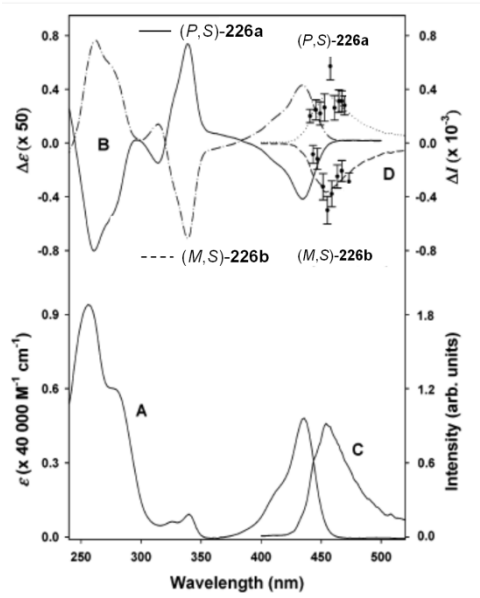

Figure 27. UV-vis (A), ECD (B), fluorescence (C) and CPL (D) spectra of (*P*,*S*)-**226a** and (*M*,*S*)-**226b**. Adapted from [204]. Copyright 2003, American Chemical Society.

Scheme 53. Preparation of dimer **229**.[207]

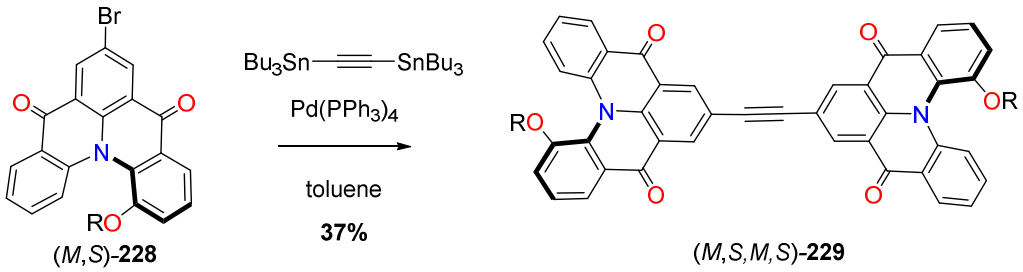

4.1.6.1.2. Oxygen-bridged triarylamine heterohelicenes

Using a similar strategy as for carboxy-bridged analogues **226**,**227**, Wakamiya, Murata *et al.* reported in 2017, the preparation of helical oxygen-bridged diphenylnaphtylamine according to Scheme 54 which were obtained as pure enantiomers after chiral HPLC over a Chiralpak-IF stationary phase (hexane/CH_2Cl_2 mixture as eluent).[215] The racemization in toluene at 100 °C for **231** and 80 °C for **232**

and **233** and the ring inversion energies were measured as 29.0 kcal mol^{-1} for **231**, 27.6 kcal mol^{-1} for **232**, and 27.1.kcal mol^{-1} for **233**, respectively, and found to be in good agreement with DFT (B3LYP/6-31G(d)) calculated ones (29.3, 27.8 and 26.4 kcal mol^{-1}).

Scheme 54. Synthesis of racemic oxygen-bridged triarylamines **231-233**. *i*) BBr_3, CH_2Cl_2, -78 °C to rt; *ii*) K_2CO_3, DMF, 120 °C, 92% (2 steps); *iii*) $POCl_3$, DMF, $C_2H_4Cl_2$, 25 °C, 80%, *iv*) malononitrile, Et_3N, $CHCl_3$, rt, 91%.[215]

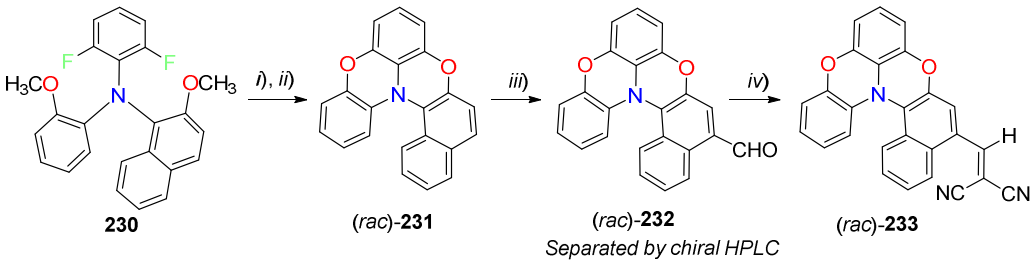

Post-functionalization of heterohelicene **231** enabled to install formyl and dicyanovinyl groups that are electroactive, to modulate and extend the π-conjugation of the system and to examine their influence on their photophysical/chiroptical properties. The tails of UV/vis and ECD together with emission and CPL bands in CH_2Cl_2 are highlighted in Figure 28. These compounds are strongly emissive, with quantum yields up to 0.86 for **231** in CH_2Cl_2. Furthermore, a clear red shift of absorption and emission was observed upon increasing the conjugation. The strong charge transfer and high polarity of these molecules were evidenced experimentally by the solvent polarity dependence of the emission properties (emission wavelength and quantum yield). Regarding the chiroptics, similar g_{abs} and g_{lum} magnitudes were found for each compound with g_{abs} / g_{lum} of $+5.6 \times 10^{-3}$ / $+4.7 \times 10^{-3}$ for (*M*)-**231**, $+2.1 \times 10^{-3}$ / $+1.4 \times 10^{-3}$ for (*M*)-**232**, and $+0.9 \times 10^{-3}$ / $+0.9 \times 10^{-3}$ for (*M*)-**233**. These properties were also compared in liquid state/solid state and in nanoparticles obtained by rapid precipitation in water. Respective g_{lum} values of 4.5×10^{-3}, 1.5×10^{-3}, and 2.8×10^{-3}, were measured for nanoparticles of **231-233** dispersed in water, showing that CPL activity was conserved.

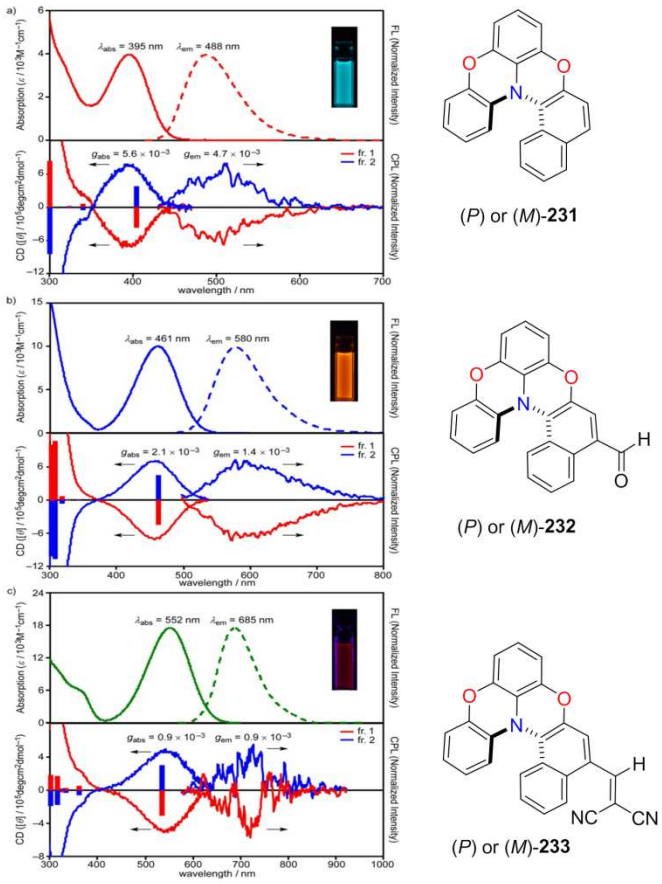

Figure 28. UV-vis absorption (solid) and fluorescence (dashed) spectra (top), and CD and CPL spectra (bottom) for (a) **231**, (b) **232**, and (c) **233** in CH_2Cl_2. The red and blue bars show the calculated CD bands (CAM-B3LYP/6-31G(d)) for the (*P*)- and (*M*)-helices, respectively. The transition energies have been calibrated using a factor of 0.88. Photographs show the emission of **231**-**233**. Adapted from ref. [215]. Copyright 2017, American Chemical Society.

4.1.6.1.3. Thia-bridged triarylamine heterohelicenes

In 2008, Menichetti and coworkers reported enantioenriched triarylamine heterohelicenes bearing sulfurated bridges. For this purpose, they proceeded through regioselective electrophilic aromatic sulfenylation of substituted triarylamine with the use of phthalimidesulfenyl chloride followed by Lewis acid catalyzed electrophilic cyclization (Scheme 55).[216] The enantiomers of heterohelicenes **236a-d** were obtained through HPLC over a Chiralpak IA chiral stationary phase giving *ee*'s > 97.5%. The enantiomers exhibited $[\alpha]_D$ values of +376 and -376 (c=0.11, hexane), respectively for **236a** and -405 and +405 (*c* 0.06, hexane), respectively for **236d**. The experimental racemization barrier of **236a** was found to be 31.6 kcal mol^{-1} at 145 °C, a value between those of [5] and [6]helicene. The absolute configuration of **236a** was determined by comparison of calculated and experimental vibrational circular dichroism (VCD) spectra of the two enantiomers. In 2017, the enantiomers of *t*-Bu-substituted analogue **236e** were prepared in a similar way and studied by Berova, Kavala *et al.*.[217] In 2016, the CPL activity of sulfurated systems

was measured by Longhi *et al.* with a g_{lum} as high as 0.9×10^{-2} at ~ 510 nm (positive for (*M*) and *vice versa*) for **236d** while excitation of the beam led to racemization for **236a**.

Scheme 55. Synthesis of thia-bridged triarylamine heterohelicenes **236a-e**.

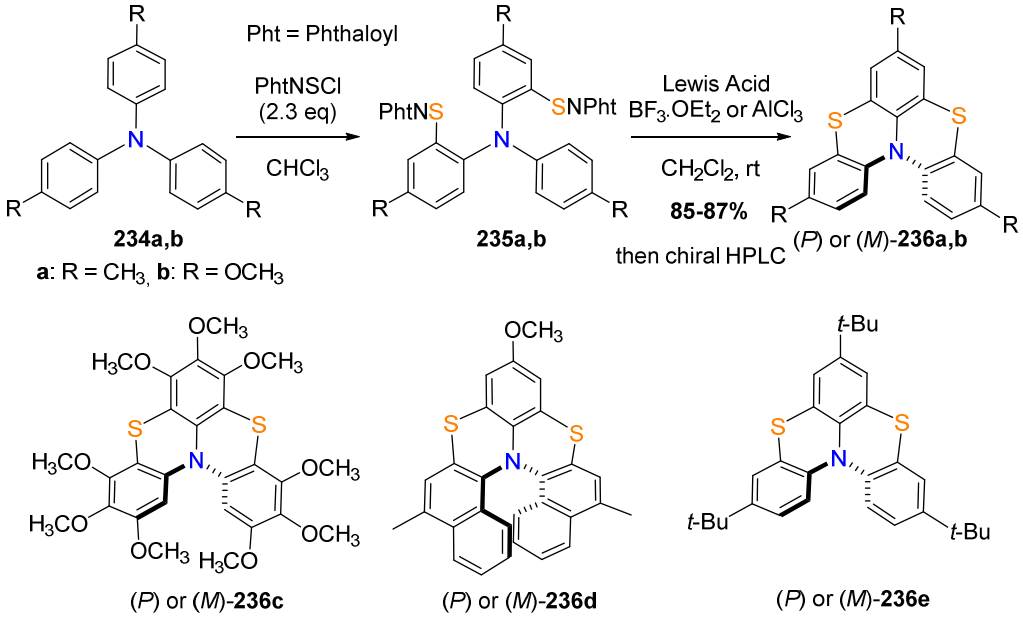

A stable chiral radical cation derived from neutral dithia-bridged triphenylamine hetero[4]helicene **236e** was generated upon reversible one-electron oxidation.[217] Indeed, purple-blue helical radical cations (*M*)- and (*P*)-**236e**$^{\cdot+}$ SbF_6^- were obtained from the colorless (*rac*)-**236e** by reaction with $AgSbF_6$ in CH_2Cl_2. The calculated Gibbs free activation energy of racemization at 298 K ($\Delta G^{\neq}_{298}$) was found ca. 5 kcal mol^{-1} lower for **236e**$^{\cdot+}$ ($\Delta G^{\neq}_{298}$=28.1 kcal mol^{-1}) than for **236e** ($\Delta G^{\neq}_{298}$=32.7 kcal mol^{-1}). They were found sufficiently high to ensure a very low racemization rate at room temperature. With the help of X-ray crystallography (Figure 29a and b) and theoretical and experimental ECD spectroscopy (Figure 29c and d), it was shown that the oxidized species retains the absolute configuration of the neutral counterpart, while exhibiting a more extensive conjugation and "flattening" of the helical motif. This was shown by a clear ECD-active band in the near-infrared region (around 1200 nm) and by the specific rotation values that changed drastically. Indeed, while (*P*)-**236e** displayed an optical rotation $[\alpha]_D$ value of +408.6 at 25 °C it increased to +1247.9 for (*P*)-**236e**$^{\cdot+}$ SbF_6^-.

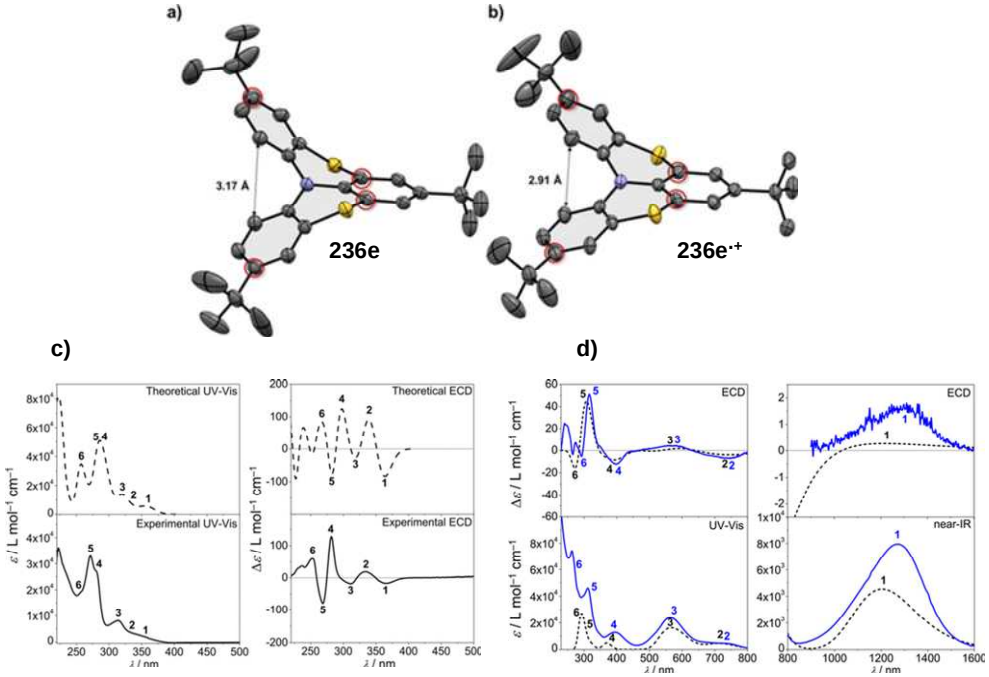

Figure 29. a), b) X-ray crystallographic structures of (*rac*)-**236e** and **236e**$^{\bullet+}$. c) Theoretical and experimental UV/Vis and ECD bands for the experimental (*P*)-(+)-**236e** (black solid lines for experimental and black dashed lines for theoretical spectra). d) Theoretical and experimental UV/Vis and ECD bands for the experimental (*P*)-(+)-**236e**$^{\bullet+}$ (blue solid lines for experimental and black dashed lines for theoretical spectra). Experimental UV and ECD spectra were recorded in THF, while corresponding theoretical spectra were simulated at B3LYP/TZVP and M06-2X/6-31+G(d,p) levels of theory. For correlation purposes, the calculated spectral data are red-shifted by 50 nm. Reproduced from ref. [217]. Copyright 2017, Wiley.

4.1.6.2. Polyaza[7]helicenes

In 2017, Shibata *et al.* reported a facile two-step synthesis of polyaza[7]helicenes possessing a 6-5-6-6-6-5-6 skeleton from commercially available 2,9-dichloro-1,10-phenanthroline via double amination with aniline derivatives followed by hypervalent iodine reagent-mediated intramolecular double-NH/CH couplings, thus yielding five different helicenic derivatives **238a-e** (Scheme 56).[218] Single-crystal X-ray analysis of **238a** revealed a unique structure with five significantly twisted central rings and nearly planar fused rings on both sides. This feature is different from classical helicenes where the entire skeleton possesses similar dihedral angles for the inner rims. The frontier molecular orbitals (FMOs) are depicted in Figure 30. The molecular coefficients of HOMO were distributed over the entire outer rim of the skeleton, while those of LUMO were on the phenanthroline-derived rings due to the electron-deficient nitrogen atoms. The azahelicenes **238a-e** show strong absorption and high fluorescent quantum yields under both neutral (Φ = 0.25-0.55, comparable to highest values for [7]helicenes[219]) and under acidic conditions (Φ up to 0.80). Enantiomers of **238a** were resolved from a racemic mixture using HPLC with a CHIRALCEL OD column (*n*-Hexane/*i*-PrOH = 7/3 as the eluent). Then the chiroptical properties of **238a**

were evaluated. The specific rotation of enantiomerically pure (+)-**238a** of +2544 (*c* 0.51, $CHCl_3$) which is larger than those of other [7]helicenes containing two five-membered rings.[220]

Figure 30 shows mirror-imaged ECD and CPL spectra of **238a** enantiomers both under neutral and acidic conditions. In both acidic and neutral conditions, the ECD spectrum of (+)-**238a** shows several positive Cotton bands in the longer wavelength region with very similar shapes for neutral and acidic forms. These observations reveal similar features in the ground state. Under both conditions, helicene **238a** also shows strong CPL activities with emission maxima consistent with those observed in the fluorescent spectrum. The value of g_{lum} under neutral conditions (0.009 at 473 nm) is quite large for a [7]helicene. Upon addition of 200 equivalent amounts of TFA the g_{lum} value remained high (0.008 at 514 nm). Overall, these systems combine both high g_{lum} value with high quantum yield of 0.80, which is highly attractive for a CPL-emitting material.

Scheme 56. Synthesis of polyaza[7]helicenes **238a-e** and X-ray structure (side view) of **238a**. Adapted from ref. [218]. Copyright 2017, Wiley.

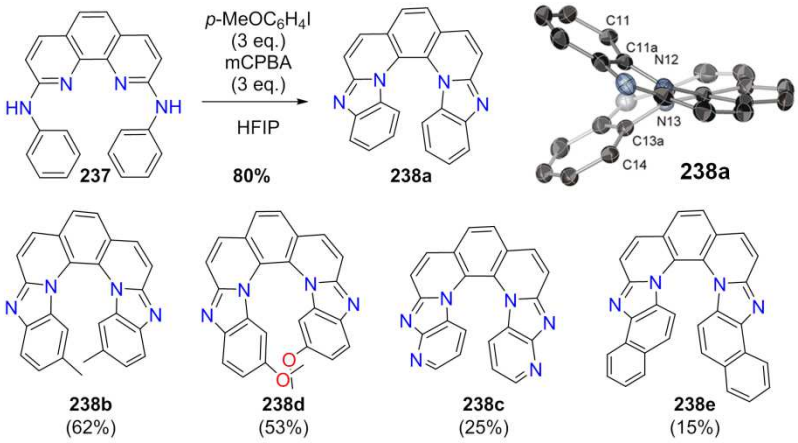

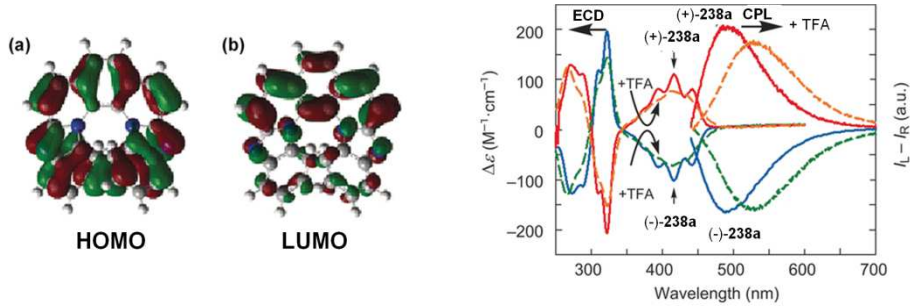

Figure 30. Frontier orbitals of **238a** and ECD and CPL spectra of neutral form and acidic form of the (*M*) and (*P*) enantiomers. Adapted from ref. [218]. Copyright 2017, Wiley.

4.1.7. Cationic azahelicenes: azahelicenia

4.1.7.1. Azonia[n]helicenes

Azoniahelicenes are a subset of nitrogen-containing helicenes in which a quaternary sp^2 nitrogen atom introduces a charge into the system. As opposed to neutral helicene species, their cationic derivatives with

quaternary nitrogen atoms in the helical backbone have been rather overlooked and a limited number of them have been reported up to now. Azonia systems may have interesting biological properties since they can bind easily to DNA and its quadruplex. See for example ref. [221].

4.1.7.1.1. Helquats: synthesis by [2+2+2] cycloisomerization and properties

Azoniahelicenes and similar cationic systems promise an attractive range of properties and applications that may be complementary to non-ionic helicenes. For example, they can strongly interact with their environment due to their positively charged helical skeleton. Furthermore, their solubility in aqueous media and electron-accepting properties associated with their cationic nature can be advantageous. In 2009, the group of Teply introduced Helquats, a class of compounds that combines the stereochemical features of pseudo-helicenes with the electronic properties of viologens (Scheme 57).[222,223] As such, Helquat are very efficient electron-transfer quenching agents thanks to their powerful electron-accepting character and are interesting for their NLO activity.[224] The group developed a scalable route of racemic [5]- and [6]Helquats,[223] based on a dicationic triyne (formed by simple quaternization of symmetrical or unsymmetrical diazaarylacetylene precursors) which can undergo a [2+2+2] cycloisomerization in the presence of a Wilkinson's catalyst or [Cp*Ru(COD)Cl] in order to form the helical backbone ([**239**][OTf]$_2$ to [**240**][OTf]$_2$, Scheme 57). This strategy could be applied to the preparation of 15 different [5]-, [6]-, and [7]Helquats, but only in their racemic form.[225] Actually the cationic character of these helicenes renders them difficult to be resolved by classical chiral HPLC separation. Therefore other methods needed to be established, such as the chiral capillary electrophoresis (CE) experiments tested analytically with salts such as **241** by using a sulfated γ-cyclodextrin as the chiral selector, with the appearance of two peaks in the two corresponding electropherograms of helical cationic enantiomers. However, these two peaks were too close to each other to be able to perform efficient enantiomeric separation.[226]

Scheme 57. Synthesis of racemic cationic azahelicenes [**240a**,**b**][OTf]$_2$ by [2+2+2] cycloisomerization.[223]

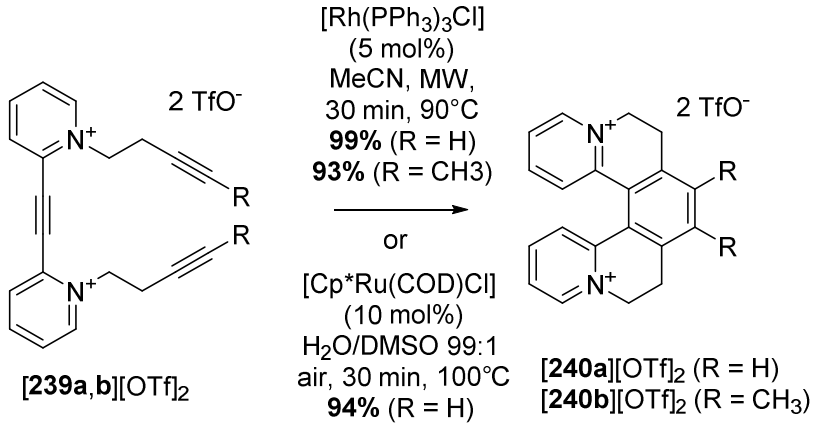

In 2010, the same group was able to prepare enantiopure samples of Helquat [**241**][OTf]$_2$ (for which configuration inversion process is hindered by the presence of two additional Me groups) by crystallization of diastereomeric salts (a process taking advantage of the different solubilities of the two

diastereomeric salts);[227] racemic [5]Helquat as its triflate salt [**241**][OTf]$_2$ was converted into a mixture containing two diastereomeric (*R*,*R*)-dibenzoyltartrate (named **X2**) salts, [(*P*)-**241**][**X2**]$_2$ and [(*M*)-**241**][**X2**]$_2$, using an ion exchange resin technique (Scheme 58). Then diffusion of ethanol vapours into a methanolic diastereomeric mixture led to the exclusive formation of [(*P*)-**241**][**X2**]$_2$ crystals. After successive crystallizations, the diastereomeric excess (*de*) could be increased to up to 98% *de*, as shown by CE with a sulfated β-cyclodextrin chiral selector. Subsequently, by using ion-exchange resin the resolved crystals of [(*P*)-(+)-**241**][**X2**]$_2$ were transformed back to ditriflate [(*P*)-(+)-**241**][OTf]$_2$ and its enantiomeric purity checked by CE showed conservation of stereointegrity of the sample occurred during the ion exchange procedure, as evidenced by the single peak in the electropherogram of [(*P*)-(+)-**241**][OTf]$_2$. To determine the configurational stability of [(*P*)-(+)-**241**][OTf]$_2$, stirred solutions in water were heated in microwave apparatus at 100 °C, and analysis using optical rotation measurements led to an activation free energy value $\Delta G^{\neq}$ = 30.4 kcal mol^{-1} and racemization half-life at 100 °C, $t_{1/2}$ = 3.79 hr. The absolute configuration was assigned using ECD spectroscopy. These results show that [5]Helquat crystallizing as its (*R*,*R*)-dibenzoyltartrate salt has (*P*) helicity.[227] In 2012, the pure enantiomers (*ee*'s> 98%) of the same Helquat were obtained by preferential crystallization. Indeed, thanks to their C_2-symmetrical topology, a most favorable case for conglomerate occurrence, several helicene derivatives undergo spontaneous resolution.[228,229] Taking advantage of this phenomenon, Teply *et al.* could perform a preferential crystallization experiment and obtain enantiopure samples up to 10.5 g-scale of [5]Helquat salt **241**.[230] Note that in 2017, in the case of similar Helquat for which diastereomeric resolution with dibenzoyltartrate alone failed, a Dutch Resolution using a family of three derivatives of tartrate anions was the key to achieve efficient separation of (*M*) and (*P*) helical enantiomers of configurationally stable [5]Helquat [**242**][OTf].[231] This latter helicene-like compounds displayed slightly longer half-life time (see Table 20). Furthermore, a [7]Helquat was also obtained in enantiopure form *via* preferential crystallization of its trifluoroacetate salt which was found to be the only conglomerate among 12 different salts studied.[232] Note that conglomerates are relatively rare and correspond to 10-15% of crystalline racemates.[228]

Scheme 58. Resolution of racemic [5]Helquat [**241**][OTf]$_2$ *via* crystallization of diastereomeric salts.[227]

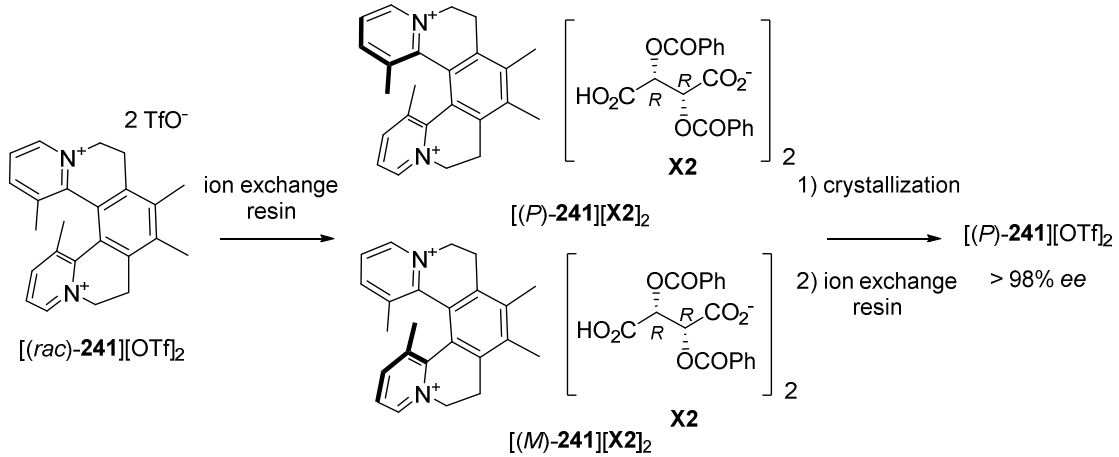

Table 20. Comparison of configurational stabilities of Helquats [**241**][OTf]$_2$ and [**242**][OTf]$_2$.[232]

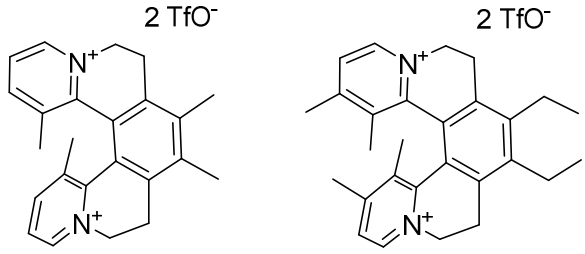

[(*rac*)-**241**][OTf]$_2$ [(*rac*)-**242**][OTf]$_2$

Compound	$\Delta G^{\#}$ (kJ mol^{-1})	$t_{1/2}$ (hr)
[**241**][OTf]$_2$	127.7	3.79
[**242**][OTf]$_2$	129.0	5.81

In 2014, Teply *et al.* reported the intense chiroptical switching activity of dicationic helicene-like derivative **241**$^{2+}$. These systems displayed nice electrochemical reversibility and they showed a two-step redox switching process in enantiopure helquat system [(*P*)-**241**]$^{2+}$ ⇌ [(*P*)-**241**]$^{\bullet+}$ ⇌ [(*P*)-**241**]^{0} (Figure 31a).[233] They showed that the viologen-type electroactive unit embedded directly in the helical scaffold of **241** was responsible for the strong chiroptical tuning at 264 nm. This process is associated with a marked sign-reversal of Cotton effect ranging between $\Delta\varepsilon$ = +35 M^{-1}cm^{-1} for [(*P*)-**241**]$^{2+}$ and $\Delta\varepsilon$ = -100 M^{-1}cm^{-1} for [(*P*)-**241**]^{0}. This helically chiral system displays the most intense chiroptical switch response observed in helicenoids up to now. Furthermore, it was possible, by gradual ramping of potentials between the three species [(*P*)-**241**]$^{2+}$, [(*P*)-**241**]$^{\bullet+}$ and [(*P*)-**241**]^{0} to perform a three-states modification of UV-vis and ECD response as depicted at 282 nm in Figure 31b. Finally, reading out the system at 550 nm led to an ON/OFF switching of the ECD signal.

The post-functionalization of [5] and [6]Helquats was shown feasible through Knoevenagel reactions at methyl groups placed at diverse positions thus yielding a class of Helquat dyes with intense colour and NLO activity,[224] such as (-)-[(*M*)-**244**][OTf]$_2$ on Scheme 59 obtained from (-)-[(*M*)-**243**][OTf]$_2$ prepared in enantiopure form by diastereomeric crystallization of its dibenzoyltartrate salts.[234] These compounds display interesting chiroptical activity. Indeed, in 2015, the same group described Helquat dyes as the first enantiopure helicene-like cationic styryl dyes for which their remarkable chiroptical properties were due to a combination of a cationic hemicyanine chromophore and a helicene-like motif (**245a**,**b** in Figure 31c).[235] The magnitude of the ECD response and the pH switching along with their positioning in the visible region was unprecedented among helicenoids (Figure 31c). Since then several other examples have been described (for a review see [22]).

Scheme 59. Post-functionalization of [6]Helquat (*M*)-[**243**][OTf]$_2$ to [6]Helquat dye (*M*)-[**244**][OTf]$_2$.[224]

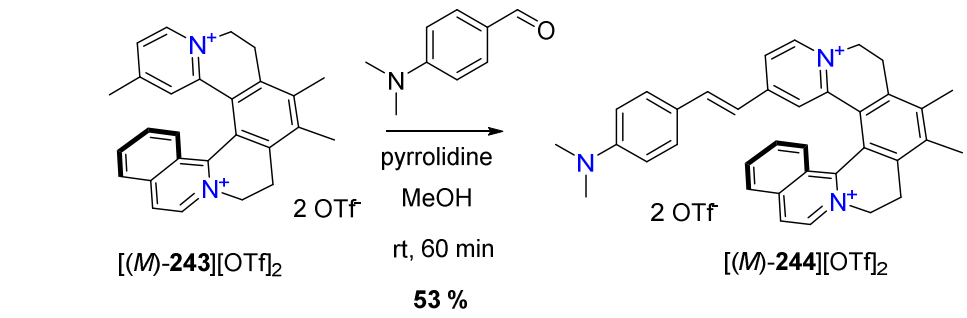

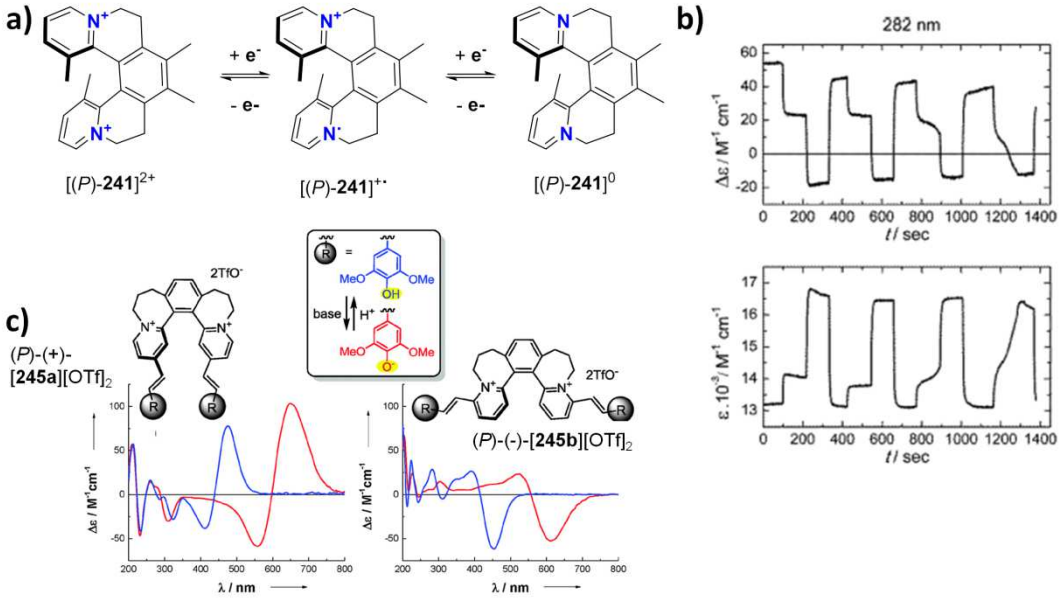

Figure 31. a) Three redox states of [(*P*)-**241**]. b) Redox-triggered ECD and UV-vis response of [(*P*)-**241**]. c) Acid-base triggered Helquat systems [**245a**,**b**][OTf]$_2$ featuring a cyanine motif. Adapted from refs. [233] and [235]. Copyrights 2014 and 2015, American Chemical Society and Royal Society of Chemistry.

Induction of optical activity from a chiral Helquat to achiral solvents was observed by ROA spectroscopy. Indeed, it was observed that [6]Helquat dye enantiomers of [**244**][OTf]$_2$ (see Scheme 59) induced exceptionally large Raman optical activity (ROA) in nitrile solvents (Figure 32). This surprising effect was partially attributed to the enhancement of Raman scattering, due to a near resonance between the green 532 nm excitation laser light and S0-S1 electronic transition of the Helquat dye.[234] This effect may give valuable insight into intermolecular interactions including the structure of solvation spheres.

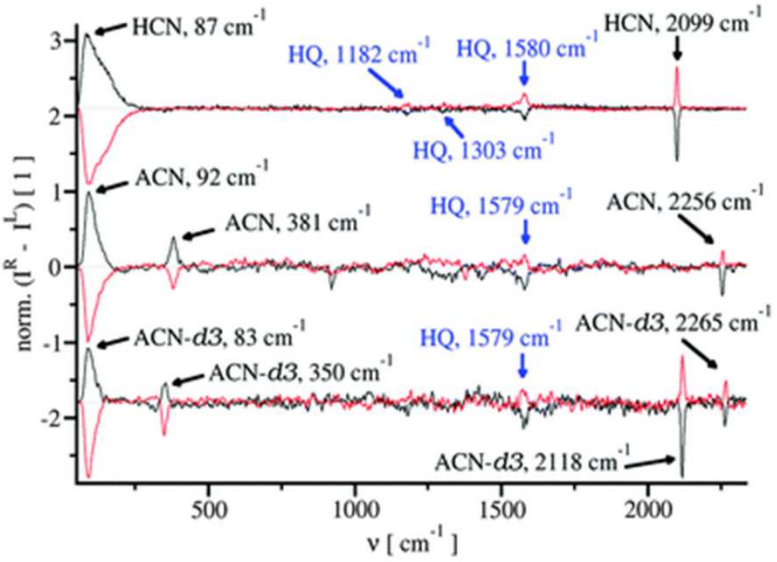

Figure 32. Experimental ROA spectra of [6]Helquat dye [**244**][OTf]$_2$ solutions in three nitrile solvents HCN, acetonitrile (ACN), and acetonitrile-d$_3$ (ACN-d$_3$). **HQ** = [**244**][OTf]$_2$. Black and red curves correspond to solutions of the (*P*)- and (*M*)-**244**, respectively. The strongest ROA peaks of [**244**][OTf]$_2$ and each solvent are indicated by arrows. Reproduced from ref. [234]. Copyright 2016, Royal Society of Chemistry.

The existence of a thermal racemization pathway equilibrating the right-handed (*P*) helix with the left-handed (*M*) helix is an important feature of helicenes [see [236] and references therein]. The helix inversion of a [6]helicene typically proceeds *via* an achiral C_S-symmetric saddle-shaped transition state (see Figure 8). In 2011, the group of Teply reported the synthesis, structure, and dynamic properties of a [6]Helquat, a dicationic [6]helicene congener captured on the racemization pathway in its saddle-shaped geometry (Scheme 60).[237] Resolution of this chiral saddle-shaped species and its highly stereocontrolled transformation into enantiopure [6]Helquat was demonstrated. Indeed, the triyne [**246**][TfO]$_2$ led to the formation of an isolable saddle-shaped species [**247**][TfO]$_2$ along with the formation of [6]Helquat [**248**][TfO]$_2$ featuring the typical helical shape, in respective 4:1 proportion and under kinetic control. The solubilities of the diastereomeric salts [**247**][TfO]$_2$ and [**248**][TfO]$_2$ were different enough in THF to separate the two stereoisomers. Notably, the saddle-shaped species [**247**][TfO]$_2$ was sufficiently long-lived to be studied experimentally. Upon heating in DMSO-d$_6$ at 100 °C saddlequat [**247**][TfO]$_2$ gradually and completely converted to Helquat [**248**][TfO]$_2$ (Scheme 60) with an activation free energy value $\Delta G^{\#}$ of 28.7 kcal mol^{-1}. This process was followed by NMR but also by ECD spectroscopy. Indeed, the pure enantiomer of **247**$^{2+}$ could be obtained similarly to **241**$^{2+}$, *i.e.* through preferential crystallization of its diastereomeric (*R*,*R*)-dibenzoyltartrate salts, thus yielding after anion resin exchange to pure stereoisomer (+)-[(S_a,R_a)-**247**][TfO]$_2$ as ascertained by X-ray crystallography. Then by heating this enantiopure sample of saddlequat (+)-[(S_a,R_a)-**247**] ditriflate at 100 °C in DMSO-d$_6$, they were able to confirm that the saddle-shaped species can be transformed into enantiopure (-)-[6]Helquat [**248**][TfO]$_2$ with no loss of chirality (Scheme 61). Furthermore, this method appeared to be the only method to prepare enantiopure samples of **248**$^{2+}$. Finally, a high stereocontrol of the chiral information transfer was observed for the enantiopure helix (-)-[(*P*)-**248**][TfO]$_2$, as established by X-ray crystallography and

optical rotation measurements. The racemization process of [**248**][OTf]$_2$ was then examined experimentally and the activation free energy value to be $\Delta G^{\#}$ = 36.7 kcal mol^{-1} and a racemization half-life $t_{1/2}$ = 4.8 h at 180 °C.

Scheme 60. Racemization of [6]Helquat *via* an isolable saddle-shaped intermediate. Synthesis of saddle-shaped species [**247**][TfO]$_2$ as the major product from triyne [**246**][TfO]$_2$. X-ray structures of [6]saddlequat and [6]Helquat (obtained as one stereoisomer, H have been omitted for clarity). Adapted from ref. [237]. Copyright 2011, Royal Society of Chemistry.

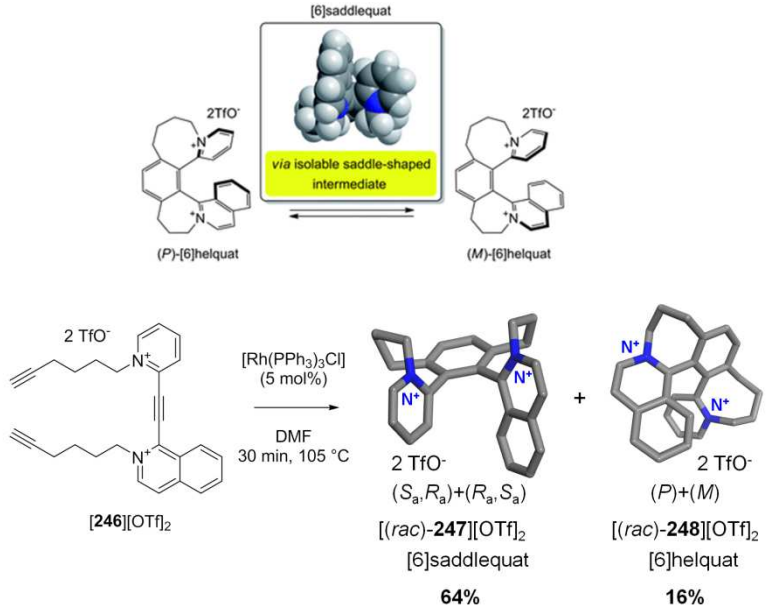

Scheme 61. ECD spectra recorded in the course of the stereocontrolled transformation (+)-[S_a,R_a-**247**][TfO]$_2$ → (-)-[(*P*)-**248**][TfO]$_2$ in DMSO at 100 °C. Reproduced with permission from ref. [237]. Copyright 2011, Royal Society of Chemistry.

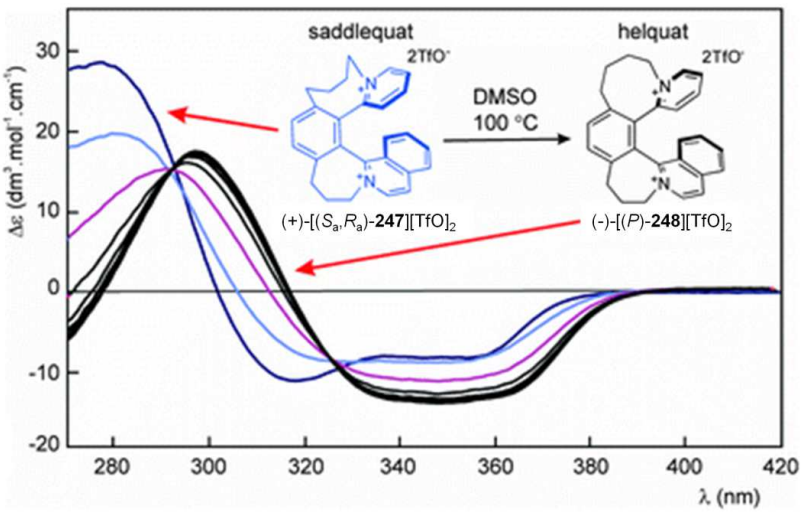

Although the helix conformer is generally energetically preferred in the free dications denoted HQ^{2+} as well as the neutral salts $[HQ^{2+}\cdot 2X^-]$, Teply, Schröder, and coworkers demonstrated, by different techniques in the condensed phase in conjunction with mass spectrometric measurements in the gas phase, and with the help of theoretical calculations, that for many counterions X^- in the singly charged binary ion pairs, the saddle conformations denoted $[SQ^{2+}\cdot X^-]$ was significantly preferred over $[HQ^{2+}\cdot X^-]$. Indeed, system **249** appeared to adopt different forms, helical or saddle-like, depending on its electronic state and on the counterion utilized.[238] The reason for this inversion of stability of the di-cationic *vs.* the mono-cationic system is explained by the fact that the saddle conformer has a central binding pocket, in which the anion can interact with both pyridinium centers, whereas the more compact helix conformer permits the anion to approach only a single cationic center efficiently. Thus, this corresponds to a counterion-induced inversion of conformer stability (see Figure 33).

Note that in a similar way, a [7]Saddlequat was prepared, which upon UV light yielded a [8]circulenoid structure, resulting from a [6+6] photocycloaddition of the terminal rings which closes the system. Upon heating, the circulenoid structure opens back to [7]saddlequat mixed with the corresponding [7]Helquat. However, these structures were studied only in racemic forms.[239] Furthermore, in 2014, Teply *et al.* developed a modular synthesis of helicene-like compounds with a central imidazolium motif based on double [2+2+2] cycloaddition reactions.[240] The two enantiomers were analyzed by chiral electrophoresis but the pure enantiomers could not be obtained yet.

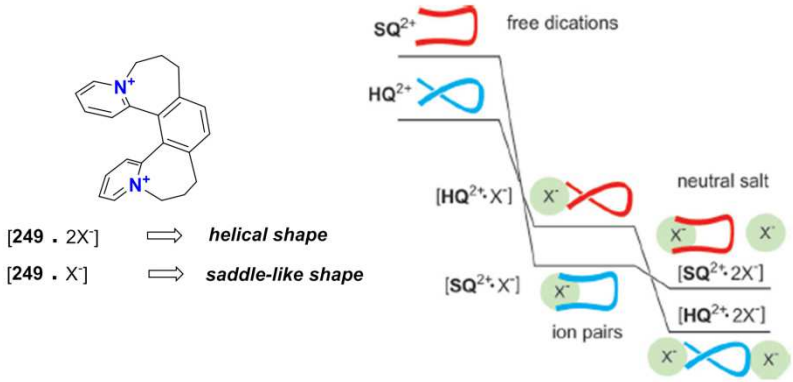

Figure 33. Sketch of the free dications with the helical form HQ^{2+} being more stable (blue) than the saddle conformer SQ^{2+} (red) and of the binary ion pairs with a counterion X^-, where the closer approach of the anion into the pocket of the saddle form can lead to an inversion of thermochemical stability for certain anions as indicated by the change in color. Adapted from ref. [238]. Copyright 2012, Wiley.

Kasicka *et al.*[226] investigated the non-covalent molecular interactions between Helquats, and several chiral acidic aromatic drugs (including warfarin, ibuprofen, mandelic acid, etodolac, binaphthylphosphate) by using the partial-filling affinity capillary electrophoresis (PF-ACE) technique. For example, enantioselective interaction was observed for (*R*) and (*S*)-enantiomers of 1,1'-binaphthyl-2,2'-diyl hydrogenphosphate (BNP) **X7** with [7]Helquat [(*P*)-**250**]$^{2+}$ (Figure 34) in favor of the (*S*): 394 ± 77 *vs.* 870 ± 138 L mol^{-1}. For mandelic acid **X6**, the recognition was below 50 L mol^{-1}. Overall, among the tested compounds, only isomers of those exhibiting helical chirality and/or possessing conjugated aromatic systems were enantioselectively separated through their differential interactions with helquats.

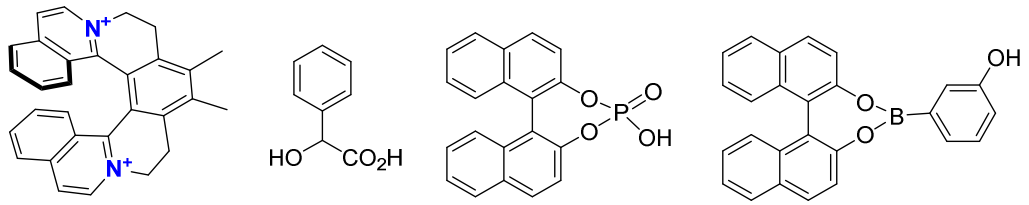

Figure 34. Molecular systems studied for enantioselective recognition of [(*P*)-**250**]$^{2+}$.[226]

Note that many helical N-heteroaromatic dications, [5], [6] and [7]Helquats were analytically separated by CE in an acidic sodium/phosphate background electrolyte (pH 2.4) and with addition of randomly sulfated α-, β- and γ-cyclodextrins. At least one of the chiral selectors was found to provide baseline separation for 22 out of 24 Helquats and partial separation for the remaining two. Individually, the sulfated γ-cyclodextrin turned out to separate 79% of the helquats, followed by the β- and α-congeners with 54 and 42% of the resolved compounds, respectively.[241] It was found that the migration order of the (*M*)- and (*P*)-helices was variable and dependent on the Helquat structure and the chiral selector. In another study by Teply, Willner, *et al.* studied the enantioselective recognition of (*R*)- or (*S*)-binaphthol phenylboronic acid ester ligands (Figure 35) by [7]Helquat **250**$^{2+}$ through donor-acceptor complexes where the Helquat acts as an electron acceptor. By following the quenching of fluorescence, the (*R*)/(*P*) or (*S*)/(*M*) complexes (in either 1:2 or 2:3 ratios depending on concentration) appeared more stable associations.[242] Au nanoparticles (NPs) were then functionalized with (*R*) or (*S*) binaphthol phenylboronic ester ligands through an amide link (see Figure 35) and preferred (*R*)/(*P*) and (*S*)/(*M*) associations were reflected in the aggregation rates of the Au-Nps, as evidenced by the UV-vis absorption decrease which was faster for the more favored association. This is a nice example of a Helquat-induced chiroselective aggregation of Au Nps. Note that circular dichroic plasmonic signal was observed in these chiral nanoparticles. Selective recognition properties of chiral ligand-functionalized Au NPs may be implemented in the future for the selective targeting to chiral biological microenvironments. Note that an interesting solid-to-solid phase transition in a helicene or a helicene-like compound was observed in single crystals of enantiopure [**250**][OTf]$_2$.[243]

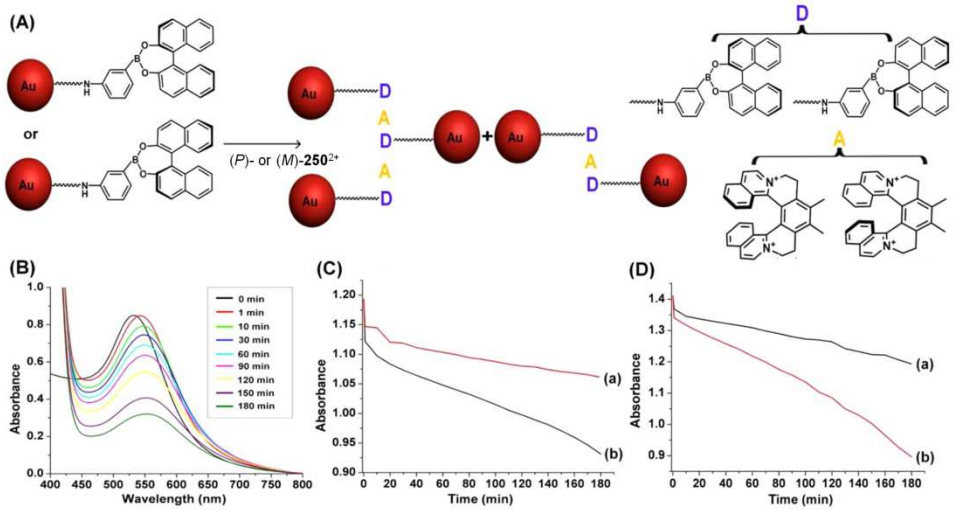

Figure 35. Schematic chiroselective helquat-induced aggregation of chiral binaphthol boronic ester-capped Au NPs using donor–acceptor interactions. (B) Time-dependent UV–vis absorption spectra upon

the aggregation of the (*R*)-modified Au NPs in the presence of [(*P*)-**250**]$^{2+}$. (C) Time-dependent absorbance changes at λ = 537 nm upon (a) aggregation of the (S)- modified Au NPs in the presence of [(*P*)-**250**]$^{2+}$ and (b) aggregation of the (*S*)-modified Au NPs in the presence of [(*M*)-**250**]$^{2+}$. (D) Time-dependent absorbance changes at λ = 537 nm upon (a) aggregation of the (*R*)- modified Au NPs in the presence of [(*M*)-**250**]$^{2+}$ and (b) aggregation of the (*R*) modified Au NPs in the presence of [(*P*)-**250**]$^{2+}$. In all systems, the Au NPs ($4.5 \pm 0.5 \times 10^{-9}$ M) were interacted in triple distilled water (TDW) with the respective dicationic helquats (2×10^{-4} M). Panels C,D: data in red color correspond to experiments with [(*P*)-**251**]$^{2+}$. Data in black color correspond to experiments with [(*M*)-**250**]$^{2+}$. Reproduced from ref. [242]. Copyright 2012, American Chemical Society.

4.1.7.1.2. Other azoniahelicenes

Sato and Arai developed the synthesis of several azonia[6]helicenes among which the ones in Figure 34. These helicenes were only obtained as racemic compounds,[244,245,246,247] except **251a** which was resolved by chiral HPLC as described in Table 21.[97]

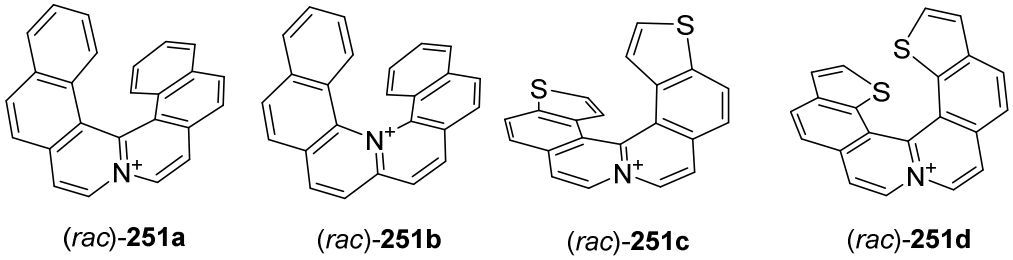

Figure 36. Azonia[6]helicenes prepared by Sato, Arai *et al*.

Note that the (*P*)- and (*M*)-3-azonia[6]helicenyl β-cyclodextrins **253** were obtained by reaction of **252** with (*P*)- or (*M*)-**41a**^{3} (Scheme 62).[248] Performing complexation studies by fluorescence spectroscopy in aqueous media, it was shown that this system displayed L/D selectivities of up to 12.4 and (*P*)/(*M*) preferences of up to 28.2 upon complexation with underivatized proteinogenic amino-acids in aqueous solution at pH 7.3. Note that racemic chemical neutral sensors recognizing explosives,[249] ions,[250,251] have been developed. Furthermore, a racemic N-methylated aza[5]helicene (**35a**^{5} derivative) was studied as DNA intercalators by using UV-vis, ECD and emission spectroscopies.[252]

Scheme 62. Azonia cyclodextrine system for recognition of amino-acids. Reproduced from ref. [248]. Copyright 2016, American Chemical Society.

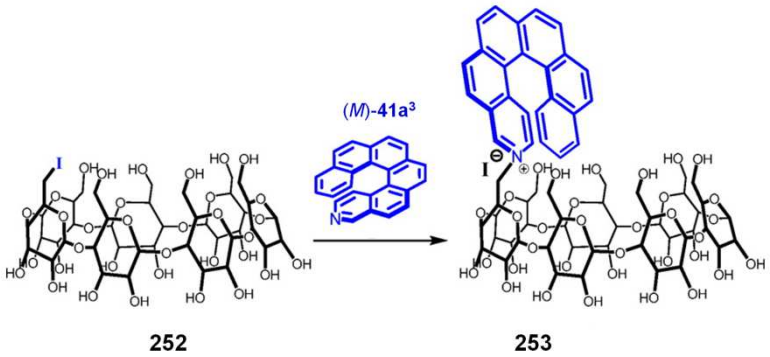

In 2017, Teply and Fuchter took advantage of the dimerization process of *N*-methyl-1-azonia[6]helicene [(*M*)-**254**]$^+$ to perform an intense chiroptical switch.[253] Indeed, a one-electron reduction of two [(*M*)-**254**]$^+$ yielded radical [(*M*)-**254**]$^{\cdot}$ which fastly dimerized to bis-helicenic system [(*M,M*)-**255**]. In its turn, the latter was bis-oxidized to [(*M,M*)-**255**]$^{2+}$ which spontaneously dissociated back to [(*M*)-**254**]$^+$ (Scheme 63a). Following the ECD responses at two different wavelengths, *i.e.* 267 and 292 nm, upon successive reduction and oxidation steps, revealed the reversible tuning of the chiroptical activity, with very strong differences in the ECD read-out signals (Scheme 63b). Note that the two reduction and oxidation steps occurred at very different potentials, thus giving a large potential range of bistability were the state of the molecule and its corresponding chiroptical read-out is solely determined by the previous redox history.

Scheme 63. a) Reversible cycle of reduction-dimerization-oxidation-dissociation of *N*-methyl-1-azonia[6]helicene [(*M*)-**254**]$^+$ and b) reversible ECD switching signal at two different wavelengths. Adapted from ref. [253]. Copyright 2017, Royal Society of Chemistry.

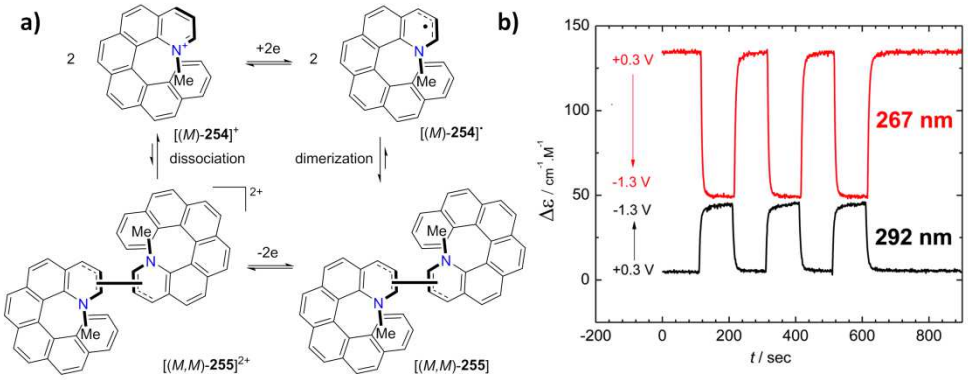

Table 21. Specific rotation values of enantioenriched Helquats.

Compound	Method of obtention	$[\alpha]_D$[a]	Conditions[b] (solvent / Conc.[c])	Enantio/diastereo-purity	Ref.
[(*P*)-**241**][OTf]$_2$	Diastereomeric crystallization[d] or Preferential crystallization	+290.6 +298.4	MeOH/0.224 H_2O/0.224	>98%[e]	227 or 230
[(*M*)-**242**][Br]$_2$	Dutch resolution[f]	-478.0	MeOH/0.201	>98% *ee*[e]	231
[(*M*)-**243**][TfO]$_2$	Diastereomeric crystallization[d]	-633.0	DMSO/0.263	98% *ee*[e]	234
[(*M*)-**244**][TfO]$_2$	From [(*M*)-**243**][TfO]$_2$	-3063.0	MeOH/3.6×10^{-4}	98% *ee*[e]	234
[(S_a,R_a)-**247**][TfO]$_2$	Diastereomeric crystallization (**A1**)[d]	+213.9	MeOH/0.129	>99% *ee*[e]	237
[(*P*)-**248**][TfO]$_2$	From [(S_a,R_a)-**247**][TfO]$_2$	-35.3	MeOH/0.232	>99% *ee*[e]	237
[(*P*)-**250**][TfO]$_2$	Preferential crystallization[d]	+572.7	MeOH/0.271	99.8% *ee*[e]	232
(*P*)-**251a**	Chiral HPLC[g]	+2700±100	ACN/0.0057	>99% *ee*[g]	97

[a] In deg·mL·g^{-1}·dm^{-1}. [b] Temperature between 20-25 °C. [c] In g/100 mL otherwise precised. [d] Crystallization of dibenzoyltartrate salts. [e] Chiral electrophoresis with a sulfated β- or γ-cyclodextrin

chiral selector. [f] crystallization with a mixture of tartrate derivatives. [g] Daicel Chiralpak OD-R, aqueous 0.1 M KPF_6/acetonitrile, 50/50.

4.1.7.2. Carbocationic azahelicenes

Cationic helicenes bearing a carbocation in the central part of the helical core have been extensively developed by the group of J. Lacour. Due to the fact that some key compounds can be readily obtained in enantiomerically forms and in large scale, and thanks to the good solubility in aqueous media, these charged helicenes have recently received great attention in the fields of chirality, physical organic chemistry, optoelectronics and biology.

4.1.7.2.1 Synthesis of configurationally stable carbocationic aza[4]helicenes

Helical derivatives of aza- and oxa-triangulenium salt, bearing nitrogen and oxygen atoms within the helix and a central carbocation, present peculiar chemical reactivity and photophysical properties owing to the very high stability of the inner carbocation under basic conditions (for a review see: [254]). The first isolation and complete characterization of such helicenium derivative was obtained by Laursen, Lacour *et al*. in 2003, following the synthesis of trimethyl triazatriangulenium salt [**258**][BF_4] through three consecutive *ortho* S_NAr reactions on *tris*(2,6-dimethoxyphenyl)-methylium cation **256**$^+$ (Scheme 64).[255]

Scheme 64. Synthesis of trimethyl triazatriangulenium salt [**258**][BF_4] through three consecutive *ortho* S_NAr reactions on carbenium salt [**256**][BF_4]. Chemical structure of 1,12-dimethylbenzo[c]phenanthrene **259**, archetype of carbo[4]helicene derivatives.[255,256]

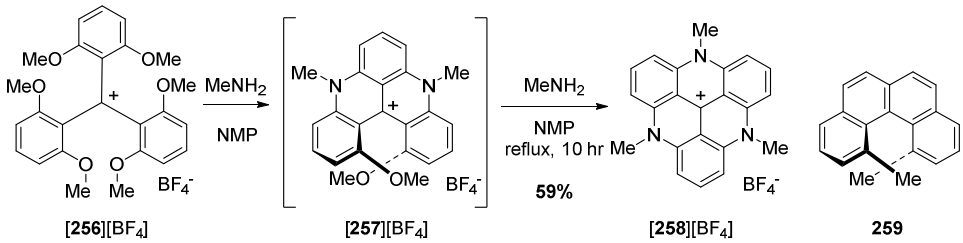

During the course of this reaction, intermediate [**257**][BF_4] was formed before the third S_NAr reaction. This intermediate can be viewed as a [4](hetero)helicenium derivative. By adjusting the reaction conditions (temperature = 110 °C and reaction time of 45 min.), the authors were able to isolate bisaza[4]helicenium salt [**257**][BF_4] as the major product in good yields (85%, Scheme 65). As in the case of 1,12-dimethylbenzo[*c*]phenanthrene [**257**][BF_4], the steric repulsion between the methoxy substituents in positions 1 and 13 forces the molecule to adopt a twisted conformation typical of helicene derivatives, which was confirmed by X-ray diffraction analysis of racemic the tetraphenylborate salt of [**260**][BF_4]. To further explore the configurational stability of [**260**]$^+$, resolution of the chiral cations through diastereomeric salt formation was attempted using enantiopure anion. The authors used chiral hexacoordinated phosphorus-centered (*Δ*)- and (*Λ*)-BINPHAT anion and succeeded in isolating the corresponding diastereomers by solubility differences and preparative achiral column chromatography (Scheme 65).

Scheme 65 Resolution of (+)- and (-)-**260**$^+$ through the formation of diastereomeric salt with (*Δ*)- and (*Λ*)-BINPHAT anion, respectively. Chemical transformation of [4]helicenium **260**$^+$ to neutral **261** for racemization studies. Experimental (blue) VCD spectrum of (-)-[**260**][PF_6] and theoretical rotational strength (red), asterisks denote regions of solvent absorption. Adapted from ref. [255]. Copyright 2003, Wiley.

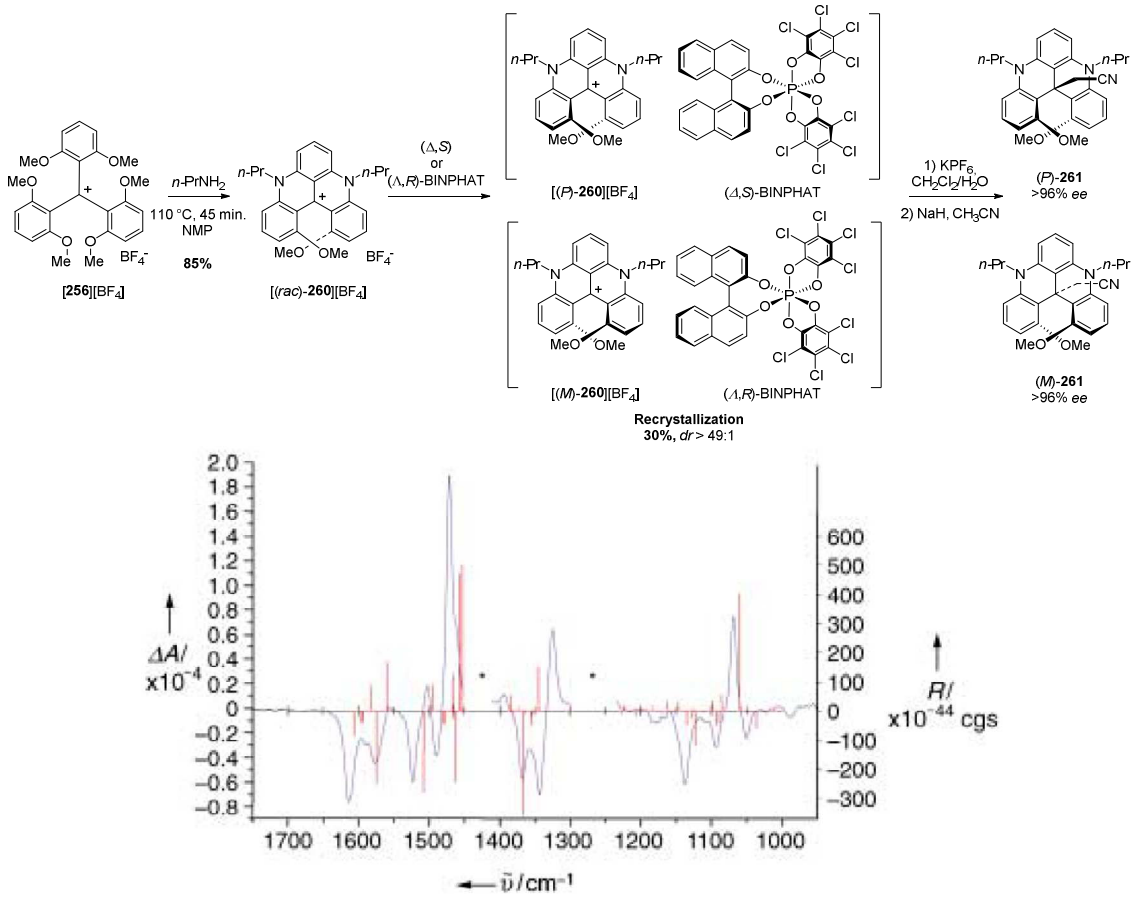

The authors characterized each enantiomer by VCD and assigned (*P*) and (*M*) configuration for (+)- and (-)-[**260**][PF_6] salts, respectively, by comparing experimental with calculated VCD signatures (Scheme 65). Determination of the interconversion barrier could not be performed on the enantiomer salt due to the presence of the cation which provides intense absorption in the visible region, ruling out optical rotations measurements and elution difficulties on available chiral stationary phase at that time. As a consequence, the authors performed chemical addition of reactive $CNCH_2^-$ carbanion to isolate neutral [4]helicene species (*M*)- and (*P*)-**261**, which occurred with retention of absolute helical configuration (Scheme 65). Remarkably, racemization of these enantiomers measured by chiral HPLC occurs at very high temperature, with a free energy of activation of 41.3 kcal mol^{-1} and a half-life of 182.7 h at 200 °C, which makes these [4]helicene derivatives more stable than the carbo[6]helicene parent **3**.

Soon after, Lacour *et al.* reported a more efficient resolution of [4]azahelicenium salts based on the specific chemical reactivity of the central carbocation.[257] They developed an unprecedented Pummerer-like reaction where [**260**][BF_4] acts as a better electrofugal group than H^+ due to its high chemical

stability. They firstly treated [**260**][BF_4] with (*R*)-(+)-Methyl-*p*-tolylsulfoxide **262** to form neutral (*R*,*M*)-**263a** and (*R*,*P*)-**263b** diastereomers, which were efficiently separated over achiral silica chromatography column (Scheme 66). They next investigated the Pummerer reaction on these derivatives using simple HPF_6 treatment in acetone at room temperature, which resulted in immediate formation of enantiomerically pure [(*M*)-**260**][PF_6] and [(*P*)-**260**][PF_6] salts. ECD spectrum of [(*P*)-**260**][PF_6] is depicted in Scheme 66 and shows active positive and negative transitions at 280 ($\Delta\varepsilon$~45 $M^{-1}cm^{-1}$), 300 ($\Delta\varepsilon$~-20 $M^{-1}cm^{-1}$), 360 nm ($\Delta\varepsilon$~-20 $M^{-1}cm^{-1}$) and 460 nm ($\Delta\varepsilon$~-20 $M^{-1}cm^{-1}$).

This non classical Pummerer bond fragmentation mechanism was further investigated to rationalize the proposed rearrangement pathway (Scheme 66), which was found to be directly related to the high stability of the helical carbocation.[258] However, the efficiency of this strategy appeared to be dependent on the nitrogen substituents, especially when *N*-methyl side chain(s) are used, resulting in poor diastereomeric separation of the corresponding sulfoxide derivatives on silica gel.[259] While the two chemical diastereomeric resolution approaches mentioned above afforded very high level of enantiopurity for [4]helicenium derivatives with high quantities of carbocationic helicenes (thus enabling reactivity and property studies), a direct and precise determination of enantiomeric purity by chiral chromatography was still problematic due to their ionic nature. In 2007, Lacour *et al.* circumvented this issue and reported the separation of [(*M*)-**260**]$^+$ and [(*P*)-**260**]$^+$ salts using chiral stationary phases based on either cellulose derivative-based HPLC (Chiralcel OD-RH) or Teicoplanin aglycon immobilized on silica gel (Chirobiotic TAG) with water-based eluents containing KPF_6 as additive.[260]

Scheme 66. Chemical Resolution of (+)- and (-)-[**260**][BF_4] *via* non classical Pummerer fragmentation of diastereomers (*R*,*M*)-**263a** and (*R*,*P*)-**263b**. ECD spectra of [(*P*)-**260**][PF_6] in ACN/H_2O (red line) and in EtOH/H_2O (blue dotted line) with KPF_6 (30 mM) in both mixture of solvent. Adapted from refs. [257] and [260]. Copyrights 2005 and 2007, Wiley.

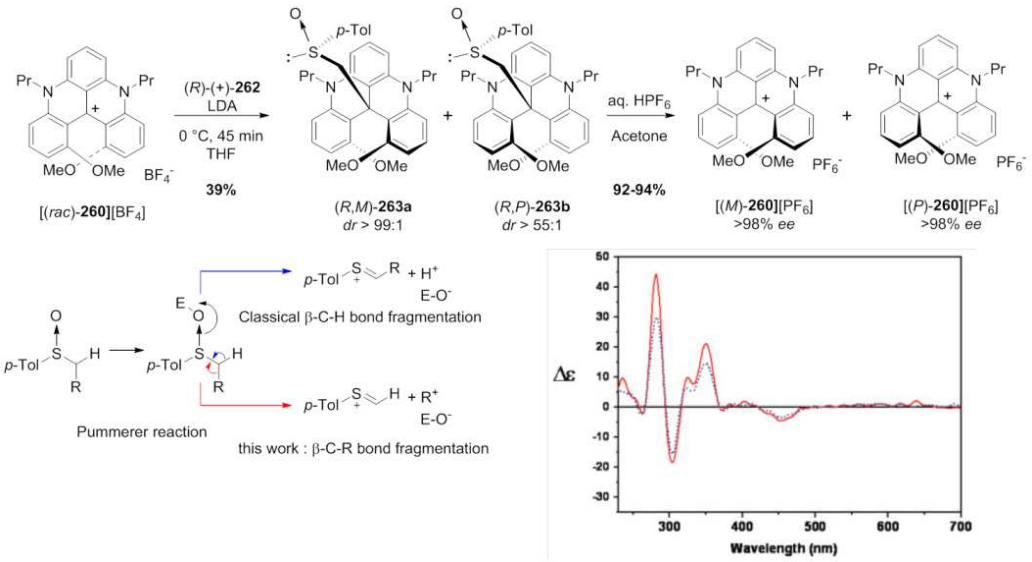

In order to extend the structural diversity of [4]helicenium derivatives, the same research group started to investigate other heteroatoms than nitrogen ones for the S_NAr substitutions reactions. The synthesis of sulfur-bridged [4]helicenium compound was reported in 2010 in its racemic form.[261] In the same year, the synthesis of cationic chromenoxanthene [4]helicene was reported (an oxygenated analogue of **260**$^+$, see

Scheme 67) along with its chiral HPLC resolution and configurational stability.[262] Starting from the carbenium salt of [**256**][BF_4], 1,13-dimethoxychromenoxanthenium salt [**265**][BF_4] was obtained in 5 steps, in a more tedious way in comparison with aza[4]helicenium derivatives.

Scheme 67. Synthesis of 1,13-dimethoxychromenoxanthenium salt **265**$^+$ and corresponding UV-vis and ECD spectra, recorded in ACN solution ((*P*)-**265**$^+$ is in blue and (*M*)-**265**$^+$ in red). Adapted from ref. [262]. Copyright 2010, American Chemical Society.

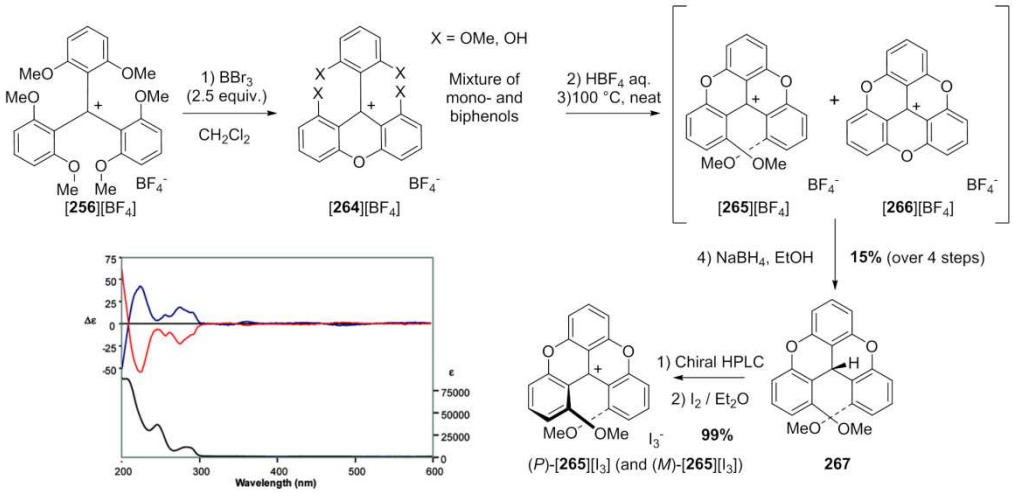

Indeed, oxa[4]helicenium **265**$^+$ appeared to be much prone to ring closure to form trioxatriangulenium **266**$^+$ than its aza analogue **260**$^+$, rendering its isolation and study quite difficult. Moreover, since compounds **265**$^+$ and **266**$^+$ were difficult to obtain in their pure forms, the authors had to proceed in two steps, *via* the formation of neutral adduct **267** to finally obtain salt **265**$^+$ in its racemic form. Resolution was also performed on neutral racemic **267** using Chiralpak IB stationary phase using organic solvents for practical reasons, followed by chemical oxidation to afford corresponding enantiomers (+)- and (-)-[**265**][I_3]. Racemization barrier was monitored by ECD and resulted in low activation barrier of 27.7 kcal mol^{-1}, much lower than for **260**$^+$ owing to the degree of flexibility brought by the presence of the two oxygen on the helical core. ECD spectra reveal significant differences between oxa[4]helicenium **265**$^+$ and aza[4]helicenium **260**$^+$, with almost no absorption and active ECD transitions after 300 nm for (*P*)- and (*M*)-**265**$^+$ in comparison with (*P*)- and (*M*)-**260**$^+$ (Scheme 67). In 2013, Laursen *et al.* reported another approach to obtain similar racemic oxahelicenium derivatives using hydrobromic or sulfuric acid as reacting agents.[263] Following this work, the same group reported for the first time the synthesis of azaoxa[4]helicenium, which includes both oxygen and nitrogen atoms as structural bridges.[264] They obtained racemic *N*-Alkyl-1,13-dimethoxychromenoacridinium salts by a stepwise ring closure strategy, using firstly primary amine derivatives and then sulfuric acid to form the desired helicenium salt. In a complementary study, Lacour *et al.* reported soon after a second synthetic approach to obtain azaoxa[4]helicenium [**268**][BF_4] and performed their resolution using chiral HPLC (Scheme 68).[265]

Scheme 68. Convergent synthetic pathway of azaoxa[4]helicenium salt. Experimental VCD spectra of [(*P*)-**268**][BF_4], (red) and [(*M*)-**268**][BF_4] (blue) with R = propyl, and calculated VCD spectrum of (*P*)-**268**$^+$. Adapted from ref. [265]. Copyright 2014, American Chemical Society.

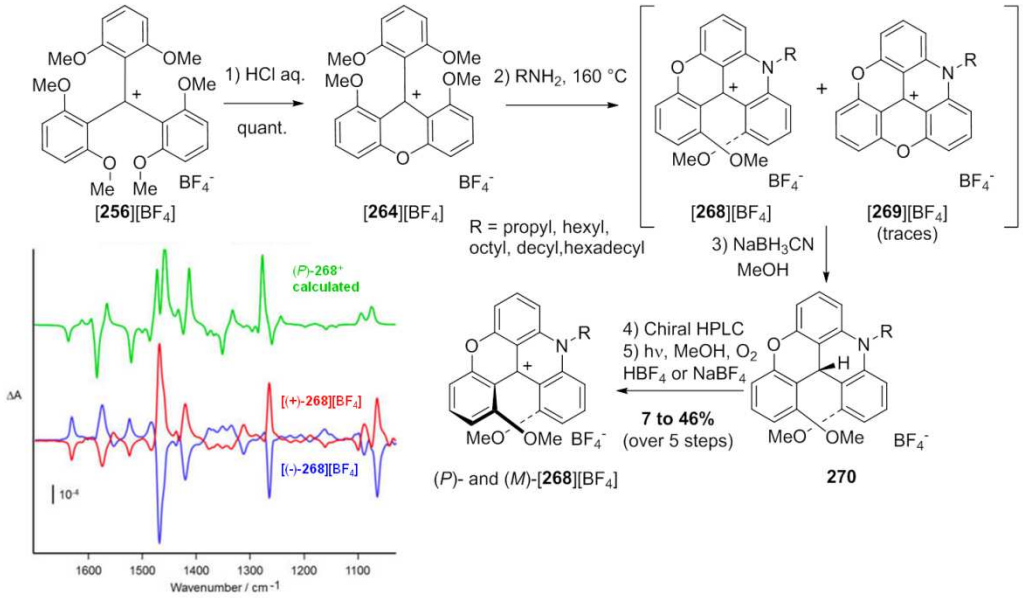

The convergent synthetic pathway involved xanthenium salt [(*P*)-**264**][BF_4] as a common precursor, which was obtained following conditions described by Martin and Smith.[266] Treatment of this intermediate with primary alkyl amine afforded a mixture of [4]helicenium [**268**][BF_4] and azadioxatriangulenium [**269**][BF_4], which were readily separated through a chemo and stereoselective reduction of the former with $NaBH_3CN$. In a final step, reoxidation of compound **270** under photochemical conditions afforded [(*M*)-**268**][BF_4]. Resolution of these new [4]helicenium derivatives were performed on neutral derivatives **270** rather than on the cationic species **268**$^+$ for practical reasons using Chirapak IC column. Here again, VCD spectroscopy helped to establish the absolute configuration of helicenes **268**$^+$ with a good agreement between the experiment and theoretical spectra (green spectrum, Scheme 68). Interestingly, the chiroptical properties of these azaoxa[4]helicenium derivatives are relatively similar as aza[4]helicenium **260**$^+$, highlighting the important role of the nitrogen atom. Racemization barrier was measured using ECD monitoring in DMSO solutions. A value of 33.3 kcal mol^{-1} was determined for the racemization barrier at 433K, being between the ones for the diaza-**260**$^+$ and the dioxo-**265**$^+$, highlighting again the degree of flexibility brought by the presence of the oxygen atom.

4.1.7.2.2. Reactivity of configurationally stable carbocationic aza[4]helicenes

The high stability of the carbocation within the helical framework and its particular reactivity towards nucleophiles such as hydride and organometallic reagents for these [4]helicenium compounds enables a number of interesting reactivity aspects to investigate. Among them, the stereoselective control of nucleophile addition by a helical stereocenter appears particularly interesting for studying diastereoselective reactions. In 2011, Lacour *et al.* addressed this question with diaza[4]helicenium compound functionalized with two different substituents on the nitrogen atoms (Scheme 69).[267] Enantiomers of compounds [**272**][BF_4] were submitted to different nucleophiles agents (hydride, alkyl

and alkynyl) which afforded diastereomers **273** in excellent yields with a high diastereomeric ratio (> 98:2) for derivatives having nitrogen substituents of different sizes. X-ray structures of the obtained diastereomers revealed that the cationic carbon adopts a sp^3 hybridization upon nucleophile addition with one nitrogen atom becoming pyramidal while the other keeping its sp^2 hybridization. This geometrical distinction probably results from the facial selectivity of the nucleophilic attack, which favors one main facial approach towards the increase of the distance between the 1 and 13 methoxy substituents, resulting in forcing the more flexible nitrogen atom to support the new geometrical constraint. The authors concluded that the helical framework may efficiently control the stereoselective addition of nucleophiles when surrounding electrophile center, which renders compound [**272**][BF_4] potentially interesting phase-transfer catalysts due to their ionic nature. Based on the reactivity of the central carbocation of chiral [4]helicenium derivatives used for purification, resolution or reactivity reasons, the same authors expended this approach with the development of functionalization through an umpolung strategy.[268] They investigated the electrophilic functionalization of neutral adducts **274**, resulting from the reduction of cationic salt **272**$^+$ (Scheme 69). Deprotonation of racemic **274** by *n*-BuLi afforded the carbanion intermediate which was subjected to different electrophiles such as thioamide, acid chlorides or anhydride reagents to obtain products **275**. This protocol was also tested with enantiopure (*P*)-(+)-**274** to yield benzyl isothiocyanate (*P*)-(+)-**275'** as a single enantiomer with complete retention of configuration.

Scheme 69. Synthesis of unsymmetrical diaza[4]helicenium salt and diastereoselective addition of nucleophiles reagents, leading to umpolung strategy for functionalization of cationic [4]helicenium compounds.[267,268]

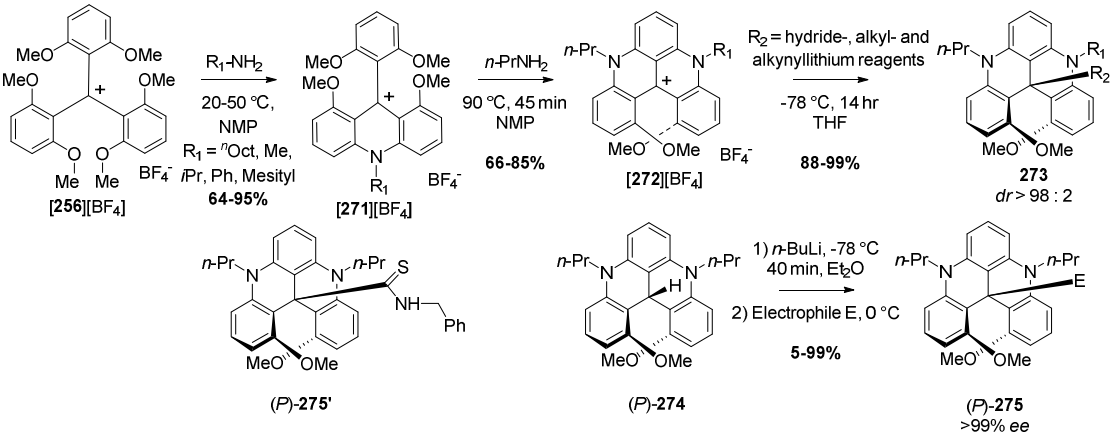

4.1.7.2.3. Synthesis of carbocationic aza[6]helicenes

In 2013, Lacour *et al.* reported the synthesis of cationic [6]helicene as new members of chiral helicenium compounds.[269] Using a modular synthetic pathway, the authors were able to obtain heterohelicenes [**278**][BF_4]-[**280**][BF_4] on a multigram scale, the latter being resolved using (Δ)- and (Λ)-BINPHAT anions in a similar way as for salt [**260**][BF_4] (Schemes 65 and 70). The key intermediate of diaza-, azaoxo- and dioxa-[6]helicene was the salt [**277**][BF_4]obtained in 5 steps from 2-methoxy-1-naphthaldehyde **276**.

Scheme 70. Top: Modular synthesis of diaza-, azaoxo- and dioxo-[6]helicenium compounds. Resolution and examples of regio functionalization on diaza[6]helicenium [**280**][BF_4] with electrophile and nucleophile reagents. Bottom: ECD and VCD spectra of (*P*)-[**280**][PF_6] (blue for ECD and red for VCD) and (*M*)-[**280**][PF_6] green for ECD and blue for VCD), with R = *n*-propyl. Adapted from ref. [269]. Copyright 2013, Wiley.

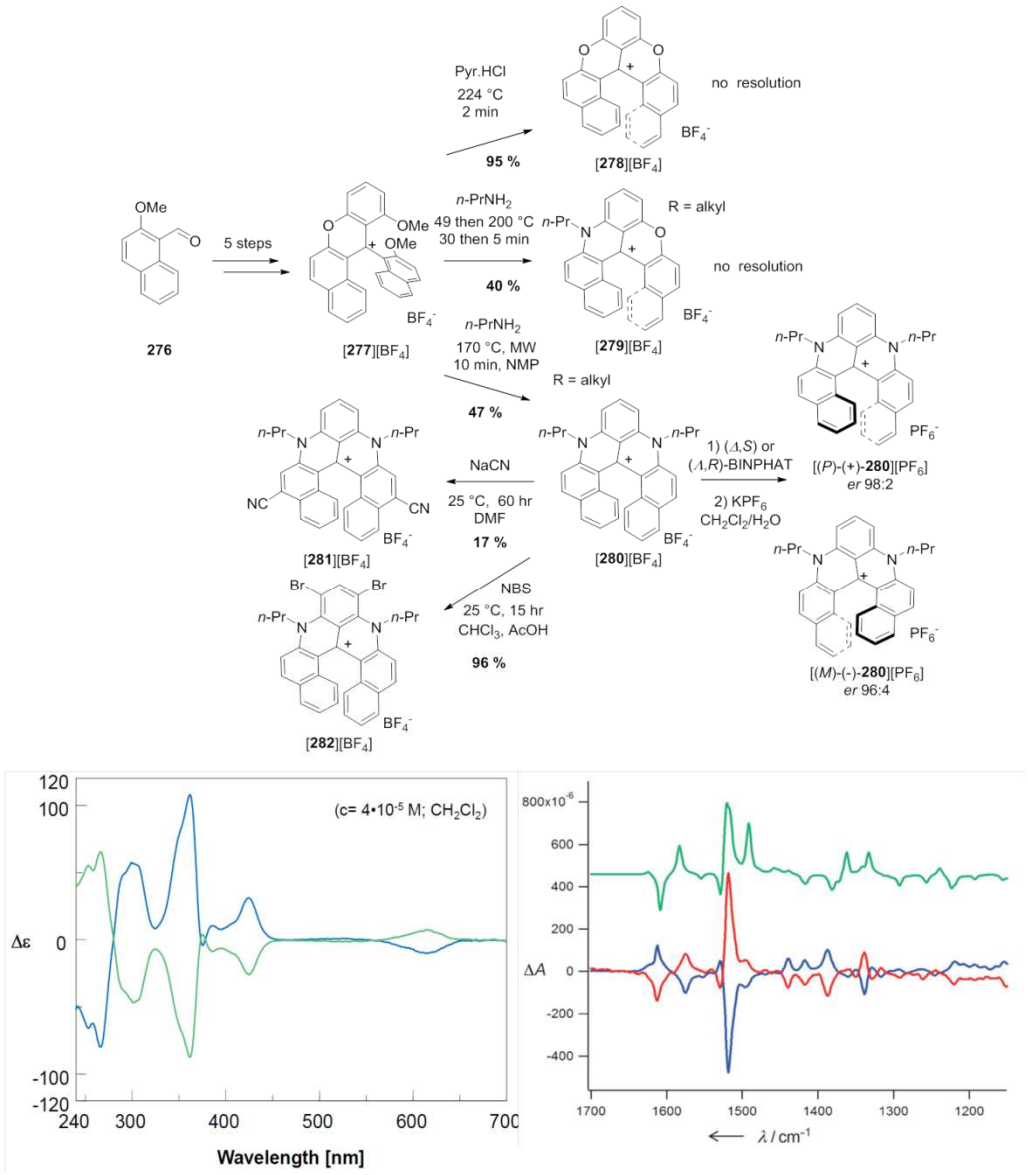

Interestingly, the presence of naphthalene substituents allows regioselective functionalization of the helicene for compound [**280**][BF_4] core depending on the nature of the reagent. Electrophilic aromatic substitutions exclusively occur at the 8,10 positions (example of bromination, [**282**][BF_4] on Scheme 70) while nucleophilic aromatic substitutions only at the 5,13 positions (example of cyanation, [**281**][BF_4] on Scheme 70). These selective reactivities were explored through the introduction of various donor acceptors units in order to modulate the resulting photophysical and chiroptical properties (*vide infra.*). X-ray analysis of diaza derivatives reveals an expected helical conformation with a larger helical pitch and

dihedral angle than the classical carbo[6]helicene, respectively 3.31 Å and 64.5 ° vs. 3.22 Å and 58.5 °. The absolute configuration of **280**$^{+}$ enantiomers were established using VCD and a racemization barrier of more than 37 kcal mol^{-1} was obtained in DMSO. Enhancing the π-conjugated helical pathway strongly increases the chiroptical properties of these aza[6]helicenium family. For instance, ECD spectra of **280**$^{+}$ displays more intense ECD transitions at 360 nm ($\Delta\varepsilon$~-20 M^{-1}cm^{-1}) and also 420 nm ($\Delta\varepsilon$~-20 M^{-1}cm^{-1}) than for aza[4]helicenium **260**$^{+}$. Interestingly, the lowest ECD band recorded at 460 nm for (*P*)-**260**$^{+}$ shows a remarkable red-shift to 610 nm in **280**$^{+}$. In 2016, the same authors reported a chiral HPLC resolution of these cationic or corresponding neutral (through hydride reduction) [6]helicenes on Chiralpak IA CSP using water-containing eluents or either Chiracel OD-I or Chiralpak ID CSP, respectively.[270] Interestingly, both species were also resolved on recently developed LARIHC columns, based on cyclofructan phases. Measurements of their racemization barrier also showed that the presence of the oxygen decreases the configurational stability of the corresponding chiral compounds.

4.1.7.2.4. Emission properties of carbocationic azahelicenes

Until 2012, Lacour *et al.* only used ECD and VCD chiroptical spectroscopy as a tool either to check the configurational stability during chemical reaction or racemization barrier experiments or to establish the absolute configuration.[255,262,268-269] In 2012, Lacour, Vauthey *et al.* used stationary and time-resolved spectroscopy to study the excited-state properties of chiral aza[4]helicene **260**$^{+}$ cations analogues,[271] where the *n*-propyl groups on the nitrogen atoms have been replaced by ethyl-1-ol side chains owing to their solubility in organic and alcohol solvents. These compounds exhibit fluorescence emissions in the red to near infrared region with quantum yields between 0.02-0.20 and lifetimes between 1 and 12 ns, depending of the solvent. As a result, and due to the transparency window of biological media in the red region, these helical derivatives may be interesting for chiral bioimaging. Following this study, the same authors investigated different [4] and [6]diazahelicenium chiral dyes **283**$^{+}$-**285**$^{+}$, functionalized in an enantiospecific way by different donor and acceptor groups in order to tune their chiroptical properties in terms of ECD and CPL responses (Figure 37).[272,273,274] Interestingly, these helical derivatives present ECD signatures up to 750 nm with moderate intensity in the visible region ($\Delta\varepsilon$ ~ 10 M^{-1}cm^{-1}), resulting from partial charge-transfer transitions involving the nitrogen atoms and central carbocation. Also, CPL emissions were recorded between 650 and 700 nm, characterized by a g_{lum} of ~10^{-3}. These features represent an unusual spectral range for helicene based chromophores, especially for fully organic ones. As a result, some of these cationic chiral dyes were used as pH-triggered ECD and CPL chiroptical switches when they presented pH-sensitive group such as carboxylic acid or quinacridine.[275,276] For instance, Lacour *et al.* reported in 2016 a zwitterionic [4]helicene [**286**][BF_4] as a reversible pH-triggered ECD/CPL chiroptical switch (Scheme 71).[276]

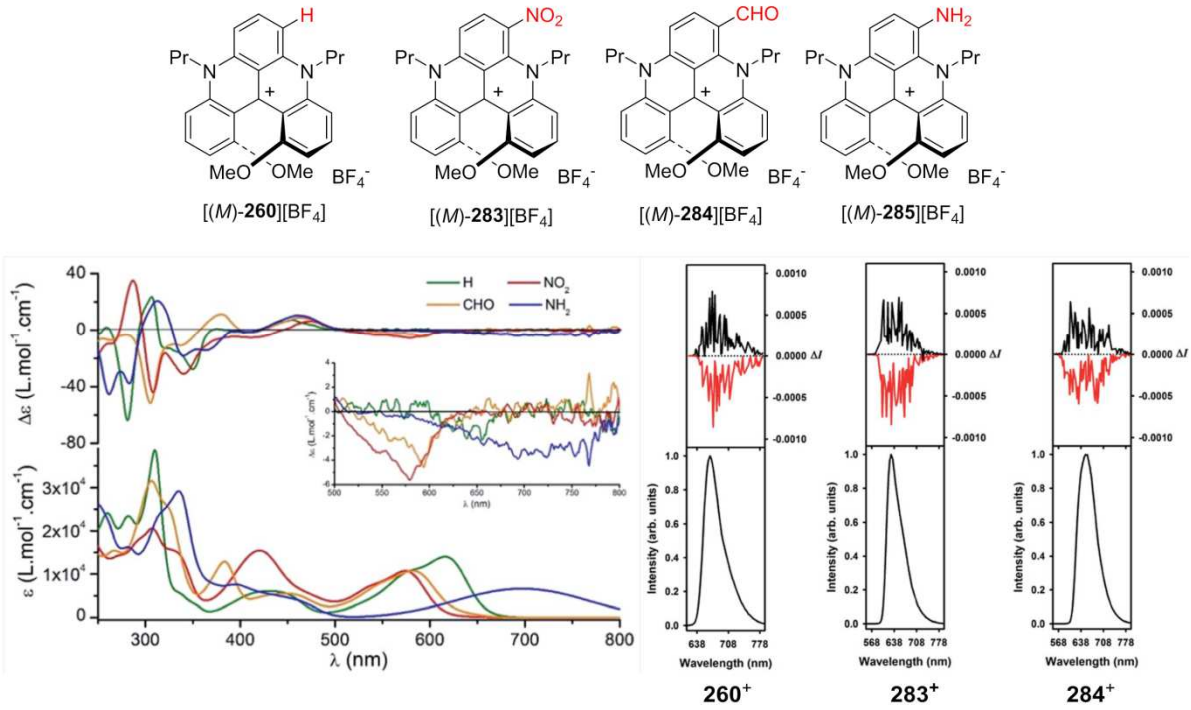

Figure 37. Chemical structures, UV-vis, and ECD spectra of (*M*)-**260**$^+$ (green), (*M*)-**283**$^+$ (red), (*M*)-**284**$^+$ (yellow), and (*M*)-**285**$^+$ (blue) along with CPL spectra of **260**$^+$, **283**$^+$, and **284**$^+$ with (*P*) and (*M*) enantiomers in black and red, respectively. Adapted from ref. [273]. Copyright 2016, Royal Society of Chemistry.

Scheme 71. Synthetic route to **286**$^+$ and **287**$^+$ along with UV-vis and ECD spectra of deprotonated and protonated of (*M*)- and (*P*)-**286**$^+$ (green) and (*M*)- and (*P*)-**287**$^+$ (red), respectively along with CPL spectra of **287**$^+$ with (*P*) and (*M*) enantiomers in blue and orange, respectively. (The CPL spectra of **286**$^+$ were not reported due to the very low emission in basic medium). Adapted with permission from ref. [276]. Copyright 2016, Royal Society of Chemistry.

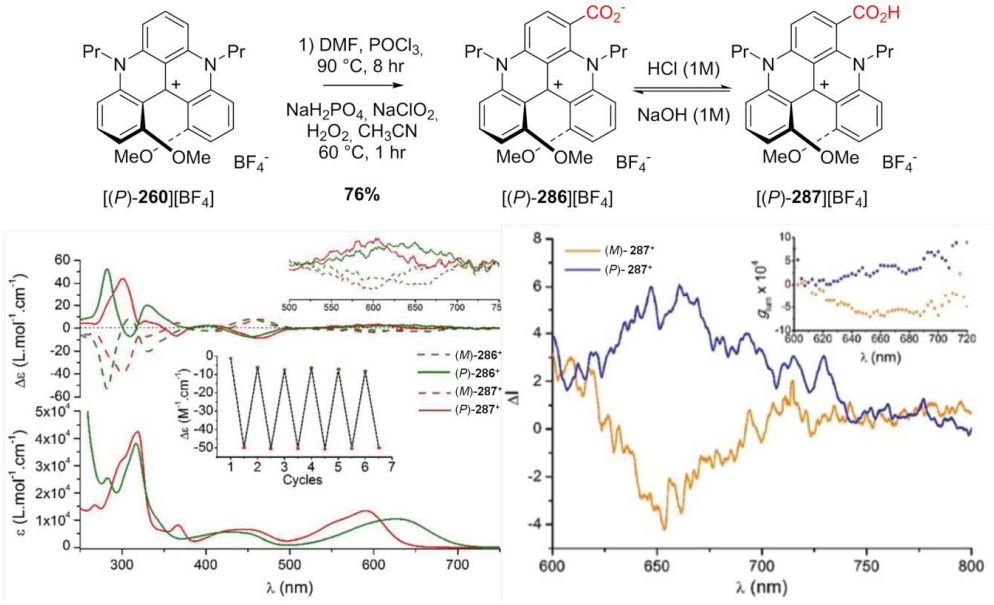

4.1.1.6.2.5. Applications of carbocationic azahelicenes

In 2006, Lacour *et al.* reported the use of diaza[4]helicenium molecule as a chiral stopper for the obtention of inherently chiral pseudorotaxane.[277] Based on the possibility of nucleophilic addition on the central carbocation, they functionalized salt [**260**][BF_4] by an ammonium species to form a chirally oriented thread **289** which may be able to discriminate oriented macrocycle **290** (Scheme 72). Although efficient pseudorotaxane formation occurred, only a low diastereomeric excess resulting from the interaction between the ring and the topologically chiral[278] thread **291** was obtained (<8% *de*).

Scheme 72. Synthesis of chiral stopper **289** and pseudorotaxane formation with oriented thread **291** (only helicenic (*P*) stereochemistry is shown while chiral topology is not specified).[277]

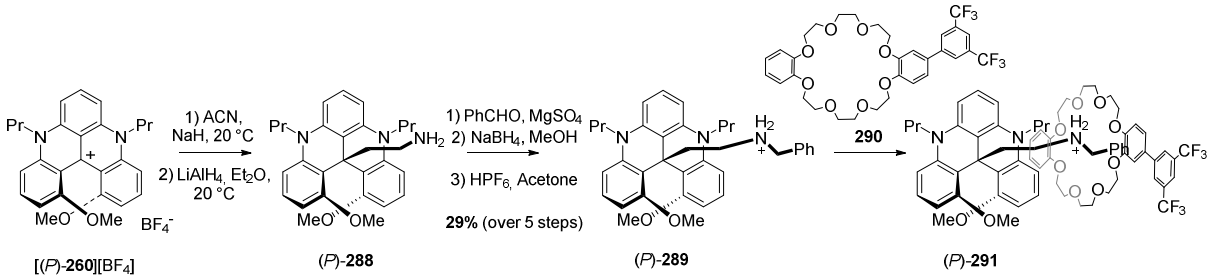

In 2013, Vauthey *et al.* studied the chiral selectivity in the binding of [4]helicenium compounds with double-stranded DNA.[279] They measured the binding constant between the (*P*) and (*M*) enantiomers with DNA sample using time-resolved fluorescence, fluorescence anisotropy and linear dichroism. They showed that both helicene monomers and aggregates interact with DNA and that the resulting binding constants are larger in both cases for the (*M*) enantiomer of the cationic dye. Further studies on bioimaging using racemic and chiral [4] and [6]helicenium dyes were also reported for specific targeting of mitochondria, which possess a central role in the regulation of cellular process such as cellular signaling, homeostasis and apoptosis.[280,281] Notably, Babic, Lacour, Allémann *et al.* described in 2017 the synthesis of [4]helicene-squalene fluorescent derivatives which form dispersed nanoassemblies in aqueous media, allowing biomedical applications of initially insoluble water dyes, along with improving therapeutic outcomes, drug stability and bioavailability.[280] Using enantiopure dye did not reveal specific response and resulting nanoassemblies behave as the racemic one. Other applications in electrochemiluminescence or ion transfer voltammetry were also reported for some [4]- and [6]helicene cationic dyes but focused only on racemic compounds.[282,283,284]

In collaboration with Prof. Naaman, Lacour investigated aza[4]helicenium derivative [**260**][BF_4] as potential organic spin filter owing to the Chirality Induced Spin Selectivity (CISS) effect.[285,286] Using magnetic conductive probe atomic force microscopy (mCP-AFM) and magnetoresistance measurements set-ups, the authors showed that spin specific electron conduction is measured on chiral helicenium films with an opposite preferred spin for (*P*) and (*M*) enantiomers (Figure 38).[287] Spin-polarization of about 45-50% was measured for each enantiomer, representing a new opportunity for designing organic spintronic devices.

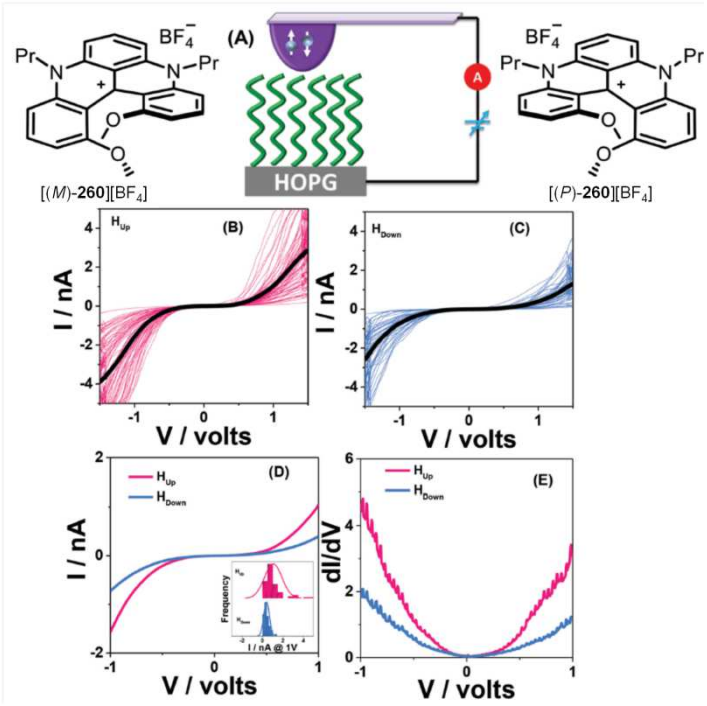

Figure 38. Schematic representation of mCP-AFM measurement with (*P*)- and [(*M*)-**260**][BF_4]. Reproduced from ref. [287]. Copyright 2016, Wiley.

Table 22. Specific rotation values and photophysical data of enantioenriched carbocationic helicenia.

Compound	Method of obtention	$[\alpha]^a$ (wavelength)	Conditions[b] (solvent/Conc.[c])	Enantio/diastereo-purity	Ref.
[(*P*)-**260**][BF_4]	From diastereomeric salts	+13900 (365 nm)	ACN/5.88×10^{-4}	>99 % *ee*[d]	257,273
[(*M*)-**260**][BF_4]	From diastereomeric salts	-13600, (365 nm)	ACN/5.80×10^{-4}	>99 % *ee*[d,e-g]	257,273
(*P*)-**267**	Chiral HPLC[h]	+497 (589 nm)	ACN/0.032	88 % *ee*[h]	262
(*P*)-**265**	From (*P*)-**267**	+2922 (589 nm)	ACN/8.9×10^{-4}	>99 % *ee*	262
(*P*)-**270**	Chiral HPLC[i]	+7500 (589 nm)	ACN/10^{-4}	>99 % *ee*[i]	265
[(*P*)-**268**][BF_4]	From (*P*)-**270**	+7500 (589 nm)	ACN/10^{-4}	>99 % *ee*	265
(*P*)-**273**	Diastereoselective reaction	N.d.	not reported	not reported	267
(*P*)-**274**	From [(*P*)-**260**][BF_4]	+1014, (578 nm)	ACN/4.14×10^{-4}	>99 % *ee* [j]	268
(*P*)-**275**	From (*P*)-**274**	+893 (589 nm)	ACN/7.4×10^{-4}	>99 % *ee*[i]	268
[(*P*)-**280**][BF_4]	Diastereomeric salts	+1840 (365 nm)	CH_2Cl_2/1.2×10^{-5}	>92 % *ee*[e]	269
[(*P*)-**283**][BF_4]	From [(*P*)-**260**][BF_4]	+7100, (365 nm)	ACN/6.36×10^{-4}	>99 % *ee*	273
[(*P*)-**284**][BF_4]	From [(*P*)-**260**][BF_4]	+11700 (365 nm)	ACN/5.88×10^{-4}	>99 % *ee*	273
[(*P*)-**285**][BF_4]	From [(*P*)-**260**][BF_4]	+4600 (365 nm)	ACN/5.92×10^{-4}	>99 % *ee*	273
[(*P*)-**286**][BF_4]	From [(*P*)-**260**][BF_4]	+5600, (365 nm)	NaOH 1M/6.36×10^{-4}	>99 % *ee*	276
[(*P*)-**287**][BF_4]	From [(*P*)-**260**][BF_4]	+5500 (365 nm)	HCl 1 M/6.36×10^{-4}	>99 % *ee*	276

(*P*)-**289**	From [(*P*)-**260**][BF_4]	+560 (589 nm)	CH_2Cl_2/0.05	>99 % *ee*	[277]
(*P*)-**291**	From (*P*)-**289**	+560 (589 nm)	CH_2Cl_2/3.8×10^{-5} M	>99 % *ee*	[277]

[a] In $deg \cdot mL \cdot g^{-1} \cdot dm^{-1}$. [b] Temperature between 20-25 °C. [c] In g/100 mL otherwise precised. [d] NMR of diastereomers. [e] Chiralpak AD-H, hexane/*i*-PrOH. [f] Chiracel OD-RH, ACN/H_2O. [g] Chirobiotic TAG, EtOH/H_2O. [h] Chiralpak IB, hexane/THF. [i] Chiralpak IC, hexane/*i*-PrOH. [j] Chiralpak OD-H, hexane/*i*-PrOH.

4.2. Helicenes grafted with nitrogen

4.2.1. Synthesis and properties of amino-substituted helicenes

Since amino-groups usually appear incompatible with the classical oxidative photocyclization process to prepare amino-substituted carbohelicenes, other methods have been developed to access this class of helical molecules. In several cases, a protected amino group is installed at the early stage of the synthesis, as shown by Stara and Stary in the case of (*M*,*R*,*R*)-**204a-g** in paragraph 4.1.5.2.[196] and more recently in the preparation of nonracemic 2-amino[6]helicene derivatives. Indeed, (*P*)-(+)-**292b** (Figure 39) and its Boc-protected analogue **292a** were prepared with 67% *ee* using enantioselective [2+2+2] cycloisomerization of an achiral triyne under [Ni(COD)$_2$]/(R)-QUINAP catalysis. An ultimate "point-to-helical" chirality transfer during the cyclization of enantiopure triynes mediated by [Ni(CO)$_2$(PPh_3)$_2$] afforded (*M*)-(-) or (*P*)-(+)-7,8-bis(*p*-tolyl)hexahelicen-2-amine **293b** (>99% *ee*) as well as its benzoderivative **294b** (>99% *ee*) together with their Boc-protected analogues (**293a** and **294a**).[288] For other (non-resolved) amino-substituted penta-, hexa- and hepta-helicenes, see references [289,290,291, 292, 293,294].

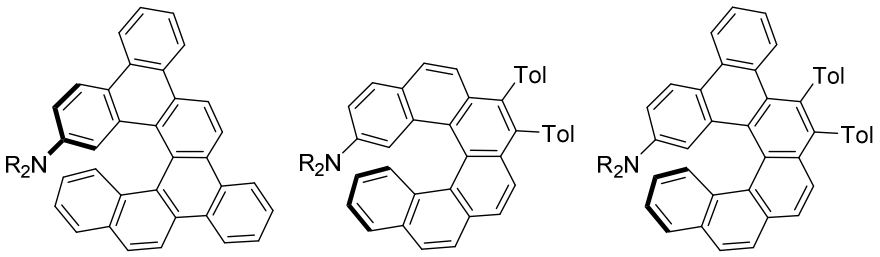

(*P*)-**292a** (R = Boc)
(*P*)-**292b** (R = H)
67% *ee*[a]

(*M*)-**293a** (R = Boc)
(*M*)-**293b** (R = H)
>99% *ee*[a]

(*M*)-**294a** (R = Boc)
(*M*)-**294b** (R = H)
>99% *ee*[b]

Figure 39. Chemical structure of 2-amino-helicenes prepared by [2+2+2] cycloisomerization. Ee's determined by [a] Chiralpak IA column, *n*-heptane-dichloromethane mixture with 0.1% diethylamine, [b] Chiralpak IA column, hexane-chloroform mixture.[288]

Stara and Stary examined the self-assembly at the air−water interface by means of the Langmuir-Blodgett (LB) technique of aminohelicene **293b** (racemic and enantiopure) endowed with a hydrophilic amino group (capable of hydrogen bonding to water molecules) and with a large lipophilic polyaromatic backbone (prone to π−π stacking).[288] Despite the absence of long alkyl or oligoethyleneglycoxy substituents, (*rac*)-, (*M*)-(-)-, and (*P*)-(+)-7,8-bis(*p*-tolyl)hexahelicen-2-amines **293b** were able to form Langmuir monolayers at the air−water interface featuring practically identical surface pressure *vs.* mean

molecular area isotherms. The corresponding Langmuir-Blodgett films on quartz or silicon substrates were characterized by AFM microscopy; their UV-vis/ECD spectra showed no clear difference from the solution state.

In 2016, Kellog *et al.* reported the use of cycloisomerization with [$PtCl_2$] to prepare 5-amino carbo[6]helicene **297** (Scheme 73) which was separated by chiral HPLC on a Chiralcel OD-H column.[295] Several attempts of resolution through crystallization of diastereomeric salts with different chiral acids failed. The optical rotations were measured on samples that were neither chemically nor enantiomerically pure. Values of -8846 (93% chemical purity and 99 % *ee*) and +7429 (83 % chemical purity and 97% *ee*) appear high for a [6]helicene derivative. For comparison 2-amino-carbo[6]helicene (*M*)-**299** in Scheme 74 displays a specific rotation of -3210 (see Table 23).[60] Finally, the half-life time $t_{1/2}$ of racemization at 210 °C was found to be approximately 1 hour. Note that the authors made many attempts to perform enantioselective cycloisomerization but with no success.

Scheme 73. Synthesis of 5-amino-carbo[6]helicene **297** by cyloisomerization.[295]

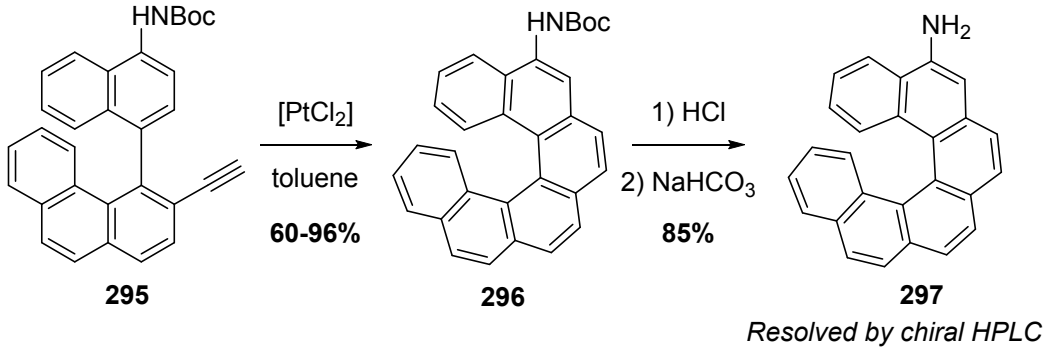

While very detailed studies have been made for carbohelicenes on different solid surfaces, [296] the study of functionalized helicenes with heteroatoms or polar groups and the substituents' influence on the self-assembly is relatively new. A few examples are: 8 hexathia[11]helicene,[297] heptahelicene-2-carboxylic acid,[298,299] 6-13-dicyano[7]helicene (*vide infra*). In 2013, Ivasenko, Kellog, Lazzaroni, De Feyter *et al.* studied the self-assembly of racemic 5-aminohelicene **297** at liquid/solid interfaces. They applied a solution of **297** in 1,2,4-trichlorobenzene (TCB) onto a Au(111) surface and found the formation of a 'three-dot' p3-(*P*3) pattern (see trimeric assembly on Figure 40a1), with partial spontaneous resolution of (*M*) and (*P*) domains on the surface.[300] One year later, Ascolani, Fuhr, Lingenfelder *et al.* reported the assembly of (*M*)-5-amino-helicene **297** on Cu(100) and Au(111) under ultra-high vacuum (UHV) studied by STM. They examined of the interplay of van der Waals (vdW) and H bonding NH_2 groups and their influence on the chiral footprint of the enantiopure adsorbates on a solid surface. The main difference between the two surfaces was found in the origin of the molecule–surface interaction. While the C6 rings-surface interaction dominates in the case of Cu(100), the amino–surface interaction is crucial on Au(111). In both cases, the amino group does not induce polar interactions *via* hydrogen bonding but rather maximizes van der Waals interactions and drive the self-assembly.[301] The self-assembly of enantiopure (*M*) and (*rac*)- **297** on Au(111) under UHV conditions was further investigated in 2016 (Figure 40a2).[295] The authors observed two rotational domains formed by rows of dimers oriented along the <1-11> Au crystallographic directions for the enantiopure aminohelicene being formed, according to DFT

calculations, by flat-lying molecules in which the NH_2 groups govern the interaction with the surface (*i.e.*, "N down"), whereas the C6 rings pack closely to maximize van der Waals interactions between neighboring molecules. Regarding the racemic compound, it showed the emergence of two enantiomorphous domains which are rotated by 6° with respect to the <1-11> crystallographic directions and have a double-row structure. This assembly of double rows under UHV appeared remarkably different from the triangular (p3) structures formed at the Au(111)/1,2,4-trichlorobenzene (TBC) interface, where the solvent plays an important role. In 2017, Fuhr, Ascolani, Lingenfelder and coworkers found a different organization and chiral expression of racemic of **297** on Cu(100) as compared to a Sn/Cu(100) alloy.[302]

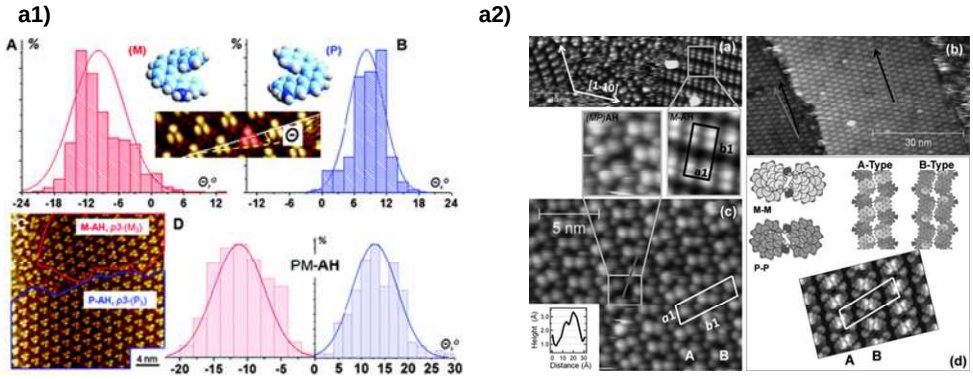

Figure 40. a1) Self-assembly of 5-aminohelicene **297** formed at Au(111)/TCB interface. (A), (B) and (D) Distribution of tilt angles (Θ) between the sides of helicene trimers and the unit cell vectors in p3-(**297**$_3$) patterns of (*M*)-, (*P*)- and (*rac*)- **297**, respectively. (C) STM image of homochiral conglomerates (p3-(M_3) and p3-(P_3), red and blue, respectively) formed from racemic **297**. Reproduced from ref. [300]. Copyright 2013, Royal Society of Chemistry. a2) (a) STM image of (*M*)-**297** on Au(111) at UHV. (b, c) STM images of racemic **297** on Au(111). (b) Two enantiomorphous domains separated by a monoatomic step of the surface. (c) High-esolution image of the molecular structure developed by the racemate. The white parallelogram indicates the unit cell. The square highlights the presence of a defect (zoomed in the inset). The gray line indicates the line profile shown in the inset. (d) DFT-based molecular model of the racemic structure in (c) that highlights the presence of *M–M* and *P–P* dimers in the A- and B-type molecular-row model. Different colors indicate different chirality: Light gray for (*M*)-**297** and dark gray for (*P*)- **297**. Constant-current STM image simulation of the fully relaxed structure. Reproduced from ref. [295]. Copyright 2016, Wiley.

As shown in Scheme 74, helicene-boronate (*M*)-**21a** was converted to a variety of amino derivatives.[60] 2-Amino-carbo[6]helicene (*M*)-**299** was prepared by copper-catalyzed azidation yielding (*M*)-**298**, followed by H_2 hydrogenation. The secondary *N*-benzyl helicenyl amine (*M*)-**300** was prepared from (*M*)-**21a** *via* conversion to the heliceneic dichloroborane and in situ treatment with benzyl azide. A Chan-Lam amination yielded the piperidino derivative (*M*)-**301**. Finally, the transformation of (*M*)-**21a** to an amino ester derivative **302** was carried out *via* a three-component Petasis reaction with glyoxylic acid and morpholine, followed by esterification with (trimethylsilyl)diazomethane. This condensation produced two diastereomeric compounds with a modest stereocontrol (*dr*: 7/3), which were then separated by flash chromatography.

Scheme 74. Synthesis of (*M*)-helicenyl derivatives **298-302** from helicene-boronate (*M*)-**21a**. Reagents and conditions: *i*) NaN_3, $CuSO_4.5H_2O$, MeOH, reflux, 19 hr; *ii*) H_2 (1 atm), 10% Pd/C, EtOAc, rt, 21 hr, 75% (2 steps); *iii*) BCl_3, CH_2Cl_2, rt, 3 hr; *iv*) $PhCH_2N_3$, CH_2Cl_2, rt, 17 hr, 68% (two steps); *v*) $Cu(OAc)_2$, $B(OH)_3$, piperidine, MeCN, 80 °C, 26 hr, 44%; *vi*) morpholine, glyoxylic acid monohydrate, 1,1,1,3,3,3-hexafluoro-2-propanol, 60 °C, 48 hr; *vii*) (trimethylsilyl)diazomethane in diethyl ether, THF/MeOH, rt, 20 hr, 84% (two steps). The X-ray structure of (*M*)-**21a** is shown. Adapted from ref. [60]. Copyright 2018, American Chemical Society.

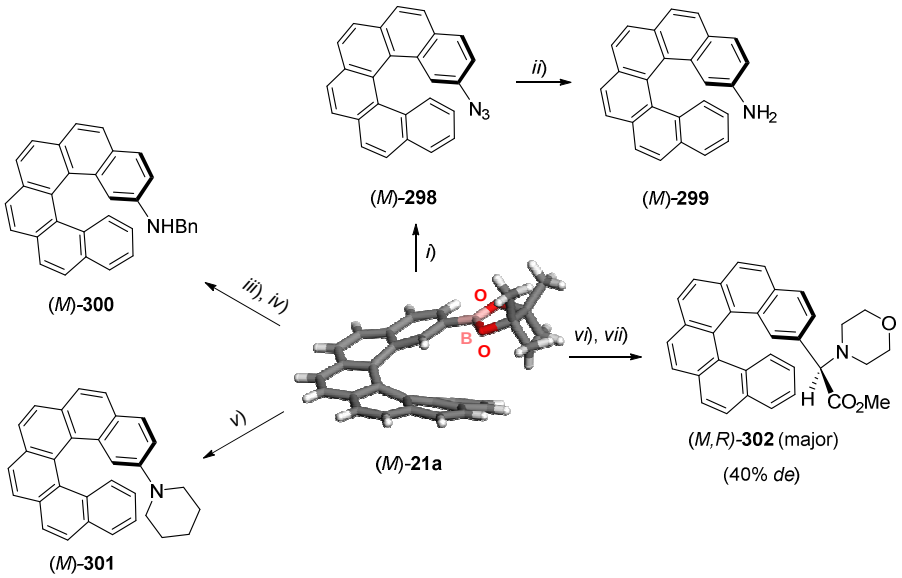

Recently, Sýkora and coworkers demonstrated that nitrogen-containing substituents such as benzylamino and cyano groups can be introduced in sterically hindered 2-position of carbo[6]helicene using microwave conditions (Scheme 75).[61] Interestingly, they found that (*P*)-2-benzylamino-carbo[6]helicene **300** with 96% *ee* could be obtained from enantiopure 2-bromo-carbo[6]helicene (*P*)-**303** *via* a coupling using Buchwald-Hartwig amination conditions at 170 °C under microwave for 2 hours, while (*M*)-2-cyano-carbo[6]helicene **304** with only 1% *ee* was obtained at 160 °C for 1 hr from (*M*)-**303** *via* Rosemund-von Braun cyanation, under microwave. The racemization process of **303** was monitored and an experimental Gibbs free energy of 36.5 kcal mol^{-1} was obtained at 465 K (a value close to unsubstituted [6]helicenes).[71] Altogether, these data showed that using temperatures lower than 160 °C were needed to safely conduct synthesis on enantiopure compounds.

Note that a configurationally stable diamino-substituted [4]helicene was prepared by Yamaguchi *et al.* (see paragraph 4.2.2.1. and Schemes 76 and 77).

Table 23. Specific rotation values of enantioenriched helicenes-amino derivatives.

Compound	Method of obtention	$[\alpha]_D$[a]	Conditions[b] (solvent/Conc.[c])	Enantiopurity	Ref
(*M*)-**293b**	Point to helical chirality transfer	-2074	$CHCl_3$/0.114	>99% *ee*[d]	288
(*M*)-**294b**	Enantioselective [2+2+2]	-931	$CHCl_3$/0.016	>99% *ee*[e]	288
(*M*)-**299**	From (*M*)-**21a**	-3210 ± 7%	CH_2Cl_2/2.85 × 10^{-4} M		60

(*P*)- **299**	From (*P*)-**21a**	+2990 ± 7%	$CH_2Cl_2/3 \times 10^{-4}$ M		[60]
(*M*)-**300**	From (*M*)-**21a**	-3260 ± 7%	$CH_2Cl_2/2.3 \times 10^{-4}$ M		[60]
(*M*)-**301**	From (*M*)-**21a**	-2600 ± 7%	$CH_2Cl_2/2 \times 10^{-4}$ M		[60]
(*P*)-**301**	From (*P*)-**21a**	+2430 ± 7%	$CH_2Cl_2/2 \times 10^{-4}$ M		[60]
(*M,R*)-**302**	From (*M*)-**21a** then diastereomeric separation[f]	-2490 ± 7%	$CH_2Cl_2/3.7 \times 10^{-4}$ M	>97% *de*[g]	[60]
(*M,S*)-**302**	From (*M*)-**21a** then diastereomeric separation[f]	-2290 ± 7%	$CH_2Cl_2/1.9 \times 10^{-4}$ M	>97% *de*[g]	[60]
(*M*)-**314**	Chiral HPLC[h]	-3456 ± 6	$CHCl_3$/0.0622	>99% *ee*[h]	[61]
(*P*)-**314**	Ibid	+3494 ± 4	$CHCl_3$/0.0534	>99% *ee*[h]	[61]

[a] In $deg \cdot mL \cdot g^{-1} \cdot dm^{-1}$. [b] Measured at 20-25 °C. [c] In g/100 mL. [d] Chiralpak IA column, *n*-heptane-dichloromethane mixture with 0.1% diethylamine; [e] Chiralpak IA column, hexane-chloroform mixture. [f] flash chromatography over silica gel. [g] ^{1}H NMR. [h] Kromasil Cellucoat column, *n*-heptane/2-propanol (99.65:0.35).

Scheme 75. Obtention of enantioenriched 2-benzylamino (**300**), 2-cyano-substituted (**304**), phosphine-borane (**305**-BH_3**)** hexahelicenes from enantiopure 2-bromohelicene **303** under microwave conditions. *Ee*'s were analyzed by HPLC over a Kromasil Cellucoat column using *n*-heptane/2-propanol mixtures.[61]

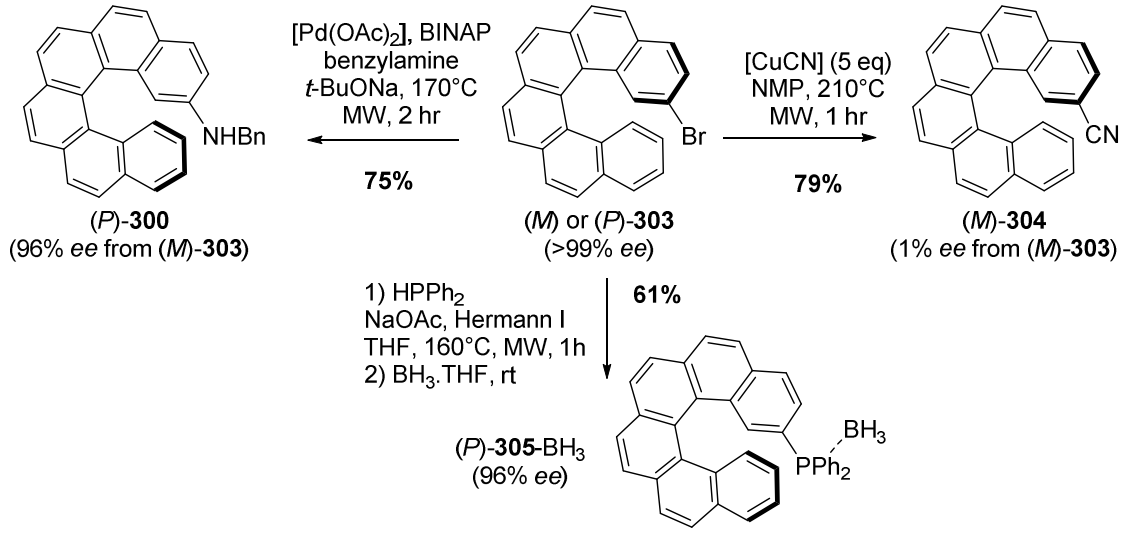

4.2.2. Synthesis and properties of cyano-substituted helicenes

4.2.2.1. Configurationally stable cyano- and amido- capped dimethyl[4]helicenes

In 1996, Yamaguchi *et al.* reported the synthesis of configurationally stable [4]helicenes by using methyl substituents at the inner positions of the helix in order to strongly increase its racemization barrier. They synthetized 1,12-dimethylbenzo[*c*]phenanthrene-5,8-dicarboxylate from the racemic diketone **306**, previously described by Newman *et al.* (Scheme 76).[303,304] They were able to resolve diacid **307** in gram scale quantities by forming diastereomeric (-)-quinine salts through repeated recrystallization steps.

Helical diacid **307** could also be resolved by column chromatography of d-(-)-camphorsultam diastereomeric derivatives.

Having access to these enantiomerically enriched building blocks, the group of Yamaguchi started to explore many facets of their chemistry and related chiroptical properties, by notably incorporating them in macrocycles and polymeric chiral materials.[305,306,307,308] For instance, they synthetized enantiopure macrocycles **308a**, **308b**, and **308c** bearing respectively two and three [4]helicene units, by condensation reaction between diacid (*M*)-**307** and 4,4'-(cyclohexane-1,1-diyl)bis(2,6-dimethylaniline) (Scheme 76), obtained as mixture with other oligomers.

Scheme 76. Synthesis and diastereomeric resolution of 1,12-dimethylbenzo[*c*]phenanthrene-5,8-dicarboxylic acid **307** and obtention of chiral macrocycles **308a**,**b**.[304,309]

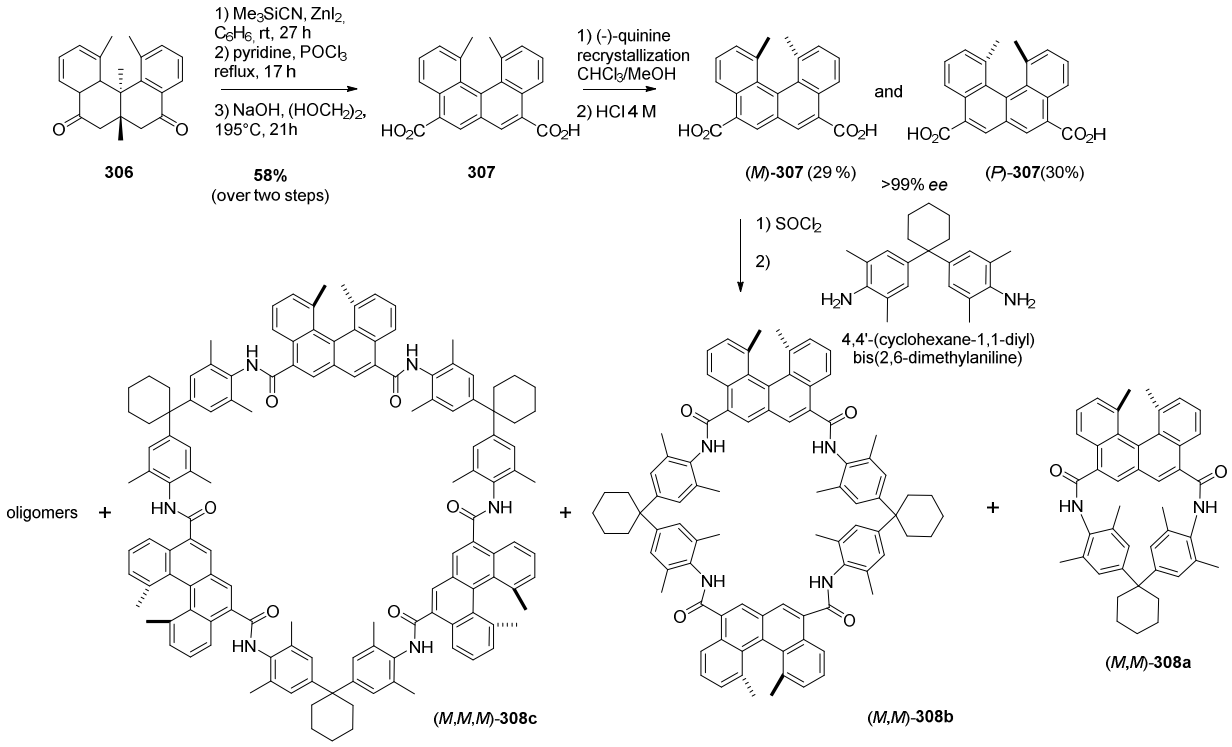

These chiral macrocycles exhibit interesting folding properties depending on both the concentration and the solvent polarity,[310,309,311,312] and also show catalytic activity in asymmetric addition of diethylzinc to aromatic aldehydes, with *ee*'s up to 50%.[309] Yamaguchi *et al.* also explored the chemical reactivity of their chiral platform in order to access to a large variety of functionalities such as electron acceptors nitro and nitrile groups or electron donors amino and hydroxyl fragments (Scheme 77).[313] In 2001, they were able to prepare cyano- and amino-substituted helicenes, *i.e.* enantiopure 5,8-bis-cyano-1,12-dimethyl-[4]helicene (*P*)-**309** and 5,8-bis-amino-1,12-dimethyl-[4]helicene (*P*)-**312**, respectively, from dicarboxylic acid (*P*)-**307** in relatively good yields (Scheme 77). They also showed that (*P*)-**309** can be nitrated at different positions by varying the reaction conditions without any racemization (compounds **310a-b**, Scheme 77). Surprisingly, compounds (*P*)-**309** and (*P*)-**310b** display negative optical rotations, while (*P*)-**307** and (*P*)-**310a** show positive ones (Table 24).[314] These functionalized [4]helicenic compounds were then investigated in chiral recognition through charge transfer complexation, or as intermediates to synthetize enantiopure macrocycles shown in Scheme 77 *i.e.* (*P*,*P*,*P*)-**313'** obtained

through a multi-step synthesis from amino helicene (*P*)-**311** and oligomers (*P*,*P*,*P*)-**313a-c** for investigating their aggregation behaviour under different solvent, concentration and temperature conditions.[306,315,316,314,317,318,319,320,321] Unexpectedly, (*P*,*P*,*P*)-**313a** and (*P*,*P*,*P*)-**313b** afforded negative optical rotations, while (*P*,*P*,*P*)-**313c** shows positive one (Table 24), results that were not discussed in ref. [314].

Scheme 77. Enantiospecific synthesis of polynitro, bis-cyano and bis-amino substituted 1,12-dimethyl-carbo[4]helicenes and their implementation into enantiopure helical oligomers or macrocycles.[304]

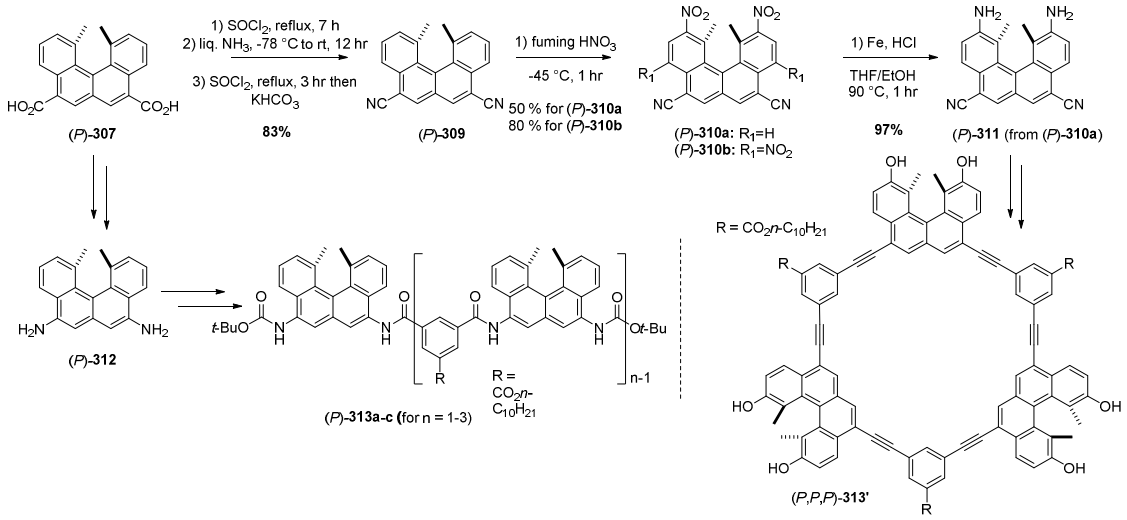

Table 24. Specific rotation values of enantiopure 1,12-dimethyl-[4]helicenes derivatives.

Compound	Method of obtention	$[\alpha]_D$[a]	Conditions[b] (solvent/Conc.[c])	Enantio-purity	λ_{Abs} (nm)	Ref
(*P*)-**307**	Diastereomeric crystallization[d]	+313	MeOH/0.690	99%[e]	310, 360	304
(*M*,*M*)-**308b**	*From* (*P*)-**307**	-179	$CHCl_3$/0.332	99%	303, 345	309
(*M*,*M*,*M*)-**308c**	*From* (*P*)-**307**	-147	$CHCl_3$/0.230	99%	302, 345	309
(*P*)-**309**	*From* (*P*)-**307**	-17	THF/0.10	99%		313
(*P*)-**310a**	*From* (*P*)-**309**	+320	DMF/0.14	99%		313
(*P*)-**310b**	*From* (*P*)-**309**	-15	THF/0.10	99% (NMR)		313
(*P*)-**312**	*From* (*P*)-**307**	+220	$CHCl_3$/0.50	99% (NMR)		313
(*P*)-**313a**	*From* (*P*)-**312**	-354	$CHCl_3$/0.35	99%		314
(*P*)-**313b**	*From* (*P*)-**312**	-363	THF/0.032	99%		314
(*P*)-**313c**	*From* (*P*)-**312**	+1345	THF/0.033	99%		314

[a] In $deg \cdot mL \cdot g^{-1} \cdot dm^{-1}$. [b] Temperature 25 °C. [c] In g/100 mL otherwise stated. [d] crystallization of quinine salts in $CHCl_3$/MeOH. [e] Chiralcel OD.

4.2.2.2. Cyano-substituted hexa- and heptahelicenes

A series of cyano-capped hexahelicenes depicted in Figure 41 have also been prepared. For racemic cyano-helicenes see ref. [322,323,324,325]. Enantioenriched **304** was prepared as described on Scheme 75).[61] Racemic 8-cyano-hexahelicene **314** was obtained by Aloui *et al.* by a classical oxidative photocyclization process as the final step and using as a key intermediate an acrylonitrile during the multistep synthesis in order to install the cyano-group in the helical backbone (Scheme 78). Its enantiomeric resolution was then

achieved by preparative HPLC using a Chiralpak IA column and *n*-heptane/2-propanol (95:5) as the mobile phase.[326] This compound displays blue emission. Similarly, the same group recently synthesized the 7-cyano-14-methoxy-5-thiahexahelicene (*M*)-**315** using a bromobenzo[*b*]naphtho[2,1-d]thiophene-7-carbonitrile as a suitable tetracyclic building block. The resolution of racemic helicene (*M*)-**315** into its enantiomers was ensured by HPLC using a Chiralpak IA column and *n*-hexane/2-propanol/chloroform (70:10:20) mixture as the mobile phase.[327]

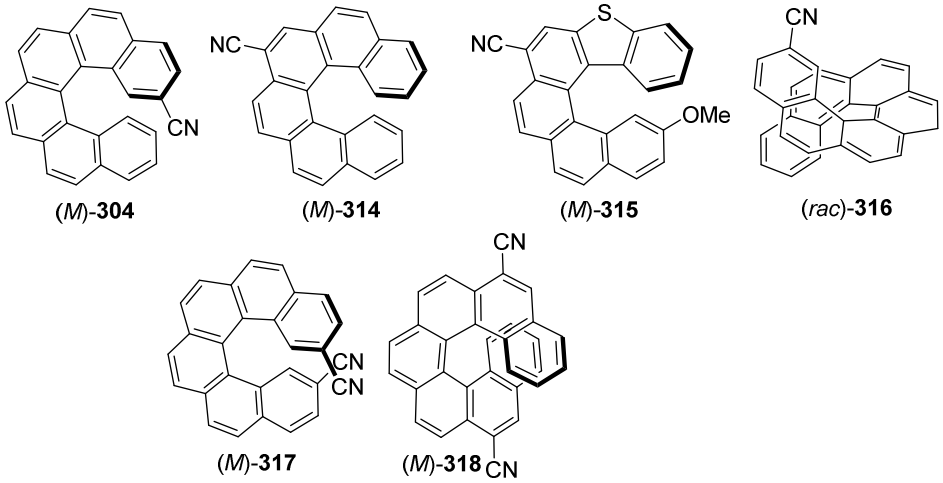

Figure 41. Different cyano-subtituted hexa and heptahelicene derivatives.

Scheme 78. Synthesis of racemic 8-cyano-hexahelicene **314**[326]

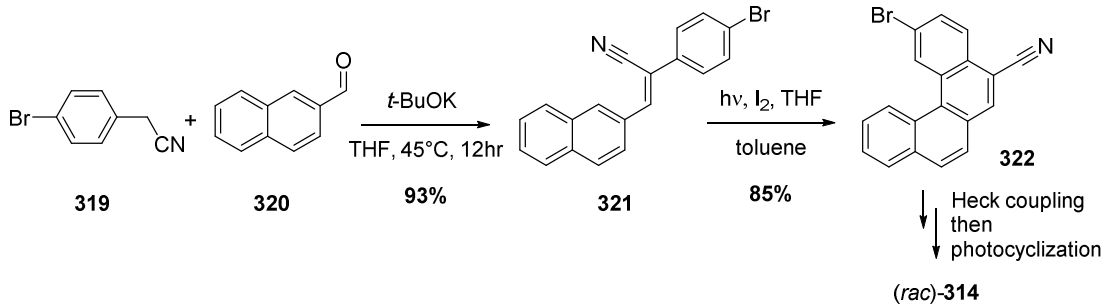

In 1986, Ben Hassine *et al.* prepared diastereomeric imine derivatives **324a**[1,2] from racemic heptahelicene-2-carboxaldehyde **323** and (*R*)-α-methyl-benzylamine and separated them by silica gel column chromatography. Each pure diastereomer (*P*,*R*)-**324a**[1] or (*M*,*R*)-**324a**[2] was then transformed into enantiopure (*P*) and (*M*)-2-cyano-heptahelicene **316** upon reduction with citric acid.[328] The authors showed that the enantioenriched 2-cyano[7]helicene **316** mediates the oxidation of *E*-stilbene into the corresponding epoxide in >99% *ee* (Scheme 79). These pioneering studies on stoichiometric reactions highlighted the undoubtedly high potential of helical auxiliaries in chiral induction processes.

Scheme 79. Preparation of pure enantiomers of 2-cyano-[7]helicene **316** and its use as chiral inducer in asymmetric epoxidation of *trans*-stilbene **325**.[328]

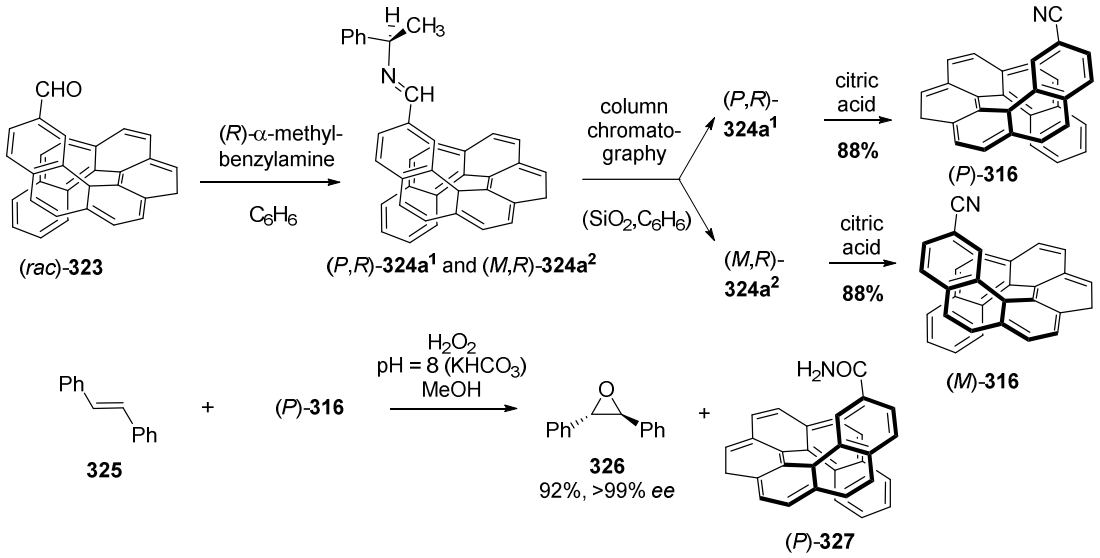

Enantiopure dicyano-helicene derivatives have also been prepared. Weber and co-workers reported the synthesis of racemic 2,15-dicyanohexahelicene **317** by a double oxidative photocyclization and its enantiomeric separation using chiral HPLC over a cellulose tris(3,5-dimethylphenylcarbamate column.[329] Crystallization of racemic dinitrile helicene derivative **317** from benzene gave orange-red crystals and the hexagonal space group $P6_122$ indicated the occurrence of spontaneous resolution.

In 2011, Diederich and colleagues prepared racemic and enantiopure 6,13-di-cyano-[7]Helicene racemic **318** according to Scheme 80 and studied the self-assembly onto Cu(111).[330] STM and DFT studies revealed a spontaneous chiral resolution process of racemic helicene on the surface (Figure 42a). Indeed, **318** formed fully segregated domains of pure enantiomers (2D conglomerate) on Cu(111). The system was able to optimize intermolecular CN···HC(Ar) hydrogen bonding and CN···CN dipolar interactions which gave preferential assembly of homochiral molecules. In 2013, Jung and coworkers reported the self-assembly of (*P*)-(+) and (*M*)-(-)-**318** on Cu(111) for which STM images revealed the formation of mirror-imaged H-bonded chains (Figure 42b).[331] Upon annealing for 1 h at 300 K, coordination with Cu adatoms occurred, thus creating Cu-coordinated chains. This corresponds to a rare case since the direction of helicene chains was found independent of the chirality (*P*) or (*M*) sense of the molecular building blocks. However, it was observed that locally the symmetry of the H-bonded dimers is mirrored when the helicene of opposite chirality sense is used. The tolerance to symmetry was observed to increase considerably and no spontaneous resolution was observed for such 1D arrangements formed by Cu coordination, contrary to more common situations found on STM of helicene on surfaces.[296]

Note that cyano-substituents are good for introducing charge transfers into helicene derivatives, thus giving rise to optimized or new chiroptical properties such as two-photon absorption circular dichroism.[332] They display also good abilities for liquid phase coordination chemistry.[333]

Scheme 80. Synthesis of bis-cyano-heptahelicene (*P*)-(+) and (*M*)-(-)-**318**. a) *hv* (Ga-doped high-pressure Hg lamp), I_2, propylene oxide, PhMe, rt, 19 hr, 73 %; b) (*S*,*S*)-Whelk-O1 CSP; c) *n*Bu_4NF, THF, rt, 1 hr; d) PCC, CH_2Cl_2, molecular sieves 3 Å, rt, 1 hr, 85 % (two steps); e) 1. $H_2NOH{\cdot}HCl$, pyridine, H_2O, 1.5 hr, rt; 2. DCC, Et_3N, $CuSO_4{\cdot}5\,H_2O$, CH_2Cl_2, 50 °C, 20 hr, 89 %; f) [$Pd(PPh_3)_4$], K_2CO_3, *n*BuOH, PhMe, 60 °C, 16 hr, 98 %. CSP=chiral stationary phase, PCC=pyridinium chlorochromate, DCC, *N*,*N*′-dicyclohexyl carbodiimide, TIPS=triisopropylsilyl. Adapted with permission from ref. [330].

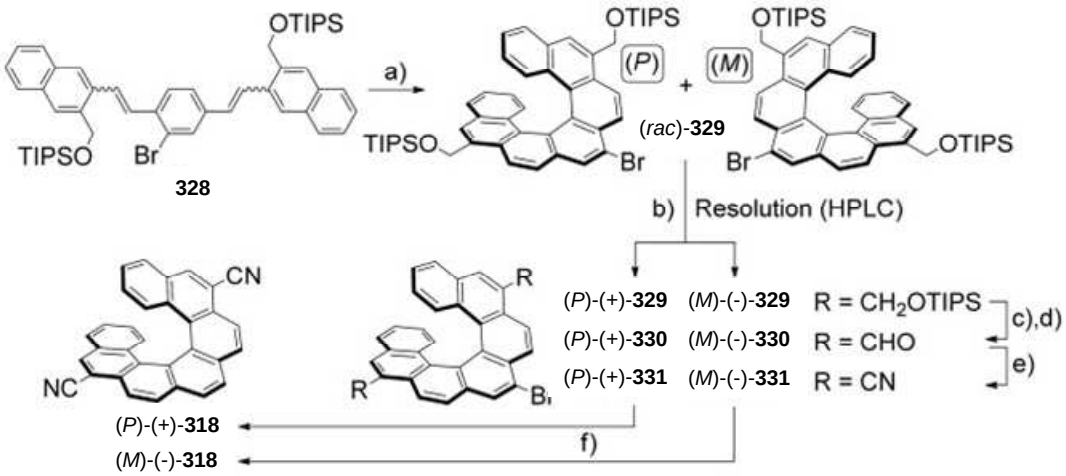

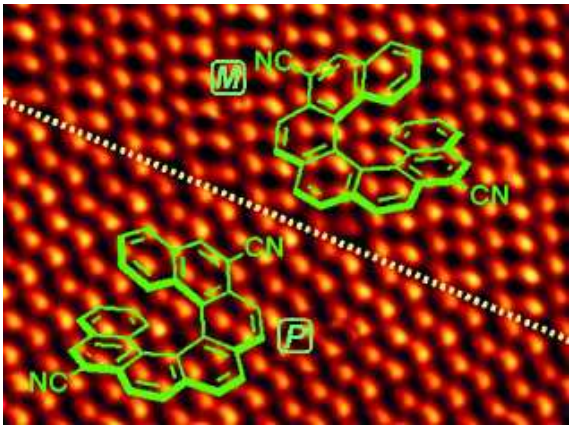

a) b)

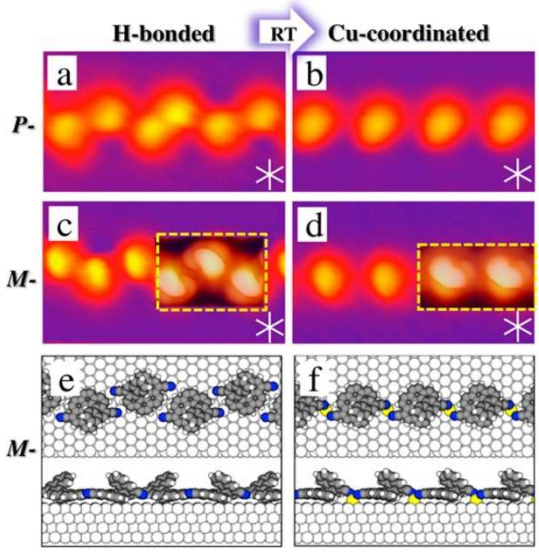

Figure 42. a) Spontaneous resolution of racemic bis-cyano-heptahelicene **318** observed by STM on a Cu(1,1,1) surface. Reproduced from ref. [330]. Copyright 2011, Wiley. b) Formation of 1D-chain and transformation to Cu-coordinated chaine observed by STM on the same Cu(111) surface from enantiopure (*P*)-(+) and (*M*)-(-)-**318**. Reproduced from ref. [331]. Copyright 2013, American Chemical Society.

Table 25. Specific rotation values and photophysical data of enantioenriched cyanohelicenes.

Compound	Method of obtention	$[\alpha]_{D\ exp}$ [a]	Conditions[b] (solvent/Conc.[c])	*ee*	λ_{Abs} (nm)	λ_{Em} [d] (nm)	Ref
(*M*)-**314**	Chiral HPLC	-3050 (c 0.051, CHCl3), respectively.	$CHCl_3$/0.051	>99.5% *ee*[d]	260,313,332, 403, 426	438	[326]
(*P*)-**315**	Chiral HPLC	+3550	$CHCl_3$/0.035	>99.5% *ee*[e]	322,356,377,403, 427	437	[327]
(*P*)-**316**	Chromatographic diastereomeric separation	+6400	$CHCl_3$/0.05				[328]
(*P*)-**317**	Chiral HPLC[f]	+3440 ± 400	$CHCl_3$/0.003				[329]
(*P*)-**318**	From (*P*)-**294**	+3539	$CHCl_3$ /0.2		282,316,382		[330]
(*P*)-**329**	Chiral HPLC[g]	+2058	$CHCl_3$/1		277,337		[330]

[a] In $deg \cdot mL \cdot g^{-1} \cdot dm^{-1}$. [b] Measured at 24-25 °C. [c] In g/100 mL. [d] Chiralpak IA, *n*-heptane/*i*-PrOH mixture. [e] Chiralpak IA, *n*-hexane/ *i*-PrOH /$CHCl_3$ mixture. [f] cellulose-tris(3,5-dimethylphenylcarbamate) (CDMPC) phase. [g] (S,S)-Whelk-O1, hexane.

4.2.3. Pyridyl-substituted carbohelicenes and cyclometallated helicenes

Coordination chemistry offers a simple way to tune the optical and electronic properties of the π-ligands since both the coordination sphere geometry and the nature of the metal-ligand interaction can be readily modified by varying the metal center. This will produce a great impact on the properties of the molecule. In 2010, Autschbach, Crassous, Réau, *et al.* prepared the first class of organometallic helicenes incorporating a metallic ion within their helical backbone. Indeed, inspired by the cyclometalation reaction of phenyl-pyridine derivatives, we developed a short and efficient strategy to prepare cyclometalated helicene derivatives, named metallahelicenes, by an *ortho*-metalation reaction of a phenyl-pyridine bearing an extended ortho-fused polycyclic π-system (Scheme 81).[334,335]

Scheme 81. General synthesis of metallahelicenes by orthometalation reaction.

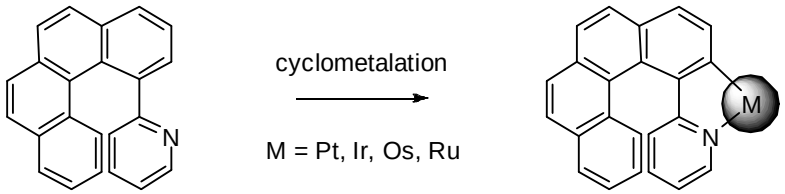

4.2.3.1. Platinahelicenes

The *ortho*-metalation reaction of 4-(2-pyridyl)-benzo[*g*]phenanthrene ligands **11a** and **332b**,**c** using K_2PtCl_4 at high temperature yielded the *μ*-chloro-bridged complexes **333a-e** bearing two C^N chelate ligands, which were then transformed under classical conditions to acetylacetonato-capped platina[6]helicene complexes **334a-c** (Scheme 82).[336,337,338] This efficient strategy consisting of adding two *ortho*-fused rings in the helical backbone enabled to prepare in half-gram scale the first racemic platina(II)-[6]helicenes bearing different substituents (OMe, F, H) and was applied to the preparation of diastereomeric Pt[6]helicene bearing a pinene moiety

(**334d**) and a longer Pt-[7]helicene (**334e**). X-ray crystallography of complex **334c** (see Scheme 83) enabled to identify it as a structural analogue of carbo[6]helicene with for example similar helicities. Except for **334b**, stable, soluble, and neutral complexes **334a-e** were prepared in enantiopure forms by HPLC separations over chiral stationary phases (see Table 26). Later on, enantiopure cycloplatinated helicenes bearing a sulfoxide ligand, being either a DMSO (**335c**) or an enantiopure methyl-*p*-tolyl-sulfoxide (**335f**,**g**) were prepared by direct cycloplatination of proligands **334c,f** and **11c** in refluxing toluene and under basic conditions. Enantiopure Pt-[6]helicene **335c** was obtained by chiral HPLC. Enantiomerically and diastereomerically pure Pt-[8]helicene **334f** was obtained by cycloplatination of 1-pyridyl-[6]helicene (*rac*)-**332f** followed by preferential crystallization of diastereomer (*M*,R_S)-**335f** over (*P*,R_S)-**335f** combined with column chromatography. Similarly, diastereomeric (*P*,R_S,R_S)-**335g** and (*M*,R_S,R_S)-**335g** consisting of bis-platina[6]helicenes were prepared from 1,3-bipyridyl-naphthalene **11c** (see Scheme 2) and obtained as pure diastereomers by taking advantage of their different solubilities in different solvents. Finally, by subsequently replacing the DMSO or chiral sulfoxide by an acac ligand, enantiopure (*M*)-(-) and (*P*)-(+) samples of **334c**,**f**,**g** were obtained (Scheme 82). A bis-platina[10]helicene **334h** was also prepared in racemic form and resolved by chiral HPLC.[45] It displayed specific rotations of similar magnitude as Pt[8]helicene **334f** (more than +3000 for the (*P*) enantiomers, see Table 26).

Scheme 82. General synthesis of platinahelicenes **334a-e** by orthoplatination reaction. Different mono-platinahelicenes prepared using this methodology. *i*) K_2PtCl_4, ethoxyethanol, H_2O, reflux, 16 hr; *ii*) pentane-2,4-dione, Na_2CO_3, ethoxyethanol, reflux, 2 hr.[40,41]

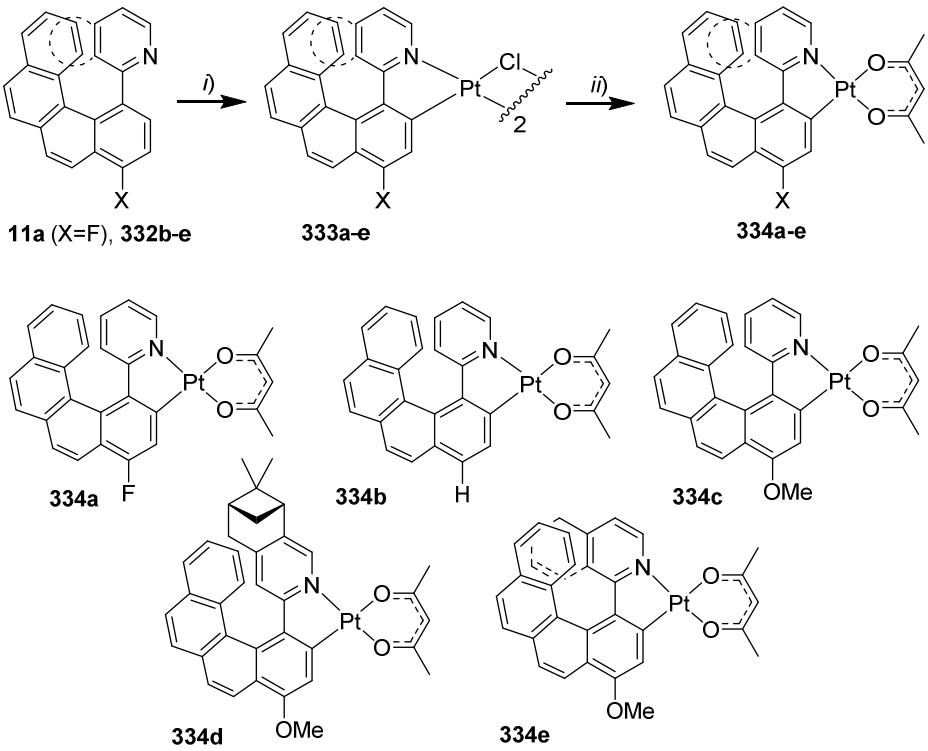

Scheme 83. Synthesis of enantiopure and CPL-active phosphorescent platinahelicenes **334a**,**g**,**f**. *i*) $[PtCl_2(dmso)_2]$, toluene, Na_2CO_3, Ar, reflux, overnight, resolution by chiral HPLC; *ii*) (R_S,R_S)-$[PtCl_2$(*p*-tolyl-MeSO)$_2]$, toluene, Na_2CO_3, Ar, reflux, overnight; *iii*) column chromatography and/or crystallization; *iv*) pentane-2,4-dione, toluene, Na_2CO_3, Ar, reflux, 2 hr. X-ray crystallographic structures of **335c**,**f**,**g**,**h** and **334c**,**f**,**g**,**h** (one enantiomer is shown).[338,45]

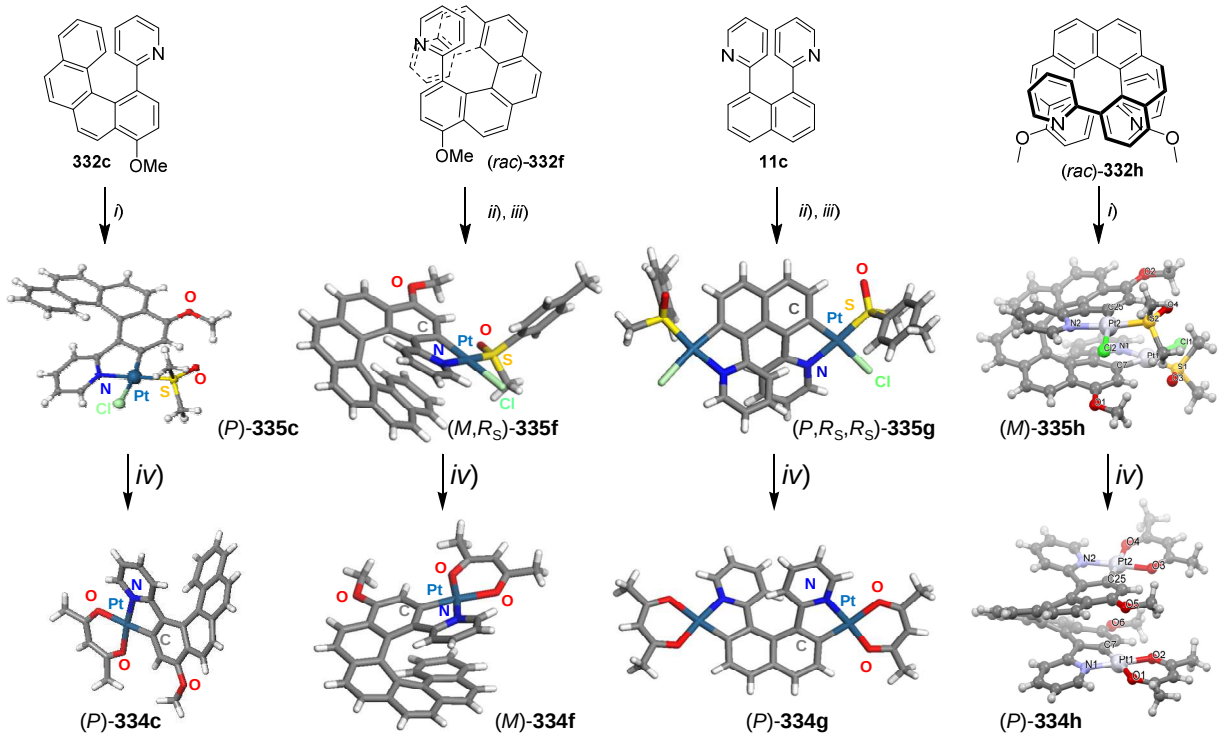

The preparation of platinahelicenes with different sizes enabled us to study and compare their photophysical (UV-vis and luminescence spectra), and chiroptical properties (ECD spectra, OR values, and CPL activity). For example, the UV-vis spectrum of compounds **334c** displayed in Figure 43 shows several intense absorption bands below 410 nm. In addition, two weak lower-energy broad bands (> 450 nm) arising from interactions between the metal and the π-ligands were observed.[337,338] The same low-energy tail was present for Pt^{II}-[8]helicene **334f** and Pt_2^{II}-[6]helicene **334g**. The ECD spectra of the organic 2-pyridyl-[6]helicene **334f** and organometallic Pt-[6]helicene **334c** displayed similar overall shape (Figure 43) but with a blue-shifted high-energy band for **334c** compared to **332f**; Pt-[8]helicene **334f** displayed a stronger and more red-shifted ECD spectrum compared to Pt-[6]helicene **334c**, a well-known tendency for helicenes that can be attributed to an enlargement of the π-electron system; Pt_2-[6]helicene **334g** displayed a significantly different ECD spectrum from **334c**,**f** and **332f**, because of cancellation effects of ECD-active transitions with opposite sign rotatory strengths and similar energies, as indicated by TD-DFT calculations.[338] Interactions between the platinum center and the π-ligands are responsible for strong phosphorescence at room temperature, thanks to efficient spin-orbit

coupling.[200] Indeed, platinahelicenes **334a-g** are efficient deep-red phosphors, with emission maxima between 630-700 nm, quantum yields around 0.05 in deoxygenated solution at room temperature (Table 26) and luminescence lifetimes of 10-20 μs.[338] Interestingly, platinahelicenes **334c**,**f**,**g** displayed circularly polarized luminescence with dissymmetry factors as high as 10^{-2}, which is one order of magnitude bigger than for usual organic helicenes.[27] These g_{lum} values appeared positive for the (*P*) enantiomers and negative for the (*M*), which was not always the case in azaborahelicenes **12a-d**.[45] Note that bis-platina[10]helicene **334h** also exhibited red phosphorescence at room temperature. However, no CPL activity was detected for this long helicene **334h**, which can be explained by two reasons: the weakly chiral environment around the two Pt centers and the high sensitivity to oxygen which readily deactivates long-time measurements necessary when CPL signals are weak. In 2016, Fuchter and Campbell succeeded in preparing a single layer CP-phosphorescent OLEDs (CP-PHOLEDs), using **334c** as a chiral emissive dopant; these PHOLEDs displayed strong circularly polarized electrophosphorescence (CPEL), with g_{EL} reaching -0.38 and +0.22 at 615 nm for (-)- and (+)-**334c**, respectively (see Figure 17C). Although not yet clearly demonstrated, the increase of g_{EL} as compared to the molecular g_{lum} value (10^{-2}) may be explained by a supramolecular organization of **334c** in the solid state.[147]

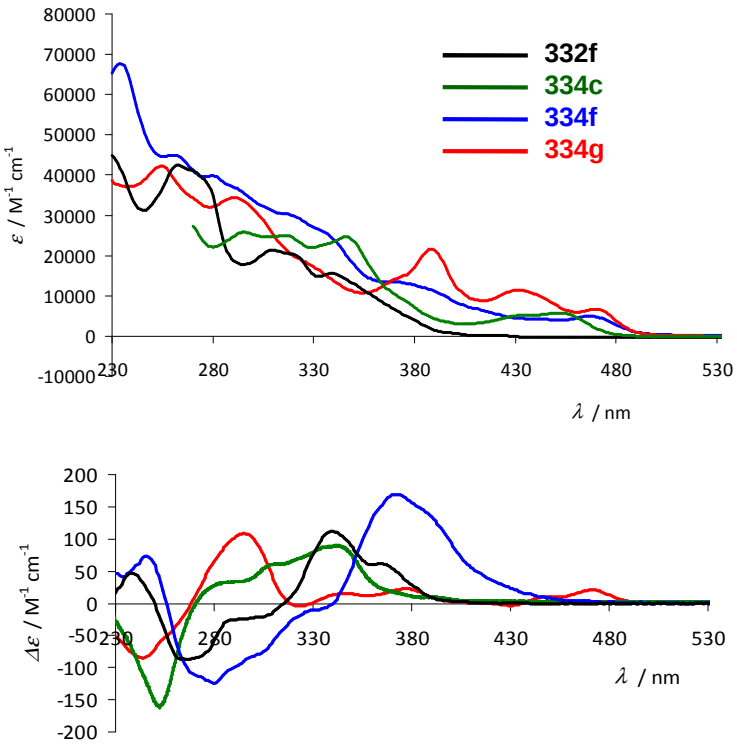

Figure 43. Comparison of the experimental UV-vis (top) and ECD spectra (bottom) of (*P*)-**332f** (black line), (*P*)-**334c** (green line), (*P*)-**334f** (blue line), and (*P*)-**334g** (red line). Reproduced from ref. [334]. Copyright 2014, Royal Chemical Society.

The platinahelicene chemistry demonstrates how powerful organometallic chemistry can be to generate new helical structures with interesting non polarized and circularly polarized

luminescence properties. An additional advantage is the redox activity of the metallic ion. Indeed, the Pt^{II} center in (*P*)-**334c** could be readily oxidized to a Pt(IV) by reaction with iodine, thus giving enantiopure Pt^{IV}-[6]helicene (*P*)-**336** with chiroptical properties that were different from (*P*)-**334c** and with the luminescence activity switched off (Scheme 84a).[337] Complex (*P*)-**336** could be reduced back to (*P*)-**334c** by reaction with zinc. Another important aspect in the chemistry of metallated helicenes is the use of coordination chemistry to assemble several helicene moieties within the same molecular architecture, as demonstrated in the bis-(Pt^{III}-helicene) scaffold **337a**[1,2][339] and in the Pt^{II}-bis-helicene[45] structure **338a**[1,2] (Scheme 84b).[340] It is worth noting that such assemblies of helicenes are impossible to prepare by using organic chemical processes. These organometallic assemblies displayed several interesting and innovative features.

Scheme 84. a) Oxidation of Pt^{II}-[6]helicene **334c** to Pt^{IV}-[6]helicene **336** and reverse reduction process accompanied with modification of the emission.[337] b) Synthesis of homochiral and heterochiral bis-(Pt^{III}[6]helicene) (**337a**[1,2])[339] and Pt^{II}-bis-([6]helicene) (**338a**[1,2]) [340] assemblies; *i*) $PhCO_2Ag$, $CHCl_3$/THF, rt, 12 hr, Ar; *ii*) $AgBF_4$, acetone then Na_2CO_3, toluene, reflux, 10 min, Ar.

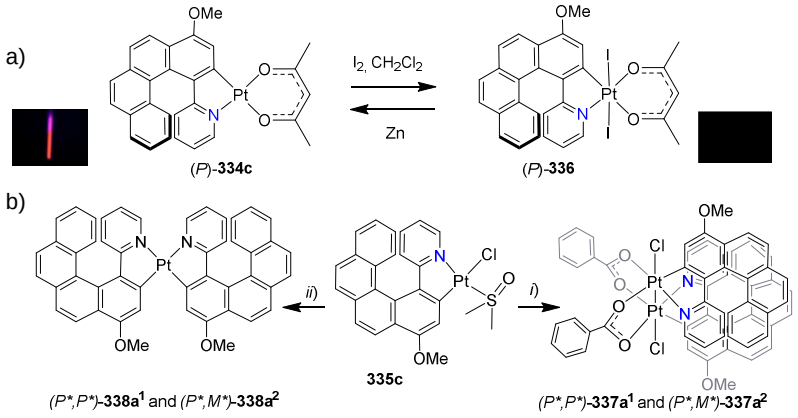

Table 26. Specific rotation values and photophysical data of enantioenriched platinahelicenes.

Compound	Method of obtention	$[\alpha]_{D\ exp}$ [a]	Conditions[b] (solvent/Conc.[c])	Enantio- or diastereo-purity	λ_{Abs} (nm)	λ_{Em} [d] (nm)	ϕ (%)	g_{lum}	Ref
(*P*)-**334a**	Chiral HPLC[e]	+1240 (± 5%)	$CH_2Cl_2/1.8\times10^{-3}$ M	99% *ee*[f]	294,317,421, 444	640	6.9		336
(*P*)-**334c**	Chiral HPLC[g]	+1300 (± 5%)	$CH_2Cl_2/2.85\times10^{-3}$ M	99.5% *ee*[g]	See Fig. 43	644	10	$+1.3\times10^{-2}$	336
(*P*,6*R*,8*R*)-**334d**[1]	Chiral HPLC[h]	+908 (± 5%)	CH_2Cl_2/0.01	>99% *ee*[h]					337
(*M*,6*R*,8*R*)-**334d**[2]	Chiral HPLC[h]	-1047 (± 5%)	CH_2Cl_2/0.01	>99% *ee*[h]					337
(*P*)-**334e**	Chiral HPLC[i]	+1320 (± 9%)	CH_2Cl_2/0.01	99.5% *ee*[i]	508,485,356, 311,266	558 (fl), 704 (ph)	0.97		337
(*P*)-**332f**	Chiral HPLC[j]	+1827 (±7%)	$CH_2Cl_2/2\times10^{-5}$ M	>99% *ee*[j]		446		$+8\times10^{-4}$	338
(*M*)-**334f**	From (*M*,R_S)-**348f**	-3111 (±5%)	$CH_2Cl_2/10^{-4}$ M		See Fig. 43	648	5.6	$+4\times10^{-3}$	338
(*P*)-**334g**	From (*M*,R_S,R_S)-**335g**	+1030 (±5%)	$CH_2Cl_2/10^{-4}$ M		See Fig. 43	633,673	13	$+5\times10^{-4}$	338

(*P*)-**334h**	Chiral HPLC[k]	+3145 (±5%)	$CH_2Cl_2/10^{-3}$ M	>99% *ee*[k]	See Fig. 5	639,663	6.6	null	45
(*P*)-**335c**	Chiral HPLC[g]	+1100 (± 9%)	$CH_2Cl_2/2.85 \times 10^{-3}$ M	99.5% *ee*[g]					339
(*M*,R_S)-**335f**	Column chromatography then crystallization of diastereomers[l]	-2435	$CH_2Cl_2/10^{-4}$ M	>99% *de*[m]					338
(*M*,R_S,R_S)-**335g**	Column chromatography then crystallization of diastereomers[l]	+916	$CH_2Cl_2/10^{-4}$ M	>99% *de*[m]					338
(*P*)-**336**	From (*P*)-**334c**	+200	$CH_2Cl_2/1.1 \times 10^{-3}$ M			Not emissive			339
(*P*,*P*)-**337a**^{1}	From (*P*)-**335c**	+2060	CH_2Cl_2/0.04						339
(*P*,*P*)-**338a**^{1}	From (*P*)-**335c** or from chiral HPLC[n]	+2136	CH_2Cl_2/0.01	60% *ee* or >99% *ee*[n]					340

[a] In deg·mL·g^{-1}·dm^{-1}. [b] Measured at 25 °C. [c] In g/100 mL otherwise specified. [d] Measured at 25 °C. [e] Chiralpak IA, hexane/*i*-PrOH/$CHCl_3$ (90:10:2). [f] Chiralpak AD-H, hexane/*i*-PrOH (9:1). [g] Chiralpak IA, hexane/EtOH/$CHCl_3$ (8:1:1) or hexane/ EtOH (70:30). [h] Chiralpak IB, hexane/ethanol/$CHCl_3$ (85:5:10). [i] Chiralcel OD, hexane/*i*-PrOH (9:1). [j] Chiralpak IB, hexane/*i*-PrOH /$CHCl_3$ (80:10:10). [k] Chiralpak IF, hexane/EtOH/$CHCl_3$ (50:10:40). [l] silica gel chromatography, heptane/ethyl acetate mixture or pure EtOAc, then crystallization. [m] ^{1}H NMR. [n] Chiralpak IA, hexane/ethanol (7:3).

As illustrated on Scheme 85a, an isomerization process from heterochiral (*M*,*P*)-**337a**^{2} to the more stable homochiral (*P**,*P**)-**337a**^{1} occurred when refluxing in toluene for several days, certainly due to high steric congestion around the Pt^{III}-Pt^{III} scaffold. In addition, enantiopure (*P*,*P*)-(+) and (*M*,*M*)-(-)-**337a**^{1} complexes were prepared from enantiopure samples of **335c** and revealed highly intense circular dichroism spectra and huge optical rotations ((*P*)-**335c**: $[\alpha]_D^{23}$ = +1100, $[\phi]_D^{23}$ = +7060 (CH_2Cl_2, *c* 0.01); (*P*,*P*)-**337a**^{1}: $[\alpha]_D^{23}$= +2060, $[\phi]_D^{23}$ = +28200 (CH_2Cl_2, *c* 0.04). Such an increase was interpreted as the consequence of efficient conjugation between the two helical π-ligands through the Pt-Pt bond (σ–π conjugation).[337,339] Concerning the synthesis of **338a**^{1,2}, the C-H activation process of the second cycloplatination step combined with a similar heterochiral to homochiral dynamic isomerization globally resulted in an unprecedented diastereoselective/enantioselective process.[340] Note that Pt^{II}-bis-helicene assemblies **338a**^{1,2} displayed the same structural features as Pt^{II}-$(ppy)_2$ complexes (ppy:2-phenyl-pyridinato) described by von Zelewsky *et al.*,[341] in which two ppy-type are arranged in mutual *cis* position (*trans* effect, Scheme 85b), and with either a bow-shaped geometry or a *Δ*/*Λ* stereochemistry around the Pt center (Scheme 85c).

Scheme 85. a) Isomerization of heterochiral (*M*,*P*)-**337a²** to homochiral (*P*,*P*)-**337a¹** Pt^{III}-Pt^{III} scaffolds; *i*) toluene, reflux, 3 days. X-ray crystallographic structures of homochiral (*P*,*P*)-**338a¹** and heterochiral (*M*,*P*)-**338a²**.[45] c) Bowlike and *Λ* geometries around the Pt^{II} center in **338a¹** and **338a²** respectively. Reproduced from ref. [334]. Copyright 2014, Royal Society of Chemistry.

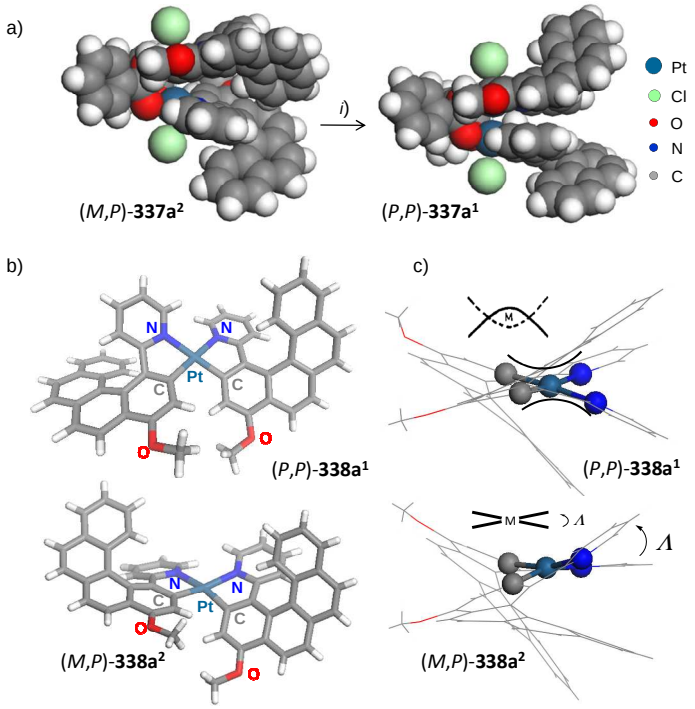

4.2.3.2. Osma- and irida-helicenes

It can be seen from the previous paragraph that the cycloplatination of π-helical ligands leads to a rich variety of platinahelicenes with different structures, redox states, and uncommon assemblies. This synthetic strategy was applied to other metallic centers such as Ir^{III} or Os^{IV} (Figure 44) thus leading to irida[6]helicenes[336] **339a** and **339b** with either two or four helicenes ligands surrounding one or two Ir centers respectively and to osmahelicene **340**.[342]

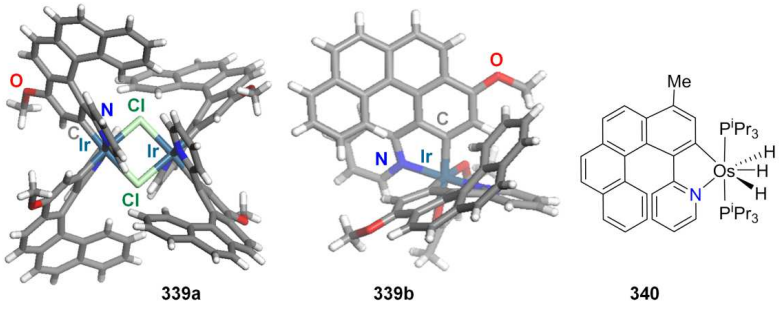

Figure 44. X-ray crystallographic structures of homochiral (*P*,*P*,*P*,*P*)-[Ir^{III}-μ-Cl-(**332c**-H)]$_2$ (**339a**) and (*P*,*P*)-Ir^{III}-(**332c**-H)$_2$ (**339b**).[336] Chemical structure of Os^{IV}-[6]helicene **340**.[342]

5. Helicenes substituted with phosphorus

It is now well-recognized that phosphorus-containing π-conjugated small molecules, oligomers, polymers, and supramolecular assemblies are important classes of heteroatomic molecular materials for applications in optoelectronics (OLEDs, polymer-based OLEDs, photovoltaic cells, field-effect transistors (FET), in electrochromic or smart windows, nonlinear optical (NLO) devices, or polymeric sensors.[343,344] Trivalent phosphorus functions and their related metal complexes are easily designed to tune the electronic and physicochemical properties of helicenes, as well as to offer a wide range of potential uses in organometallic chemistry and catalysis.[345,346]

Therefore, since these P-containing building blocks can lead to materials with unique properties (emission, charge transport, coordination, (anti)aromaticity, etc), and due to the interest of chiral phosphanes as ligands in asymmetric transition metal catalysis, different approaches are currently being developed to incorporate phosphorus atoms in graphene-type molecules including helicene-type molecules. So far, most phosphorus derivatives having helical chirality display polyaromatic (or heteroaromatic) helical scaffolds with pendant phosphorus functions (phosphites, trivalent phosphines and phosphine oxides, helicene-phospholes derivatives, …) but a few classes of P-containing heterohelicenes have appeared in the literature in the last years.

5.1. Helicenes incorporating a phosphorus atom: phosphahelicenes

5.1.1. Synthesis, structural and physicochemical properties of P-containing helicenes

5.1.1.1. Oxidative photocyclization

In 2012, the group of Voituriez and Marinetti constructed phosphahelicenes in which the phosphole ring is placed at the external edge of the fused ring sequence. In this case, the helical phosphines take full advantage of the dissymmetric steric environment generated by the helical chirality at the external edge. Moreover, systems where the P atom is pointing inward the helix can be created. For this purpose, phosphahelicenes were prepared from functionalized *1H*-phosphindoles or dibenzophospholes as starting materials. A first strategy was to use the classical oxidative photocyclization of diarylolefins. For instance, 1*H*-oxaphosphindol-5-yl tosylates **341a**,**b** bearing respectively a P-menthyl or a P-phenyl substituent, were incorporated within *cis* olefins **342a**,**b** (Scheme 86).[347] Starting from diastereomerically pure L-menthyl substituted olefin (R_P)-**342a**, the photocyclization appeared both regio- and stereochemically controlled, with the obtention of oxaphospha[6]helicene (R_P,*P*)-**343a** as the major product (27% isolated yield, $[\alpha]_D^{25}$ +1860 (*C* = 1, $CHCl_3$), absolute configuration determined by X-ray crystallography), as a result of C-C bond formation between a and b carbon atoms. Furthermore, this helical 1*H*-oxophosphindoles terminated by a phosphole unit appeared highly reactive upon UV light and dimerized into **344a** and **344a'** (1:1 ratio) through an intermolecular photochemical [2+2] cyclization. The solid-state structure of compound **344a** was unambiguously established by X-ray crystallography and depicts a head-to-head dimerization of (R_P,*P*)-**343a** through a [2+2] cyclization of the terminal olefinic functions. The two homochiral helical units, of *P* stereochemistry are connected by a cyclobutane moiety having a (*R*,*S*,*S*,*R*) configuration, while the stereogenic phosphorus center displays an (*R*) configuration

($[\alpha]_D^{25}$ +1505, (*C* = 1, $CHCl_3$)). The compound **344a'** ($[\alpha]_D^{25}$ +1150, (*C* = 1, $CHCl_3$)) was assumed to be the epimer of the head-to-head dimer, *i.e.* with (*S*,*R*,*R*,*S*) configuration of the cyclobutane ring.

Scheme 86. Photochemical approach to oxaphosphahelicenes **343a**,**b** and **345b** from oxophosphindoles **341a**,**b**. Intermolecular photochemical dimerization of **343a** to **344a,a'**.[347]

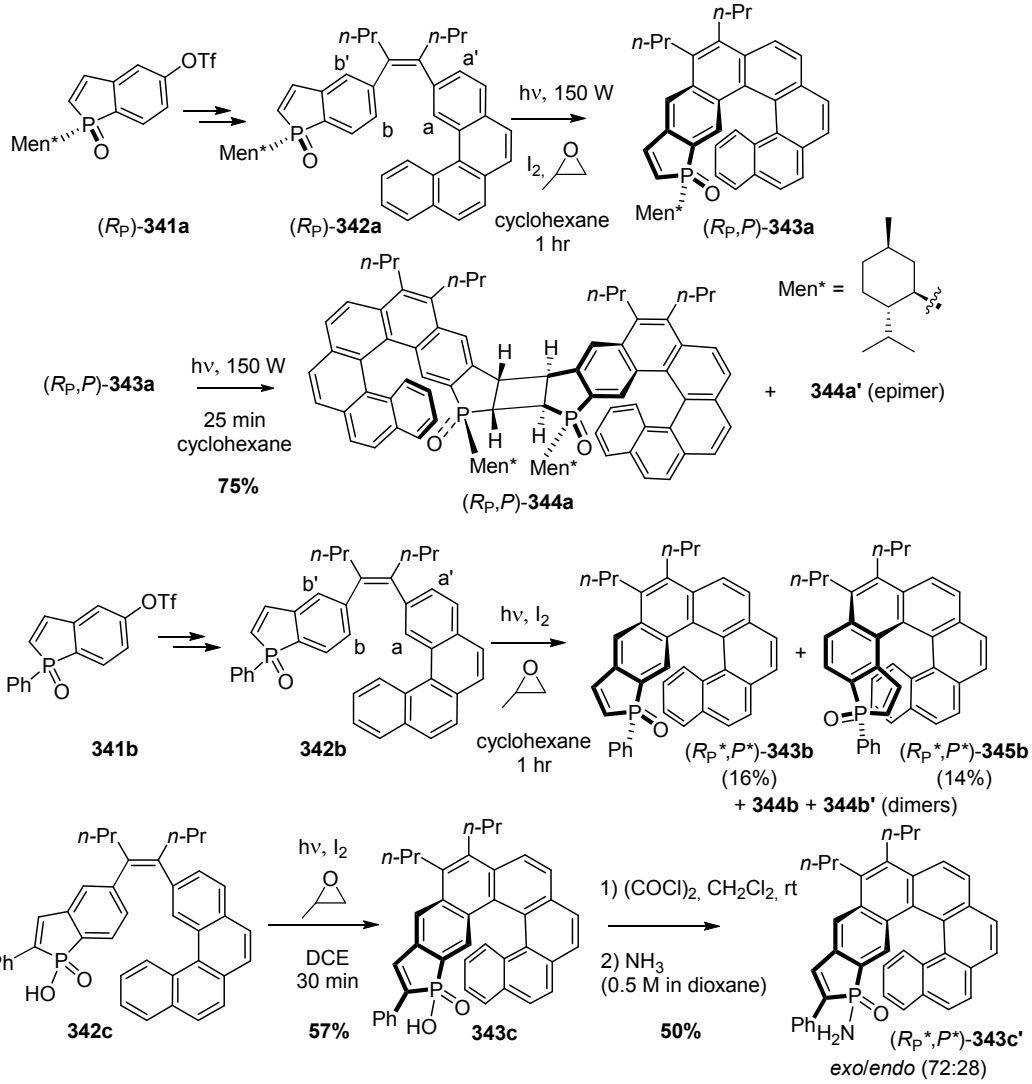

Racemic phenyl substituted **342b** was subsequently oxidatively photocyclized[347] into regioisomers (*R*P*,*P**)-**343b** and (*R*P*,*P**)-**345b** (Scheme 86), which correspond to phospha[6]helicene and phospha[7]helicene, respectively, and result from either Ca-Cb or Ca-Cb' bond formation. Here again, dimeric structures were obtained as evidenced by X-ray crystallographic structures depicted in Figure 45. Furthermore, the homochiral self-assembly of columnar arrangements in the solid state was observed for compound **345b** as observed below for **361**,[70] probably as a result of dipoles alignment. These final compounds obtained in racemic forms could subsequently be resolved into pure enantiomers by HPLC over chiral stationary phases using SFC technique. An important characteristic feature can be drawn from these experimental results: the (*R*)-configured stereogenic phosphorus center induced the (*P*) helical configuration in the final products, whatever the P-substituent, which means that the phosphorus substituents are oriented toward the polyaromatic scaffold, *i.e.* in the most hindered space region. This

rather rare highly diastereoselective photocyclization process is probably due to a kinetic control, as suggested by the experiments shown in Scheme 87 and describing epimerization of the P-atom to the epimeric mixture of (R_P*,*P**)-**343b** and (S_P*,*P**)-**343b'** upon a reduction-reoxidation process of (R_P*,*P**)-**343b**.

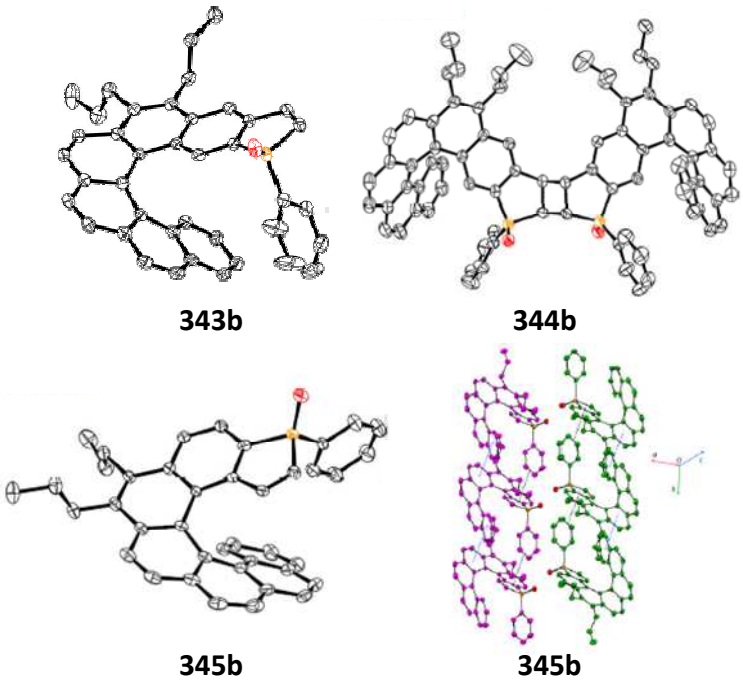

Figure 45. X-ray structures (ORTEP) of the phosphahelicenes **343b** and **345b** (only (*M*) helicenes shown) together with heterochiral dimer **344b**. Supramolecular organization of **345b**. Adapted from ref.[347]. Copyright 2012, Wiley.

Scheme 87. Epimerization process of **343b** upon a reduction-oxidation process.[347]

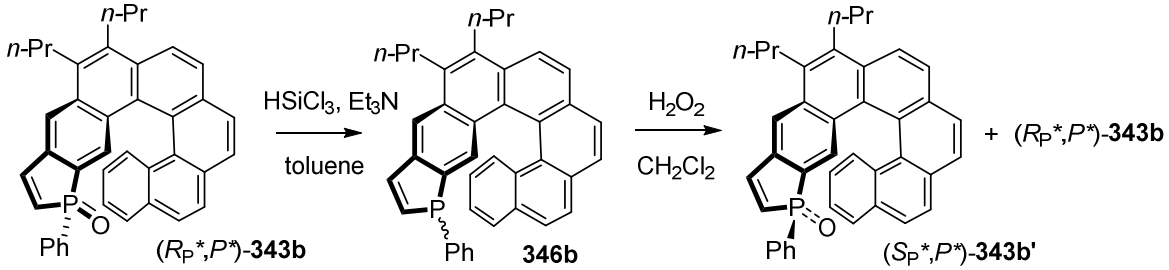

Later on, Voituriez, Marinetti *et al.* enlarged the scope of their strategy by preparing a diversity of phosphahelicenes, *i.e.* P/N-bi-heterosubstituted dimeric helicenes (R_P,*P*)-**347**, as well as for the syntheses of oxophospha[6]- (**348a,b**) and oxophospha[8]helicenes (**349a,b**) starting from dibenzophospholes oxides as structural units (Figure 46).[348] Here again the menthyl and the phenyl groups are directed toward the helix, *i.e.* the P-stereochemistry controls the helicene's configuration. Interestingly, in oxophospha[6]helicenes **348a,b** the P atom points internally within the helical polyaromatic backbone while in (**349a,b**) the P atom points outward. This has an important implication in the asymmetric catalytic activity of these helical phosphine ligands (*vide infra*).[349] Note also that (R_P*,*P**)-**349a** arranges

into homochiral columns in the solid state. Finally, the pseudo-enantiomeric form (S_P,*M*)-**349a** was not observed during the reaction due to different reactivities between pseudoenantiomeric L-Menthyl-substituted (S_P)-dibenzophosphole oxide as compared to the L-Menthyl-(R_P) precursor, thus highlighting the influence of the (S_P)/(R_P) on the fate of the reaction. Finally, taking advantage of the P-reactivity and of the modularity of the photocyclization reaction, several phosphahelicenic systems were prepared, such as for instance the thiooxophosphahelicene (R_P,*M*)-**350**,[348] oxophosphathiahelicene (*S*)-**351**,[350] phosphahelicene (*S*)-**352** bearing an enantiopure isopinocampheyl unit at the P atom,[351] Au^I complexes such as (R_P*,*M**)-*endo*-**353a**[348] and (S_P,*P*)-*endo*-**354**[350] and Ir^{III} complex (*P*)-**355** (Figure 46).[348] Overall, this family of phosphahelicenes displays strong specific rotations, with values ranging from 1080 to 3300 (see Table 27). As described in Scheme 86, the oxidative photochemical process also enabled to prepare phosphahelicene **343c'** which entails a phosphinamide function from helican phosphinic acid **343c**.[352] Two *exo*/*endo* diastereomers were obtained in a 72:28 ratio and were readily separated through column chromatography. Note that *endo*-**343c** isomer underwent intermolecular photochemical [2+2] cyclization to a bis-phosphahelicene affording a head-to-tail heterochiral dimer with total regio- and diastereoselectivity. Interestingly, this process occurred not only in solution but also in the solid state, as a single-crystal-to-single-crystal process, under either X-ray or sunlight irradiation.[352]

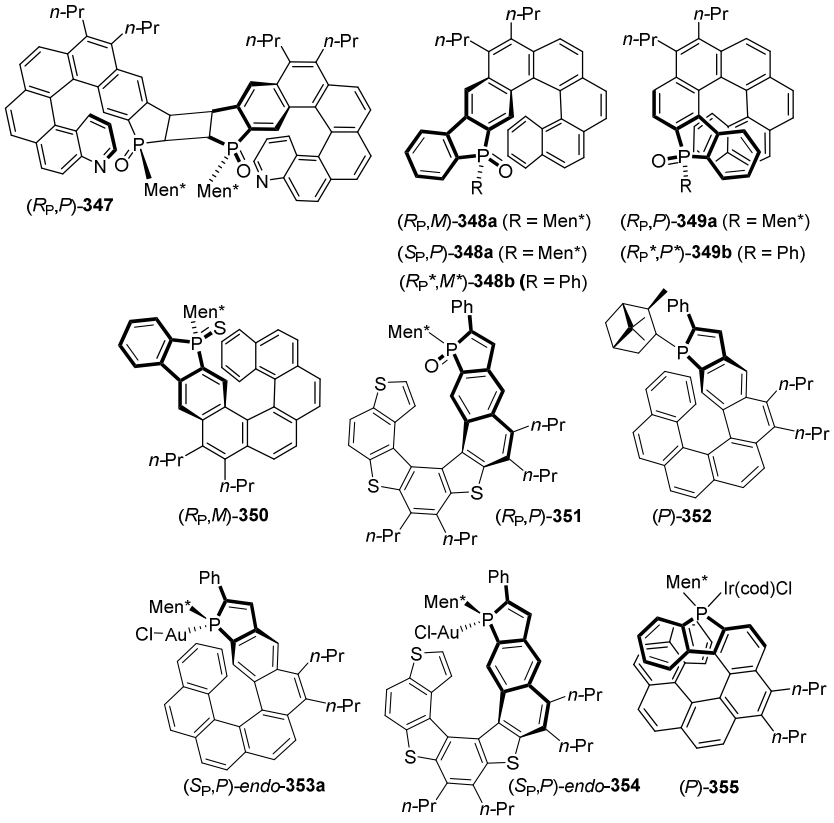

Figure 46. Phosphahelicene derivatives prepared from phosphindole and dibenzophosphole oxides and thiooxides precursors using the diastereoselective photocyclization method and taking advantage of P-reactivity.

5.1.1.2. Intramolecular P-arylation

In 2012, Nozaki and coworkers described the synthesis of racemic λ^5-phospha[7]helicene derivatives, their photophysical and chiroptical properties, and their columnar aggregation within homochiral columns.[70] Oxo- and thiooxo-phospha[7]helicenes **360** and **361** were synthesized as shown in Scheme 88. The palladium-catalyzed cross-coupling of racemic 4,4'-biphenanthryl-3,3'-diyl-bis(trifluoromethanesulfonate), (*rac*)-**356**, with ethyl phenylphosphinate gave the monophosphorous compound (*rac*)-**357** as a mixture of diastereomers displaying both axial and phosphorus centered chiralities. Subsequent reduction with $LiAlH_4$ followed by a palladium-catalyzed intramolecular P-arylation yielded λ^3-phospha[7]helicene (*rac*)-**359**, which contains a phosphole unit as the central cycle. (*rac*)-**359** was directly oxidized without purification to give racemic oxophospha[7]helicene (*rac*)-**360**, which in its turn could give the thiooxophosphahelicene (*rac*)-**361** by using Lawesson's reagent. Racemic **360** was then separated into enantiopure (*P*) and (*M*)-**360** by HPLC over a chiral stationary phase, while (*rac*)-**361** could not be resolved by chiral HPLC and was prepared in enantiopure forms (*P*)- and (*M*)-**361** from enantiopure (*P*)- and (*M*)-**360**, respectively (see Table 27).

Scheme 88. a) Synthesis of racemic λ^5-oxo and thiooxo-phospha[7]helicenes **360** and **361**. b) Homochiral supramolecular arrangement of in the solid state of **361**. c) UV-vis absorption and photoluminescence spectra of **360** in $CHCl_3$. d) ECD spectra of **360** enantiomers in $CHCl_3$. Adapted from ref.[70]. Copyright 2012, Wiley.

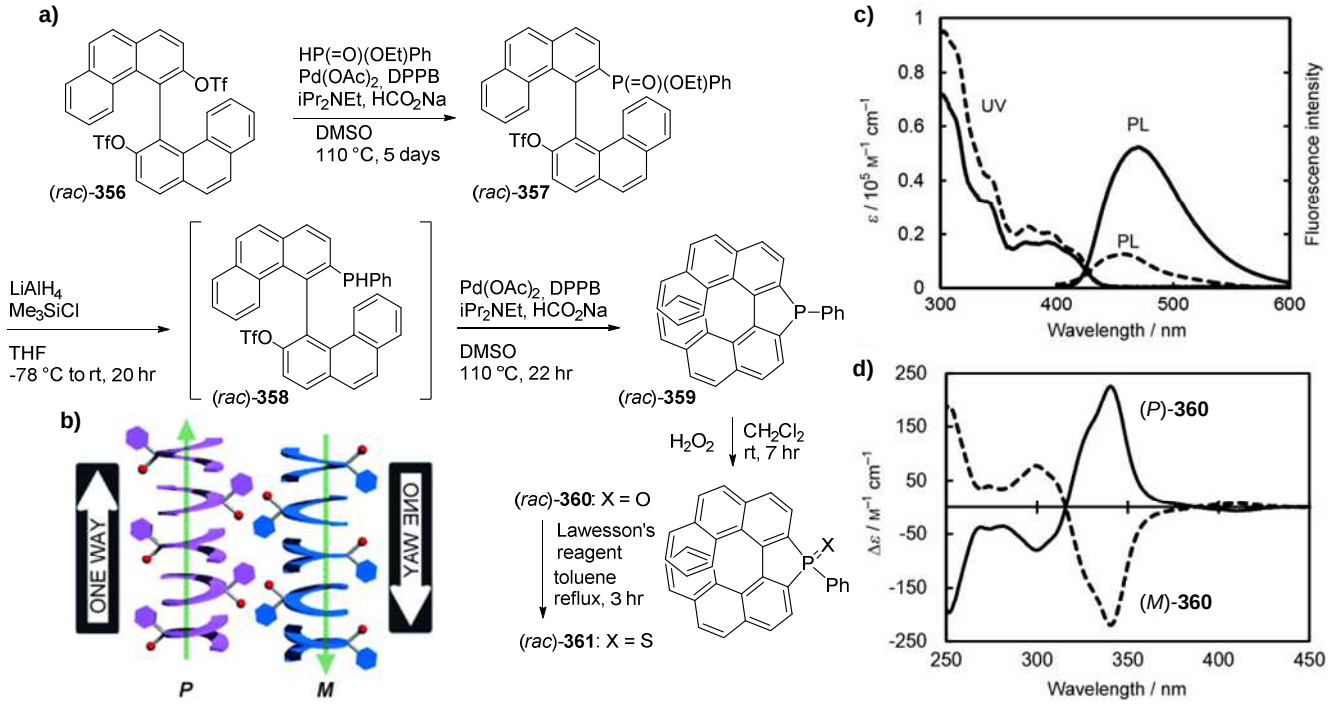

The photophysical properties of λ^5-phospha[7]helicenes 3**60** and **361** were evaluated by UV/Vis absorption and photoluminescence spectroscopy (see Scheme 88 and Table 27), together with cyclic voltammetry, and theoretical calculations. Compounds **360** and **361** display similar absorption spectra

with the longest absorption maxima λ_{Abs} at 416 nm (Scheme 88c) which is significantly red-shifted in comparison to that of 5-phenyldibenzophosphole-5-oxide (332 nm),[353] and 5-phenyldibenzophosphole-5-sulfide (330 nm),[353] as a result of the extended π-conjugation over the helical frameworks. Similarly, the absorption spectra appeared bathochromically shifted compared to the related oxo and aza[7]helicenes **147** and **149** (see Scheme 37).[69] Phospha[7]helicenes **360** and **361** have similar broad luminescent spectra in solution, with maxima λ_{Em} at 462 nm and 460 nm, respectively but with different quantum yields (0.078 and 0.001 respectively) and with large Stokes shifts (Scheme 88c). Such large Stokes shifts suggest a strong rearrangement of the π-conjugated framework upon photoexcitation. Based on DFT calculations, the HOMOs of **360** and **361** are mainly located on the two phenanthrene moieties and chalcogen atoms, and contain a nodal plane at the phosphorus atom. In contrast, the LUMOs are largely located on the phosphole/chalcogenide moieties, where (thio)phosphoryl groups work as electron-withdrawing groups through σ*–π* hyperconjugation (Figure 47A).[68] Such electronic perturbation of the phosphole/chalcogenide moieties may cause an intramolecular charge transfer and may be responsible for the large Stokes shift. The chiroptical properties of **360** and **361** that are incorporated by their helically chiral structures were also characterized. Similar to other known (*P*)-heterohelicenes, both (*P*)-**360** and (*P*)-**361** are dextrorotatory, with strong specific rotations that are much larger than those of **147** and **149** (see Table 12) and of similar magnitude as sila[7]helicene (*P*)-**32** (+2980, see Table 3). This can be directly related to the bigger distortion found by X-ray crystal structures for **360**/**361** as compared to **147**/**149**; but similar as Si (see their dihedral angles on Figure 47B). As a result, the larger angle causes a larger overlap of the two terminal benzene rings in the λ^5-phospha[7]helicenes and, therefore, a stronger steric repulsion. These larger distortions in **360** and **361** also explain their higher tolerance towards racemization, with enantiopurity of **360** and **361** that remain stable after heating up to 170 °C for 68 hr in CH_2Cl_2, whereas the enantiopurity of **147** and **149** decrease upon heating (*ee* drops from >90% to 40% at 150 °C after 68 hr in mesitylene for **147** and after 20 min for **149**). The ECD spectra of (*P*)-**360** and (*P*)-**361** displayed a small negative dichroic signal at around 410 nm, an intense positive signal around 340 nm, and a relatively intense negative signal around 250 nm (Scheme 88d for (*P*)-**360**) together with an additional negative one around 300 nm, which is not present in other heterohelicenes. The (*P*)-(+) and (*M*)-(-) absolute configurations of **360** and **361** were further determined by X-ray crystallographic analysis. Upon crystallization, the authors observed that (*rac*)-**360** spontaneous resolved into enantiopure crystals, while single crystals of (*rac*)-**361** contained both enantiomers, that organized into homochiral columns (Scheme 89b).[70]

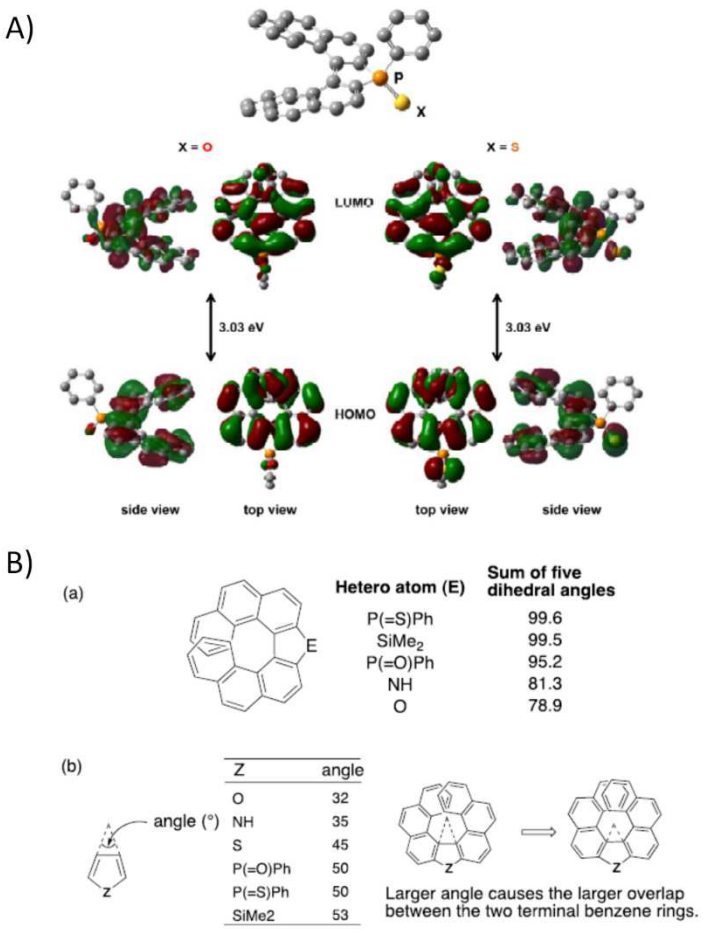

Figure 47. A) Frontier orbitals of phospha[7]helicenes **360** and **361**. B) (a) Summary of sum of five dihedral angles of various heterole-fused [7]helicene. (b) Relation between the angle derived from two double bonds of heteroles and the overlap between the two terminal benzene rings of hetero[7]helicenes. Reproduced from ref. [68].Copyright 2013, American Chemical Society.

Table 27. Specific rotation values of enantioenriched phosphahelicenes and their photophysical data.

Compound	$[\alpha]_D$[a]	Conditions[b] (solvent/Conc.[c])	Enantiopurity	λ_{Abs} (nm)	λ_{Em} (nm)	Φ (% / solvent)	*Ref.*
(R_P,*P*)-**343a**	+1860	$CHCl_3$/1					347
(R_P,*P*)-**343b**	+2028	$CHCl_3$/0.3					347
(S_P,*M*)-**343b**	-2024	$CHCl_3$/0.3					347
(R_P,*P*)-**344a**	+1505	$CHCl_3$/1					347
(R_P,*P*)-**344a'**	+1150	$CHCl_3$/1					347
(R_P,*P*)-**347**	+1846	$CHCl_3$/0.5					348
(R_P,*M*)-**348a**	-2367	$CHCl_3$/0.5					348
(S_P,*P*)-**348a**	+2394	$CHCl_3$/0.7					348
(R_P,*P*)-**349a**	+2048	$CHCl_3$/0.5					348
(R_P,*M*)-**350**	-3306	$CHCl_3$/0.2					348
(S_P,*P*)-**351**	+1358	$CHCl_3$/1					350
(S_P,*P*)-**354**	+1080	$CHCl_3$/1					350

(*P*)-**355**	+1426	$CHCl_3$/0.4					[348]
(*P*)-**360**	+3014	$CHCl_3$/0.10		416	462	7.8/$CHCl_3$	[354]
(*P*)-**361**	+3198	$CHCl_3$/0.10		416	460	0.1/$CHCl_3$	[354]
(*P*)-**364ff**	+1230[d]	$CHCl_3$/3 × 10^{-5} M	68% *ee*[e]			21.8/$CHCl_3$	[67]
(*M*)-**368a**	-961	$CHCl_3$/1					[355]
(*P*)-**368b**	+1725	$CHCl_3$/1					[355]

[a] In deg·mL·g^{-1}·dm^{-1}. [b] Temperatures between 20-25 °C. [c] In g/100 mL otherwise stated. [d] Values calculated as 100% *ee*. [e] SUMICHIRAL, hexane/EtOH (80:20).

5.1.1.3. [2+2+2] Cycloaddition

Using a similar method as the one described for silaheptahelicene **28** in Scheme 6, Tanaka *et al.* reported in 2010 the preparation of enantioenriched benzopyrano- and naphthopyrano-fused helical phosphafluorenes **364** by rhodium-catalyzed enantioselective double [2+2+2] cycloaddition of dialkynyl phosphorus compounds **362** with phenol- or naphthol-linked tetraynes **363**.[356] A whole set of enantioenriched oxaphospha[7,9]helicene-like molecules **364** were prepared with moderate yields and variable *ee*'s (between 9 and 73%) and their photophysical properties were studied. The results are summarized in Figure 48. In 2012, Tanaka reported improved conditions to prepare helicenic structures with higher *ee*'s (up to 75%) when using the (*S*)-Segphos ligand (Scheme 89).[67] The obtained phospha[7]helicene **364** revealed strong fluorescence with good quantum yield (>0.20), and high specific rotations (see Table in Figure 48).

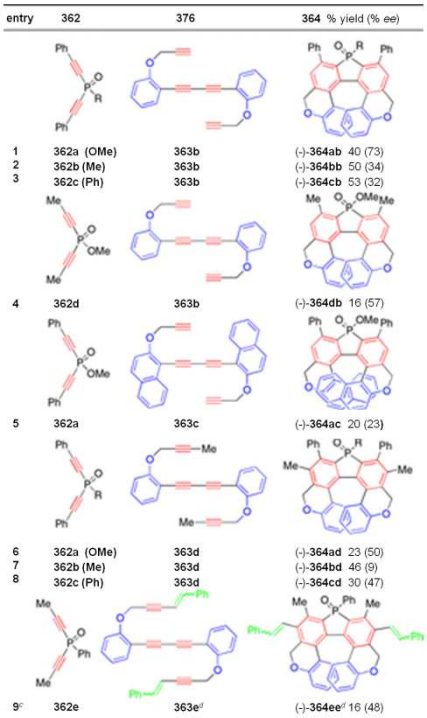

Compound	λ_{abs} (nm)[a,b]	λ_{em} (nm)[a,b,c]	$[\alpha]_D^{25}$ [a,d]
(−)-**364ab**	288, 341	477	699
(−)-**364bb**	288, 344	471	546
(−)-**364cb**	289, 337	474	636
(−)-**364db**	281, 338	469	584
(+)-**364ac**	308, 386	490	420
(−)-**364ad**	285, 343	464	586
(+)-**364ee**	281, 348[e]	482[e]	279[e]

[a] Measured in $CHCl_3$. [b] Concentration: 1.0 10^{-5} M. [c] Excited at 280 nm. [d] Values are calculated as 100% *ee*. [e] Values were measured with use of a mixture of olefin geometric isomers.

Figure 48. Rh-catalyzed asymmetric synthesis of benzopyrano- or naphthopyrano-fused helical phosphafluorenes **364**. [a] Reactions were conducted with $[Rh(cod)_2]BF_4$ (20 mol %), ligand (20 mol %), **362a-e** (1 equiv), and **363a-e** (1.2 equiv) in $(CH_2Cl)_2$ at rt for 1 hr. Ligand: (*R*)-tol-BINAP (entries 1-4 and 9), (*R*)-H8-BINAP (entries 5-8). [b] Isolated yield. [c] For 6 hr. [d] A mixture of olefin geometric isomers. [e]

ee value of the major olefin geometric isomer. *ee's* were measured by analytical HPLC using a CHIRALPAK AD-H column. Adapted from ref. [356]. Copyright 2010, American Chemical Society.
Table: Photophysical properties in and specific rotation of representative phosphafluorenes **364**.[356]

Scheme 89. Efficient enantioselective synthesis of bistriphenylene-fused phospha[7]helicene *via* Rh-catalyzed double [2+2+2] cycloaddition. *ee*'s measured by HPLC using a SUMICHIRAL column (eluent hexane/EtOH = 80:20).[67]

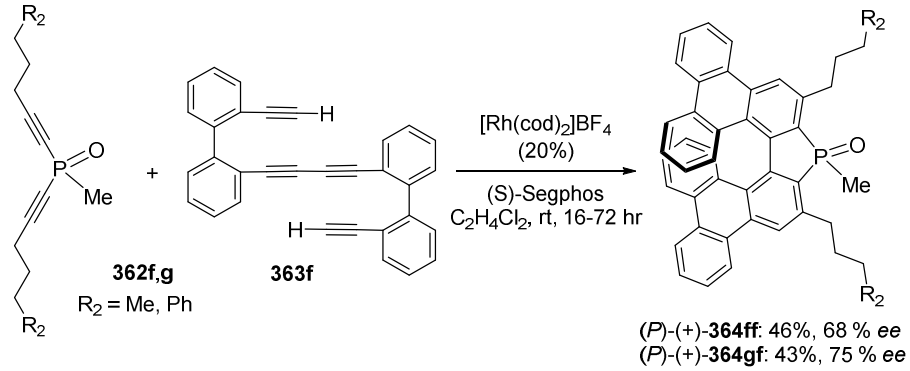

Oxaphospha[7,9]helicene-like molecules **364** from Figure 48 possess both properties of phosphafluorene-type and tetrahydro-oxaphosphahelicenic molecules, therefore showing good emission properties and high optical rotation values. The derivatives displaying the higher emission wavelength correspond to the most extended π-conjugated systems *i.e.* [9]helicene-like derivative **364ac** and [7]helicene-like derivative **364ee** grafted with two styryl groups. However, these two compounds displayed the smallest specific rotation values among the whole series.[356] Bistriphenylene-fused phospha[7]helicene **364ff** display strong blue fluorescence with quantum yield almost reaching 0.218, but still modest specific rotation (1230) for a heptahelicenic structure (see Table 27).[67]

The metal promoted [2+2+2] cyclization of triynes[357] was also applied to the synthesis of phosphahelicene analogues, as an alternative method to oxidative photocyclization. Indeed, phosphahelicene-like structures **366** and **368** were prepared from triynes displaying phosphindole units, **365** and **367**, respectively, by nickel(0)-promoted intramolecular cyclotrimerization of the alkyne functions; as shown on Scheme 90, two examples were either racemic phosphahelicene such as **366** or enantiopure ones like (*M*)-**368a** and (*P*)-**368b** obtained in enantiopure forms after silica gel column chromatography (see their specific rotations in Table 27).[358,355] Recently, highly distorted helicene-phosphanes displaying a homochiral bis-helicenic structure and incorporating two P=S functions was prepared in its racemic form.[359]

Scheme 90. Synthesis of phosphahelicenes **366** and **368** by nickel-promoted cyclotrimerization.[358,355]

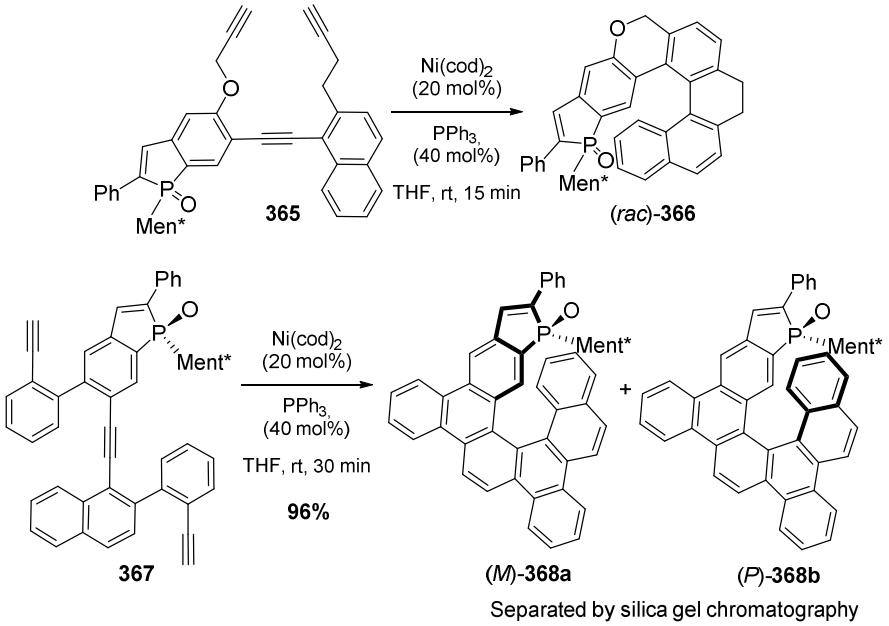

5.1.2. P-incorporating helicenes in asymmetric catalysis

These phosphahelicenes structures revealed as efficient platforms for asymmetric gold catalysis in cycloisomerizations[349] of N-tethered 1,6-enynes and dienynes. Several gold complexes have been prepared and are depicted in Figure 49. Fine-tuning of the phosphahelicene ligands furnished efficient catalytic systems such as (S_P,*P*)-*endo*-**353** and **354** (see Figure 46) displaying high activity and giving high *ee's*.[360,350] In (S_P,*P*)-*endo*-**353** and **354**, the P atom is embedded within the helical structure and the *endo* stems for the gold atom pointing towards the helical groove. This topology is well-fitted for efficient enantioselectivity even with the linear Au^I environment. Complexes **353** and **354** were used as a precatalysts in enyne cycloisomerization reactions, studying a benchmark reaction is the cycloisomerization of the *N*-tethered 1,6-enynes **369** into aza-bicyclo-[4.1.0]heptenes **370** shown in Scheme 91. Good catalytic activity at room temperature, was observed, after activation with $AgBF_4$. Changing the activating agent from $AgBF_4$ to $AgNTf_2$ did not change the enantioselectivity level (75% *ee*), while other silver salts such as AgOTf or $AgSbF_6$ decreased the *ee* to 45 and 63%, respectively. Cycloisomerization of other classes of enynes was then investigated. Dienynes **371** were considered that display conjugated enyne moieties. Depending on the nature of the R substituent, the gold-catalyzed cycloisomerization afforded either the aza-bicyclo[4.1.0]heptene **372** (for R=H) or the tricyclic derivative **373** (for R=Ph), which resulted from a vinylcyclopropane-cyclopentene rearrangement of the intermediate aza-bicyclo[4.1.0]heptene. In the cycloisomerization of **371** (R=Ph), the nature of the silver salt was shown to have a remarkable effect on the enantioselectivity level, going from a moderate 65% *ee* for $AgBF_4$ to an excellent 96% *ee* for $AgNTf_2$. The thiaphosphahelicene–Au^I catalyst (S_P,*P*)-*endo*-**354** gave the highest *ee*'s attained in such cycloisomerization reactions. Note that in 2014, the group studied the influence of the structure and stereochemistry of both the P atom and the helical core of phosphahelicenes depicted in Figure 49 on the fate of the asymmetric intramolecular cyclization of **369** to **370** (Table 28).[360]

The general results on catalysis using phosphahelicenes and more generally helical phosphine ligands and organocatalysts have been the focus of reviews.[16,361]

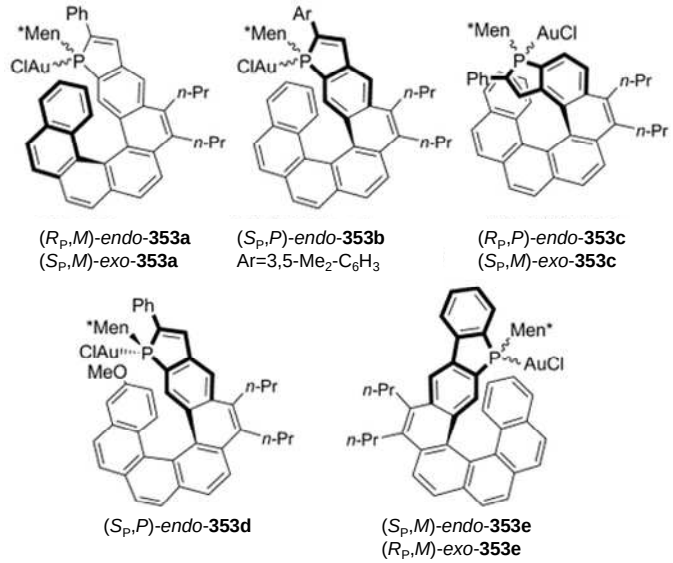

Figure 49. Gold-complexes with different structures and stereochemistries studied in the asymmetric intramolecular cyclization of **369** to **370**.[360]

Scheme 91. Enantioselective catalysis with gold(I) complexes **353a** and **354**.

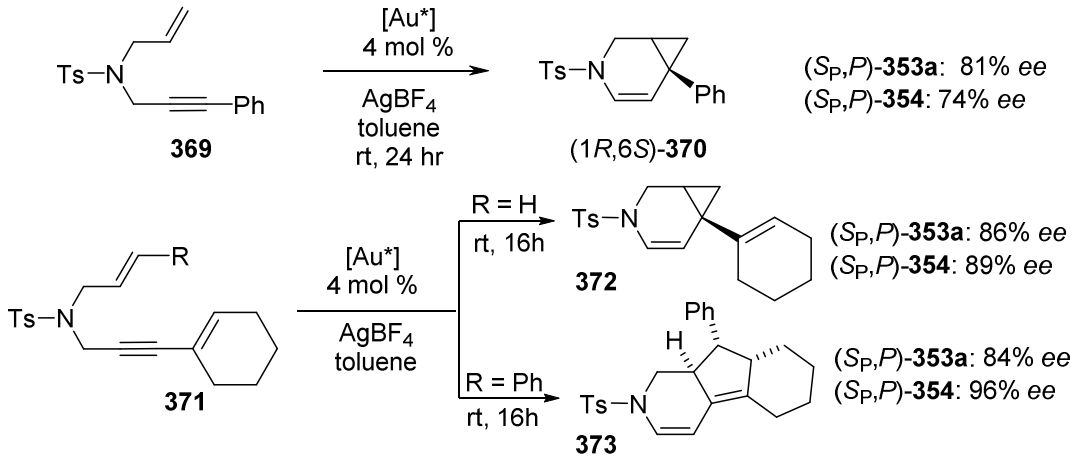

Table 28. Stereochemical influence of phosphahelicene-gold complexes in enantioselective enyne cycloisomerizations.[a]

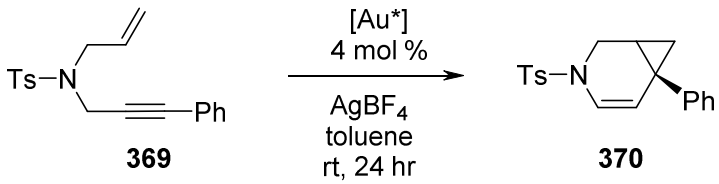

Entry	Catalyst	*ee* [%][b]	Conv. [%]	Config.[c]
1	(S_P ,M)-*endo*-**353e**	7	70	(1*S*,6*R*)

Entry	Catalyst	*ee* [%][b]	Conv. [%]	Config.[c]
2	(R_P,*P*)-*endo*-**353c**	35	43	(1*S*,6*R*)
3	(R_P,*M*)-*endo*-**353a**	42	90	(1*S*,6*R*)
4	(S_P,*M*)-*exo*-**353a**	n.d.	<10	–
5	(R_P,*P*)-*exo*-**353a′**	n.d.	<5	–
6	(S_P ,*P*) -*endo*-**353a′**	81	>95	(1*R*,6*S*)
7	(S_P ,*P*)-*endo*-**353b**	84	>95	(1*R*,6*S*)
8	(S_P ,*P*)-*endo*-**353d**	82	>95	(1*R*,6*S*)

[a] Ts: toluene-4-sulfonyl. [b] n.d.: not determined. [c] The configuration of the bicyclic derivative **370** was assigned by comparison with known samples. The (1*R*,6*S*)-configured bicycles display positive optical rotation values (*c*=1, CH_2Cl_2).

In an additional study, gold complexes were prepared from enantiopure (*M*)-**368a** and (*P*)-**368b** by first reducing the phosphine oxides with $PhSiH_3$ in the presence of bis(4-nitrophenyl) phosphate, then by reacting the trivalent phosphines obtained with chloro(dimethylsulfide)gold(I) (Scheme 92).[355] The gold complexes *exo*-(*M*)-**374a** and *endo*-(*M*)-**374a'** were obtained from (*M*)-**368a** in 78% yield, in a 75:25 ratio similar to the corresponding trivalent phosphine, and with the AuCl moiety placed in the outer groove or in the inner groove, respectively. Both isomers were isolated and characterized by NMR and the stereochemistry of the minor isomer (*M*)-**374a'** was assigned by X-ray crystallography (Scheme 92). Similarly, gold(I) complexes *exo*-(*P*)-**374b** and *endo*-(*P*)-**374b'** were obtained as a 45:55 mixture from (*P*)-**368b**. This set of four stereoisomeric complexes were then investigated as catalysts in the intramolecular [2+2] cyclization of 1,6-allenenes into bicyclo[3.2.0]-heptane derivatives, as shown in Scheme 92 for the transformation of **375** into (-)-**376** obtained in 88% *ee*, were catalyzed by *endo*-(*P*)-**374b'**. Different phosphahelicenic gold(I) complexes have been compared for this type of reaction, and the complexes of the series (**374a-b'**) have proven more efficient than gold(I) complexes of **353** and **354**.[355]

Scheme 92. Synthesis of gold(I) complexes **374** and use in catalysis. *i*) $PhSiH_3$, $(4\text{-}NO_2\text{-}C_6H_4O)_2P(O)OH$, toluene, 100 °C, 2 hrs. *ii*) $(Me_2S)AuCl$, CH_2Cl_2, rt, 1hr. *iii*) Column chromatography. X-ray crystal structure of *endo*-(*M*)-**374a'** showing one molecule in the asymmetric unit. Ellipsoids are drawn at the 50% probability level, H atoms are not shown for clarity. Reproduced from ref. [355] . Copyright 2015, Wiley.

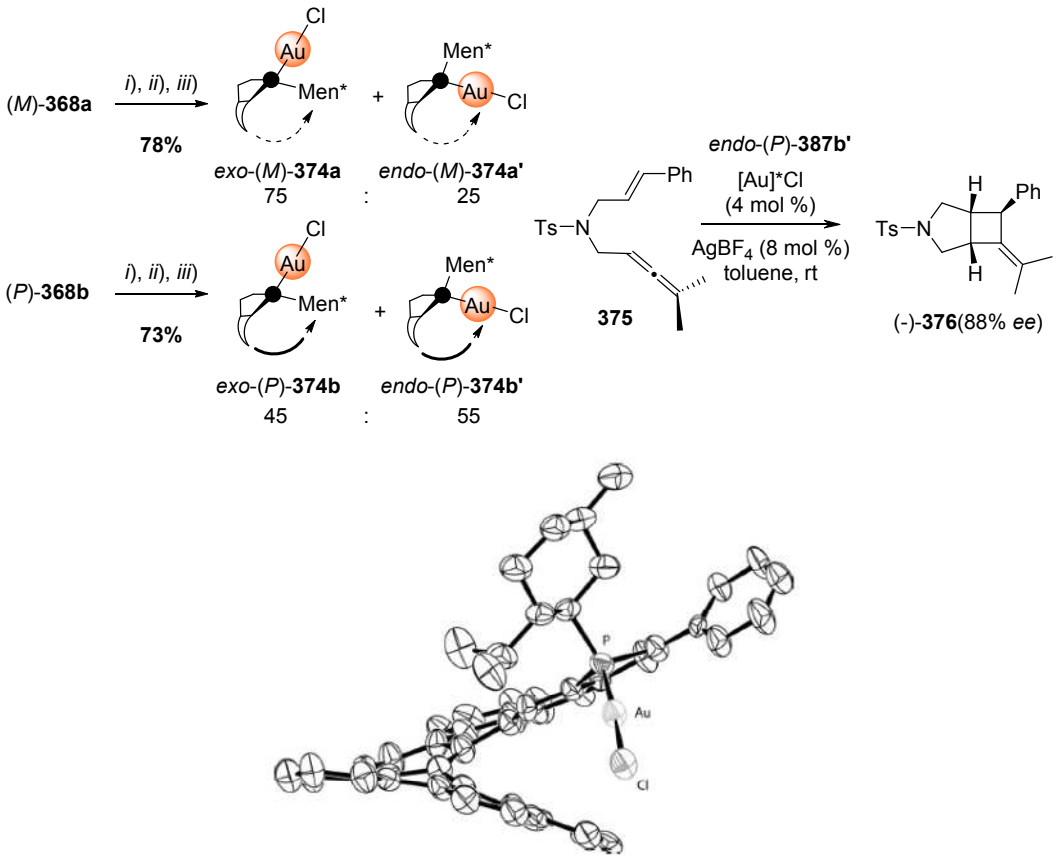

Phosphahelicenes have also revealed efficient chiral organocatalysts in the enantioselective [3+2] annulation of arylidenemalononitriles with allenoates (Table 29).[351] The reaction proved to be successful with a large series of γ-substituted allenoates and γ-substituted buta-2,3-dienenitriles with very high diastereoselectivities (>95:5 *dr*) and enantioselectivities (20 examples, *ee's* 85-97 %). More recently, benzophosphahelicene analogues such the reduced form **352** proved also efficient in this type of enantioselective organocatalytic reaction.[362]

Table 29. Screening of the HelPhos catalysts in an organocatalytic [3+2] cyclization reaction yielding enantioenriched **379**. [351]

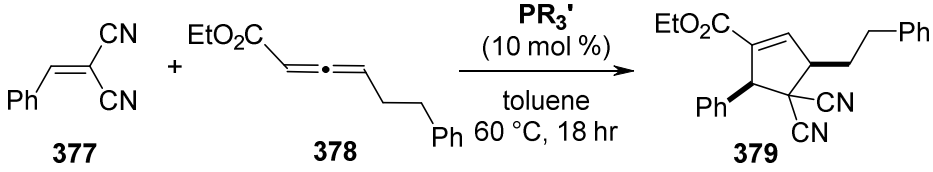

Entry	PR_3*	d.r. (%)	Yield (%)	*ee* [(%)]

Entry	PR_3*	d.r. (%)	Yield (%)	*ee* [(%)]
1	(*P*)-Men*-HelPhos (*P*)-**351**	>95:5	30	89 (+)
2	(*P*)-Ipc*-HelPhos (*P*)-**352**	>95:5	37	95 (+)
3[a,b]	(*P*)-Ipc*-HelPhos (*P*)-**352**	>95:5	91	96 (+)
4	(*P*)-Ipc*-HelPhos (*M*)-**352**	85:15	83	68 (−)

[a] Reaction temperature 80 °C. [b] As an additional experiment, reaction in entry 3 has been carried out at a 5 mol % catalyst loading: total conversion was attained after 48 hr at 80 °C, yielding **379** in 96 % *ee*.

5.2. Helicenes grafted with phosphorus atoms

Helical compounds of this class in which phosphorated functions are appended onto an azahelicene structure are still rare, although varying the pendant substituents enables the modulation of the chemical and physical properties of the helical structure. In addition, the presence of substituents with different steric demands can tune the distance between the two terminal rings yielding variations in the dihedral angle of the molecules, which can accommodate a metallic ion for further use as chiral ligands for enantioselective catalysis. Chiral phosphanes are indeed the most universal ligands for coordination chemistry and for transition-metal asymmetric catalysis.[346]

5.2.1. Synthesis of P-grafted helicenes

5.2.1.1. Configurationally stable carbo[5]helicene phosphanes

The preparation of configurationally stable carbo[5]helicene phosphanes was successfully accomplished only recently. In 2016, Usui and coworkers reported the synthesis of configurationally stable 1-substituted carbo[5]helicene phosphanes **385** and **387** and used them as highly efficient catalysts.[363] As depicted in Scheme 93, [5]helicene-derived phosphines either with a 7,8-dihydro[5]helicene core (**385**) or with a fully aromatic [5]helicene structure (**387**) were prepared in enantiopure forms. First, the Suzuki-Miyaura coupling 4-chloro-3-formy-l,2 dihydrophenanthrene **380** with 2-bromophenylboronic acid **381** gave compound **382** in 89% yield, then homologation using diethyl(1-diazo-2-oxopropyl)phosphonate) followed by cycloisomerization with 10 mol% [$PtCl_2$] resulted in 1-bromo-7,8-dihydro[5]helicene (*rac*)-**383** (54% yield for the two steps). Lithiation of (*rac*)-**383** followed by reaction with chlorodiphenylphosphine and treatment with hydrogen peroxide afforded racemic phosphine oxide (*rac*)-**384** with 63% yield. Using (-)- (resp. (+)-) spiro-TADDOL as a resolving agent yielded, after column chromatography and recrystallization processes, enantiopure (*P*)-**384** (resp. (*M*)-**384**). Phosphine oxides (*P*)-**384** were then reduced into the desired (*P*)-**385** using trichlorosilane and $P(OEt)_3$ (in 72% yield) while ligand (*P*)-**387** was obtained in 70% yield over two steps consisting of oxidative aromatization of (*P*)-**385** with 2,3-dichloro-5,6-dicyano-1,4-benzoquinone (DDQ), and subsequent reduction of (*P*)-**386**. Similar procedures were used for the (*M*) series. The chiroptical properties of enantiopure **385** and **387** were measured. They revealed strong specific rotations with higher values for partially hydrogenated (*P*)-**385** (+1730) than for the fully aromatic (*P*)-**387** (+920). The experimental and calculated ECD spectra are depicted in Figure 50b and 50c, respectively. For example, the ECD spectrum of (+)-**385** displays two bands, a first positive band at ~325 nm and a second negative

one at ~280 nm, corresponding to a (*P*) helicity, as observed by the same authors for 1-methoxy-functionalized [5]helicenes.[364]

The structures of **385** and **387** were confirmed by X-ray crystallography (Figure 50a), with the helical pitch diameter for **385** (3.54-3.50 Å) longer than that for **387** (3.39-3.34 Å). Interestingly, the complex Pd(dba)[**385**] complex was prepared and showed a phosphine-metal-arene interaction, with the double bond (C8a–C14b) of the helicene ligand coordinated with the palladium center in a side-on (η^2) fashion.

Scheme 93. 1-substituted carbo[5]helicenic phosphanes **385** and **387**.[363]

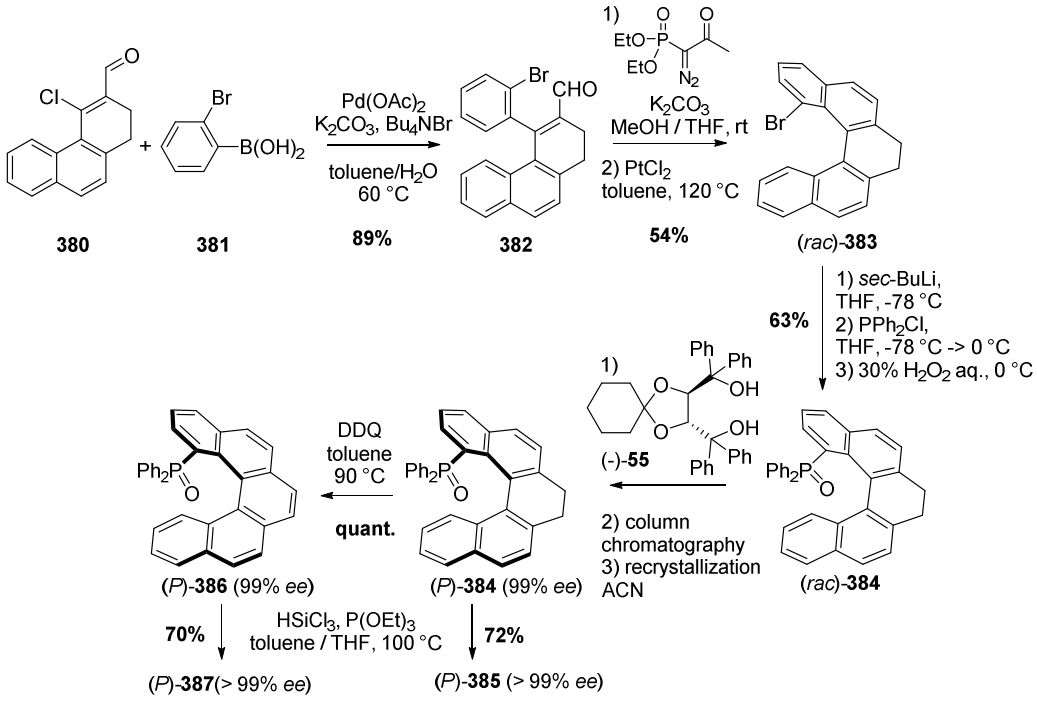

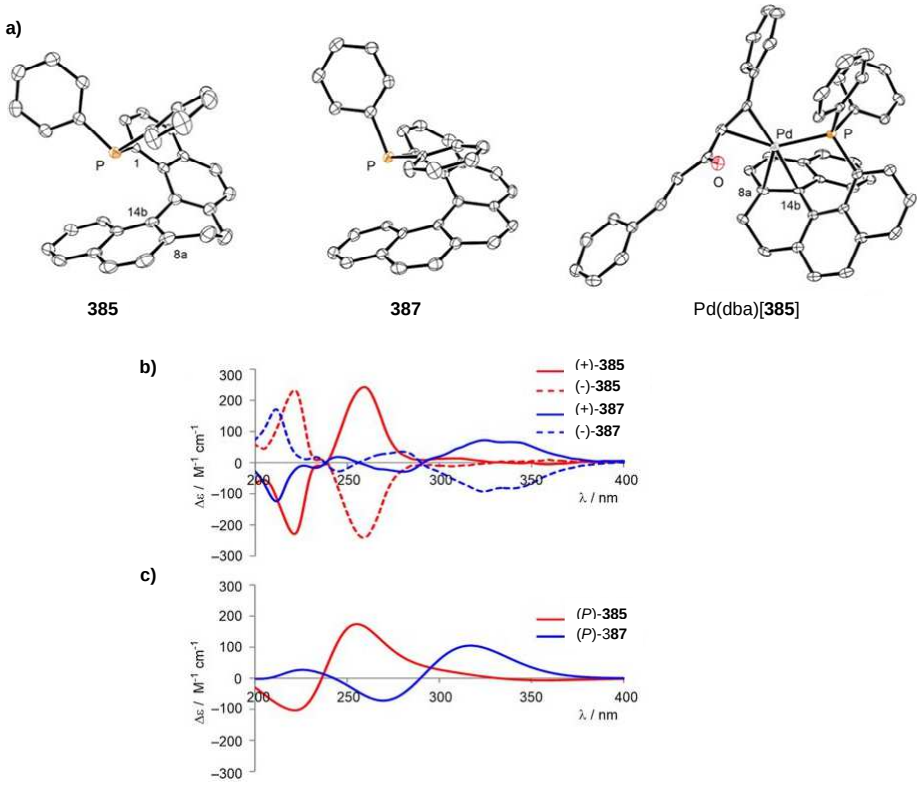

Figure 50. a) X-ray crystallographic structures of **385**,**387** and of complex Pd(dba)[**385**]. b) Experimental ECD/UV-vis spectra of **385**,**387** enantiomers. c) Calculated (CAM-B3LYP/6-31 + G**//B97-D/6-31G*) ECD spectra of (*P*)-**385** and (*P*)-**387**. Reproduced from ref. [363]. Copyright 2016, Nature Publishers.

5.2.1.2. Carbo[6]Helicene phosphanes and related derivatives

In 1997, Reetz *et al.* reported for the first time the preparation of enantiopure 2,15-bis(diphenylphosphino)-hexahelicene **390** (Scheme 94),[365] named Heliphos or more often PHel and previously prepared in its racemic form by Brunner *et al.* in 1997.[366] The synthetic strategy was the classical one, *i.e.* first the preparation of racemic 2,15-dibromo-hexahelicene **389** by a classical photocyclization reaction then replacement of the two bromides by diphenylphosphino groups. HPLC separation using a Chiralcel stationary phase furnished the enantioenriched (>96% *ee*) of *P*-(+) and *M*-(-)-dibromohelicenes which in turn yielded almost enantiopure (>98% *ee*) helical diphosphane enantiomers **390** through lithiation/phosphinylation. To our knowledge, no ECD or OR was reported for this helicene phosphane, although the absolute configuration was obtained from the sign of OR compared to the X-ray structure of enantiomer.

Scheme 94. Synthesis of enantioenriched 2,15-bis(diphenylphosphino)-hexahelicene **390** from enantioenriched dibromohexahelicene **389**.[365]

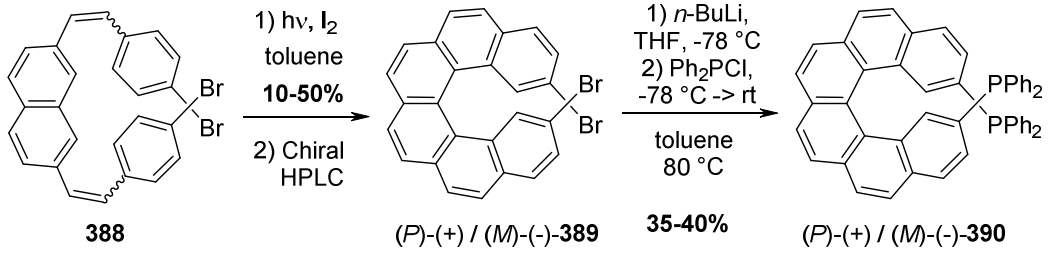

As shown in the example presented above, the phosphorated function is introduced at a late stage of the synthetic sequence on a preformed helical scaffold, *i.e.* a helical dibromide. Using a similar strategy, Stary *et al.* prepared in 2003, *rac*-3-(diphenylphosphino)hexahelicene **393** and its oxide **392** from *rac*-3-(trifluoromethanesulfonato)hexahelicene (Scheme 95). Note that attempts to resolve the former triflate by kinetic resolution failed.[290] In 2009, Aloui and Ben Hassine proposed a modified preparation of (*rac*)-**393** and its oxide (*rac*)-**392**.[367] Marinetti, Ben Hassine and co-workers reported in 2007 the preparation of 3-methoxy-14-(diphenylphosphino)hexahelicene (*rac*)-**395** and its oxide (*rac*)-**396** from 3-methoxy-14-bromohexahelicene (*rac*)-**394**. It is mentioned that the helical phosphine oxide **396** can be separated by chiral HPLC separation while the corresponding phosphine **395** was not stable enough. As a result, its performances in asymmetric catalysis could not be investigated.[368]

Scheme 95. Preparation of hexahelicene monophosphines.

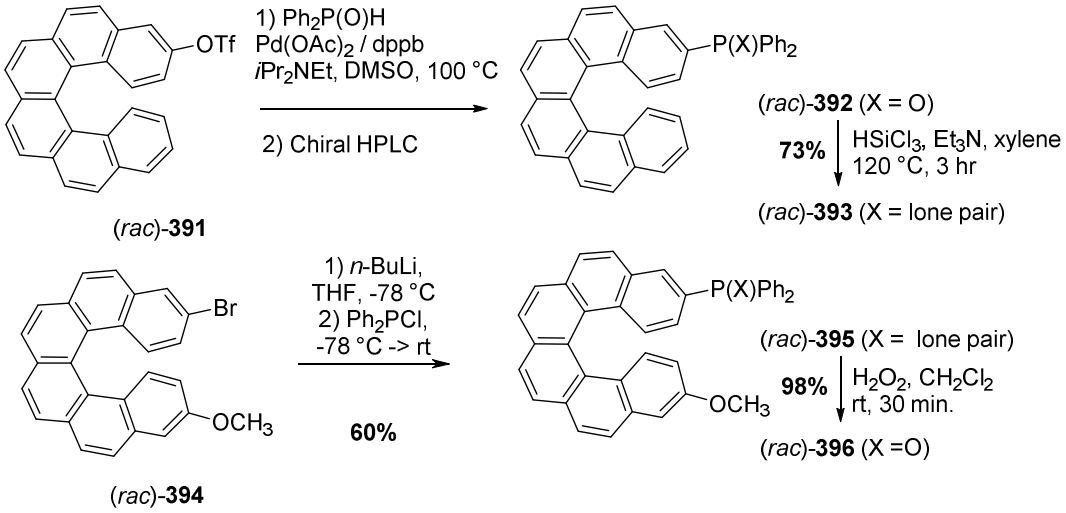

Recently, borane 2-(diphenylphosphanyl)[6]helicene complex **305**-BH_3 was obtained with 96 % *ee* from 2-bromo-hexahelicene (99% *ee*) **303** by a coupling reaction of diphenylphosphine in a microwave reactor at 160 °C for 1 hour, followed by borane protection (see Scheme 75).[61]

In 2016, Tsujihara, Kawano *et al.* reported the preparation of enantiopure helicenic derivatives 1-substituted with a diphenylphosphinoxy group,[369] namely (*P*)-**398** and (*P*)-**400** which were obtained from 1-hydroxy-5,6,9,10-tetrahydro[6]helicene (*P*)-**397** and 1-hydroxy-carbo[6]helicene (*P*)-**399** respectively (and similarly for the (*M*) enantiomers) (Scheme 96). These helical phosphinites were used as enantiopure

chiral ligands in the Pd-catalyzed asymmetric allylic alkylation (see Table 31). Note that enantiopure **397** and **399** pentahelicenic alcohols were prepared through column chromatography of camphanate esters.

Scheme 96. Synthesis of phosphinoxy-substituted hexahelicenic derivatives.[369]

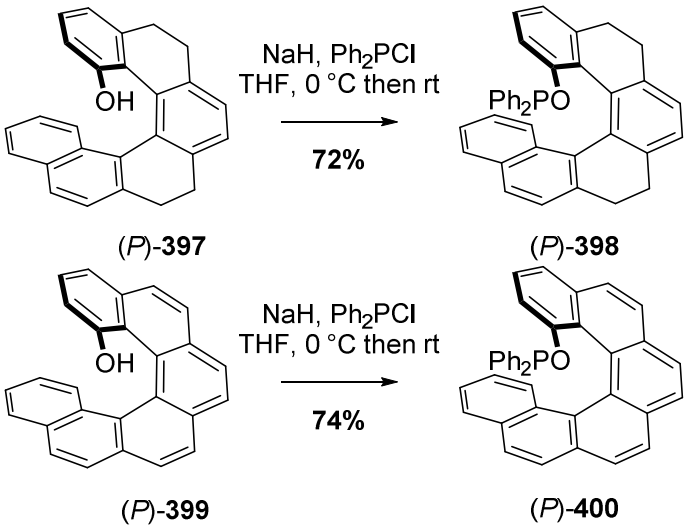

5.2.1.3. Carbo[7]helicene phosphanes

The same year, these groups reported the synthesis and resolution of 2-(diphenylphosphino)heptahelicene **403**.[370] In this case, the diphenylphosphine oxide group was introduced at the early stage of the synthesis and it was shown that oxidative photocyclization was compatible with the presence of such function (Scheme 97). Finally, the phosphine oxide **402** was reduced to phosphine **403** using $HSiCl_3/NEt_3$. The resolution of this monodentate phosphine **403** was performed using a chiral cyclopalladated amine complex, namely ortho-palladated (*R*)-1-(naphthyl)ethylamine complex (*R*,*R*)-**404**, which reacted with **403** giving diastereomeric Pd complexes (*R*,*M*)-**405a**$^{\mathbf{1}}$ and (*R*,*P*)-**405a**$^{\mathbf{2}}$ which were separated by silica gel chromatography. Removal of the enantiomerically enriched phosphines from their palladium complexes was carried out by reaction with bis(diphenylphosphino)ethane (dppe) at room temperature. The specific rotation values obtained for the (*M*)-**403** and (*P*)-**403** monodentate phosphines were -2980 and +2985 (*c* = 0.1, $CHCl_3$), respectively (Table 30). Note that the dichloro[heptahelicen-2-yl(diphenyl)phosphine]-(*p*-cymene)ruthenium complex **406** was also prepared but only in its racemic form.

Scheme 97. Synthesis and resolution of carbo[7]helicene phosphane **403**.[370]

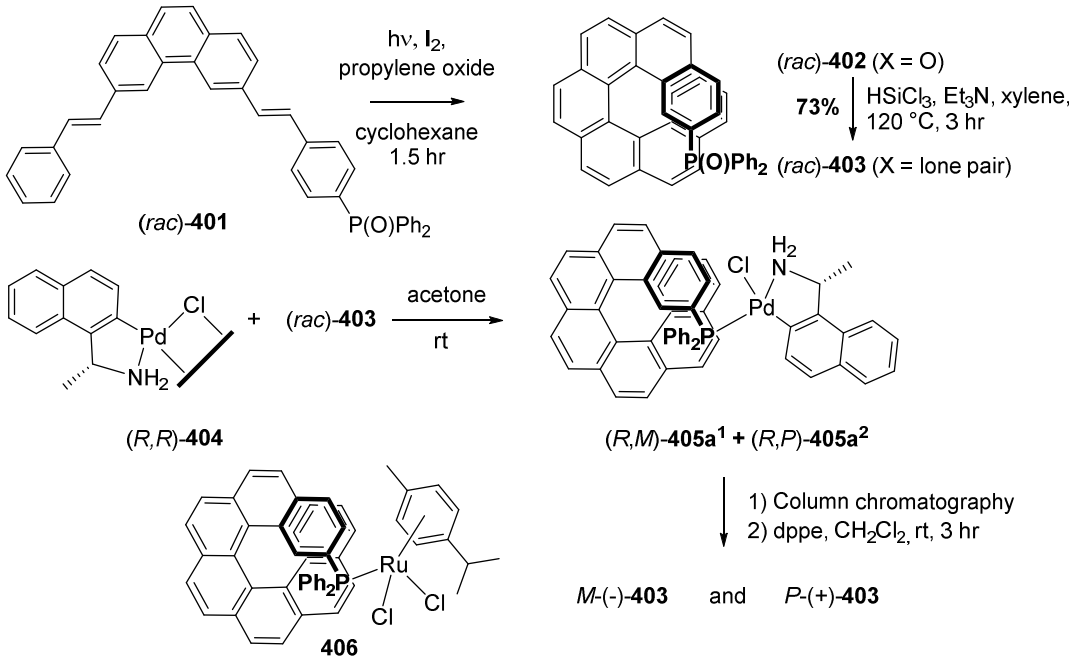

5.2.1.4. Tetrathiahelicene phosphanes

In 2011, Forni, Licandro *et al.* reported the synthesis of tetrathiahelicene phosphanes (named Thiaheliphos) (*rac*)-**408a-c** from tetrathiahelicene **407a-c**.[371] The functionalization at the alpha positions of the two terminal thiophene rings is indeed straightforward by deprotonation and reaction with electrophilic dichlorophosphine chloride. The alkyl chains in the 7- and 8-positions of the helical system improve the solubility but render the phosphorus atoms of substituted thiaheliphos more electron-rich and therefore more sensitive to oxidation. Therefore compound **408c** was reacted with BH_3.THF and gave bis-phosphine-borane (*rac*)**-410** accompanied by mono-phosphine-borane (*rac*)**-411**. The free phosphanes (*rac*)-**408c** and (*rac*)**-412** could then be obtained by refluxing in EtOH. Furthermore, reaction with either precursors $[Rh(COD)_2]BF_4$ or $[Rh(COD)_2]B(Ar_F)_4$ (Ar_F = 3,5-$(CF_3)_2C_6H_3$) gave access to Rh(I) complexes (*rac*)**-413a**,**b**. The structure of these complexes, notably the ligand acting as a chelate of one Rh center, was ascertained by ^{31}P NMR (with the two P atoms coupling together) and by ESI-HRMS. Note that *in situ* oxidation of one P atom was observed for complex (*rac*)**-413a**, thus yielding stable phosphane-phosphane oxide Rh(I) complex. Tetrathiahelicene **407c** was first resolved into its enantiomers using HPLC with a chiral stationary phase (Chiralpak IA) and hexane/dichloromethane (19:1, *v*/*v*) as the mobile phase. Then the (*P*)-(+)-**407c** enantiomer was transformed into (*P*)-(+)-**408c** (see their specific rotations in Table 30) with similar *ee* (as verified by HPLC analysis of its di-phosphine oxide). Note that the tetrathiahelicene-diphosphonate (*rac*)-**409a** was also generated from (*rac*)-**407a** as described in Scheme 98 and as characterized by X-ray crystallography.[371] Furthermore, other similar thia[6]helicene-phosphane,[372] or [7]helicene-phosphane[293] together with some transition metal complexes have been prepared but only in their racemic forms.

Scheme 98. Synthesis of tetrathiahelicene-phosphine/phosphonate derivatives.[371]

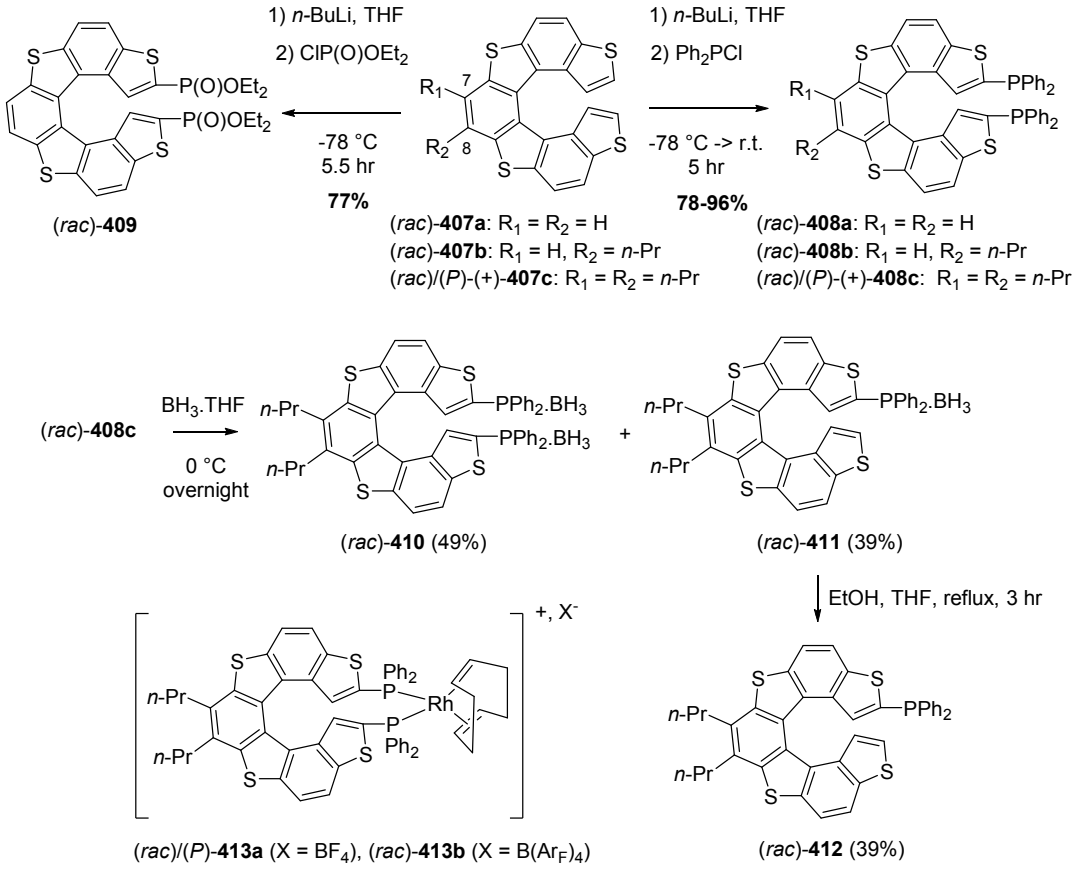

Furthermore, the functionalization of tetrahelicene **407c** by grafting P-dialkyl-borane substituents in position 2 of the terminal thiophene rings has been investigated in 2015. The two enantiomers of **410'** substituted with di(*n*-butyl)phosphine-borane were obtained from resolution of the racemic mixture by HPLC over a chiral Chiralpack IA stationary phase and their chiroptical properties (ECD and OR) studied. The specific and molar rotation were determined and were 3 fold higher than the unsubstituted tetra[7]helicene **407c**.[373]. The experimental ECD spectra is given in Figure 51. The spectra showed an intense band around 300-340 nm with opposite sign for *P* and *M* enantiomers. Computational analyses with RI-CC2 level of theory are in good agreement with the experimental UV-vis and ECD spectra. Interestingly, it was found that the first electronically excited state (S1) was centered in the central helicene core and similar in all tetra[7]thiahelicenes molecules whereas the ECD was more sensitive to the structure modification in the helicene moiety since at the low energy region of the ECD spectrum compensation of bands with opposite signs occurred, such that any difference in the helicene structure could modulate the relative energetic position of the first and the second singlet excited states, S1 and S2, respectively.

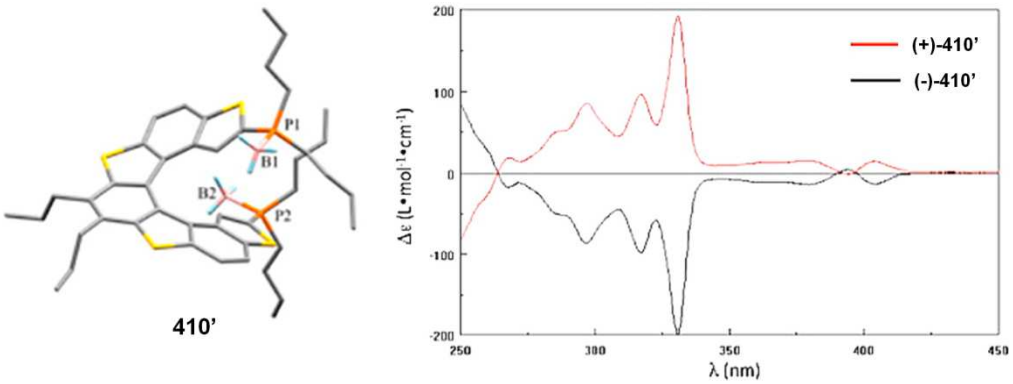

Figure 51. Chemical structure of **410'** and experimental ECD spectra of its enantiomers. Reproduced from ref. [373]. Copyright 2015, American Chemical Society.

Table 30. Specific rotation values of enantioenriched helicene phosphane derivatives.

Compound	Method of obtention	$[\alpha]_D$ [a]	Conditions[b] (solvent/Conc.[c])	Enantiopurity	Ref
(*P*)-**385**	Diastereomeric resolution[d]	+1730	$CHCl_3$/0.0032	99% *ee*[e]	363
(*P*)-**487**	From (*P*)-**385**	+920	$CHCl_3$/0.005	99% *ee*[f]	363
(*P*)-**397**	Diastereomeric resolution[g]	+1010	$CHCl_3$/0.01	> 99% *ee*[f]	369
(*P*)-**498**	From (*P*)-**397**	+1227	$CHCl_3$/0.01		369
(*P*)-**399**	From (*P*)-**397**	+3548	$CHCl_3$ /0.01	> 99% *ee*[f]	369
(*P*)-**400**	From (*P*)-**399**	+2897	$CHCl_3$/0.01		369
(*P*)-**403**	Diastereomeric resolution[h]	+2985	$CHCl_3$/0.1		370
(*P*)-**407c**	Chiral HPLC[i]	+685	$CHCl_3$/0.187	98.9% *ee*[i]	371
(*P*)-**408c**	From (*P*)-**407c**	+2344	CH_2Cl_2/0.058	*ee*~94.9%[j]	371
(*P*)-**410'**	Chiral HPLC[k]	+1320	$CHCl_3$/0.14		373
(*M*,*M*,*S*,1*R*,2*S*,5*R*)-**414**	Chiral pool	+603	$CHCl_3$/0.5		374

[a] In $deg \cdot mL \cdot g^{-1} \cdot dm^{-1}$. [b] Temperatures between 20-25 °C. [c] In g/100 mL otherwise stated. [d] silica gel chromatographic resolution of diastereomeric complexes with spiro-TADDOL. [e] CHIRALPAK IA, hexane/*i*-PrOH mixture. [f] CHIRALCEL OD-H, hexane/*i*-PrOH mixture. [g] silica gel chromatographic resolution of covalent diastereomeric camphanate esters. [h] silica gel column chromatography of diastereomeric complexes with *ortho*-palladated (*R*)-1-(naphthyl)ethylamine. [i] Chiralpak IA, hexane/CH_2Cl_2 (19:1). [j] Chiralpack IA,*i*-PrOH/CH_2Cl_2/MeOH mixture on bis-phosphine-oxide. [k] Chiralpack IA, hexane/ CH_2Cl_2/*i*-PrOH mixture.

5.2.1.5. Helical phosphites and phosphamidates

Earlier examples of phosphites[374,375,376] and phosphamidates[377] are shown in Figure 52. In 2003, the Yamaguchi group prepared phosphite displaying helical, axial, and central chirality, such as (*M*,*M*,*S*,1*R*,2*S*,5*R*)-**414**. Phosphamidate **415** displays a (*P*) helicity. Phosphinites **414** and **417** were utilized in asymmetric catalysis (*vide infra*), while Helol derivative **416** was also investigated in enantioselective recognition.

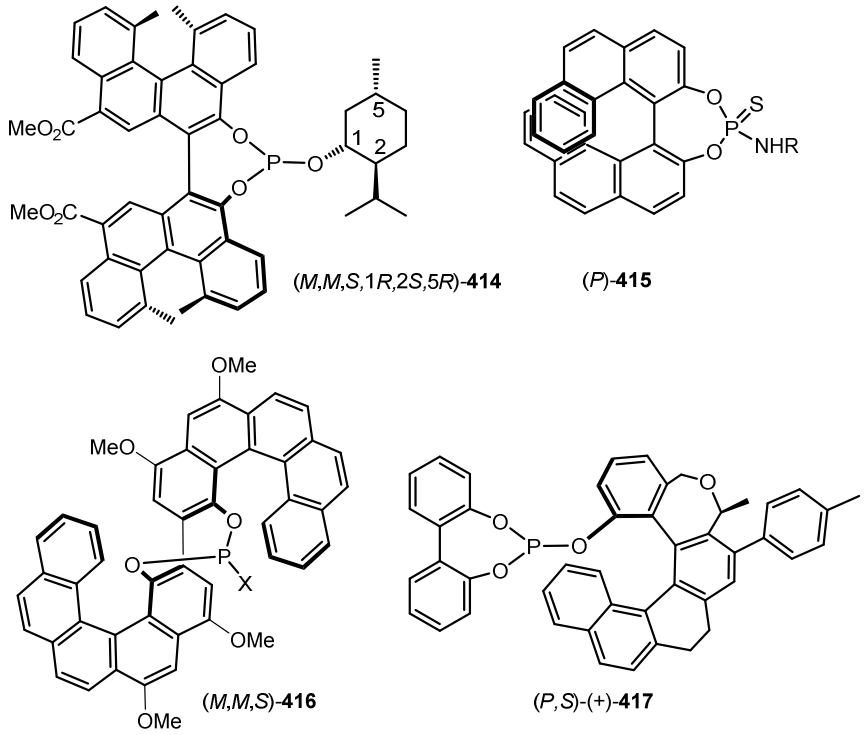

Figure 52. Example of helical phosphites and phosphinates prepared in enantioenriched forms.

5.2.2. Applications in enantioselective catalysis

The rhodium complex of **390** was prepared by reaction with $[Rh(COD)_2][BF_4]$ and used as a chiral catalyst in the asymmetric hydrogenation of di-methyl itaconic acid ester **418** (Table 31). A 39% *ee* was obtained in this pioneering example of asymmetric catalysis using a helicene-based complex (entry 1).[365] The organometallic catalyst was not clearly characterized; the intramolecular P-P distance (6.48Å) obtained from the X-ray crystallographic structure is too large for PHel to act as a ditopic chelating ligand and suggests that it rather behaved as a monodentate one. In 2000, the (*P*) enantiomer of the same helical phosphane was employed as a chiral ligand to form a structurally undefined Pd allyl complex (probably also not chelated) in a Pd-catalyzed kinetic resolution consisting of allylic substitution of acetate by dimethylmalonate in 1,3-diphenylpropenylacetate **422** (entry 6); the left starting material displayed *ee*'s up to 99% while the allylic malonate product **424** showed *ee*'s up to 85.7%.[378]

Enantiopure complex (*P*)-**413a** was tested in the asymmetric hydrogenation of 2-methylene-succinate **418** (entry 2), and methyl-2-acetamidoacrylate **420** (entries 4,5). The hydrogenated (*S*) enantiomers were obtained with moderate *ee*'s (31-40%) (Table 31). The phosphinoxi-substituted hexahelicenic molecules **398** and **400** were also tested as enantiopure chiral ligands in the Pd-catalyzed asymmetric allylic alkylation of **422** giving *ee*'s as high as 97% (entries 9,10).

The two pentahelicenic ligands **385** and **387** proved very effective in asymmetric catalysis.[363] Indeed, the Pd-catalyzed asymmetric allylic substitution reactions were first studied, and the alkylation of racemic 1,3-diphenylallyl acetate **422** with dimethyl malonate **423**, using Cs_2CO_3 as the base and $[PdCl(C_3H_5)]_2$ (0.5 mol%) as the palladium source, in the presence of a catalytic amount of **385** and **387** (1 mol%) in CH_2Cl_2 at room temperature (Table 31, entries 7,8) as a model reaction. Ligand (*M*)-**385** was highly effective in this reaction, affording (*S*)-**424** in 99% yield with 94% *ee*, while (*M*)-**387** afforded (*S*)-**424** in

99% yield with only 71% *ee*. Similarly, (*M*)-**385** was also highly effective in the asymmetric allylation of indoles with 1,3-diphenylallyl acetate (up to 99% *ee*, entry 11), and in the etherification of alcohols (up to 96% *ee*, entry 12). In contrast, **385** and **387** were was highly effective in the stereocontrol of helical chirality in Suzuki-Miyaura coupling (SMC) reactions as illustrated in entries 13-14 of Table 31, with the Suzuki coupling between diisopropyl (1-bromonaphthalen-2-yl) phosphonate **429** and *o*-tolylboronic acid **429'** (up to 99% *ee* for product **430**). The stereoselectivity of the reactions was elucidated with the help of DFT calculations.

In 2003, Yamaguchi *et al.* used phosphites displaying helical, axial, and central chirality, such as (*M*,*M*,*S*,1*R*,2*S*,5*R*)-**414**, as effective ligands for the rhodium-catalyzed enantioselective hydrogenation of di-Me itaconate with *ee*'s up to 96% (entry 3).[374] It was shown that the stereochemistry of the helicene moiety plays an important role in the asymmetric induction, and matched/mismatched phenomena were observed between helical and axial chirality. In 2011, Stary *et al.* used chiral ligands such as (*P*,*S*)-(+)-**417** bearing a pendant phosphite moiety either in asymmetric Rh-catalyzed hydroformylations (moderate *ee*'s up to 32%) or in Ir-catalyzed allylic amination reactions (high *ee*'s up to 94% using an analogue of **417**).[376] For selected reviews on helicenes in asymmetric catalysis, see: [15,16,17,361]. Note that gold-catalyzed cycloisomerizations such as intramolecular allene hydroarylation were performed recently by Hashmi, Licandro *et al*. using tetrathiahelicene phosphane ligands Thiaheliphos **408c** or **412** but those were tested as racemic catalysts.[379]

Table 31. Enantioselective hydrogenation of 2-methylene-succinate **418**, methyl-2-acetamidoacrylate **420** using helicene-phosphanes as catalysts.

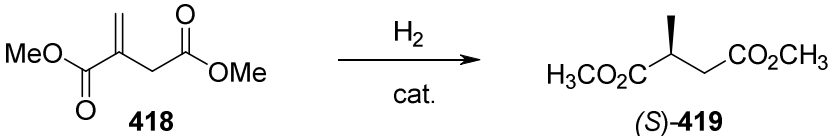

418 *(S)*-**419**

Entry	Catalyst	Conditions H_2 / % catalyst	*ee*	Yield	Ref
1	[(*M*)-**390**-Rh(COD)$_2$][BF$_4$]	1 bar / 0.2 mol % cat.	39%	54%	365
2	(*P*)-**413a**	5 bars / 0.2 mol % cat.	31%	27%	371
3	[(*M*,*M*)-**414**-Rh(COD)$_2$][BF$_4$]	90 bars / 1 mol % cat. -78 to 20 °C	96%	Quant.	374

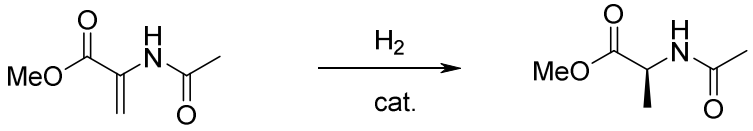

420 *(S)*-**421**

4	(*P*)-**413a**	5 bars / 0.2 mol % cat.	32%	67% (conv.)	371
5	(*P*)-**413a**	5 bars / 0.2 mol % cat.	40%	Quant.	371

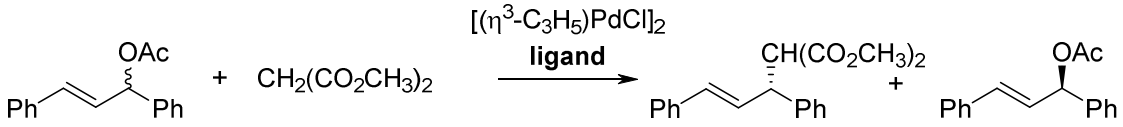

(*rac*)-**422** **423** (*R*)-**424** (*R*)-**422**

6	(*P*)-**390**	BSA, KOAc, 0.5 mol% cat. ligand-metal (2:1)/2h	82.7% ((*R*)-**424**) and 99% ((*R*)-**422**)	98%	378
7	(*M*)-**385**	Cs_2CO_3, 0.5 mol% cat.	94% ((*S*)-**424**)	99%	363
8	(*M*)-**387**	Cs_2CO_3, 0.5 mol% cat.	71% ((*S*)-**424**)	99%	363
9	(*P*)-**398**	BSA, LiOAc, 10 mol% ligand/2.5mol% [Pd]	90% ((*R*)-**424**)	96%	369
10	(*P*)-**400**	BSA, LiOAc, 10 mol% ligand/2.5mol% [Pd]	84% ((*R*)-**424**)	97%	369

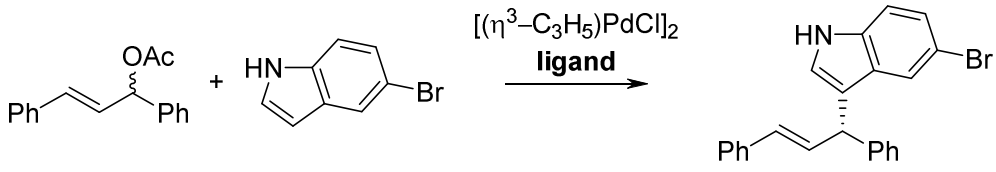

(*rac*)-**422** **425** (*S*)-**426**

11	(*M*)-**385**	Cs_2CO_3 , 1 mol% cat. CH_2Cl_2, rt	99% (*S*)	99%	363

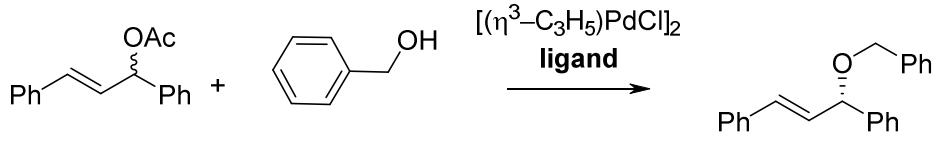

(*rac*)-**422** **427** (*S*)-**428**

12	(*M*)-**385**	Cs_2CO_3 , 1 mol% cat. CH_2Cl_2, rt	96% (*S*)	95%	[363]

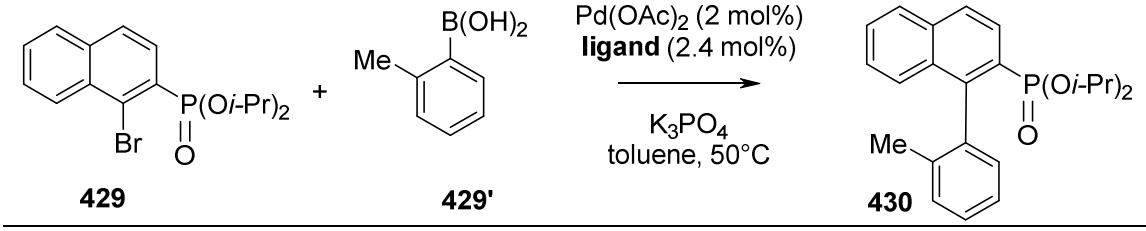

429 **429'** **430**

13	(*P*)-**385**		81% (*R*)	87%	[363]
14	(*P*)-**387**		95% (*R*)	97%	[363]

In 2006, Soai, and collaborators reported the use of unsubstituted enantiomerically pure **420a** and **420c** as chiral inducers in the famous autocatalytic "Soai reaction" (see Scheme 33).[380]

5.2.3. Aza[6]helicene phospholes: synthesis and coordination chemistry

Phospholes are weakly aromatic heteroles with a reactive P atom.[343,344] This weak aromatic character is a consequence of two intrinsic properties of phospholes: (i) the tricoordinate P-atom adopts a pyramidal geometry and (ii) its lone pair exhibits a high degree of σ-character. The aromatic character of the phosphole ring results from hyperconjugation involving the exocyclic P-R σ-bond and the π-system of the dienic moiety. One consequence of such weak aromaticity is that the parent phosphole is stable only below -100 °C. However, introducing a phenyl, a cyano, a bulky alkyl or an alkoxy group at the P-atom allows derivatives to be obtained that are stable at room temperature. The aromaticity of phospholes can also be strongly influenced by the nature (steric hindrance, electronegativity) of the substituent on the P-atom. Calculations have shown that phospholes with a planar P-atom would be more aromatic than pyrrole, due to the good π-donor ability of planar-P centers. However, this stabilization is not sufficient to overcome the high planarization barrier of the P-atom (35 kcal·mol^{-1}), but is responsible for the reduced P-inversion barrier in phosphole (*ca*. 16 kcal·mol^{-1} versus 36 kcal·mol^{-1} for phospholanes). Together, these electronic properties (low aromatic character, σ–π hyperconjugation) set phosphole apart from pyrrole and thiophene.

Phosphole **433a**$^{\mathbf{1,2}}$ having an aza[6]helicene-phosphole motif has been prepared in 2009 by our group *via* the 'Fagan-Nugent method' using enantiopure diyne **432** possessing a $(CH_2)_4$ spacer and a 4-aza[6]helicene unit obtained by regular oxidative photocyclization process followed by chiral HPLC resolution.[381] Starting with a diyne bearing an enantiomerically pure helix that can be obtained by chiral HPLC resolution (for example (*P*)-configuration, Scheme 99), two diastereomeric phospholes (*ie* (*P*,S_P)-**433a**$^{\mathbf{1}}$ and (*P*,R_P)-**433a**$^{\mathbf{2}}$) were obtained due to the presence of the stereogenic P-atom. Their mirror

images (*ie* (*M*,R_P)-**433a^1** and (*M*,S_P)-**433a^2**) were synthesized using the (*M*)-azahelicene. A variable temperature ^{31}P NMR spectroscopic study revealed an inversion barrier between **433a^1** and **433a^2** of 16 kcal mol^{-1} at 330 K in $CDCl_3$. Slow crystallization at room temperature of the diastereomeric mixture of phospholes **433^{1,2}** afforded single crystals of **433a^1** only (see X-ray structure on Scheme 99). The helicity of aza[6]helicene fragment showed a classical value of 45.8° between the pyridine ring and the terminal phenyl ring. Furthermore, the low twist angle (26.3°) measured between the phosphole ring and the aza[6]helicene unit allows a good electronic interaction between the two π–systems. This is illustrated in the UV-visible spectrum with lower energy at 430 nm, a red-shifted value compared to 2-pyridyl-1-phenyl-5-phenyl-phosphole (390 nm).[343,382] In Table 32 are summarized the photophysical data of precursor **432** and of phosphole **433^{1,2}**. While **432** displays the classical structured blue fluorescence at 422 nm, the phosphole displays a large fluorescence signal centered at 502 nm, originating from both the azahelicene and phosphole fluorophores.

Scheme 99. Synthesis of (*P*,S_P)-**433a^1** and (*P*,R_P)-**433a^2** diastereomers from one diyne (*P*)-**432** enantiomer. X-Ray structures of phospholes **433a^1**.[381]

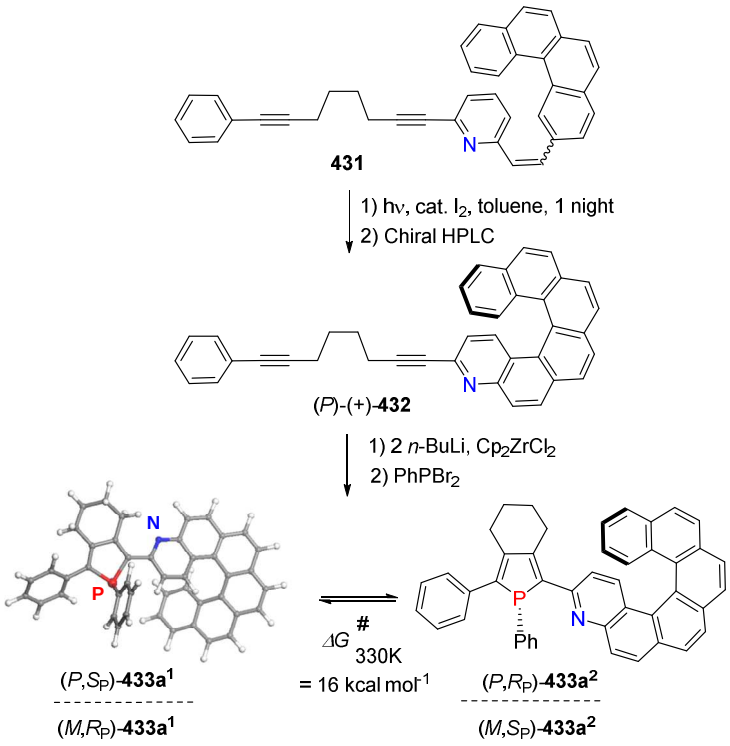

Table 32. Photophysical data for the azahelicene diyne **432** and of azahelicene phospholes **433^{1,2}**. Data at 298 K in CH_2Cl_2; at 77 K in ether/isopentane/ethanol (2:2:1 v/v).

Compound	λ_{max}^{abs} (nm) (ε in $M^{-1}cm^{-1}$)	λ_{fluo}^{RT} (nm)	Φ_{fluo}^{RT} (%)	τ_{fluo}^{RT} (ns)	$\lambda_{fluo}^{77\,K}$ (nm)	$\tau_{fluo}^{77\,K}$ (ns)	$\lambda_{phos}^{77\,K}$ (nm)	$\tau_{phos}^{77\,K}$ (s)

432	265 (48700), 321 (18000), 331 (17500), 352 (8510), 393 (1560), 416 (1270)	422, 446, 472	6	5.9	420, 445, 473	9.3	532, 578, 626	1.5
433a^{1,2}	265 (67500), 326 (21000), 395 (15900), 430 (12700)	502	--	6, 1.2	425 and 490	8.5 , 2.6	~ 550	1.3

Table 33. Specific rotation values of enantioenriched helicene phosphane derivatives.[382, 383]

Compound	$[\alpha]_D^{23}$ [a]	$[\phi]_D^{23}$	Conditions[b] (solvent / Conc.[c])	$[\phi]$ [b]
(*P*)-**432**	+2010	+10240	CH_2Cl_2 / 0.01	
(*P*,*R**)-**433a**^{1,2}	+1350	+8200	CH_2Cl_2 / 0.3	
(*P*,*P*)-[Pd(**433**)$_2$]$^{2+}$	+ 1275	+23100	CH_2Cl_2 / 0.01	(*P*,*P*,*R*$_P$,*R*$_P$,Δ_{Pd})-[Pd(**5c**^{1})$_2$]$^{2+}$ +26660
(*P*,*P*)-[Cu(**433**)$_2$]$^+$	+ 910	+13150	$CHCl_3$ / 0.01	(*P*,*P*,*R*$_P$,*R*$_P$,Δ_{Cu})-[Cu(**433a**^{1})$_2$]$^{2+}$ +13230
				(*P*,*P*,*R*$_P$,*R*$_P$,Λ_{Cu})-[Cu(**433a**^{1})$_2$]$^{2+}$ +30340
(*P*,*P*)-**448**	+2230	+21000	CH_2Cl_2 / 1 × 10^{-4} M	
(*P*,*P*)-**449**	+1690	+19560	CH_2Cl_2 / 1 × 10^{-4} M	
(*P*,*P*)-**450**	+658	+19200	CH_2Cl_2 / 1 × 10^{-4} M	

[a] Within an error of ± 2%. [b] TD-DFT calculated using the **433a**^{1} diastereomer.

Heteroditopic 2-pyridylphosphole derivatives have been utilized as 1,4-chelating ligands towards transition metals.[345] They possess two coordination centres with different stereo-electronic properties ("hard" nitrogen and "soft" phosphorus centres) which, in accordance with Pearson's antisymbiotic effect (*trans* effect), can control the orientation of two 1,4-P,N ligands around a square planar d^8-metal centre (Pd^{2+}, Pt^{2+}); C_2-symmetrical complexes with optimized optical properties such as second order NLO activity are obtained in this way.[384] Indeed, complexation of aza[6]helicene phosphole **433** to Pd(II) and Cu(I) gave stable metal-bis(helicene) complexes of respective formula [Pd(**433**)$_2$]$^{2+}$ and [Cu(**433**)$_2$]$^+$ (Scheme 100). Pd(II) appeared more efficient than Cu(I) to stereoselectively organize two aza[6]helicene phosphole ligands around the metallic ion thanks to steric hindrance combined with *trans* effects and configurational lability at the phosphole's P atom. Indeed, in complex (*P*,*P*)-[Pd(**433**)$_2$]$^{2+}$, the lability enabled the P atom to adapt its configuration upon coordination in order to minimize the steric congestion induced by the two helical units, while the *trans* effect resulted in aligning the two P,N chelates in a *cis* fashion around the Pd(II) center. Overall, the (*P*) handedness of the aza[6]helicene unit was transferred to the P atom fixed at (*R*) stereochemistry which in turn imposed the (Δ) configuration to the Pd center (ligand found as **432a**^{1} stereoisomer).

DFT calculations performed at the BP/SV(P) level of theory on the Pd(II) complex [Pd(**433**)$_2$]$^{2+}$ with a (*P*) ligand, and where the P-atom is (*R*) and the Pd center is Δ , *i.e.* (R_P,Δ_{Pd}) diastereomer, is 19.4 kcal/mol more stable than the (S_P,Δ_{Pd}) diastereomer (Figure 53).[382] On the contrary, in the case of Cu(I) complex, the two stereoisomeric complexes (*P*,*P*,*R*,*R*,Δ_{Cu}), and (*P*,*P*,*R*,*R*,Λ_{Cu}) were found to have the same energy.

Thanks to such a highly controlled stereoselective process, the chiroptical properties of the Pd^{II}-bis(helicene) assemblies [Pd(**433**)$_2$]$^{2+}$ were significantly enhanced as compared to the starting ligand **433** and to the Cu^{I}-bis(helicene) assembly [Cu(**433**)$_2$]$^{+}$ (see Scheme 100C). The ECD spectrum observed for **433** was characteristic of an extended π-conjugated helical ligand over the whole helicene-phosphole skeleton. In the Pd(II) complex [Pd(**433**)$_2$]$^{2+}$, efficient metal-ligand electronic interaction induced MLCT type transitions responsible for the low-energy ECD-active tails (400-500 nm). This was not the case for Cu(I) complex [Cu(**433**)$_2$]$^{+}$ since metal-ligand electronic interactions appeared much weaker and the stereoselectivity very low (*vide supra*).[79] In conclusion, the heteroditopic *P*,*N*-moiety of derivative **433** dictates its coordination behaviour allowing a predictable coordination-driven molecular engineering to be performed.

Enantiopure aza[6]helicene diyne (*P*)-**432** (Scheme 100) displays a high MR value $[\phi]_D^{23}$= +10240 (Table 33) that is comparable to (*P*)-hexacarbohelicene ($[\phi]_D^{23}$= 11950).[25] The specific MR of phosphole (*P*)-**433** is lower ($[\phi]_D^{23}$= + 8200) since it corresponds to a mixture of diastereomers ((*P*,S_P)-**433** and (*P*,R_P)-**433**). In comparison, complex (*P*,*P*)-[Pd(**433**)$_2$]$^{2+}$ displays a huge specific MR ($[\phi]_D^{23}$ = +23100), which is much larger than that of its Cu^{I}-analogue (*P*,*P*)-[Cu(**433**)$_2$]$^{+}$ ($[\phi]_D^{23}$= 13100).

Scheme 100. Synthesis of Pd- and Cu-bis(aza[6]helicenephosphole) from **433a^{1,2}**. UV-vis and ECD spectra in CH_2Cl_2 at 293 K of (*P*) enantiomers (plain line) and of their respective (*M*) enantiomers (dashed lines).[381,382]

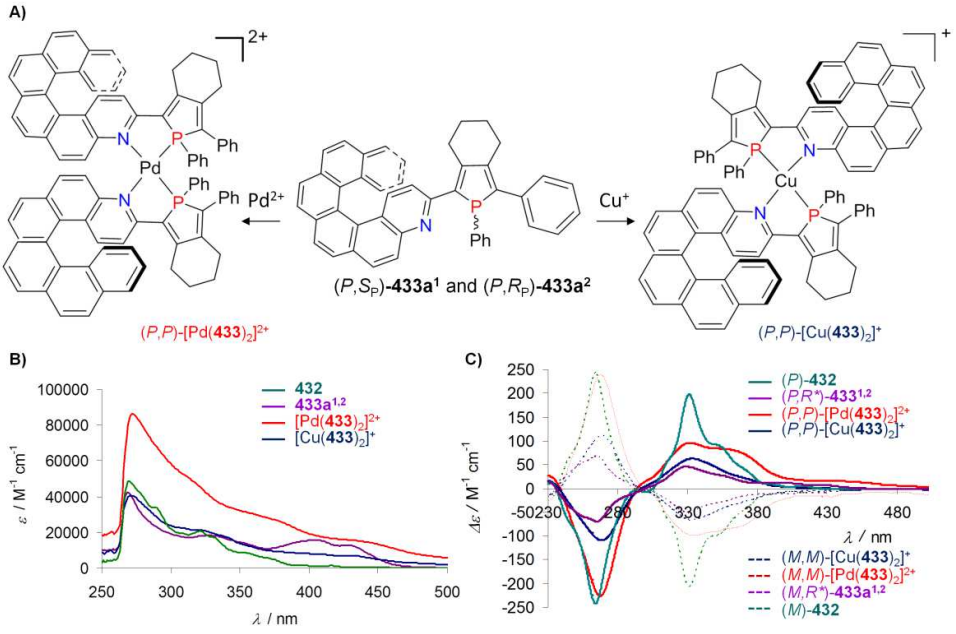

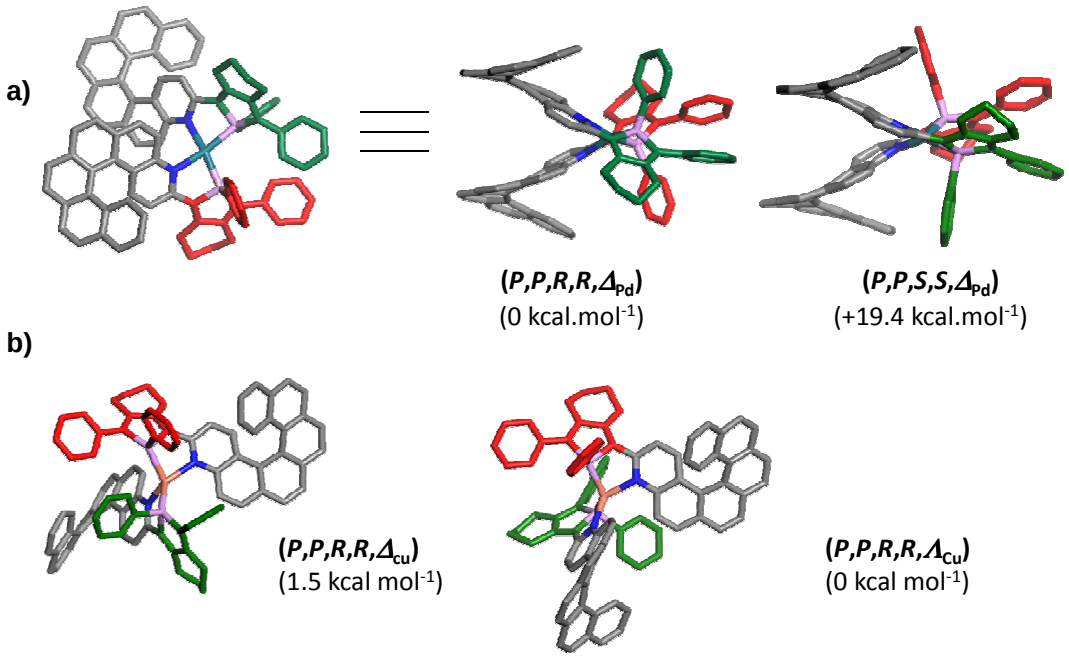

Figure 53. Optimized structures and relative energies for $([Pd(\mathbf{433})_2]^{2+}$ (*a*) and $([Cu(\mathbf{433})_2]^{+}$ obained by DFT calculations.[382]

Finally, it was shown in the former paragraph that phosphole-modified azahelicenes are well designed to self-assemble onto metallic ions in a highly stereoselective way, affording original chiral architectures. Along these lines, multitopic 2,6-bis(aza[6]helicene-phosphole)-pyridine **435** was prepared and appeared well-suited to generate structural diversity within helicate chemistry. Indeed, helicates and helicenes are two prototypes of helical structures in molecular chemistry (Scheme 101). Since their introduction by Lehn *et al.*,[385] helicates have attracted attention for their potential applications such as for instance functional chiral supramolecular assemblies,[386] efficient chiral emitters,[387] α-helices mimics and antimicrobial agents.[388] Ligand **445** prepared from enantiopure diyne **434** acted as a N,P,N,P,N-helicand upon an original coordination mode on Cu^{I}-dimers.[383] Enantiopure helicates (*M*,*M*)- and (*P*,*P*)-**436** were thus obtained, which assembled two helicene-capped helicands **435** around four Cu(I) centers. Their chiroptical properties were studied; their specific rotations are displayed in Table 33 and the ECD spectra are depicted in Scheme 101. Theoretical calculations evidenced the efficient chiral induction from azahelicene moieties to the Cu^{I}-helicate core and emphasized the presence of helicand-to-helicand charge transfer (LLCT type) transitions that significantly impacted the ECD active bands. These assemblies possess an original skeleton based on metal-dimers and mixed pentadentate phosphole-pyridine helicands exhibiting unusual coordination modes.

Scheme 101. Coordination-driven synthesis of supramolecular helicate **436** from helicand **435**. ECD spectra of (*P*) (plain lines) and (*M*) (dotted lines) enantiomers of diyne **434** (red colour), ligand **435** (purple colour) and Cu-helicate **436** (green colour).[383]

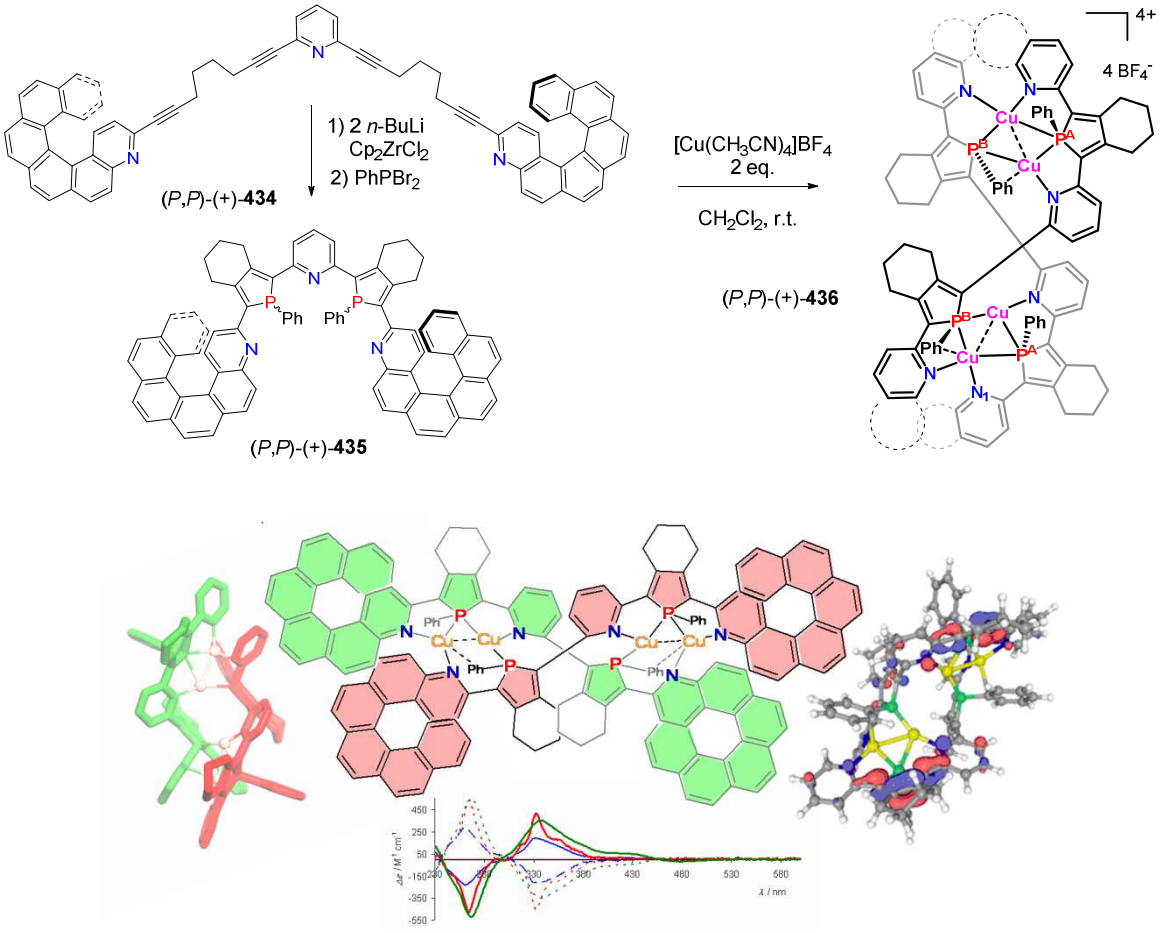

6. Conclusion and perspectives

In conclusion, helicenes and helicenoids decorated with main-group elements represent a particular type of helical non-planar scaffolds that could powerfully extend the arsenal of helicene chemistry generating novel architectures with undiscovered structural, optical, chiroptical properties and physicochemical qualities, determined by the nature and the number of the present heterocycles and/or the type of the substituted groups. In this review, we discussed the different strategies offering such chiral helical systems based on boron, silicon, nitrogen and phosphorus helicenes. There is certainly an avenue to develop novel and improved synthetic approaches toward helicenes containing main-group elements. A special focus on methods enabling large-scale preparation will be greatly needed to be able to screen the properties and to use these materials in diverse applications. Indeed, these aesthetically pleasant structures are eminently useful in a broad range of advanced applications including materials science, asymmetric organo- or transition metal catalysis, molecular recognition, or biology. Although the enantiomeric resolution through chiral HPLC separation appears the method of choice to access enantiopure helicene derivatives, the development of stereoselective approaches are greatly needed. The presence of the heteroatom offers opportunities to investigate new types of reactivity for stereoselective synthetic

methods (for instance through diastereomeric covalent derivatives or coordination complexes). Chiroptical activity is a focal point research and has been thoroughly detailed in the present review. Improved anisotropy factors g_{abs} in the fundamental state and g_{lum} in the excited state can guide the use of helicenes in some chiral devices. As exemplified in this work, the heteroatom alters the chiroptical properties of the helicene moiety, generating different shapes and intensity of the circular dichroic response and the circularly polarized light in comparison with their simpler carbohelicene counterparts. However, these small-organic molecules including helicene structures usually give limited g_{abs} and g_{lum} values in the range of 10^{-4}-10^{-2}. In order to increase these low dissymmetric factors, an alternative approach will consist in constructing higher-order molecular architectures of main-group element containing helicenes that will assemble in a controlled manner and form supramolecular arrangements. Thus, helicenes and helicenoids may be meticulously tailored with a precise molecular design and then engaged in higher-order structures with controlled self-assembly, thus paving the way to the development of robust and promising CPL active systems. The coordination chemistry toolbox can also afford novel helicene-based structures type with novel properties appearing, such as for instance circularly polarized phosphorescence or redox-triggered chiroptical switching activity. Ditopic and multitopic helicenic ligands could indeed self-assemble onto metallic ions with the aid of a controlled stereoselective process providing unprecedented chiral supramolecular architectures. Additionally, theoretical work undergoes expeditious and efficient progress which provides not only complementary information to the experimental features but also a decent guideline to chiroptical materials engineering.

For optoelectronics and photonic applications, optically active helicenes can interact differently with a circularly polarized light, depending on their handedness. This property along with their exceptional thermal and photostability, their strong absorption and their moderate quantum yield of photoluminescence justify their use as semiconductors in some post-silicon electronics. Yet, there are still some critical aspects that should be controlled in order to integrate chiral molecules in such devices which are: *i)* the chiral structure: the nature, the number and the position of the heteroatom in the helicene scaffold *ii)* the enantiopurity of the chiral semiconductor *iii)* the packing in the solid state. The latter parameter has shown to have a crucial effect in the photophysics behavior of the chiral molecules[389] and the fact that racemic and the enantiopure versions have different organization and morphology at the condensed state,[143] may open a new research area in which the homo- and heterochiral composition represent an alternative parameter to structural modification in order to ameliorate and to tune the device's efficiency and properties.[390]

It appears that helicene derivatives have been underexplored in asymmetric catalysis, although, the few works that have been published show promising results in some precise reactions in which the chiral helically moiety was decorated with oxygen, nitrogen, and phosphorus functionalities. After the earlier examples employing a substituted [7]helicene moiety as chiral auxiliary and as chiral reagent for some diastereoselective reactions,[391] a variety of helicenic molecules have been employed in asymmetric catalysis reaction as organocatalysts, organometallic catalyst and chiral inducers. Helicenes with alcohol functions, phosphines, phospholes, bipyridines, aminopyridines, NHCs, revealed efficient in enantioselective organocatalysis and organometallic catalysis, where the rigidity, the bulkiness, and the dissymmetric environment, match-mismatch effects, appeared as important features for the stereocontrol of the reaction. The development of new helical systems will give new opportunities to develop efficient

catalysts that can enrich the existing catalytic strategies for asymmetric reactions which is of great interest for a synthetic chemist at the laboratory and the industry levels.

In biology, few works have been published on the use of heterohelicene in enantioselective recognition of biologically relevant molecules, with specific binding between heterohelicene and DNA fragments, nucleic acids, or proteins. With the aid of some spectroscopic tools such as the absorption, the fluorescence, ECD, CPL and NMR, researchers were able to monitor the change and the gradual alteration of the shape and the intensity of the output signal after interactions. These studies have shed the light in the importance of the heterohelicene in some critical biological applications and may open up a window on future prospects of helicene chirality in some fields such as inhibitory activity, drug delivery, photodynamic therapy and bioimaging.

Recently, the field of the multiple helicenes has become the focus of interest of many research groups.[392,393,394] The presence of two or more helicene molecules in the same scaffold provide the structure with intriguing properties that could be absent in the single helicene, *i.e*, more complicated stereochemistry that incorporates a variety of inherent multihelicity giving rise to a plethora of 3D diastereomers configurations, fascinating molecular dynamics and complex interconversion mechanisms for the existing stereoisomers. One can expect that incorporation of heteroatoms within the multiple helicene architectures may provide further added values by generating a new molecular materials with excellent carrier mobility and special semiconducting properties that differ from the multiple carbohelicene spiral structures. *In fine*, the literature on enantioenriched helicenic derivatives with main-group elements is constantly growing; this review addresses the results before the end of 2018 but many references on the topics have appeared in early 2019; they have not been detailed in the present review.[395,396,397,398,399,400]

Acknowledgements

We thank the Ministère de l'Education Nationale, de la Recherche et de la Technologie, the Centre National de la Recherche Scientifique (CNRS), and the French National Agency (HE-LNHC, ANR-16-CE07-0019-01-HEL-NHC and HELPHOS, ANR-15-CE29-0012-03). KD thanks the University of Gabès and Campus France for financial support and Prof. Bassem Jamoussi for his strong support. JC warmly thanks all her coworkers and all the students who have been involved in helicenes chemistry.

Supplementary Information

References with complete list of authors.

Notes

[#] Molar rotations $[\phi]_D^{25}$ and specific rotations $[\alpha]_D^{25}$ are related by: $[\phi]_D^{25} = [\alpha]_D^{25} \, x \, \frac{MW}{100}$, where *MW* is the molar weight. Units are in degree [dm (g cm^{-3})]$^{-1}$ for specific rotations and in degree cm^2 $dmol^{-1}$ for molar rotations. UV/vis and ECD are commonly expressed by ε and $\Delta\varepsilon$ and are given in M^{-1} cm^{-1} units.

List of catalysts and chiral resolving agents

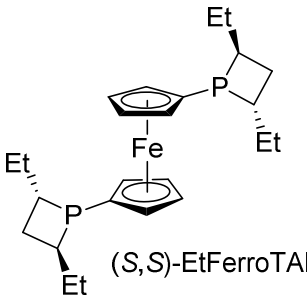

(*S*,*S*)-EtFerroTANE

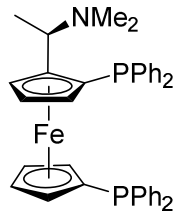

(*R*)-(*S*)-BPPFA

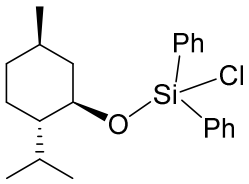

(-)-MenthSiCl

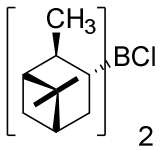

(-)-B-Chlorodiisopino-campheylborane

(-)-**X1**

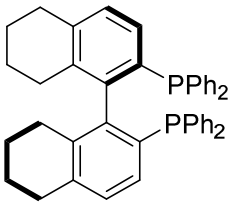

(*R*)-H8-BINAP

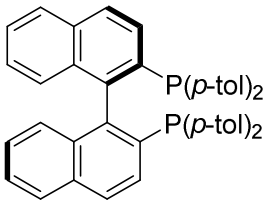

(*R*)-tol-BINAP

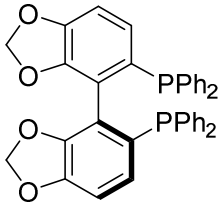

(*S*)-Segphos

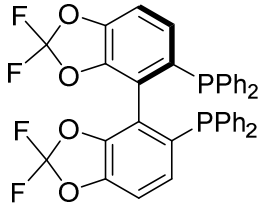

(*R*)-difluorphos

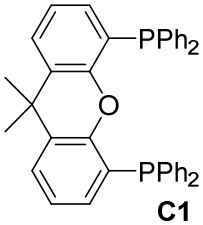

C1

xantphos

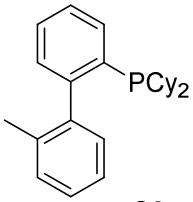

C2

biphenyl-phosphine

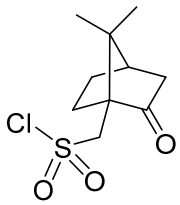

C3

(1*S*)-(+)-10-camphor-sulfonyl chloride

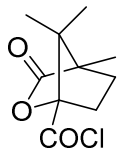

C4

(*S*)-(-)-camphanoyle chloride

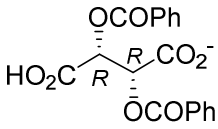

X2

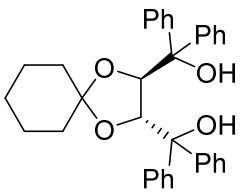

(-)-spiro-TADDOL

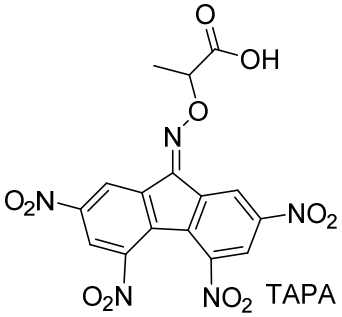

TAPA

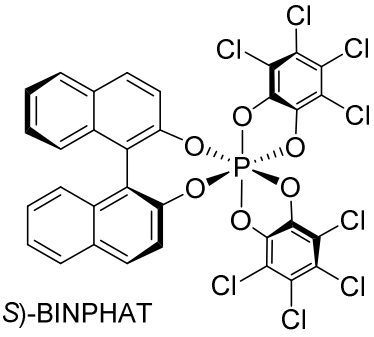

(*Δ*,*S*)-BINPHAT

List of abbreviations

ACN: acetonitrile

APTS: *p*-toluenesulfonic acid

[BDMIM][BF4]: 1-butyl-2,3-dimethylimidazolium tetrafluoroborate

BSA: *N*,*O*-bis(trimethylsilyl)acetamide

CBP: 4,4'-bis(9-carbazolyl)-1,1'-biphenyl

CCDC: Cambridge Crystallographic Data Centre

CE: Capillary Electrophoresis

CISS: Chirality Induced Spin Selectivity

COD: cycloocta-1,5-diene

***m*-CPBA**: *meta*-chloro-perbenzoic acid

CPL: Circularly Polarized Luminescence

1,2-DCB: 1,2-dichlorobenzene

DCE: dichloroethane

DDQ: 2,3-dichloro-5,6-dicyano-1,4-benzoquinone

de: diastereomeric excess

DFT: Density Functional Theory

DHPLC: Dynamic High-Pressure Liquid Chromatography

dppe: bis(diphenylphosphino)ethane

dppp: bis(diphenylphosphino)propane

ee: enantiomeric excess

ECD: Electronic Circular Dichroism

Fum: dimethyl fumarate

hfac: 1,1,1,5,5,5-hexafluoroacetylacetonate

HMDS: 1,1,1,3,3,3-hexamethyldisilazane

HOMO: Highest Occupied Molecular Orbital

HPLC: High-Pressure Liquid Chromatography

HRMS: High-Resolution Mass Spectrometry

ISC: Inter-System Crossing

LUMO: Lowest Unoccupied Molecular Orbital

MJ: Molecular Junction

MR: Molar Rotations

MW: Microwave

NICS: Nuclear Independent Spin Chemical Shift

NMP: *N*-methyl-2-pyrrolidone

NLO: Non Linear Optics/ Non Linear Optical

***o*-DCB:** *ortho*-dichlorobenzene

OFET: Organic Field-Effect Transistor

OLED: Organic Light-Emitting Diode

OPV: Organic PhotoVoltaics

PAH: PolyAromatic Hydrocarbon

PLED: Polymer Light-Emitting Diode

ROA: Raman Optical Activity

TCB: trichlorobenzene

TD-DFT: Time-Dependent Density Functional Theory

TFA: trifluoroacetic acid

TMS: trimethylsilyl

TOF: Time of Flight

tta: 2-thienyltrifluoroaacetonate

UHP: urea-hydrogen peroxide

UHV: Ultra-High Vacuum

VCD: Vibrational Circular Dichroism

References

(1) Bonner, W. A. In *Origins Life Evol. Biospheres* 1995; Vol. 25.

(2) Meurer, K. P.; Vogtle, F. Helical Molecules In Organic-Chemistry, *Topics in Current Chemistry* **1985**, *127*, 1-76.

(3) Hecht , S.; Huc, I. *Foldamers: Structure, Properties and Applications*; Wiley - VCH, 2007.

(4) Yashima, E.; Ousaka, N.; Taura, D.; Shimomura, K.; Ikai, T.; Maeda, K. Supramolecular Helical Systems: Helical Assemblies of Small Molecules, Foldamers, and Polymers with Chiral Amplification and Their Functions, *Chem. Rev.* **2016**, *116*, 13752-13990.

(5) Shen, Y.; Chen, C.-F. Helicenes: Synthesis and Applications, *Chem. Rev.* **2012**, *112*, 1463-1535.

(6) Chen, C.-F.; Shen, Y. In *Helicene Chemistry: From Synthesis to Applications*; Springer Berlin Heidelberg: Berlin, Heidelberg, 2017.

(7) Gingras, M. One Hundred Years of Helicene Chemistry. Part 1: Non-Stereoselective Syntheses of Carbohelicenes, *Chem. Soc. Rev.* **2013**, *42*, 968-1006.

(8) Gingras, M.; Felix, G.; Peresutti, R. One Hundred Years of Helicene Chemistry. Part 2: Stereoselective Syntheses And Chiral Separations of Carbohelicenes, *Chem. Soc. Rev.* **2013**, *42*, 1007-1050.

(9) Gingras, M. One Hundred Years of Helicene Chemistry. Part 3: Applications And Properties of Carbohelicenes, *Chem. Soc. Rev.* **2013**, *42*, 1051-1095.

(10) Meisenheimer, J.; Witte, K. Reduction von 2-Nitronaphtalin, *Berichte der deutschen chemischen Gesellschaft* **1903**, *36*, 4153-4164.

(11) Newman, M. S.; Lednicer, D. The Synthesis and Resolution of Hexahelicene, *J. Am. Chem. Soc.* **1956**, *78*, 4765-4770.

(12) Wynberg, H.; Groen, M. B. Synthesis, Resolution, And Optical Rotatory Dispersion Of A Hexa- And A Heptaheterohelicene, *J. Am. Chem. Soc.* **1968**, *90*, 5339-5341.

(13) Stępień, M.; Gońka, E.; Żyła, M.; Sprutta, N. Heterocyclic Nanographenes and Other Polycyclic Heteroaromatic Compounds: Synthetic Routes, Properties, and Applications, *Chem. Rev.* **2017**, *117*, 3479-3716.

(14) Márquez, I. R.; Castro-Fernández, S.; Millán, A.; Campaña, A. G. Synthesis of Distorted Nanographenes Containing Seven- and Eight-Membered Carbocycles, *Chem. Comm.* **2018**, *54*, 6705-6718.

(15) Narcis, M. J.; Takenaka, N. Helical-Chiral Small Molecules in Asymmetric Catalysis, *Eur. J. Org. Chem.* **2014**, *2014*, 21-34.

(16) Aillard, P.; Voituriez, A.; Marinetti, A. Helicene-Like Chiral Auxiliaries In Asymmetric Catalysis, *Dalton Trans.* **2014**, *43*, 15263-15278.

(17) Hasan, M.; Borovkov, V. Helicene-Based Chiral Auxiliaries and Chirogenesis, *Symmetry* **2017**, *10*, 10.

(18) Cahn, R. S.; Ingold, C.; Prelog, V. Specification of Molecular Chirality, *Angew. Chem. Int. Ed.* **1966**, *5*, 385-415.

(19) Wolf, C. *Dynamic Stereochemistry of Chiral Compounds: Principles and Applications*; RSC Publishing, 2008.

(20) Murai, M.; Okada, R.; Nishiyama, A.; Takai, K. Synthesis and Properties of Sila[n]helicenes via Dehydrogenative Silylation of C-H Bonds under Rhodium Catalysis, *Org. Lett.* **2016**, *18*, 4380-4383.

(21) Tian, Y.-H.; Park, G.; Kertesz, M. Electronic Structure of Helicenes, C_2S Helicenes, and Thiaheterohelicenes, *Chem. Mater.* **2008**, *20*, 3266-3277.

(22) Isla, H.; Crassous, J. Helicene-Based Chiroptical Switches, *C. R. Chimie* **2016**, *19*, 39-49.

(23) Schmidt, K.; Brovelli, S.; Coropceanu, V.; Beljonne, D.; Cornil, J.; Bazzini, C.; Caronna, T.; Tubino, R.; Meinardi, F.; Shuai, Z.; Brédas, J.-L. Intersystem Crossing Processes in Nonplanar Aromatic Heterocyclic Molecules, *J. Phys. Chem. A* **2007**, *111*, 10490-10499.

(24) Lightner, D. A.; Hefelfinger, D. T.; Powers, T. W.; Frank, G. W.; Trueblood, K. N. Hexahelicene. Absolute Configuration, *J. Am. Chem. Soc.* **1972**, *94*, 3492-3497.

(25) Furche, F.; Ahlrichs, R.; Wachsmann, C.; Weber, E.; Sobanski, A.; Vögtle, F.; Grimme, S. Circular Dichroism of Helicenes Investigated by Time-Dependent Density Functional Theory, *J. Am. Chem. Soc.* **2000**, *122*, 1717-1724.
(26) Abbate, S.; Longhi, G.; Lebon, F.; Castiglioni, E.; Superchi, S.; Pisani, L.; Fontana, F.; Torricelli, F.; Caronna, T.; Villani, C.; *et al.*. Helical Sense-Responsive and Substituent-Sensitive Features in Vibrational and Electronic Circular Dichroism, in Circularly Polarized Luminescence, and in Raman Spectra of Some Simple Optically Active Hexahelicenes, *J. Phys. Chem. C* **2014**, *118*, 1682-1695.
(27) Tanaka, H.; Inoue, Y.; Mori, T. Circularly Polarized Luminescence and Circular Dichroisms in Small Organic Molecules: Correlation Between Excitation and Emission Dissymmetry Factors, *ChemPhotoChem* **2018**, *2*, 386-402.
(28) Brandt, J. R.; Salerno, F.; Fuchter, M. J. The Added Value of Small-Molecule Chirality in Technological Applications, *Nat. Rev. Chem.* **2017**, *1*, 0045.
(29) Laarhoven, W. H.; Prinsen, W. J. C. Carbohelicenes and Heterohelicenes, *Topics in Current Chemistry* **1984**, *125*, 63-130.
(30) Weissman, S. I.; Chang, R. Optical and Magnetic Properties of Anions of Hexahelicene, *J. Am. Chem. Soc.* **1972**, *94*, 8683-8685.
(31) Weissman, S. I. Selectivity in the Reduction of Enantiomers of Hexahelicene in an Optically Active Solvent, *J. Org. Chem.* **1976**, *41*, 4040-4041.
(32) Makrlík, E.; Sýkora, D.; Böhm, S.; Vaňura, P. Cation-π Interaction of Li^+ with [6]Helicene: Experimental and Theoretical Study, *Chem. Phys. Lett.* **2016**, *665*, 162-165.
(33) Katz, T. J. Syntheses of Functionalized and Aggregating Helical Conjugated Molecules, *Angew. Chem. Int. Ed.* **2000**, *39*, 1921-1923.
(34) Urbano, A. Recent Developments in the Synthesis of Helicene-Like Molecules, *Angew. Chem. Int. Ed.* **2003**, *42*, 3986-3989.
(35) Stary, I.; Stara, I. G.; Alexandrova, Z.; Sehnal, P.; Teply, F.; Saman, D.; Rulisek, L. Helicity Control in The Synthesis of Helicenes and Related Compounds, *Pure Appl. Chem.* **2006**, *78*, 495-499.
(36) Wynberg, H. Some Observations on the Chemical, Photochemical, and Spectral Properties of Thiophenes, *Acc. Chem. Res.* **1971**, *4*, 65-73.
(37) Collins, S. K.; Vachon, M. P. Unlocking the Potential of Thiaheterohelicenes: Chemical Synthesis as the Key, *Org. Biomol. Chem.* **2006**, *4*, 2518-2524.
(38) Rajca, A.; Miyasaka, M. In *Functional Organic Materials*; Wiley-VCH, 2007.
(39) Licandro, E.; Cauteruccio, S.; Dova, D. In *Advances in Heterocyclic Chemistry*; Scriven, E. F. V., Ramsden, C. A., Eds.; Academic Press, 2016; Vol. 118.
(40) Wang, X. Y.; Wang, J. Y.; Pei, J. BN Heterosuperbenzenes: Synthesis and Properties, *Chem. – Eur. J.* **2015**, *21*, 3528-3539.
(41) Hatakeyama, T.; Hashimoto, S.; Oba, T.; Nakamura, M. Azaboradibenzo[6]Helicene: Carrier Inversion Induced by Helical Homochirality, *J. Am. Chem. Soc.* **2012**, *134*, 19600-19603.
(42) Si, Y.; Yang, G. Photophysical Properties of Azaboradibenzo[6]Helicene Derivatives, *J. Mater. Chem. C* **2013**, *1*, 2354.
(43) Hirai, H.; Nakajima, K.; Nakatsuka, S.; Shiren, K.; Ni, J.; Nomura, S.; Ikuta, T.; Hatakeyama, T. One-Step Borylation of 1,3-Diaryloxybenzenes Towards Efficient Materials for Organic Light-Emitting Diodes, *Angew. Chem. Int. Ed.* **2015**, *54*, 13581-13585.
(44) Janke, R. H.; Haufe, G.; Würthwein, E.-U.; Borkent, J. H. Racemization Barriers of Helicenes: A Computational Study1, *J. Am. Chem. Soc.* **1996**, *118*, 6031-6035.
(45) Shen, C.; Srebro-Hooper, M.; Jean, M.; Vanthuyne, N.; Toupet, L.; Williams, J. A. G.; Torres, A. R.; Riives, A. J.; Muller, G.; Autschbach, J.; *et al.*. Synthesis and Chiroptical Properties of Hexa-, Octa-, and Deca-azaborahelicenes: Influence of Helicene Size and of the Number of Boron Atoms, *Chem. – Eur. J.* **2017**, *23*, 407-418.
(46) Nakai, Y.; Mori, T.; Inoue, Y. Circular Dichroism of (Di)methyl- and Diaza[6]helicenes. A Combined Theoretical and Experimental Study, *J. Phys. Chem. A* **2013**, *117*, 83-93.

(47) Domínguez, Z.; López-Rodríguez, R.; Álvarez, E.; Abbate, S.; Longhi, G.; Pischel, U.; Ros, A. Azabora[5]helicene Charge-Transfer Dyes Show Efficient and Spectrally Variable Circularly Polarized Luminescence, *Chem. – Eur. J.* **2018**, *24*, 12660-12668.
(48) Li, C.; Yang, Y.; Miao, Q. Recent Progress in Chemistry of Multiple Helicenes, *Chem. Asian J.* **2018**,
(49) Lin, W.-B.; Li, M.; Fang, L.; Chen, C.-F. Recent progress on multidimensional construction of helicenes, *Chin. Chem. Lett.* **2018**, *29*, 40-46.
(50) Kato, K.; Segawa, Y.; Itami, K. Symmetric Multiple Carbohelicenes, *Synlett* **2019**,
(51) Katayama, T.; Nakatsuka, S.; Hirai, H.; Yasuda, N.; Kumar, J.; Kawai, T.; Hatakeyama, T. Two-Step Synthesis of Boron-Fused Double Helicenes, *J. Am. Chem. Soc.* **2016**, *138*, 5210-5213.
(52) Wang, X.-Y.; Wang, X.-C.; Narita, A.; Wagner, M.; Cao, X.-Y.; Feng, X.; Müllen, K. Synthesis, Structure, and Chiroptical Properties of a Double [7]Heterohelicene, *J. Am. Chem. Soc.* **2016**, *138*, 12783-12786.
(53) Goedicke, C.; Stegemeyer, H. Resolution and Racemization of Pentahelicene, *Tetrahedron Lett.* **1970**, *11*, 937-940.
(54) Wang, X.-Y.; Dienel, T.; Di Giovannantonio, M.; Barin, G. B.; Kharche, N.; Deniz, O.; Urgel, J. I.; Widmer, R.; Stolz, S.; De Lima, L. H.; *et al.*. Heteroatom-Doped Perihexacene from a Double Helicene Precursor: On-Surface Synthesis and Properties, *J. Am. Chem. Soc.* **2017**, *139*, 4671-4674.
(55) Miyamoto, F.; Nakatsuka, S.; Yamada, K.; Nakayama, K.; Hatakeyama, T. Synthesis of Boron-Doped Polycyclic Aromatic Hydrocarbons by Tandem Intramolecular Electrophilic Arene Borylation, *Org. Lett.* **2015**, *17*, 6158-6161.
(56) Hatakeyama, T.; Shiren, K.; Nakajima, K.; Nomura, S.; Nakatsuka, S.; Kinoshita, K.; Ni, J.; Ono, Y.; Ikuta, T. Ultrapure Blue Thermally Activated Delayed Fluorescence Molecules: Efficient HOMO-LUMO Separation by the Multiple Resonance Effect, *Adv. Mater.* **2016**, *28*, 2777-2781.
(57) Li, D.; Zhang, H.; Wang, Y. Four-Coordinate Organoboron Compounds for Organic Light-Emitting Diodes (OLEDS), *Chem. Soc. Rev.* **2013**, *42*, 8416-8433.
(58) Rao, Y.-L.; Amarne, H.; Wang, S. Photochromic Four-Coordinate N,C-Chelate Boron Compounds, *Coord. Chem. Rev.* **2012**, *256*, 759-770.
(59) Wang, Y.; Huang, H. Y.; Zhang, Q. L.; Zhang, P. Y. Chirality in Metal-Based Anticancer Agents, *Dalton Trans.* **2018**, *47*, 4017-4026.
(60) Hellou, N.; Mace, A.; Martin, C.; Dorcet, V.; Roisnel, T.; Jean, M.; Vanthuyne, N.; Berree, F.; Carboni, B.; Crassous, J. Synthesis of Carbo[6]helicene Derivatives Grafted with Amino or Aminoester Substituents from Enantiopure [6]Helicenyl Boronates, *J. Org. Chem.* **2018**, *83*, 484-490.
(61) Jakubec, M.; Beránek, T.; Jakubík, P.; Sýkora, J.; Žádný, J.; Církva, V.; Storch, J. 2-Bromo[6]helicene as a Key Intermediate for [6]Helicene Functionalization, *J. Org. Chem.* **2018**, *83*, 3607-3616.
(62) Yamaguchi, S.; Tamao, K. Silole-containing σ- and π-conjugated compounds, *Dalton Trans.* **1998**, 3693-3702.
(63) Tamao, K.; Uchida, M.; Izumizawa, T.; Furukawa, K.; Yamaguchi, S. Silole Derivatives as Efficient Electron Transporting Materials, *J. Am. Chem. Soc.* **1996**, *118*, 11974-11975.
(64) Shibata, T.; Uchiyama, T.; Yoshinami, Y.; Takayasu, S.; Tsuchikama, K.; Endo, K. Highly Enantioselective Synthesis of Silahelicenes Using Ir-Catalyzed [2+2+2] Cycloaddition, *Chem. Comm.* **2012**, *48*, 1311-1313.
(65) Murayama, K.; Oike, Y.; Furumi, S.; Takeuchi, M.; Noguchi, K.; Tanaka, K. Enantioselective Synthesis, Crystal Structure, and Photophysical Properties of a 1,1′-Bitriphenylene-Based Sila[7]helicene, *Eur. J. Org. Chem.* **2015**, *2015*, 1409-1414.
(66) Tanaka, K.; Kimura, Y.; Murayama, K. Enantioselective Helicene Synthesis by Rhodium-Catalyzed [2+2+2] Cycloadditions, *Bull. Chem. Soc. Jpn.* **2015**, *88*, 375-385.
(67) Sawada, Y.; Furumi, S.; Takai, A.; Takeuchi, M.; Noguchi, K.; Tanaka, K. Rhodium-Catalyzed Enantioselective Synthesis, Crystal Structures, and Photophysical Properties of Helically Chiral 1,1 '-Bitriphenylenes, *J. Am. Chem. Soc.* **2012**, *134*, 4080-4083.
(68) Oyama, H.; Nakano, K.; Harada, T.; Kuroda, R.; Naito, M.; Nobusawa, K.; Nozaki, K. Facile Synthetic Route to Highly Luminescent Sila[7]helicene, *Org. Lett.* **2013**, *15*, 2104-2107.

(69) Nakano, K.; Hidehira, Y.; Takahashi, K.; Hiyama, T.; Nozaki, K. Stereospecific Synthesis of Hetero[7]helicenes by Pd-Catalyzed Double N-Arylation and Intramolecular O-Arylation, *Angew. Chem. Int. Ed.* **2005**, *44*, 7136-7138.
(70) Nakano, K.; Oyama, H.; Nishimura, Y.; Nakasako, S.; Nozaki, K. λ5-Phospha[7]helicenes: Synthesis, Properties, and Columnar Aggregation with One-Way Chirality, *Angew. Chem. Int. Ed.* **2012**, *51*, 695-699.
(71) Martin, R. H.; Marchant, M.-J. Thermal racemisation of [6], [7], [8] and [9] helicene, *Tetrahedron Lett.* **1972**, *13*, 3707-3708.
(72) Zak, J. K.; Miyasaka, M.; Rajca, S.; Lapkowski, M.; Rajca, A. Radical Cation of Helical, Cross-Conjugated β-Oligothiophene, *J. Am. Chem. Soc.* **2010**, *132*, 3246-3247.
(73) Rajca, A.; Miyasaka, M.; Pink, M.; Wang, H.; Rajca, S. Helically Annelated and Cross-Conjugated Oligothiophenes: Asymmetric Synthesis, Resolution, and Characterization of a Carbon−Sulfur [7]Helicene, *J. Am. Chem. Soc.* **2004**, *126*, 15211-15222.
(74) Miyasaka, M.; Rajca, A.; Pink, M.; Rajca, S. Chiral Molecular Glass: Synthesis and Characterization of Enantiomerically Pure Thiophene-Based [7]Helicene, *Chem. – Eur. J.* **2004**, *10*, 6531-6539.
(75) Li, C.; Wu, L.; Xu, W.; Song, J.; Shi, J.; Yu, P.; Kan, Y.; Wang, H. Silicon Spiro Double Helicene-like Compounds Based on Dithieno[2,3-b:3′,2′-d]thiophene: Syntheses and Crystal Structures, *J. Org. Chem.* **2015**, *80*, 11156-11161.
(76) Sato, K. A. S. In Cyclophane Chemistry for the 21st Century, Takemura, H., Ed.; Research Signpost: Trivandrum,, **2002**,
(77) Dumitrascu, F.; Dumitrescu, D. G.; Aron, I. Azahelicenes and Other Similar Tri and Tetracyclic Helical Molecules, *Arkivoc* **2010**, 1-32.
(78) Bazzini, C.; Brovelli, S.; Caronna, T.; Gambarotti, C.; Giannone, M.; Macchi, P.; Meinardi, F.; Mele, A.; Panzeri, W.; Recupero, F.; *et al.*. Synthesis and Characterization of Some Aza[5]helicenes, *Eur. J. Org. Chem.* **2005**, *2005*, 1247-1257.
(79) Hoffmann, N. Photochemical reactions applied to the synthesis of helicenes and helicene-like compounds, *J. Photochem. Photobiol. C* **2014**, *19*, 1-19.
(80) Mori, K.; Murase, T.; Fujita, M. One-Step Synthesis of [16]Helicene, *Angew. Chem. Int. Ed.* **2015**, *54*, 6847-6851.
(81) Abbate, S.; Bazzini, C.; Caronna, T.; Fontana, F.; Gambarotti, C.; Gangemi, F.; Longhi, G.; Mele, A.; Sora, I. N.; Panzeri, W. Monoaza[5]helicenes. Part 2: Synthesis, Characterisation and Theoretical Calculations, *Tetrahedron* **2006**, *62*, 139-148.
(82) Caronna, T.; Gabbiadini, S.; Mele, A.; Recupero, F. Approaches to the azahelicene system: Synthesis and spectroscopic characterization of some diazapentahelicenes, *Helv. Chim. Acta* **2002**, *85*, 1-8.
(83) Lebon, F.; Longhi, G.; Gangemi, F.; Abbate, S.; Priess, J.; Juza, M.; Bazzini, C.; Caronna, T.; Mele, A. Chiroptical Properties of Some Monoazapentahelicenes, *J. Phys. Chem. A* **2004**, *108*, 11752-11761.
(84) Kuroda, R. Crystal and molecular-structure of 5 helicene - crystal packing modes, *J. Chem. Soc., Perkin Trans. 2* **1982**, 789-794.
(85) Abbate, S.; Bazzini, C.; Caronna, T.; Fontana, F.; Gangemi, F.; Lebon, F.; Longhi, G.; Mele, A.; Natali Sora, I. Experimental and Calculated Circular Dichroism Spectra of Monoaza[5]Helicenes, *Inorg. Chim. Acta* **2007**, *360*, 908-912.
(86) Caronna, T.; Fontana, F.; Mele, A.; Natali Sora, I.; Panzeri, W.; Vigano, L. A Simple Approach for the Synthesis of 7,8-Diaza[5]Helicene, *Synthesis* **2008**, 413-416.
(87) Caronna, T.; Fontana, F.; Longhi, G.; Mele, A.; Natali Sora, I.; Vigano, L. 2,13-Diaza 5 helicene: synthesis, theoretical calculations and spectroscopic properties, *Arkivoc* **2009**, 145-155.
(88) Reist, M.; Testa, B.; Carrupt, P. A.; Jung, M.; Schurig, V. Racemization, Enantiomerization, Diastereomerization, and Epimerization - Their Meaning and Pharmacological Significance, *Chirality* **1995**, *7*, 396-400.
(89) Trapp, O. Fast and Precise Access to Enantiomerization Rate Constants in Dynamic Chromatography, *Chirality* **2006**, *18*, 489-497.

(90) Caronna, T.; Mele, A.; Famulari, A.; Mendola, D.; Fontana, F.; Juza, M.; Kamuf, M.; Zawatzky, K.; Trapp, O. A Combined Experimental and Theoretical Study on the Stereodynamics of Monoaza[5]helicenes: Solvent-Induced Increase of the Enantiomerization Barrier in 1-Aza-[5]helicene, *Chem. – Eur. J.* **2015**, *21*, 13919-13924.
(91) Vacek Chocholoušová, J.; Vacek, J.; Andronova, A.; Míšek, J.; Songis, O.; Šámal, M.; Stará, I. G.; Meyer, M.; Bourdillon, M.; Pospíšil, L.; *et al.*. On the Physicochemical Properties of Pyridohelicenes, *Chem. – Eur. J.* **2014**, *20*, 877-893.
(92) Misek, J.; Teply, F.; Stara, I. G.; Tichy, M.; Saman, D.; Cisarova, I.; Vojtisek, P.; Stary, I. A Straightforward Route To Helically Chiral N-Heteroaromatic Compounds: Practical Synthesis Of Racemic 1,14-Diaza 5 Helicene And Optically Pure 1-And 2-Aza 6 Helicenes, *Angew. Chem. Int. Ed.* **2008**, *47*, 3188-3191.
(93) Waghray, D.; Zhang, J.; Jacobs, J.; Nulens, W.; Basarić, N.; Meervelt, L. V.; Dehaen, W. Synthesis and Structural Elucidation of Diversely Functionalized 5,10-Diaza[5]Helicenes, *J. Org. Chem.* **2012**, *77*, 10176-10183.
(94) Aloui, F.; El Abed, R.; Ben Hassine, B. Synthesis of A New N-Containing Hexahelicene, *Tetrahedron Lett.* **2008**, *49*, 1455-1457.
(95) Aloui, F.; El Abed, R.; Marinetti, A.; Ben Hassine, B. Synthesis and Resolution of A New Helically Chiral Azahelicene, *Tetrahedron Lett.* **2008**, *49*, 4092-4095.
(96) Newman, M. S.; Darlak, R. S.; Tsai, L. L. Optical properties of hexahelicene, *J. Am. Chem. Soc.* **1967**, *89*, 6191-6193.
(97) Nakai, Y.; Mori, T.; Sato, K.; Inoue, Y. Theoretical and Experimental Studies of Circular Dichroism of Mono- and Diazonia[6]helicenes, *J. Phys. Chem. A* **2013**, *117*, 5082-5092.
(98) Martin, R. H.; Deblecker, M. Synthesis of 4-azahexahelicene (benzo [c] phénanthro [1,2-f] quinoline), *Tetrahedron Lett.* **1969**, *10*, 3597-3598.
(99) Mendola, D.; Saleh, N.; Vanthuyne, N.; Roussel, C.; Toupet, L.; Castiglione, F.; Caronna, T.; Mele, A.; Crassous, J. Aza[6]helicene Platinum Complexes: Chirality Control of cis–trans Isomerism, *Angew. Chem. Int. Ed.* **2014**, *53*, 5786-5790.
(100) Mendola, D.; Saleh, N.; Hellou, N.; Vanthuyne, N.; Roussel, C.; Toupet, L.; Castiglione, F.; Melone, F.; Caronna, T.; Fontana, F.; *et al.*. Synthesis and Structural Properties of Aza[n]helicene Platinum Complexes: Control of Cis and Trans Stereochemistry, *Inorg. Chem.* **2016**, *55*, 2009-2017.
(101) Raczynska, E. D.; Gal, J.-F.; Maria, P.-C. Gas-phase basicity of aromatic azines: A short review on structural effects, *Int. J. Mass Spectrom.* **2017**, *418*, 130-139.
(102) Roithova, J.; Schroeder, D.; Misek, J.; Stara, I. G.; Stary, I. Chiral superbases: the proton affinities of 1-and 2-aza 6 helicene in the gas phase, *J. Mass Spectrom.* **2007**, *42*, 1233-1237.
(103) Ehala, S.; Misek, J.; Stara, I. G.; Stary, I.; Kasicka, V. Determination of Acid-Base Dissociation Constants of Azahelicenes by Capillary Zone Electrophoresis, *J. Sep. Sci.* **2008**, *31*, 2686-2693.
(104) Napagoda, M.; Rulisek, L.; Jancarik, A.; Klivar, J.; Samal, M.; Stara, I. G.; Stary, I.; Solinova, V.; Kasicka, V.; Svatos, A. Azahelicene Superbases as MAILD Matrices for Acidic Analytes, *Chempluschem* **2013**, *78*, 937-942.
(105) Staab, H. A.; Zirnstein, M. A.; Krieger, C. Benzo[1,2-h:4,3-h']diquinoline ("1,14-Diaza[5]helicene"): Synthesis, Structure, and Properties, *Angew. Chem. Int. Ed.* **1989**, *28*, 86-88.
(106) Platt, J. R. Classification of Spectra of Cata-Condensed Hydrocarbons, *J. Chem. Phys.* **1949**, *17*, 484-495.
(107) Nakai, Y.; Mori, T.; Inoue, Y. Theoretical and Experimental Studies on Circular Dichroism of Carbo[n]helicenes, *J. Phys. Chem. A* **2012**, *116*, 7372-7385.
(108) Saleh, N.; Moore, B.; Srebro, M.; Vanthuyne, N.; Toupet, L.; Williams, J. A. G.; Roussel, C.; Deol, K. K.; Muller, G.; Autschbach, J.; *et al.*. Acid/Base-Triggered Switching of Circularly Polarized Luminescence and Electronic Circular Dichroism in Organic and Organometallic Helicenes, *Chem. Eur. J* **2015**, *21*, 1673-1681.
(109) Baryshnikov, G.; Minaev, B.; Ågren, H. Theory and Calculation of the Phosphorescence Phenomenon, *Chem. Rev.* **2017**, *117*, 6500-6537.

(110) Liu, Y.; Cerezo, J.; Mazzeo, G.; Lin, N.; Zhao, X.; Longhi, G.; Abbate, S.; Santoro, F. Vibronic Coupling Explains the Different Shape of Electronic Circular Dichroism and of Circularly Polarized Luminescence Spectra of Hexahelicenes, *J. Chem. Theory Comput.* **2016**, *12*, 2799-2819.
(111) Isla, H.; Srebro-Hooper, M.; Jean, M.; Vanthuyne, N.; Roisnel, T.; Lunkley, J. L.; Muller, G.; Williams, J. A. G.; Autschbach, J.; Crassous, J. Conformational Changes And Chiroptical Switching Of Enantiopure Bis-Helicenic Terpyridine Upon Zn^{2+} Binding, *Chem. Comm.* **2016**, *52*, 5932-5935.
(112) Deshayes, K.; Broene, R. D.; Chao, I.; Knobler, C. B.; Diederich, F. Synthesis of the helicopodands: novel shapes for chiral clefts, *J. Org. Chem.* **1991**, *56*, 6787-6795.
(113) Fox, J. M.; Katz, T. J. Conversion of a [6]Helicene into an [8]Helicene and a Helical 1,10-Phenanthroline Ligand, *J. Org. Chem.* **1999**, *64*, 302-305.
(114) Takenaka, N.; Chen, J.; Captain, B.; Sarangthem, R. S.; Chandrakumar, A. Helical Chiral 2-Aminopyridinium Ions: A New Class of Hydrogen Bond Donor Catalysts, *J. Am. Chem. Soc.* **2010**, *132*, 4536-4537.
(115) Takenaka, N.; Sarangthem, R. S.; Captain, B. Helical Chiral Pyridine N-Oxides: A New Family of Asymmetric Catalysts, *Angew. Chem. Int. Ed.* **2008**, *47*, 9708-9710.
(116) Chen, J.; Captain, B.; Takenaka, N. Helical Chiral 2,2'-Bipyridine N- Monoxides as Catalysts in the Enantioselective Propargylation of Aldehydes with Allenyltrichlorosilane, *Org. Lett.* **2011**, *13*, 1654-1657.
(117) Murguly, E.; McDonald, R.; Branda, N. R. Chiral Discrimination in Hydrogen-Bonded [7]Helicenes, *Org. Lett.* **2000**, *2*, 3169-3172.
(118) Tanaka, K.; Kitahara, Y.; Suzuki, H.; Osuga, H.; Kawai, Y. Synthesis and crystal structure of chiral bifunctional helicenes with π-deficient pyridine and π-excessive thiophene units, *Tetrahedron Lett.* **1996**, *37*, 5925-5928.
(119) Waghray, D.; Cloet, A.; Van Hecke, K.; Mertens, S. F. L.; De Feyter, S.; Van Meervelt, L.; Van der Auweraer, M.; Dehaen, W. Diazadithia[7]helicenes: Synthetic Exploration, Solid-State Structure, and Properties, *Chem. – Eur. J.* **2013**, *19*, 12077-12085.
(120) Groen, M. B.; Wynberg, H. Optical properties of some heterohelicenes. Absolute configuration, *J. Am. Chem. Soc.* **1971**, *93*, 2968-2974.
(121) Staab, H. A.; Diehm, M.; Krieger, C. Synthesis, Structure and Basicity of 1,16-Diaza[6]Helicene, *Tetrahedron Lett.* **1994**, *35*, 8357-8360.
(122) Chen, J.; Takenaka, N. Helical Chiral Pyridine N-Oxides: A New Family of Asymmetric Catalysts, *Chem. – Eur. J.* **2009**, *15*, 7268-7276.
(123) Chercheja, S.; Klívar, J.; Jančařík, A.; Rybáček, J.; Salzl, S.; Tarábek, J.; Pospíšil, L.; Vacek Chocholoušová, J.; Vacek, J.; Pohl, R.; *et al.*. The Use of Cobalt-Mediated Cycloisomerisation of Ynedinitriles in the Synthesis of Pyridazinohelicenes, *Chem. – Eur. J.* **2014**, *20*, 8477-8482.
(124) Songis, O.; Míšek, J.; Schmid, M. B.; Kollárovič, A.; Stará, I. G.; Šaman, D.; Císařová, I.; Starý, I. A Versatile Synthesis of Functionalized Pentahelicenes, *J. Org. Chem.* **2010**, *75*, 6889-6899.
(125) Jančařík, A.; Rybáček, J.; Cocq, K.; Vacek Chocholoušová, J.; Vacek, J.; Pohl, R.; Bednárová, L.; Fiedler, P.; Císařová, I.; Stará, I. G.; *et al.*. Rapid Access to Dibenzohelicenes and their Functionalized Derivatives, *Angew. Chem. Int. Ed.* **2013**, *52*, 9970-9975.
(126) Klívar, J.; Jančařík, A.; Šaman, D.; Pohl, R.; Fiedler, P.; Bednárová, L.; Starý, I.; Stará, I. G. [2+2+2] Cycloisomerisation of Aromatic Cyanodiynes in the Synthesis of Pyridohelicenes and Their Analogues, *Chem. – Eur. J.* **2016**, *22*, 14401-14405.
(127) Žádný, J.; Jančařík, A.; Andronova, A.; Šámal, M.; Vacek Chocholoušová, J.; Vacek, J.; Pohl, R.; Šaman, D.; Císařová, I.; Stará, I. G.; *et al.*. A General Approach to Optically Pure [5]-, [6]-, and [7]Heterohelicenes, *Angew. Chem. Int. Ed.* **2012**, *51*, 5857-5861.
(128) Šámal, M.; Chercheja, S.; Rybáček, J.; Vacek Chocholoušová, J.; Vacek, J.; Bednárová, L.; Šaman, D.; Stará, I. G.; Starý, I. An Ultimate Stereocontrol in Asymmetric Synthesis of Optically Pure Fully Aromatic Helicenes, *J. Am. Chem. Soc.* **2015**, *137*, 8469-8474.
(129) Klívar, J.; Šámal, M.; Jančařík, A.; Vacek, J.; Bednárová, L.; Buděšínský, M.; Fiedler, P.; Starý, I.; Stará, I. G. Asymmetric Synthesis of Diastereo- and Enantiopure Bioxahelicene 2,2'-Bipyridines, *Eur. J. Org. Chem.* **2018**, *2018*, 5164-5178.

(130) Andronova, A.; Szydlo, F.; Teply, F.; Tobrmanova, M.; Volot, A.; Stara, I. G.; Stary, I.; Rulisek, L.; Saman, D.; Cvacka, J.; *et al.*. The Quest For Alternative Routes To Racemic And Nonracemic Azahelicene Derivatives, *Collect. Czech. Chem. Commun.* **2009**, *74*, 189-215.
(131) Storch, J.; Čermák, J.; Karban, J.; Císařová, I.; Sýkora, J. Synthesis of 2-Aza[6]helicene and Attempts To Synthesize 2,14-Diaza[6]helicene Utilizing Metal-Catalyzed Cycloisomerization, *J. Org. Chem.* **2010**, *75*, 3137-3140.
(132) Weimar, M.; Correa da Costa, R.; Lee, F.-H.; Fuchter, M. J. A Scalable and Expedient Route to 1-Aza[6]helicene Derivatives and Its Subsequent Application to a Chiral-Relay Asymmetric Strategy, *Org. Lett.* **2013**, *15*, 1706-1709.
(133) Nakamura, K.; Furumi, S.; Takeuchi, M.; Shibuya, T.; Tanaka, K. Enantioselective Synthesis and Enhanced Circularly Polarized Luminescence of S-Shaped Double Azahelicenes, *J. Am. Chem. Soc.* **2014**, *136*, 5555-5558.
(134) Tanaka, M.; Shibata, Y.; Nakamura, K.; Teraoka, K.; Uekusa, H.; Nakazono, K.; Takata, T.; Tanaka, K. Gold-Catalyzed Enantioselective Synthesis, Crystal Structure, and Photophysical/Chiroptical Properties of Aza[10]helicenes, *Chem. – Eur. J.* **2016**, *22*, 9537-9541.
(135) Tanaka, H.; Ikenosako, M.; Kato, Y.; Fujiki, M.; Inoue, Y.; Mori, T. Symmetry-based rational design for boosting chiroptical responses, *Commun. Chem.* **2018**, *1*, 38.
(136) Rau, H.; Schuster, O. Simple Synthesis and Resolution of a Diaza[7]helicene, *Angew. Chem. Int. Ed.* **1976**, *15*, 114-115.
(137) Newman, M. S.; Lutz, W. B. α-(2,4,5,7-Tetranitro-9-fluorenylideneaminoöxy)-propionic Acid, a New Reagent for Resolution by Complex Formation, *J. Am. Chem. Soc.* **1956**, *78*, 2469-2473.
(138) Mikeš, F.; Boshart, G. Binaphthyl-2,2′-diyl hydrogen phosphate. A new chiral atropisomeric selectro for the resolution of helicenes using high performance liquid chromatography, *J. Chem. Soc., Chem. Comm.* **1978**, 173-175.
(139) Greiner, G.; Rau, H.; Bonneau, R. Spectroscopy of *o*-diazahelicenes of $C_{2v}C_2$ symmetry, *J. Photochem. Photobiol., A* **1996**, *95*, 115-125.
(140) Vacek, J.; Chocholousova, J. V.; Stara, I. G.; Stary, I.; Dubi, Y. Mechanical Tuning Of Conductance And Thermopower In Helicene Molecular Junctions, *Nanoscale* **2015**, *7*, 8793-8802.
(141) Guo, Y.-D.; Yan, X.-H.; Xiao, Y.; Liu, C.-S. U-shaped relationship between current and pitch in helicene molecules, *Sci. Rep.* **2015**, *5*, 16731.
(142) Yang, Y.; da Costa, R. C.; Fuchter, M. J.; Campbell, A. J. Circularly Polarized Light Detection By A Chiral Organic Semiconductor Transistor, *Nature Photonics* **2013**, *7*, 634.
(143) Yang, Y.; Rice, B.; Shi, X.; Brandt, J. R.; Correa da Costa, R.; Hedley, G. J.; Smilgies, D.-M.; Frost, J. M.; Samuel, I. D. W.; Otero-de-la-Roza, A.; *et al.*. Emergent Properties of an Organic Semiconductor Driven by its Molecular Chirality, *ACS Nano* **2017**, *11*, 8329-8338.
(144) Josse, P.; Favereau, L.; Shen, C.; Dabos-Seignon, S.; Blanchard, P.; Cabanetos, C.; Crassous, J. Enantiopure versus Racemic Naphthalimide End-Capped Helicenic Non-fullerene Electron Acceptors: Impact on Organic Photovoltaics Performance, *Chem. – Eur. J.* **2017**, *23*, 6277-6281.
(145) Rice, B.; LeBlanc, L. M.; Otero-de-la-Roza, A.; Fuchter, M. J.; Johnson, E. R.; Nelson, J.; Jelfs, K. E. A computational exploration of the crystal energy and charge-carrier mobility landscapes of the chiral [6]helicene molecule, *Nanoscale* **2018**, *10*, 1865-1876.
(146) Yang, Y.; da Costa, R. C.; Smilgies, D.-M.; Campbell, A. J.; Fuchter, M. J. Induction of Circularly Polarized Electroluminescence from an Achiral Light-Emitting Polymer via a Chiral Small-Molecule Dopant, *Adv. Mater.* **2013**, *25*, 2624-2628.
(147) Brandt, J. R.; Wang, X.; Yang, Y.; Campbell, A. J.; Fuchter, M. J. Circularly Polarized Phosphorescent Electroluminescence with a High Dissymmetry Factor from PHOLEDs Based on a Platinahelicene, *J. Am. Chem. Soc.* **2016**, *138*, 9743-9746.
(148) Misek, J.; Tichy, M.; Stara, I. G.; Stary, I.; Schroder, D. Preferential formation of homochiral Silver(i) complexes upon coordination of two aza[6]helicene ligands to Ag+ ions, *Collect. Czech. Chem. Commun.* **2009**, *74*, 323-333.

(149) Alkorta, I.; Blanco, F.; Elguero, J.; Schröder, D. Distinction between homochiral and heterochiral dimers of 1-aza[n]helicenes (n=1–7) with alkaline cations, *Tetrahedron: Asymmetry* **2010**, *21*, 962-968.
(150) Caronna, T.; Castiglione, F.; Famulari, A.; Fontana, F.; Malpezzi, L.; Mele, A.; Mendola, D.; Natali Sora, I. Quantum Mechanics Calculations, Basicity and Crystal Structure: The Route to Transition Metal Complexes of Azahelicenes, *Molecules* **2012**, *17*, 463-479.
(151) C. Constable, E.; J. Steel, P. N,N'-Chelating biheteroaromatic ligands; a survey, *Coord. Chem. Rev.* **1989**, *93*, 205-223.
(152) Maidich, L.; Dettori, G.; Stoccoro, S.; Cinellu, M. A.; Rourke, J. P.; Zucca, A. Electronic and Steric Effects in Rollover C-H Bond Activation, *Organometallics* **2015**, *34*, 817-828.
(153) Ittel, S. D.; Johnson, L. K.; Brookhart, M. Late-Metal Catalysts for Ethylene Homo- and Copolymerization, *Chem. Rev.* **2000**, *100*, 1169-1204.
(154) Saleh, N.; Srebro, M.; Reynaldo, T.; Vanthuyne, N.; Toupet, L.; Chang, V. Y.; Muller, G.; Williams, J. A. G.; Roussel, C.; Autschbach, J.; *et al.*. Enantio-Enriched CPL-Active Helicene-Bipyridine-Rhenium Complexes, *Chem. Comm.* **2015**, *51*, 3754-3757.
(155) Ou-Yang, J. K.; Saleh, N.; Garcia, G. F.; Norel, L.; Pointillart, F.; Guizouarn, T.; Cador, O.; Totti, F.; Ouahab, L.; Crassous, J.; *et al.*. Improved Slow Magnetic Relaxation In Optically Pure Helicene-Based Dy-III Single Molecule Magnets, *Chem. Comm.* **2016**, *52*, 14474-14477.
(156) Fernandez-Garcia, G.; Gonzalez, J. F.; Ou-Yang, J.-K.; Saleh, N.; Pointillart, F.; Cador, O.; Guizouarn, T.; Totti, F.; Ouahab, L.; Crassous, J.; *et al.*. Slow Magnetic Relaxation in Chiral Helicene-Based Coordination Complex of Dysprosium, *Magnetochemistry* **2017**, *3*,
(157) Gonzalez, J. F.; Montigaud, V.; Saleh, N.; Cador, O.; Crassous, J.; le Guennic, B.; Pointillart, F. Slow Relaxation of the Magnetization in Bis-Decorated Chiral Helicene-Based Coordination Complexes of Lanthanides, *Magnetochemistry* **2018**, *4*,
(158) Galland, M.; Riobé, F.; Ouyang, J.; Saleh, N.; Pointillart, F.; Dorcet, V.; Le Guennic, B.; Cador, O.; Crassous, J.; Andraud, C.; *et al.*. Helicenic Complexes of Lanthanide: Influence of f-Element on the Inter-System Crossing Efficiency and Competition Between Luminescence and Oxygen Sensitization, *Eur. J. Inorg. Chem.* **2019**, 118-125.
(159) Mulzer, J. In *Comprehensive Asymmetric Catalysis, Vol. 1* E. N. Jacobsen, A. P., H. Yamamoto Ed.; Springer, Berlin, 1999.
(160) Samal, M.; Misek, J.; Stara, I. G.; Stary, I. Organocatalysis with azahelicenes: The first use of helically chiral pyridine-based catalysts in the asymmetric acyl transfer reaction, *Collect. Czech. Chem. Commun.* **2009**, *74*, 1151-1159.
(161) Matsumoto, A.; Yonemitsu, K.; Ozaki, H.; Míšek, J.; Starý, I.; Stará, I. G.; Soai, K. Reversal of the sense of enantioselectivity between 1- and 2-aza[6]helicenes used as chiral inducers of asymmetric autocatalysis, *Org. Biomol. Chem.* **2017**, *15*, 1321-1324.
(162) I. F. Perepichka, D. F. P. *Handbook of Thiophene-Based Materials*; John Wiley & Sons, Ltd., 2009.
(163) Grigalevicius, S. 3,6(2,7),9-Substituted carbazoles as electroactive amorphous materials for optoelectronics, *Synthetic Metals* **2006**, *156*, 1-12.
(164) Sathiyan, G.; Sivakumar, E. K. T.; Ganesamoorthy, R.; Thangamuthu, R.; Sakthivel, P. Review of Carbazole Based Conjugated Molecules for Highly Efficient Organic Solar Cell Application, *Tetrahedron Lett.* **2016**, *57*, 243-252.
(165) Janosik, T.; Rannug, A.; Rannug, U.; Wahlström, N.; Slätt, J.; Bergman, J. Chemistry and Properties of Indolocarbazoles, *Chem. Rev.* **2018**, *118*, 9058-9128.
(166) Tsuji, H.; Nakamura, E. Design and Functions of Semiconducting Fused Polycyclic Furans for Optoelectronic Applications, *Acc. Chem. Res.* **2017**, *50*, 396-406.
(167) Bucinskas, A.; Waghray, D.; Bagdziunas, G.; Thomas, J.; Grazulevicius, J. V.; Dehaen, W. Synthesis, Functionalization, and Optical Properties of Chiral Carbazole-Based Diaza[6]helicenes, *J. Org. Chem.* **2015**, *80*, 2521-2528.
(168) Upadhyay, G. M.; Talele, H. R.; Sahoo, S.; Bedekar, A. V. Synthesis of Carbazole Derived Aza[7]Helicenes, *Tetrahedron Lett.* **2014**, *55*, 5394-5399.

(169) Upadhyay, G. M.; Talele, H. R.; Bedekar, A. V. Synthesis and Photophysical Properties of Aza[n]helicenes, *J. Org. Chem.* **2016**, *81*, 7751-7759.
(170) Arae, S.; Mori, T.; Kawatsu, T.; Ueda, D.; Shigeta, Y.; Hamamoto, N.; Fujimoto, H.; Sumimoto, M.; Imahori, T.; Igawa, K.; *et al.*. Synthesis and Stereochemical Properties of Chiral Hetero[7]helicenes Structured by a Benzodiheterole Ring Core, *Chem. Lett.* **2017**, *46*, 1214-1216.
(171) Ryo, I.; Akihiro, T.; Suguru, U.; Tatsushi, I.; Kazunobu, I.; Taisuke, M.; Katsuhiko, T.; Shinsuke, K.; Tatsuya, U.; Tsutomu, K. Synthesis and Stereochemical Behavior of a New Chiral Oxa[7]heterohelicene, *Chem. Lett.* **2011**, *40*, 1343-1345.
(172) Nakano, K.; Hidehira, Y.; Takahashi, K.; Hiyama, T.; Nozaki, K. Stereospecific synthesis of hetero[7]helicenes by Pd-catalyzed double N-arylation and intramolecular O-arylation, *Angew Chem Int Ed Engl* **2005**, *44*, 7136-7138.
(173) Fuchs, W.; Niszel, F. Über die Tautomerie der Phenole, IX.: Die Naphtho-carbazol-Bildung aus Naphtholen, *Berichte der deutschen chemischen Gesellschaft (A and B Series)* **1927**, *60*, 209-217.
(174) Pischel, I.; Grimme, S.; Kotila, S.; Nieger, M.; Vögtle, F. A Configurationally Stable Pyrrolohelicene: Experimental and Theoretical Structure-Chiroptic Relationships, *Tetrahedron: Asymmetry* **1996**, *7*, 109-116.
(175) Kötzner, L.; Webber, M. J.; Martínez, A.; De Fusco, C.; List, B. Asymmetric Catalysis on the Nanoscale: The Organocatalytic Approach to Helicenes, *Angew. Chem. Int. Ed.* **2014**, *53*, 5202-5205.
(176) Chen, F.; Tanaka, T.; Hong, Y. S.; Mori, T.; Kim, D.; Osuka, A. Closed Pentaaza[9]helicene and Hexathia[9]/[5]helicene: Oxidative Fusion Reactions of ortho-Phenylene-Bridged Cyclic Hexapyrroles and Hexathiophenes, *Angew. Chem. Int. Ed.* **2017**, *56*, 14688-14693.
(177) Chen, F.; Tanaka, T.; Mori, T.; Osuka, A. Synthesis, Structures, and Optical Properties of Azahelicene Derivatives and Unexpected Formation of Azahepta[8]circulenes, *Chem. – Eur. J.* **2018**, *24*, 7489-7497.
(178) Goto, K.; Yamaguchi, R.; Hiroto, S.; Ueno, H.; Kawai, T.; Shinokubo, H. Intermolecular Oxidative Annulation of 2-Aminoanthracenes to Diazaacenes and Aza[7]helicenes, *Angew. Chem. Int. Ed.* **2012**, *51*, 10333-10336.
(179) Sakamaki, D.; Kumano, D.; Yashima, E.; Seki, S. A Facile and Versatile Approach to Double N-Heterohelicenes: Tandem Oxidative C-N Couplings of N-Heteroacenes via Cruciform Dimers, *Angew. Chem. Int. Ed.* **2015**, *54*, 5404-5407.
(180) Dreher, S. D.; Weix, D. J.; Katz, T. J. Easy Synthesis of Functionalized Hetero[7]helicenes, *J. Org. Chem.* **1999**, *64*, 3671-3678.
(181) Liégeois, V.; Champagne, B. Vibrational Raman optical activity of π-conjugated helical systems: Hexahelicene and heterohelicenes, *J. Comput. Chem.* **2009**, *30*, 1261-1278.
(182) Wang, Y.; Zhang, H.; Pink, M.; Olankitwanit, A.; Rajca, S.; Rajca, A. Radical Cation and Neutral Radical of Aza-thia[7]helicene with SOMO–HOMO Energy Level Inversion, *J. Am. Chem. Soc.* **2016**, *138*, 7298-7304.
(183) Yamamoto, Y.; Sakai, H.; Yuasa, J.; Araki, Y.; Wada, T.; Sakanoue, T.; Takenobu, T.; Kawai, T.; Hasobe, T. Synthetic Control of the Excited-State Dynamics and Circularly Polarized Luminescence of Fluorescent "Push–Pull" Tetrathia[9]helicenes, *Chem. – Eur. J.* **2016**, *22*, 4263-4273.
(184) Fox, J. M.; Katz, T. J.; Van Elshocht, S.; Verbiest, T.; Kauranen, M.; Persoons, A.; Thongpanchang, T.; Krauss, T.; Brus, L. Synthesis, Self-Assembly, and Nonlinear Optical Properties of Conjugated Helical Metal Phthalocyanine Derivatives, *J. Am. Chem. Soc.* **1999**, *121*, 3453-3459.
(185) Dai, Y.; Katz, T. J.; Nichols, D. A. Synthesis of a Helical Conjugated Ladder Polymer, *Angew. Chem. Int. Ed.* **1996**, *35*, 2109-2111.
(186) Dai, Y.; Katz, T. J. Synthesis of Helical Conjugated Ladder Polymers, *J. Org. Chem.* **1997**, *62*, 1274-1285.
(187) Waghray, D.; Bagdziunas, G.; Jacobs, J.; Van Meervelt, L.; Grazulevicius, J. V.; Dehaen, W. Diastereoselective Strategies towards Thia[n]helicenes, *Chem. – Eur. J.* **2015**, *21*, 18791-18798.
(188) Li, M.; Lu, H.-Y.; Zhang, C.; Shi, L.; Tang, Z.; Chen, C.-F. Helical aromatic imide based enantiomers with full-color circularly polarized luminescence, *Chem. Comm.* **2016**, *52*, 9921-9924.
(189) Tsuji, G.; Kawakami, K.; Sasaki, S. Enantioselective binding of chiral 1,14-dimethyl[5]helicene–spermine ligands with B- and Z-DNA, *Bioorg. Med. Chem.* **2013**, *21*, 6063-6068.

(190) Kawara, K.; Tsuji, G.; Taniguchi, Y.; Sasaki, S. Synchronized Chiral Induction between [5]Helicene–Spermine Ligand and B–Z DNA Transition, *Chem. – Eur. J.* **2017**, *23*, 1763-1769.
(191) Schuster, N. J.; Paley, D. W.; Jockusch, S.; Ng, F.; Steigerwald, M. L.; Nuckolls, C. Electron Delocalization in Perylene Diimide Helicenes, *Angew. Chem. Int. Ed.* **2016**, *55*, 13519-13523.
(192) Schuster, N. J.; Hernández Sánchez, R.; Bukharina, D.; Kotov, N. A.; Berova, N.; Ng, F.; Steigerwald, M. L.; Nuckolls, C. A Helicene Nanoribbon with Greatly Amplified Chirality, *J. Am. Chem. Soc.* **2018**, *140*, 6235-6239.
(193) Zhong, Y.; Sisto, T. J.; Zhang, B.; Miyata, K.; Zhu, X. Y.; Steigerwald, M. L.; Ng, F.; Nuckolls, C. Helical Nanoribbons for Ultra-Narrowband Photodetectors, *J. Am. Chem. Soc.* **2017**, *139*, 5644-5647.
(194) Milton, M.; Schuster, N. J.; Paley, D. W.; Hernández Sánchez, R.; Ng, F.; Steigerwald, M. L.; Nuckolls, C. Defying strain in the synthesis of an electroactive bilayer helicene, *Chem. Sci.* **2019**,
(195) Hellou, N.; Srebro-Hooper, M.; Favereau, L.; Zinna, F.; Caytan, E.; Toupet, L.; Dorcet, V.; Jean, M.; Vanthuyne, N.; Williams, J. A. G.; *et al.*. Enantiopure Cycloiridiated Complexes Bearing a Pentahelicenic N-Heterocyclic Carbene and Displaying Long-Lived Circularly Polarized Phosphorescence, *Angew. Chem. Int. Ed.* **2017**, *56*, 8236-8239.
(196) Sanchez, I. G.; Samal, M.; Nejedly, J.; Karras, M.; Klivar, J.; Rybacek, J.; Budesinsky, M.; Bednarova, L.; Seidlerova, B.; Stara, I. G.; *et al.*. Oxahelicene NHC ligands in the asymmetric synthesis of nonracemic helicenes, *Chem. Comm.* **2017**, *53*, 4370-4373.
(197) Karras, M.; Dąbrowski, M.; Pohl, R.; Rybáček, J.; Vacek, J.; Bednárová, L.; Grela, K.; Starý, I.; Stará, I. G.; Schmidt, B. Helicenes as Chirality-Inducing Groups in Transition-Metal Catalysis: The First Helically Chiral Olefin Metathesis Catalyst, *Chem. – Eur. J.* **2018**, *24*, 10994-10998.
(198) Hellou, N.; Jahier-Diallo, C.; Basle, O.; Srebro-Hooper, M.; Toupet, L.; Roisnel, T.; Caytan, E.; Roussel, C.; Vanthuyne, N.; Autschbach, J.; *et al.*. Electronic And Chiroptical Properties Of Chiral Cycloiridiated Complexes Bearing Helicenic NHC Ligands, *Chem. Comm.* **2016**, *52*, 9243-9246.
(199) Biet, T.; Martin, K.; Hankache, J.; Hellou, N.; Hauser, A.; Bürgi, T.; Vanthuyne, N.; Aharon, T.; Caricato, M.; Crassous, J.; *et al.*. Triggering Emission with the Helical Turn in Thiadiazole-Helicenes, *Chem. – Eur. J.* **2017**, *23*, 437-446.
(200) Yersin, H. *Highly efficient OLEDs with phosphorescent materials*; Wiley, 2008.
(201) Ma, D.-L.; He, H.-Z.; Leung, K.-H.; Chan, D. S.-H.; Leung, C.-H. Bioactive Luminescent Transition-Metal Complexes for Biomedical Applications, *Angew. Chem. Int. Ed.* **2013**, *52*, 7666-7682.
(202) Storch, J.; Zadny, J.; Strasak, T.; Kubala, M.; Sykora, J.; Dusek, M.; Cirkva, V.; Matejka, P.; Krbal, M.; Vacek, J. Synthesis and Characterization of a Helicene-Based Imidazolium Salt and Its Application in Organic Molecular Electronics, *Chem. – Eur. J.* **2015**, *21*, 2343-2347.
(203) Storch, J.; Kalíková, K.; Tesařová, E.; Maier, V.; Vacek, J. Development of separation methods for the chiral resolution of hexahelicenes, *J. Chromatogr., A* **2016**, *1476*, 130-134.
(204) Field, J. E.; Muller, G.; Riehl, J. P.; Venkataraman, D. Circularly polarized luminescence from bridged triarylamine helicenes, *J. Am. Chem. Soc.* **2003**, *125*, 11808-11809.
(205) Phillips, K. E. S.; Katz, T. J.; Jockusch, S.; Lovinger, A. J.; Turro, N. J. Synthesis and Properties of an Aggregating Heterocyclic Helicene, *J. Am. Chem. Soc.* **2001**, *123*, 11899-11907.
(206) Riehl, J. P.; Richardson, F. S. Circularly polarized luminescence spectroscopy, *Chem. Rev.* **1986**, *86*, 1-16.
(207) Cyphersmith, A.; Surampudi, S.; Casey, M. J.; Jankowski, K.; Venkataraman, D.; Barnes, M. D. Chiroptical Dissymmetries in Fluorescence Excitation from Single Molecules of (M-2) Helicene Dimers, *J. Phys. Chem. A* **2012**, *116*, 5349-5352.
(208) Hassey, R.; Swain, E. J.; Hammer, N. I.; Venkataraman, D.; Barnes, M. D. Probing the Chiroptical Response of a Single Molecule, *Science* **2006**, *314*, 1437-1439.
(209) Tang, Y.; Cook, T. A.; Cohen, A. E. Limits on Fluorescence Detected Circular Dichroism of Single Helicene Molecules, *J. Phys. Chem. A* **2009**, *113*, 6213-6216.
(210) Hassey, R.; McCarthy, K. D.; Swain, E.; Basak, D.; Venkataraman, D.; Barnes, M. D. Single-molecule chiroptical spectroscopy: Fluorescence excitation of individual helicene molecules in polymer-supported thin-films, *Chirality* **2008**, *20*, 1039-1046.

(211) Pandith, A. H.; Islam, N.; Syed, Z. F.; Rehman, S.-u.; Bandaru, S.; Anoop, A. Density functional theory prediction of geometry and vibrational circular dichroism of bridged triarylamine helicenes, *Chem. Phys. Lett.* **2011**, *516*, 199-203.
(212) Longhi, G.; Castiglioni, E.; Villani, C.; Sabia, R.; Menichetti, S.; Viglianisi, C.; Devlin, F.; Abbate, S. Chiroptical Properties of the Ground and Excited States of Two Thia-Bridged Triarylamine Heterohelicenes, *J. Photochem. Photobiol., A* **2016**, *331*, 138-145.
(213) Islam, N.; Pandith, A. H. Chiro-optic and nonlinear optical studies of bridged triarylamine heterohelicenes; A DFT study, *J. Mol. Struct.* **2017**, *1142*, 1-10.
(214) Spassova, M.; Asselberghs, I.; Verbiest, T.; Clays, K.; Botek, E.; Champagne, B. Theoretical investigation on bridged triarylamine helicenes: UV/visible and circular dichroism spectra, *Chem. Phys. Lett.* **2007**, *439*, 213-218.
(215) Nishimura, H.; Tanaka, K.; Morisaki, Y.; Chujo, Y.; Wakamiya, A.; Murata, Y. Oxygen-Bridged Diphenylnaphthylamine as a Scaffold for Full-Color Circularly Polarized Luminescent Materials, *J. Org. Chem.* **2017**, *82*, 5242-5249.
(216) Lamanna, G.; Faggi, C.; Gasparrini, F.; Ciogli, A.; Villani, C.; Stephens, P. J.; Devlin, F. J.; Menichetti, S. Efficient Thia-Bridged Triarylamine Heterohelicenes: Synthesis, Resolution, and Absolute Configuration Determination, *Chem. – Eur. J.* **2008**, *14*, 5747-5750.
(217) Gliemann, B. D.; Petrovic, A. G.; Zolnhofer, E. M.; Dral, P. O.; Hampel, F.; Breitenbruch, G.; Schulze, P.; Raghavan, V.; Meyer, K.; Polavarapu, P. L.; *et al.*. Configurationally Stable Chiral Dithia-Bridged Hetero[4]helicene Radical Cation: Electronic Structure and Absolute Configuration, *Chem. Asian J.* **2017**, *12*, 31-35.
(218) Otani, T.; Tsuyuki, A.; Iwachi, T.; Someya, S.; Tateno, K.; Kawai, H.; Saito, T.; Kanyiva, K. S.; Shibata, T. Facile Two-Step Synthesis of 1,10-Phenanthroline-Derived Polyaza[7]helicenes with High Fluorescence and CPL Efficiency, *Angew. Chem. Int. Ed.* **2017**, *56*, 3906-3910.
(219) Oyama, H.; Akiyama, M.; Nakano, K.; Naito, M.; Nobusawa, K.; Nozaki, K. Synthesis and Properties of [7]Helicene-like Compounds Fused with a Fluorene Unit, *Org. Lett.* **2016**, *18*, 3654-3657.
(220) Numan, H.; Helder, R.; Wynberg, H. The resolution of heterohelicenes, a facile method using HPLC: (Preliminary communication), *Recl. Trav. Chim. Pays-Bas* **1976**, *95*, 211-212.
(221) Granzhan, A.; Ihmels, H.; Jäger, K. Diazonia- and tetraazoniapolycyclic cations as motif for quadruplex-DNA ligands, *Chem. Comm.* **2009**, 1249-1251.
(222) Wanda, S.; Barbara, B.; Tomasz, G. Viologens as Components of Supramolecular Structures, *Curr. Org. Chem.* **2007**, *11*, 497-513.
(223) Adriaenssens, L.; Severa, L.; Šálová, T.; Císařová, I.; Pohl, R.; Šaman, D.; Rocha, S. V.; Finney, N. S.; Pospíšil, L.; Slavíček, P.; *et al.*. Helquats: A Facile, Modular, Scalable Route to Novel Helical Dications, *Chem. – Eur. J.* **2009**, *15*, 1072-1076.
(224) Coe, B. J.; Rusanova, D.; Joshi, V. D.; Sánchez, S.; Vávra, J.; Khobragade, D.; Severa, L.; Císařová, I.; Šaman, D.; Pohl, R.; *et al.*. Helquat Dyes: Helicene-like Push–Pull Systems with Large Second-Order Nonlinear Optical Responses, *J. Org. Chem.* **2016**, *81*, 1912-1920.
(225) Severa, L.; Adriaenssens, L.; Vávra, J.; Šaman, D.; Císařová, I.; Fiedler, P.; Teplý, F. Highly Modular Assembly Of Cationic Helical Scaffolds: Rapid Synthesis Of Diverse Helquats Via Differential Quaternization, *Tetrahedron* **2010**, *66*, 3537-3552.
(226) Růžička, M.; Koval, D.; Vávra, J.; Reyes-Gutiérrez, P. E.; Teplý, F.; Kašička, V. Interactions of Helquats with Chiral Acidic Aromatic Analytes Investigated by Partial-Filling Affinity Capillary Electrophoresis, *J. Chromatogr., A* **2016**, *1467*, 417-426.
(227) Severa, L.; Koval, D.; Novotná, P.; Ončák, M.; Sázelová, P.; Šaman, D.; Slavíček, P.; Urbanová, M.; Kašička, V.; Teplý, F. Resolution of A Configurationally Stable [5]Helquat: Enantiocomposition Analysis of A Helicene Congener by Capillary Electrophoresis, *New J. Chem.* **2010**, *34*, 1063-1067.
(228) Jacques, J.; Collet, A.; Wilen, S. H. *Enantiomers, Racemates, and Resolutions*; 2nd ed. ed.; Krieger: Malabar, FL.

(229) Collet, A.; Brienne, M. J.; Jacques, J. Optical Resolution By Direct Crystallization Of Enantiomer Mixtures, *Chem. Rev.* **1980**, *80*, 215-230.
(230) Vavra, J.; Severa, L.; Svec, P.; Cisarova, I.; Koval, D.; Sazelova, P.; Kasicka, V.; Teply, F. Preferential Crystallization of a Helicene-Viologen Hybrid - An Efficient Method to Resolve [5]Helquat Enantiomers on a 20 g Scale, *Eur. J. Org. Chem.* **2012**, 489-499.
(231) Severa, L.; Sázelová, P.; Císařová, I.; Šaman, D.; Koval, D.; Devadig, P.; Kašička, V.; Teplý, F. Dutch Resolution of A Configurationally Stable [5]Helquat, *Chirality* **2018**, *30*, 254-260.
(232) Vávra, J.; Severa, L.; Císařová, I.; Klepetářová, B.; Šaman, D.; Koval, D.; Kašička, V.; Teplý, F. Search for Conglomerate in Set of [7]Helquat Salts: Multigram Resolution of Helicene–Viologen Hybrid by Preferential Crystallization, *J. Org. Chem.* **2013**, *78*, 1329-1342.
(233) Pospíšil, L.; Bednárová, L.; Štěpánek, P.; Slavíček, P.; Vávra, J.; Hromadová, M.; Dlouhá, H.; Tarábek, J.; Teplý, F. Intense Chiroptical Switching in a Dicationic Helicene-Like Derivative: Exploration of a Viologen-Type Redox Manifold of a Non-Racemic Helquat, *J. Am. Chem. Soc.* **2014**, *136*, 10826-10829.
(234) Šebestík, J.; Teplý, F.; Císařová, I.; Vávra, J.; Koval, D.; Bouř, P. Intense Chirality Induction In Nitrile Solvents By A Helquat Dye Monitored By Near Resonance Raman Scattering, *Chem. Comm.* **2016**, *52*, 6257-6260.
(235) Reyes-Gutiérrez, P. E.; Jirásek, M.; Severa, L.; Novotná, P.; Koval, D.; Sázelová, P.; Vávra, J.; Meyer, A.; Císařová, I.; Šaman, D.; *et al.*. Functional Helquats: Helical Cationic Dyes with Marked, Switchable Chiroptical Properties in The Visible Region, *Chem. Comm.* **2015**, *51*, 1583-1586.
(236) Barroso, J.; Cabellos, J. L.; Pan, S.; Murillo, F.; Zarate, X.; Fernandez-Herrera, M. A.; Merino, G. Revisiting the racemization mechanism of helicenes, *Chem. Comm.* **2018**, *54*, 188-191.
(237) Adriaenssens, L.; Severa, L.; Koval, D.; Císařová, I.; Belmonte, M. M.; Escudero-Adán, E. C.; Novotná, P.; Sázelová, P.; Vávra, J.; Pohl, R.; *et al.*. [6]Saddlequat: A [6]Helquat Captured on Its Racemization Pathway, *Chem. Sci.* **2011**, *2*, 2314-2320.
(238) Severa, L.; Jirásek, M.; Švec, P.; Teplý, F.; Révész, Á.; Schröder, D.; Koval, D.; Kašička, V.; Císařová, I.; Šaman, D. Counterion-Induced Inversion of Conformer Stability of a [5]Helquat Dication, *Chempluschem* **2012**, *77*, 624-635.
(239) Severa, L.; Ončák, M.; Koval, D.; Pohl, R.; Šaman, D.; Císařová, I.; Reyes-Gutiérrez, P. E.; Sázelová, P.; Kašička, V.; Teplý, F.; *et al.*. Chiral Dicationic [8]Circulenoid: Photochemical Origin and Facile Thermal Conversion into a Helicene Congener, *Angew. Chem. Int. Ed.* **2012**, *51*, 11972-11976.
(240) Čížková, M.; Šaman, D.; Koval, D.; Kašička, V.; Klepetářová, B.; Císařová, I.; Teplý, F. Modular Synthesis of Helicene-Like Compounds Based on the Imidazolium Motif, *Eur. J. Org. Chem.* **2014**, *2014*, 5681-5685.
(241) Koval, D.; Severa, L.; Adriaenssens, L.; Vávra, J.; Teplý, F.; Kašička, V. Chiral Analysis of Helquats by Capillary Electrophoresis: Resolution of Helical N-Heteroaromatic Dications Using Randomly Sulfated Cyclodextrins, *Electrophoresis* **2011**, *32*, 2683-2692.
(242) Balogh, D.; Zhang, Z.; Cecconello, A.; Vavra, J.; Severa, L.; Teply, F.; Willner, I. Helquat-Induced Chiroselective Aggregation of Au NPs, *Nano Lett.* **2012**, *12*, 5835-5839.
(243) Nath, N. K.; Severa, L.; Kunetskiy, R. A.; Císařová, I.; Fulem, M.; Růžička, K.; Koval, D.; Kašička, V.; Teplý, F.; Naumov, P. Single-Crystal-to-Single-Crystal Transition in an Enantiopure [7]Helquat Salt: The First Observation of a Reversible Phase Transition in a Helicene-Like Compound, *Chem. – Eur. J.* **2015**, *21*, 13508-13512.
(244) Arai, S.; Ishikura, M.; Yamagishi, T. Synthesis of polycyclic azonia-aromatic compounds by photo-induced intramolecular quaternization: Azonia derivatives of benzo[c]phenanthrene, [5]helicene and [6]helicene, *J. Chem. Soc., Perkin Trans. 1* **1998**, 1561-1568.
(245) Sato, K.; Arai, S.; Yamagishi, T.; Tanase, T. An azonia derivative of hexahelicene, *Acta Cryst. C* **2003**, *59*, o162-o164.
(246) Sato, K.; Okazaki, S.; Yamagishi, T.; Arai, S. The synthesis of azoniadithia 6 helicenes, *J. Heterocycl. Chem.* **2004**, *41*, 443-447.
(247) Sato, K.; Katayama, Y.; Yamagishi, T.; Arai, S. The synthesis of new azoniathiahelicenes, *J. Heterocycl. Chem.* **2006**, *43*, 177-181.

(248) Huang, Q.; Jiang, L.; Liang, W.; Gui, J.; Xu, D.; Wu, W.; Nakai, Y.; Nishijima, M.; Fukuhara, G.; Mori, T.; *et al.*. Inherently Chiral Azonia[6]helicene-Modified β-Cyclodextrin: Synthesis, Characterization, and Chirality Sensing of Underivatized Amino Acids in Water, *J. Org. Chem.* **2016**, *81*, 3430-3434.
(249) Zhou, L.-L.; Li, M.; Lu, H.-Y.; Chen, C.-F. Benzo[5]helicene-based conjugated polymers: synthesis, photophysical properties, and application for the detection of nitroaromatic explosives, *Polymer Chemistry* **2016**, *7*, 310-318.
(250) Tounsi, M.; Ben Braiek, M.; Barhoumi, H.; Baraket, A.; Lee, M.; Zine, N.; Maaref, A.; Errachid, A. A Novel EIS Field Effect Structures Coated with TESUD-PPy-PVC-Dibromoaza[7]Helicene Matrix for Potassium Ions Detection, *Mater. Sci. Eng. C* **2016**, *61*, 608-615.
(251) Tounsi, M.; Ben Braiek, M.; Baraket, A.; Lee, M.; Zine, N.; Zabala, M.; Bausells, J.; Aloui, F.; Ben Hassine, B.; Maaref, A.; *et al.*. Electrochemical Capacitive K+ EMIS Chemical Sensor Based on the Dibromoaza[7]helicene as an Ionophore for Potassium Ions Detection, *Electroanalysis* **2016**, *28*, 2892-2899.
(252) Passeri, R.; Aloisi, G. G.; Elisei, F.; Latterini, L.; Caronna, T.; Fontana, F.; Sora, I. N. Photophysical Properties of N-Alkylated Azahelicene Derivatives as DNA Intercalators: Counterion Effects, *Photochem. Photobiol. Sci.* **2009**, *8*, 1574-1582.
(253) Brandt, J. R.; Pospíšil, L.; Bednárová, L.; da Costa, R. C.; White, A. J. P.; Mori, T.; Teplý, F.; Fuchter, M. J. Intense Redox-Driven Chiroptical Switching With A 580 Mv Hysteresis Actuated Through Reversible Dimerization Of An Azoniahelicene, *Chem. Comm.* **2017**, *53*, 9059-9062.
(254) Bosson, J.; Gouin, J.; Lacour, J. Cationic Triangulenes and Helicenes: Synthesis, Chemical Stability, Optical Properties and Extended Applications of These Unusual Dyes, *Chem. Soc. Rev.* **2014**, *43*, 2824-2840.
(255) Herse, C.; Bas, D.; Krebs, F. C.; Bürgi, T.; Weber, J.; Wesolowski, T.; Laursen, B. W.; Lacour, J. A Highly Configurationally Stable [4]Heterohelicenium Cation, *Angew. Chem. Int. Ed.* **2003**, *42*, 3162-3166.
(256) Laursen, B. W.; Krebs, F. C. Synthesis of a Triazatriangulenium Salt, *Angew. Chem. Int. Ed.* **2000**, *39*, 3432-3434.
(257) Laleu, B.; Mobian, P.; Herse, C.; Laursen, B. W.; Hopfgartner, G.; Bernardinelli, G.; Lacour, J. Resolution of [4]Heterohelicenium Dyes with Unprecedented Pummerer-like Chemistry, *Angew. Chem. Int. Ed.* **2005**, *44*, 1879-1883.
(258) Laleu, B.; Machado, M. S.; Lacour, J. Pummerer fragmentation vs. Pummerer rearrangement: a mechanistic analysis, *Chem. Comm.* **2006**, 2786-2788.
(259) Mehanna, N.; Grass, S.; Lacour, J. Surprisingly Difficult Resolution of N-Methylated Cationic [4]Helicenes, *Chirality* **2012**, *24*, 928-935.
(260) Villani, C.; Laleu, B.; Mobian, P.; Lacour, J. Effective HPLC Resolution of [4]Heterohelicenium Dyes on Chiral Stationary Phases Using Reversed-Phase Eluents, *Chirality* **2007**, *19*, 601-606.
(261) Nicolas, C.; Bernardinelli, G.; Lacour, J. On the synthesis and optical properties of sulfur-bridged analogues of triangulenium cations and their precursors, *J. Phys. Org. Chem.* **2010**, *23*, 1049-1056.
(262) Guin, J.; Besnard, C.; Lacour, J. Synthesis, Resolution, and Stabilities of a Cationic Chromenoxanthene [4]helicene, *Org. Lett.* **2010**, *12*, 1748-1751.
(263) Sørensen, T. J.; Madsen, A. Ø.; Laursen, B. W. Synthesis and fluorescence properties of DMCX+—a stable oxygen-bridged [4]helicenium dye, *Tetrahedron Lett.* **2013**, *54*, 587-590.
(264) Sørensen, T. J.; Madsen, A. Ø.; Laursen, B. W. Synthesis and Structures of N-Alkyl-1,13-dimethoxychromeno- [2,3,4-kl]acridinium Salts: The Missing Azaoxa[4]helicenium, *Chem. – Eur. J.* **2014**, *20*, 6391-6400.
(265) Gouin, J.; Bürgi, T.; Guénée, L.; Lacour, J. Convergent Synthesis, Resolution, and Chiroptical Properties of Dimethoxychromenoacridinium Ions, *Org. Lett.* **2014**, *16*, 3800-3803.
(266) Martin, J. C.; Smith, R. G. Factors Influencing the Basicities of Triarylcarbinols. The Synthesis of Sesquixanthydrol, *J. Am. Chem. Soc.* **1964**, *86*, 2252-2256.
(267) Guin, J.; Besnard, C.; Pattison, P.; Lacour, J. Highly Selective Additions of Hydride and Organolithium Nucleophiles to Helical Carbenium Ions, *Chem. Sci.* **2011**, *2*, 425-428.

(268) Conreaux, D.; Mehanna, N.; Herse, C.; Lacour, J. From Cationic to Anionic Helicenes: New Reactivity through Umpolung, *J. Org. Chem.* **2011**, *76*, 2716-2722.
(269) Torricelli, F.; Bosson, J.; Besnard, C.; Chekini, M.; Bürgi, T.; Lacour, J. Modular Synthesis, Orthogonal Post-Functionalization, Absorption, and Chiroptical Properties of Cationic [6]Helicenes, *Angew. Chem. Int. Ed.* **2013**, *52*, 1796-1800.
(270) Labrador, G. M.; Bosson, J.; Breitbach, Z. S.; Lim, Y.; Francotte, E. R.; Sabia, R.; Villani, C.; Armstrong, D. W.; Lacour, J. High-Performance Liquid Chromatographic Resolution of Neutral and Cationic Hetero[6]Helicenes, *Chirality* **2016**, *28*, 282-289.
(271) Kel, O.; Sherin, P.; Mehanna, N.; Laleu, B.; Lacour, J.; Vauthey, E. Excited-State Properties of Chiral [4]Helicene Cations, *Photochem. Photobiol. Sci.* **2012**, *11*, 623-631.
(272) Bosson, J.; Labrador, G. M.; Pascal, S.; Miannay, F. A.; Yushchenko, O.; Li, H.; Bouffier, L.; Sojic, N.; Tovar, R. C.; Muller, G.; *et al.*. Physicochemical and Electronic Properties of Cationic [6]Helicenes: from Chemical and Electrochemical Stabilities to Far-Red (Polarized) Luminescence, *Chem. – Eur. J.* **2016**, *22*, 18394-18403.
(273) Delgado, I. H.; Pascal, S.; Wallabregue, A.; Duwald, R.; Besnard, C.; Guenee, L.; Nancoz, C.; Vauthey, E.; Tovar, R. C.; Lunkley, J. L.; *et al.*. Functionalized cationic [4]helicenes with unique tuning of absorption, fluorescence and chiroptical properties up to the far-red range, *Chem. Sci.* **2016**, *7*, 4685-4693.
(274) Duwald, R.; Pascal, S.; Bosson, J.; Grass, S.; Besnard, C.; Bürgi, T.; Lacour, J. Enantiospecific Elongation of Cationic Helicenes by Electrophilic Functionalization at Terminal Ends, *Chem. – Eur. J.* **2017**, *23*, 13596-13601.
(275) Wallabregue, A.; Sherin, P.; Guin, J.; Besnard, C.; Vauthey, E.; Lacour, J. Modular Synthesis of pH-Sensitive Fluorescent Diaza[4]helicenes, *Eur. J. Org. Chem.* **2014**, *2014*, 6431-6438.
(276) Pascal, S.; Besnard, C.; Zinna, F.; Di Bari, L.; Le Guennic, B.; Jacquemin, D.; Lacour, J. Zwitterionic [4]Helicene: A Water-Soluble and Reversible Ph-Triggered ECD/CPL Chiroptical Switch in the UV and Red Spectral Regions, *Org. Biomol. Chem.* **2016**, *14*, 4590-4594.
(277) Mobian, P.; Banerji, N.; Bernardinelli, G.; Lacour, J. Towards the Stereoselective Synthesis of Inherently Chiral Pseudorotaxanes, *Org. Biomol. Chem.* **2006**, *4*, 224-231.
(278) Schalley, C. A.; Beizai, K.; Vögtle, F. On the Way to Rotaxane-Based Molecular Motors: Studies in Molecular Mobility and Topological Chirality, *Acc. Chem. Res.* **2001**, *34*, 465-476.
(279) Kel, O.; Fürstenberg, A.; Mehanna, N.; Nicolas, C.; Laleu, B.; Hammarson, M.; Albinsson, B.; Lacour, J.; Vauthey, E. Chiral Selectivity in the Binding of [4]Helicene Derivatives to Double-Stranded DNA, *Chem. – Eur. J.* **2013**, *19*, 7173-7180.
(280) Babič, A.; Pascal, S.; Duwald, R.; Moreau, D.; Lacour, J.; Allémann, E. [4]Helicene–Squalene Fluorescent Nanoassemblies for Specific Targeting of Mitochondria in Live-Cell Imaging, *Adv. Func. Mater.* **2017**, *27*, 1701839-n/a.
(281) Bauer, C.; Duwald, R.; Labrador, G. M.; Pascal, S.; Moneva Lorente, P.; Bosson, J.; Lacour, J.; Rochaix, J.-D. Specific Labeling of Mitochondria of Chlamydomonas with Cationic Helicene Fluorophores, *Org. Biomol. Chem.* **2018**, *16*, 919-923.
(282) Li, H.; Wallabregue, A.; Adam, C.; Labrador, G. M.; Bosson, J.; Bouffier, L.; Lacour, J.; Sojic, N. Bright Electrochemiluminescence Tunable in the Near-Infrared of Chiral Cationic Helicene Chromophores, *J. Phys. Chem. C* **2016**, *121*, 785-792.
(283) Li, H.; Voci, S.; Wallabregue, A.; Adam, C.; Labrador, G. M.; Duwald, R.; Hernández Delgado, I.; Pascal, S.; Bosson, J.; Lacour, J.; *et al.*. Efficient Annihilation Electrochemiluminescence of Cationic Helicene Luminophores, *ChemElectroChem* **2017**, *4*, 1750-1756.
(284) Jarolímová, Z.; Bosson, J.; Labrador, G. M.; Lacour, J.; Bakker, E. Ion Transfer Voltammetry at Thin Films Based on Functionalized Cationic [6]Helicenes, *Electroanalysis* **2018**, *30*, 650-657.
(285) Michaeli, K.; Kantor-Uriel, N.; Naaman, R.; Waldeck, D. H. The electron's spin and molecular chirality - how are they related and how do they affect life processes?, *Chem. Soc. Rev.* **2016**, *45*, 6478-6487.
(286) Mondal, P. C.; Fontanesi, C.; Waldeck, D. H.; Naaman, R. Spin-Dependent Transport through Chiral Molecules Studied by Spin-Dependent Electrochemistry, *Acc. Chem. Res.* **2016**, *49*, 2560-2568.

(287) Kiran, V.; Mathew, S. P.; Cohen, S. R.; Hernández Delgado, I.; Lacour, J.; Naaman, R. Helicenes—A New Class of Organic Spin Filter, *Adv. Mater.* **2016**, *28*, 1957-1962.
(288) Karras, M.; Holec, J.; Bednárová, L.; Pohl, R.; Schmidt, B.; Stará, I. G.; Starý, I. Asymmetric Synthesis of Nonracemic 2-Amino[6]helicenes and Their Self-Assembly into Langmuir Films, *J. Org. Chem.* **2018**, *83*, 5523-5538.
(289) Wang, Z. Y.; Qi, Y.; Bender, T. P.; Gao, J. P. Condensation Polyimides from AB-Type Amino Anhydride Monomers, *Macromolecules* **1997**, *30*, 764-769.
(290) Teplý, F.; Stará, I. G.; Starý, I.; Kollárovič, A.; Šaman, D.; Vyskočil, Š.; Fiedler, P. Synthesis of 3-Hexahelicenol and Its Transformation to 3-Hexahelicenylamines, Diphenylphosphine, Methyl Carboxylate, and Dimethylthiocarbamate, *J. Org. Chem.* **2003**, *68*, 5193-5197.
(291) Perzyna, A.; Zotto, C. D.; Durand, J.-O.; Granier, M.; Smietana, M.; Melnyk, O.; Stará, I. G.; Starý, I.; Klepetářová, B.; Šaman, D. Reaction of Isocyanate-Functionalised Silicon Wafers with Complex Amino Compounds, *Eur. J. Org. Chem.* **2007**, *2007*, 4032-4037.
(292) Pieters, G.; Gaucher, A.; Prim, D.; Marrot, J. First expeditious synthesis of 6,11-diamino-[6]carbohelicenes, *Chem. Comm.* **2009**, 4827-4828.
(293) Zadny, J.; Velisek, P.; Jakubec, M.; Sykora, J.; Cirkva, V.; Storch, J. Exploration Of 9-Bromo[7]Helicene Reactivity, *Tetrahedron* **2013**, *69*, 6213-6218.
(294) Jhulki, S.; Mishra, A. K.; Chow, T. J.; Moorthy, J. N. Helicenes as All-in-One Organic Materials for Application in OLEDs: Synthesis and Diverse Applications of Carbo- and Aza[5]helical Diamines, *Chem. – Eur. J.* **2016**, *22*, 9375-9386.
(295) van der Meijden, M. W.; Gelens, E.; Quirós, N. M.; Fuhr, J. D.; Gayone, J. E.; Ascolani, H.; Wurst, K.; Lingenfelder, M.; Kellogg, R. M. Synthesis, Properties, and Two-Dimensional Adsorption Characteristics of 5-Amino[6]hexahelicene, *Chem. – Eur. J.* **2016**, *22*, 1484-1492.
(296) Ernst, K.-H. Stereochemical Recognition of Helicenes on Metal Surfaces, *Acc. Chem. Res.* **2016**, *49*, 1182-1190.
(297) Taniguchi, M.; Nakagawa, H.; Yamagishi, A.; Yamada, K. STM observation of molecular chirality and alignment on solid surface, *J. Mol. Catal. A Chem.* **2003**, *199*, 65-71.
(298) Rahe, P.; Nimmrich, M.; Greuling, A.; Schütte, J.; Stará, I. G.; Rybáček, J.; Huerta-Angeles, G.; Starý, I.; Rohlfing, M.; Kühnle, A. Toward Molecular Nanowires Self-Assembled on an Insulating Substrate: Heptahelicene-2-carboxylic acid on Calcite (10$\bar{1}$4), *J. Phys. Chem. C* **2010**, *114*, 1547-1552.
(299) Hauke, C. M.; Rahe, P.; Nimmrich, M.; Schütte, J.; Kittelmann, M.; Stará, I. G.; Starý, I.; Rybáček, J.; Kühnle, A. Molecular Self-Assembly of Enantiopure Heptahelicene-2-Carboxylic Acid on Calcite (10$\bar{1}$4), *J. Phys. Chem. C* **2012**, *116*, 4637-4641.
(300) Balandina, T.; W. van der Meijden, M.; Ivasenko, O.; Cornil, D.; Cornil, J.; Lazzaroni, R.; Kellogg, R. M.; De Feyter, S. Self-assembly of an asymmetrically functionalized [6]helicene at liquid/solid interfaces, *Chem. Comm.* **2013**, *49*, 2207-2209.
(301) Ascolani, H.; van der Meijden, M. W.; Cristina, L. J.; Gayone, J. E.; Kellogg, R. M.; Fuhr, J. D.; Lingenfelder, M. Van der Waals interactions in the self-assembly of 5-amino[6]helicene on Cu(100) and Au(111), *Chem. Comm.* **2014**, *50*, 13907-13909.
(302) Fuhr, J. D.; van der Meijden, M. W.; Cristina, L. J.; Rodríguez, L. M.; Kellogg, R. M.; Gayone, J. E.; Ascolani, H.; Lingenfelder, M. Chiral expression of adsorbed (MP) 5-amino[6]helicenes: from random structures to dense racemic crystals by surface alloying, *Chem. Comm.* **2017**, *53*, 130-133.
(303) Newman, M. S.; Wise, R. M. The Synthesis and Resolution of 1, 12-Dimethylbenzo [c] phenanthrene-5-acetic Acid1, *J. Am. Chem. Soc.* **1956**, *78*, 450-454.
(304) Yamaguchi, M.; Okubo, H.; Hirama, M. Synthesis of optically active macrocycles consisting of helical chiral unit 1,12-dimethylbenzo[c]phenanthrene-5,8-dicarboxylate as a novel chiral building block, *Chem. Comm.* **1996**, 1771-1772.
(305) Amemiya, R.; Yamaguchi, M. Synthesis and structure of built-up organic macromolecules containing helicene, *The Chemical Record* **2008**, *8*, 116-127.

(306) Amemiya, R.; Yamaguchi, M. Chiral recognition in noncovalent bonding interactions between helicenes: right-handed helix favors right-handed helix over left-handed helix, *Org. Biomol. Chem.* **2008**, *6*, 26-35.
(307) Shigeno, M.; Kushida, Y.; Yamaguchi, M. Molecular Thermal Hysteresis in Helix-Dimer Formation of Sulfonamidohelicene Oligomers in Solution, *Chem. – Eur. J.* **2013**, *19*, 10226-10234.
(308) Yamaguchi, M.; Arisawa, M.; Shigeno, M.; Saito, N. Equilibrum and Nonequilibrium Chemical Reactions of Helicene Oligomers in the Noncovalent Bond Formation, *Bull. Chem. Soc. Jpn.* **2016**, *89*, 1145-1169.
(309) Okubo, H.; Yamaguchi, M.; Kabuto, C. Macrocyclic Amides Consisting of Helical Chiral 1,12-Dimethylbenzo[c]phenanthrene-5,8-dicarboxylate, *J. Org. Chem.* **1998**, *63*, 9500-9509.
(310) Feng, F.; Miyashita, T.; Okubo, H.; Yamaguchi, M. Spreading Behavior of Optically Active Macrocycloamides Consisting of Helical Chiral Units at the Air−Water Interface and the Formation of Langmuir−Blodgett Films, *J. Am. Chem. Soc.* **1998**, *120*, 10166-10170.
(311) Okubo, H.; Feng, F.; Nakano, D.; Hirata, T.; Yamaguchi, M.; Miyashita, T. Synthesis and monolayer behaviors of optically active 1,12- dimethylbenzo[c]phenanthrene-5,8-diamides and the formation of chiral langmuir-blodgett films, *Tetrahedron* **1999**, *55*, 14855-14864.
(312) Okubo, H.; Yamaguchi, M. A Building Block Method for the Synthesis of Higher Cycloamides, *J. Org. Chem.* **2001**, *66*, 824-830.
(313) Okubo, H.; Nakano, D.; Anzai, S.; Yamaguchi, M. Synthesis of Symmetrical Polynitrohelicenes and Their Chiral Recognition in the Charge Transfer Complexation, *J. Org. Chem.* **2001**, *66*, 557-563.
(314) Ichinose, W.; Miyagawa, M.; Ito, J.; Shigeno, M.; Amemiya, R.; Yamaguchi, M. Synthesis and duplex formation of the reverse amidohelicene tetramer, *Tetrahedron* **2011**, *67*, 5477-5486.
(315) Sugiura, H.; Takahira, Y.; Yamaguchi, M. Functionalized [3 + 3]Cycloalkynes: Substituent Effect on Self-Aggregation by Nonplanar π−π Interactions, *J. Org. Chem.* **2005**, *70*, 5698-5708.
(316) Ryo, A.; Wataru, I.; Masahiko, Y. Synthesis and Thermally Stable Helix-Dimer Formation of Amidohelicene Oligomers, *Bull. Chem. Soc. Jpn.* **2010**, *83*, 809-815.
(317) Yamamoto, K.; Sugiura, H.; Amemiya, R.; Aikawa, H.; An, Z.; Yamaguchi, M.; Mizukami, M.; Kurihara, K. Formation of double helix self-assembled monolayers of ethynylhelicene oligomer disulfides on gold surfaces, *Tetrahedron* **2011**, *67*, 5972-5978.
(318) Ichinose, W.; Shigeno, M.; Yamaguchi, M. Multiple States of Dimeric Aggregates Formed by (Amido–ethynyl)helicene Bidomain Compound and (Amido–ethynyl–amido)helicene Tridomain Compound, *Chem. – Eur. J.* **2012**, *18*, 12644-12654.
(319) Ichinose, W.; Ito, J.; Yamaguchi, M. Tetrameric αααβ Aggregate Formation by Stereoisomeric Bidomain Helicene Oligomers, *Angew. Chem. Int. Ed.* **2013**, *52*, 5290-5294.
(320) Shigeno, M.; Kushida, Y.; Yamaguchi, M. Heating/Cooling Stimulus Induces Three-State Molecular Switching of Pseudoenantiomeric Aminomethylenehelicene Oligomers: Reversible Nonequilibrium Thermodynamic Processes, *J. Am. Chem. Soc.* **2014**, *136*, 7972-7980.
(321) Kushida, Y.; Sawato, T.; Saito, N.; Shigeno, M.; Satozono, H.; Yamaguchi, M. Spatially Heterogeneous Nature of Self-Catalytic Reaction in Hetero-Double Helix Formation of Helicene Oligomers, *ChemPhysChem* **2016**, *17*, 3283-3288.
(322) Ben Braiek, M.; Aloui, F.; Moussa, S.; Ben Hassine, B. Synthesis and Characterization of New Helically Chiral Heptacyclic Systems, *Tetrahedron Lett.* **2015**, *56*, 6580-6584.
(323) Liu, L.; Yang, B.; Katz, T. J.; Poindexter, M. K. Improved Methodology For Photocyclization Reactions, *J. Org. Chem.* **1991**, *56*, 3769-3775.
(324) van Meerssche, M.; Declercq, J. P.; Soubrier-Payen, B. Études Structurales En Série Helicenique. IV. Structures Du Fluoro-1 Heptahelicene C30H17F Et Du Cyano-17 Fluoro-1 Heptahelicene C31H16Fn, *Bull. Soc. Chim. Bel.* **1986**, *95*, 609-618.
(325) Vanmeerssche, M.; Declercq, J. P.; Soubrierpayen, B. Structural Studies in Helicenic Series .4. Structures of 1-Fluoroheptahelicene $C_{30}H_{17}F$ and 17-Cyano-1-Fluoroheptahelicene $C_{31}H_{16}FN$, *Bull. Soc. Chim. Bel.* **1986**, *95*, 609-618.
(326) Ben Braiek, M.; Aloui, F.; Ben Hassine, B. Synthesis, Enantiomeric Resolution and Optical Properties of 8-Cyanohexahelicene, *Tetrahedron Lett.* **2016**, *57*, 4273-4276.

(327) Hafedh, N.; Aloui, F.; Raouafi, S. Synthesis, enantiomeric resolution and photophysical properties of 7-cyano-14-methoxy-5-thiahexahelicene, *J. Mol. Struct.* **2018**, *1165*, 126-131.
(328) Benhassine, B.; Gorsane, M.; Geertsevrard, F.; Pecher, J.; Martin, R. H.; Castelet, D. Potential Inducers of Asymmetric Syntheses - Use of The Atrolactic Synthesis to Evaluate their Efficiency, *Bull. Soc. Chim. Bel.* **1986**, *95*, 547-556.
(329) Wachsmann, C.; Weber, E.; Czugler, M.; Seichter, W. New Functional Hexahelicenes − Synthesis, Chiroptical Properties, X-ray Crystal Structures, and Comparative Data Bank Analysis of Hexahelicenes, *Eur. J. Org. Chem.* **2003**, *2003*, 2863-2876.
(330) Stöhr, M.; Boz, S.; Schär, M.; Nguyen, M.-T.; Pignedoli, C. A.; Passerone, D.; Schweizer, W. B.; Thilgen, C.; Jung, T. A.; Diederich, F. Self-Assembly and Two-Dimensional Spontaneous Resolution of Cyano-Functionalized [7]Helicenes on Cu(111), *Angew. Chem. Int. Ed.* **2011**, *50*, 9982-9986.
(331) Shchyrba, A.; Nguyen, M.-T.; Wäckerlin, C.; Martens, S.; Nowakowska, S.; Ivas, T.; Roose, J.; Nijs, T.; Boz, S.; Schär, *et al.*. Chirality Transfer in 1D Self-Assemblies: Influence of H-Bonding vs Metal Coordination between Dicyano[7]helicene Enantiomers, *J. Am. Chem. Soc.* **2013**, *135*, 15270-15273.
(332) Díaz, C.; Vesga, Y.; Echevarria, L.; Stará, I. G.; Starỳ, I.; Anger, E.; Shen, C.; El Sayed Moussa, M.; Vanthuyne, N.; Crassous, J.; *et al.*. Two-Photon Absorption And Two-Photon Circular Dichroism Of Hexahelicene Derivatives: A Study Of The Effect Of The Nature Of Intramolecular Charge Transfer, *RSC Advances* **2015**, *5*, 17429-17437.
(333) Garcia, M. H.; Florindo, P.; Piedade, M. d. F. M.; Maiorana, S.; Licandro, E. New organometallic Ru(II) and Fe(II) complexes with tetrathia-[7]-helicene derivative ligands, *Polyhedron* **2009**, *28*, 621-629.
(334) Saleh, N.; Shen, C. S.; Crassous, J. Helicene-Based Transition Metal Complexes: Synthesis, Properties And Applications, *Chem. Sci.* **2014**, *5*, 3680-3694.
(335) OuYang, J.; Crassous, J. Chiral Multifunctional Molecules Based On Organometallic Helicenes: Recent Advances, *Coord. Chem. Rev.* **2018**, *376*, 533-547.
(336) Norel, L.; Rudolph, M.; Vanthuyne, N.; Williams, J. A. G.; Lescop, C.; Roussel, C.; Autschbach, J.; Crassous, J.; Réau, R. Metallahelicenes: Easily Accessible Helicene Derivatives with Large and Tunable Chiroptical Properties, *Angew. Chem. Int. Ed.* **2010**, *49*, 99-102.
(337) Anger, E.; Rudolph, M.; Norel, L.; Zrig, S.; Shen, C. S.; Vanthuyne, N.; Toupet, L.; Williams, J. A. G.; Roussel, C.; Autschbach, J.; *et al.*. Multifunctional and Reactive Enantiopure Organometallic Helicenes: Tuning Chiroptical Properties by Structural Variations of Mono- and Bis(platinahelicene)s, *Chem. Eur. J* **2011**, *17*, 14178-14198.
(338) Shen, C.; Anger, E.; Srebro, M.; Vanthuyne, N.; Deol, K. K.; Jefferson, T. D.; Muller, G.; Williams, J. A. G.; Toupet, L.; Roussel, C.; *et al.*. Straightforward Access To Mono- And Bis-Cycloplatinated Helicenes Displaying Circularly Polarized Phosphorescence By Using Crystallization Resolution Methods, *Chem. Sci.* **2014**, *5*, 1915-1927.
(339) Anger, E.; Rudolph, M.; Shen, C.; Vanthuyne, N.; Toupet, L.; Roussel, C.; Autschbach, J.; Crassous, J.; Réau, R. From Hetero- to Homochiral Bis(metallahelicene)s Based on a PtIII−PtIII Bonded Scaffold: Isomerization, Structure, and Chiroptical Properties, *J. Am. Chem. Soc.* **2011**, *133*, 3800-3803.
(340) Shen, C.; Anger, E.; Srebro, M.; Vanthuyne, N.; Toupet, L.; Roussel, C.; Autschbach, J.; Réau, R.; Crassous, J. Diastereo-and Enantioselective Synthesis of Organometallic Bis (helicene) s by a Combination of C□ H Activation and Dynamic Isomerization, *Chem. Eur. J.* **2013**, *19*, 16722-16728.
(341) Chassot, L.; Mueller, E.; Von Zelewsky, A. cis-Bis(2-phenylpyridine)platinum(II) (CBPPP): a simple molecular platinum compound, *Inorg. Chem.* **1984**, *23*, 4249-4253.
(342) Crespo, O.; Eguillor, B.; Esteruelas, M. A.; Fernandez, I.; Garcia-Raboso, J.; Gomez-Gallego, M.; Martin-Ortiz, M.; Olivan, M.; Sierra, M. A. Synthesis and Characterisation of [6]-Azaosmahelicenes: the First d4-Heterometallahelicenes, *Chem. Comm.* **2012**, *48*, 5328-5330.
(343) Baumgartner, T.; Réau, R. Organophosphorus π-Conjugated Materials, *Chem. Rev.* **2006**, *106*, 4681-4727.
(344) Duffy, M. P.; Delaunay, W.; Bouit, P. A.; Hissler, M. π-Conjugated phospholes and their incorporation into devices: components with a great deal of potential, *Chem. Soc. Rev.* **2016**, *45*, 5296-5310.

(345) Lescop, C. Coordination-Driven Syntheses of Compact Supramolecular Metallacycles toward Extended Metallo-organic Stacked Supramolecular Assemblies, *Acc. Chem. Res.* **2017**, *50*, 885-894.
(346) Zhou, Q. L. *Privileged Chiral Ligands and Catalysts*; Wiley-VCH, 2011.
(347) Yavari, K.; Moussa, S.; Ben Hassine, B.; Retailleau, P.; Voituriez, A.; Marinetti, A. 1H-Phosphindoles as Structural Units in the Synthesis of Chiral Helicenes, *Angew. Chem. Int. Ed.* **2012**, *51*, 6748-6752.
(348) Yavari, K.; Retailleau, P.; Voituriez, A.; Marinetti, A. Heterohelicenes with Embedded P-Chiral 1H-Phosphindole or Dibenzophosphole Units: Diastereoselective Photochemical Synthesis and Structural Characterization, *Chem. – Eur. J.* **2013**, *19*, 9939-9947.
(349) Marinetti, A.; Jullien, H.; Voituriez, A. Enantioselective, Transition Metal Catalyzed Cycloisomerizations, *Chem. Soc. Rev.* **2012**, *41*, 4884-4908.
(350) Aillard, P.; Voituriez, A.; Dova, D.; Cauteruccio, S.; Licandro, E.; Marinetti, A. Phosphathiahelicenes: Synthesis and Uses in Enantioselective Gold Catalysis, *Chem. – Eur. J.* **2014**, *20*, 12373-12376.
(351) Gicquel, M.; Zhang, Y.; Aillard, P.; Retailleau, P.; Voituriez, A.; Marinetti, A. Phosphahelicenes in Asymmetric Organocatalysis: [3+2] Cyclizations of γ-Substituted Allenes and Electron-Poor Olefins, *Angew. Chem. Int. Ed.* **2015**, *54*, 5470-5473.
(352) Demmer, C. S.; Aillard, P.; Febvay, J.; Retailleau, P.; Voituriez, A.; Marinetti, A. Photochemical 2+2 Cyclization of Helical Phosphinamides in Solution and in the Solid State, *ChemPhotoChem* **2017**, *1*, 535-538.
(353) Su, H. C.; Fadhel, O.; Yang, C. J.; Cho, T. Y.; Fave, C.; Hissler, M.; Wu, C. C.; Réau, R. Toward Functional Pi-Conjugated Organophosphorus Materials: Design Of Phosphole-Based Oligomers For Electroluminescent Devices, *J. Am. Chem. Soc.* **2006**, *128*, 983-995.
(354) Nakano, K.; Oyama, H.; Nishimura, Y.; Nakasako, S.; Nozaki, K. λ5-Phospha[7]helicenes: Synthesis, Properties, and Columnar Aggregation with One-Way Chirality, *Angew. Chem. Int. Ed.* **2012**, *51*, 695-699.
(355) Aillard, P.; Retailleau, P.; Voituriez, A.; Marinetti, A. Synthesis of New Phosphahelicene Scaffolds and Development of Gold(I)-Catalyzed Enantioselective Allenene Cyclizations, *Chem. – Eur. J.* **2015**, *21*, 11989-11993.
(356) Fukawa, N.; Osaka, T.; Noguchi, K.; Tanaka, K. Asymmetric Synthesis and Photophysical Properties of Benzopyrano- or Naphthopyrano-Fused Helical Phosphafluorenes, *Org. Lett.* **2010**, *12*, 1324-1327.
(357) Stará, I. G.; Starý, I.; Kollárovič, A.; Teplý, F.; Šaman, D.; Tichý, M. A Novel Strategy for the Synthesis of Molecules with Helical Chirality. Intramolecular [2 + 2 + 2] Cycloisomerization of Triynes under Cobalt Catalysis, *J. Org. Chem.* **1998**, *63*, 4046-4050.
(358) Aillard, P.; Retailleau, P.; Voituriez, A.; Marinetti, A. *Chem. Commun.* **2014**, *50*, 2199-2201.
(359) Hashimoto, S.; Nakatsuka, S.; Nakamura, M.; Hatakeyama, T. Construction of a Highly Distorted Benzene Ring in a Double Helicene, *Angew. Chem. Int. Ed.* **2014**, *53*, 14074-14076.
(360) Yavari, K.; Aillard, P.; Zhang, Y.; Nuter, F.; Retailleau, P.; Voituriez, A.; Marinetti, A. Helicenes with Embedded Phosphole Units in Enantioselective Gold Catalysis, *Angew. Chem. Int. Ed.* **2014**, *53*, 861-865.
(361) Demmer, C. S.; Voituriez, A.; Marinetti, A. Catalytic Uses Of Helicenes Displaying Phosphorus Functions, *C. R. Chimie* **2017**, *20*, 860-879.
(362) Aillard, P.; Gicquel, M.; Yavari, K.; Retailleau, P.; Voituriez, A.; Marinetti, A. Tuning the Structure of Phosphahelicenes for Targeted Applications in Enantioselective Phosphine Organocatalysis, *Eur. J. Org. Chem.* **2018**, *2018*, 5853-5860.
(363) Yamamoto, K.; Shimizu, T.; Igawa, K.; Tomooka, K.; Hirai, G.; Suemune, H.; Usui, K. Rational Design and Synthesis of [5]Helicene-Derived Phosphine Ligands and Their Application in Pd-Catalyzed Asymmetric Reactions, *Sci. Rep.* **2016**, *6*, 36211.
(364) Yamamoto, K.; Okazumi, M.; Suemune, H.; Usui, K. Synthesis of [5]Helicenes with a Substituent Exclusively on the Interior Side of the Helix by Metal-catalyzed Cycloisomerization, *Org. Lett.* **2013**, *15*, 1806-1809.
(365) Reetz, M. T.; Beuttenmüller, E. W.; Goddard, R. First Enantioselective Catalysis Using A Helical Diphosphane, *Tetrahedron Lett.* **1997**, *38*, 3211-3214.
(366) Terfort, A.; Gorls, H.; Brunner, H. The First Helical-Chiral Phosphane Ligands: Rac-[5]- And Rac-[6]-Heliphos, *Synthesis* **1997**, 79-86.

(367) Aloui, F.; Ben Hassine, B. An Alternative Approach to 3-(Diphenylphosphino)Hexahelicene, *Tetrahedron Lett.* **2009**, *50*, 4321-4323.
(368) Aloui, F.; El Abed, R.; Marinetti, A.; Ben Hassine, B. Synthesis and characterization of new hexahelicene derivatives, *Tetrahedron Lett.* **2007**, *48*, 2017-2020.
(369) Tsujihara, T.; Inada-Nozaki, N.; Takehara, T.; Zhou, D.-Y.; Suzuki, T.; Kawano, T. Nickel-Catalyzed Construction of Chiral 1-[6]Helicenols and Application in the Synthesis of [6]Helicene-Based Phosphinite Ligands, *Eur. J. Org. Chem.* **2016**, *2016*, 4948-4952.
(370) El Abed, R.; Aloui, F.; Genêt, J.-P.; Ben Hassine, B.; Marinetti, A. Synthesis and Resolution of 2-(Diphenylphosphino)Heptahelicene, *J. Organomet. Chem.* **2007**, *692*, 1156-1160.
(371) Monteforte, M.; Cauteruccio, S.; Maiorana, S.; Benincori, T.; Forni, A.; Raimondi, L.; Graiff, C.; Tiripicchio, A.; Stephenson, G. R.; Licandro, E. Tetrathiaheterohelicene Phosphanes as Helical-Shaped Chiral Ligands for Catalysis, *Eur. J. Org. Chem.* **2011**, *2011*, 5649-5658.
(372) Moussa, S.; Aloui, F.; Ben Hassine, B. Synthesis and Optoelectronic Properties of Some New Thiahelicenes, *Synth. Commun.* **2011**, *41*, 1006-1016.
(373) Dova, D.; Cauteruccio, S.; Prager, S.; Dreuw, A.; Graiff, C.; Licandro, E. Chiral Thiahelicene-Based Alkyl Phosphine–Borane Complexes: Synthesis, X-ray Characterization, and Theoretical and Experimental Investigations of Optical Properties, *J. Org. Chem.* **2015**, *80*, 3921-3928.
(374) Nakano, D.; Yamaguchi, M. Enantioselective Hydrogenation Of Itaconate Using Rhodium Bihelicenol Phosphite Complex. Matched/Mismatched Phenomena Between Helical And Axial Chirality, *Tetrahedron Lett.* **2003**, *44*, 4969-4971.
(375) Weix, D. J.; Dreher, S. D.; Katz, T. J. [5] HELOL Phosphite: A Helically Grooved Sensor Of Remote Chirality, *J. Am. Chem. Soc.* **2000**, *122*, 10027-10032.
(376) Krausová, Z.; Sehnal, P.; Bondzic, B. P.; Chercheja, S.; Eilbracht, P.; Stará, I. G.; Šaman, D.; Starý, I. Helicene-Based Phosphite Ligands in Asymmetric Transition-Metal Catalysis: Exploring Rh-Catalyzed Hydroformylation and Ir-Catalyzed Allylic Amination, *Eur. J. Org. Chem.* **2011**, *2011*, 3849-3857.
(377) Dore, A.; Fabbri, D.; Gladiali, S.; Valle, G. New Axially Chiral Sulfur-Compounds - Synthesis And Conformational Stability Of Enantiopure 4,4'-Biphenanthrene-3,3'-Dithiol And Related Atropisomeric Derivatives, *Tetrahedron-Asymmetry* **1995**, *6*, 779-788.
(378) Reetz, M. T.; Sostmann, S. Kinetic Resolution in Pd-Catalyzed Allylic Substitution Using the Helical PHelix Ligand, *J. Organomet. Chem.* **2000**, *603*, 105-109.
(379) Cauteruccio, S.; Loos, A.; Bossi, A.; Blanco Jaimes, M. C.; Dova, D.; Rominger, F.; Prager, S.; Dreuw, A.; Licandro, E.; Hashmi, A. S. K. Gold(I) Complexes of Tetrathiaheterohelicene Phosphanes, *Inorg. Chem.* **2013**, *52*, 7995-8004.
(380) Kawasaki, T.; Suzuki, K.; Licandro, E.; Bossi, A.; Maiorana, S.; Soai, K. Enantioselective Synthesis Induced by Tetrathia-[7]-Helicenes in Conjunction with Asymmetric Autocatalysis, *Tetrahedron: Asymmetry* **2006**, *17*, 2050-2053.
(381) Graule, S.; Rudolph, M.; Vanthuyne, N.; Autschbach, J.; Roussel, C.; Crassous, J.; Réau, R. Metal−Bis(helicene) Assemblies Incorporating π-Conjugated Phosphole-Azahelicene Ligands: Impacting Chiroptical Properties by Metal Variation, *J. Am. Chem. Soc.* **2009**, *131*, 3183-3185.
(382) Graule, S.; Rudolph, M.; Shen, W.; Williams, J. A. G.; Lescop, C.; Autschbach, J.; Crassous, J.; Réau, R. Assembly of π-Conjugated Phosphole Azahelicene Derivatives into Chiral Coordination Complexes: An Experimental and Theoretical Study, *Chem. – Eur. J.* **2010**, *16*, 5976-6005.
(383) Vreshch, V.; El Sayed Moussa, M.; Nohra, B.; Srebro, M.; Vanthuyne, N.; Roussel, C.; Autschbach, J.; Crassous, J.; Lescop, C.; Réau, R. Assembly of Helicene-Capped N,P,N,P,N-Helicands within Cu^{I} Helicates: Impacting Chiroptical Properties by Ligand–Ligand Charge Transfer, *Angew. Chem. Int. Ed.* **2013**, *52*, 1968-1972.
(384) Crassous, J.; Réau, R. Pi-Conjugated Phosphole Derivatives: Synthesis, Optoelectronic Functions And Coordination Chemistry, *Dalton Trans.* **2008**, 6865-6876.

(385) Lehn, J. M.; Rigault, A.; Siegel, J.; Harrowfield, J.; Chevrier, B.; Moras, D. Spontaneous Assembly of Double-Stranded Helicates from Oligobipyridine Ligands and Copper(I) Cations: Structure of an Inorganic Double Helix, *Proc. Nat. Acad. Sci.* **1987**, *84*, 2565-2569.
(386) Lehn, J.-M. *Supramolecular Chemistry*; Wiley, 1995.
(387) Stomeo, F.; Lincheneau, C.; Leonard, J. P.; O'Brien, J. E.; Peacock, R. D.; McCoy, C. P.; Gunnlaugsson, T. Metal-Directed Synthesis of Enantiomerially Pure Dimetallic Lanthanide Luminescent Triple-Stranded Helicates, *J. Am. Chem. Soc.* **2009**, *131*, 9636-9637.
(388) Howson, S. E.; Bolhuis, A.; Brabec, V.; Clarkson, G. J.; Malina, J.; Rodger, A.; Scott, P. Optically pure, water-stable metallo-helical 'flexicate' assemblies with antibiotic activity, *Nature Chem.* **2011**, *4*, 31.
(389) Josse, P.; Favereau, L.; Shen, C.; Dabos-Seignon, S.; Blanchard, P.; Cabanetos, C.; Crassous, J. Enantiopure versus Racemic Naphthalimide End-Capped Helicenic Non-fullerene Electron Acceptors: Impact on Organic Photovoltaics Performance, *Chemistry* **2017**, *23*, 6277-6281.
(390) Hatakeyama, T.; Hashimoto, S.; Oba, T.; Nakamura, M. Azaboradibenzo[6]helicene: Carrier Inversion Induced by Helical Homochirality, *J. Am. Chem. Soc.* **2012**, *134*, 19600-19603.
(391) Ben Hassine, B.; Gorsane, M.; Pecher, J.; Martin, R. H. Diastereoselective NaBH4 Reductions of (dl) α-Keto Esters, *Bull. Soc. Chim. Bel.* **1985**, *94*, 597-603.
(392) Kato, K.; Segawa, Y.; Itami, K. Symmetric Multiple Carbohelicenes, *Synlett*
(393) Li, C.; Yang, Y.; Miao, Q. Recent Progress in Chemistry of Multiple Helicenes, *Chemistry – An Asian Journal* **2018**, *13*, 884-894.
(394) Li, L.; Zhao, C.; Wang, H. Recent Progress in Synthesis and Application of Thiophene Oligomers Based on Bithiophene Dicarbanions, *The Chemical Record* **2016**, *16*, 797-809.
(395) Isla, H.; Saleh, N.; Ou-Yang, J.-K.; Dhbaibi, K.; Jean, M.; Dziurka, M.; Favereau, L.; Vanthuyne, N.; Toupet, L.; Jamoussi, B.; *et al.*. Bis-4-aza[6]helicene: A Bis-helicenic 2,2'-Bipyridine with Chemically Triggered Chiroptical Switching Activity, *J. Org. Chem.* **2019**, *84*, 5383-5393.
(396) Chen, S.; Ge, Z.; Jia, Q.; Wang, K.-P.; Gan, L.-H.; Hu, Z.-Q. The Preparation of Enantiopure [6]- and [7]Helicenes from Binaphthanol, *Chemistry – An Asian Journal* **2019**, *14*, 1462-1466.
(397) Yan, Z.-P.; Luo, X.-F.; Liu, W.-Q.; Wu, Z.-G.; Liang, X.; Liao, K.; Wang, Y.; Zheng, Y.-X.; Zhou, L.; Zuo, J.-L.; *et al.*. Configurationally Stable Platinahelicene Enantiomers for Efficient Circularly Polarized Phosphorescent Organic Light-Emitting Diodes, *Chem. – Eur. J.* **2019**, *25*, 5672-5676.
(398) Macé, A.; Hellou, N.; Hammoud, J.; Martin, C.; Gauthier, E. S.; Favereau, L.; Roisnel, T.; Caytan, E.; Nasser, G.; Vanthuyne, N.; *et al.*. An Enantiopure Cyclometallated Iridium Complex Displaying Long-Lived Phosphorescence both in Solution and in the Solid State, *Helv. Chim. Acta* **2019**, *102*, e1900044.
(399) Yen-Pon, E.; Champagne, P. A.; Plougastel, L.; Gabillet, S.; Thuéry, P.; Johnson, M.; Muller, G.; Pieters, G.; Taran, F.; Houk, K. N.; *et al.*. Sydnone-Based Approach to Heterohelicenes through 1,3-Dipolar-Cycloadditions, *J. Am. Chem. Soc.* **2019**, *141*, 1435-1440.
(400) Yavari, K.; Delaunay, W.; De Rycke, N.; Reynaldo, T.; Aillard, P.; Srebro-Hooper, M.; Chang, V. Y.; Muller, G.; Tondelier, D.; Geffroy, B.; *et al.*. Phosphahelicenes: From Chiroptical and Photophysical Properties to OLED Applications, *Chem. – Eur. J.* **2019**, *25*, 5303-5310.

Biographies

Kais Dhbaibi obtained his Engineer degree in analytical chemistry in 2015 from Tunis-El Manar University (Tunisia). He is a PhD student since February 2016, preparing his research doctorate between the University of Rennes 1 in France and the University of Gabés in Tunisia and under the joint supervision of Prof. B. Jamoussi and Dr. J. Crassous. His doctoral studies focus on the synthesis and the photophysical characterization of helicene derivatives and the exploration of possible applications in optoelectronic and spintronic devices. His research interests lie in the field of the development of optically active materials based on helicenes.

Dr. Ludovic Favereau received his master degree in organic chemistry in 2011 from the National Institute of Applied Sciences (INSA) in Rouen. He obtained his PhD in 2014 from the University of Nantes under the supervision of Dr. F. Odobel on the synthesis of molecular architectures for mimicking the photosynthetic Z scheme function. After a one-year postdoctoral fellow at the University of Oxford with Prof. Harry L. Anderson on the synthesis of porphyrin nanorings, he was recruited as CNRS researcher at the "*Institut des Sciences Chimiques de Rennes*" (University of Rennes, France) in 2015 in Jeanne Crassous' group. In 2019, he received the Dina Surdin prize from the Société Chimique de France. His research focuses on the design of chiral organic molecules with intense chiroptical properties (circular dichroism, circularly polarized luminescence) to explore the potential of chirality property in optoelectronic applications (OLED, OPV, …).

Dr. Jeanne Crassous (born Costante) received her PhD in 1996 under supervision of Prof. André collet (ENS, Lyon, France), working on the absolute configuration of bromochlorofluoromethane. After a one-year postdoctoral period studying the chirality of fullerenes in Prof. François Diederich's group (ETH Zurich, Switzerland), she received a CNRS researcher position at the ENS Lyon in 1998, and she joined the "*Institut des Sciences Chimiques de Rennes*" (University of Rennes, France) in 2005. She is currently Director of Research at the CNRS. In 2013, she became a distinguished member of French Chemical Society (Société Chimique de France, SCF). Her group is dealing with many fields related to chirality (organometallic and heteroatomic helicenes, fundamental aspects of chirality such as parity violation effects, chiroptical activity such as electronic and vibrational circular dichroism and circularly polarized luminescence). She has published more than 110 papers and a French monography on the Stereochemistry of Chiral Molecules. She is responsible for a National Network on "Chirality and Multifunctionality".

TOC